komunikácie

COMMUNICATIONS

SCIENTIFIC LETTERS OF THE UNIVERSITY OF ŽILINA

Volume 26

UNIVERSITY
OF ŽILINA

ISSN 1335-4205

2/2024

UNIVERSITY OF ŽILINA
EDIS-Publishing House
UNIZA

EDIS-Publishing House of the University of Žilina (UZ) is one of the University of Žilina's consituents. The beginning of its existence dates back to 1990. In the course of its work, the publishing house has published more than 4 900 titles of book publications, especially university textbooks, scientific monographs, scripts, prose, but also enriched the book market with titles of regional, children's and popular literature.
Students and professional public have the opportunity to purchase published titles in the „Selling Study Literature" directly on the premises of the University of Žilina, in the EDIS shop or upon order on a „cash on delivery" basis. All published titles are available at: www.edis.uniza.sk.

EDIS-Publishing House of the University of Žilina offers book titles in English

Lenka Černá, Jozef Daniš
APPLICATION OF COST ALCULATIONS IN THE TARIFF POLICY FORMATION IN RAILWAY TRANSPORT
ISBN 978-80-554-1391-4 Price 7.61 €

Eva Nedeliaková, Jana Sekulová
EVALUATION OF QUALITY IN RAILWAY TRANSPORT
ISBN 978-554-1272-6 Price 8.00 €

Martin Bugaj
AEROMECHANICS 1
ISBN 978-80-554-1675-5 Price 14.50 €

Ján Bujňák, Ružica Nikolić, Jelena Djoković
STEEL STRUCTURES COLLECTION OF SOLVED PROBLEMS WITH EXCERPTS FROM T HEORY
ISBN 978-80554-0404-2 Price 9.34 €

Anna Tomová
ECONOMICS OF AIR NAVIGATION SERVICES
ISBN 978-80-554-0905-4 Price 14.30 €

Marica Mazurek
MODELS OF BRANDING AND THEIR APPLICATION
ISBN 978-80-554-1705-9 Price 9.00 €

Jozef Melcer
DYNAMICS OF STRUCTURES
ISBN 978-80-554-1698-4 Price 19.00 €

Jozef Gašparík et al.
RAILWAY TRAFFIC OPERATION
ISBN 978-80-554-1281-8 Price 15.80 €

Tetiana Hovorushchenko et.al.
CD - INTELLIGENT INFORMATION-ANALYTICAL TECHNOLOGIES...
ISBN 978-80-554-1729-5 Price 3.50 €

Karol Matiaško, Michal Kvet, Marek Kvet
CD - PRACTICES FOR DATABASE SYSTEMS
ISBN 978-80-554-1397-6 Price 2.20 €

Michal Kvet, Karol Matiaško, Štefan Toth
USB - PRACTICAL SQL FOR ORACLE CLOUD
ISBN 978-80-554-1880-3 Price: 11,30 €

Veronika Valašková, Daniela Kucharová
USB - STATICS OF STRUCTURES 3
ISBN 978-80-554-1826-1 Price: 8,90 €

Michal Kvet, Karol Matiaško, Marek Kvet
USB - BECOME EXPERT IN MYSQL PRACTICES FOR DATABASE SYSTEMS IN MYSQL
ISBN 978-80-554-1786-8 Price 13.50 €

EDIS-Publishing House UNIZA
Univerzitná 8215/1,
010 26 Žilina,
Slovakia

e-mail: edis_objednavky@uniza.sk, edis@uniza.sk
www.edis.uniza.sk

B - MECHANICAL ENGINEERING

C - ELECTRICAL ENGINEERING IN TRANSPORT

D - CIVIL ENGINEERING IN TRANSPORT

E - MANAGEMENT SCIENCE AND INFORMATICS IN TRANSPORT

PECULIARITIES OF DESIGNING THE FRAME OF A UNIVERSAL CONTAINER MADE OF RECTANGULAR PIPES

Juraj Gerlici[1], Alyona Lovska[1,*], Mykhailo Pavliuchenkov[2], Oleksandr Kravchenko[1]

[1]University of Zilina, Zilina, Slovak Republic
[2]Ukrainian State University of Railway Transport, Kharkiv, Ukraine

*E-mail of corresponding author: alyonaLovskaya.vagons@gmail.com

Juraj Gerlici 0000-0003-3928-0567,
Alyona Lovska 0000-0002-8604-1764,
Mykhailo Pavliuchenkov 0000-0003-0542-7284,
Oleksandr Kravchenko 0000-0003-4677-2535

Resume

The features of designing the frame of a universal container made of square pipes are presented in this paper. The two frame loading schemes are taken into account: the effect of vertical loading on the container frame when it is lifted by the upper corner fittings (I loading mode); the effect of longitudinal loading on the frame during transportation by the rail transport (II loading mode). Mathematical modeling was performed to determine the longitudinal loading acting on the container in the II loading mode. The determined acceleration is taken into account when constructing the schemes of force factors that arise in the frame. The strength of the frame was calculated using the finite element method, which was implemented in SolidWorks Simulation. The conducted research could contribute to creation of recommendations and developments regarding the design of modern structures of modular vehicles.

Article info

Received 10 November 2023
Accepted 10 January 2024
Online 26 January 2024

Keywords:

container
container frame
container loading
container strength
container transportation

Available online: https://doi.org/10.26552/com.C.2024.016

ISSN 1335-4205 (print version)
ISSN 2585-7878 (online version)

1 Introduction

Container transportation has long been one of the most successful symbioses of transport interaction. Due to the mobility of their design, containers are transported by all types of transport [1-3]. One of the most common logistics schemes is the transportation of containers by rail transport with subsequent transshipment onto the decks of railway vessels. In this case, the transshipment of containers from one type of transport to another is carried out with the help of lifting and transporting equipment - spreaders, fork-lift trucks, etc. Containers can be damaged as a result of loading and unloading operations. Such damages include a rupture of the cladding, deformation of the frame elements, broken welds, etc. These damages not only cause the need for additional capital costs for the operation of containers, in particular for repairs, but can also cause damage to the cargo placed in them. In addition, such damages threaten the traffic safety of vehicles transporting such containers. In this regard, there is a need to create modern container designs with improved technical properties, including operational ones.

2 Analysis of recent research and publications

Currently, there is a large number of developments on design of the modern container structures. Some of them are considered hereon. For example, in work [4], an analysis of the stresses occurring in the structure of the container during its transportation by water transport is carried out. A 40-foot container of standard size 1AA is taken into account. The calculation results made it possible to formulate the main requirements for operation of such a container.

Authors of publication [5] also analyzed the strength of the universal container, however, in the case of transporting it by rail. They obtained the dependence of the influence of the container's own movements on its strength. It must be said that the works [4-5] do not propose solutions for improving the container, which would enable the enhancement of its operational properties.

The creation of a new design of a specialized container is covered in publication [6]. The container is intended for transportation of fruit and vegetable products. The authors not only highlighted the features

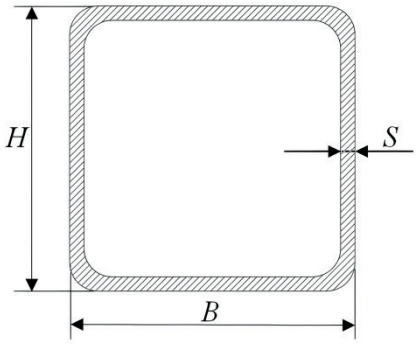

H - height; B - width; S - wall thickness

Figure 1 *Pipe section*

of its design, but also performed the strength calculation. The paper also mentions the prospects for operation of such a container. Similar studies are also covered in work [7], where a design of a container for fruit and vegetable products is also proposed.

Peculiarities of designing a container, according to the ISO standard size, are considered in the work [8]. The main loading patterns of the container in operation are analyzed. The influence of operational loadings on the strength qualities of the container was studied. Further prospects for creation of modern container designs have been determined. Along with this, the authors of works [6-8] did not propose solutions for improving the design of the container frame, as its most loaded component.

To reduce the dynamic loading of the container during transportation by rail, works [9-10] proposed to make its walls from sandwich panels with a layer of energy-absorbing material. These panels are supposed to be attached to the frame. To justify such an implementation, the simulation of the container loading (longitudinal and lateral) and the calculation of strength of its structure were carried out. The obtained results proved the effectiveness of the proposed improvement. At the same time, the authors' team did not pay attention to the improvement of the container's frame.

Determination of the stress-deformation state of the container body with a variable volume is carried out in work [11]. The calculation was carried out in the ANSYS software. Experimental studies were carried out on the lateral skew of the container at insignificant loads to check the adequacy of the obtained results.

The study of the stress-deformed state of the container body when it is lifted by a crane and moved by a drag is carried out in the publication [12]. The theoretical determination of strength indicators was carried out in the WinMachine ARM software package. The experimental study of strength was carried out using the method of electrical strain measurement.

The determination of the dynamic load of the container under operational load modes was carried out in work [13]. The obtained values of dynamic loads are taken into account when calculating the strength of the container in the Ansys software.

However, solutions for improving the supporting structure of the container and its technical and economic indicators are not given in these works.

The literary review of sources [4-13] proves that the creation of modern container designs is a very relevant issue, but it needs further development.

The purpose of this study was to highlight the features of creating a frame of a universal container from square pipes. To achieve this goal, the authors set the following tasks:

- to determine the force factors that occur in the structure of the container frame during operational loading modes;
- to choose the profile of the container frame execution and calculate its strength.

3 The proposal of the new container frame design

To reduce the damage to the container during the operational modes, it is suggested to make its frame from the closed profiles - square pipes (Figure 1) [14]. When designing this container, the requirements of the international standard ISO 668 "Series 1 cargo containers. Classification, dimensions and nominal characteristics" were taken into account.

To justify the expediency of such an implementation, a frame scheme is proposed, which is shown in Figure 2. The study was carried out on the example of a 24-ton container (1CC).

To determine the parameters of the frame pipes, the corresponding calculations were carried out in the Lira - SAPR. Lira - SAPR is a multifunctional software complex designed for the design and calculation of machine-building and construction structures for various purposes. Calculations in the program are performed for both static and dynamic effects. The finite element method is the basis of calculations in this software. Various available modules can be connected to select and to check cross-sections of steel and reinforced concrete structures, model of soil, calculation of bridges

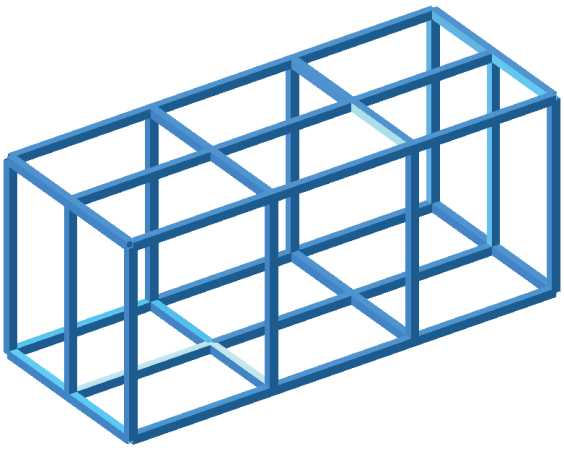

Figure 2 *Container frame*

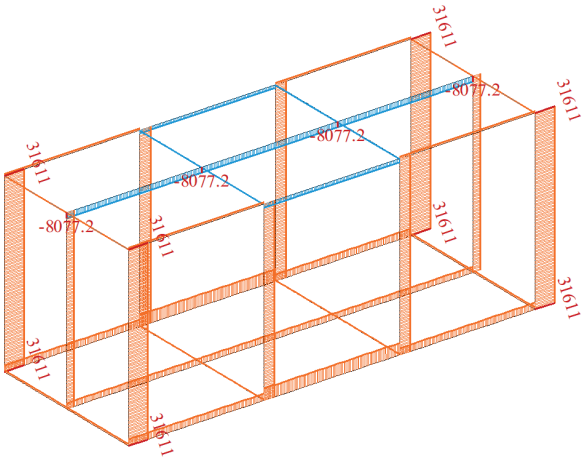

Figure 4 *Scheme of the longitudinal forces acting in the frame (N)*

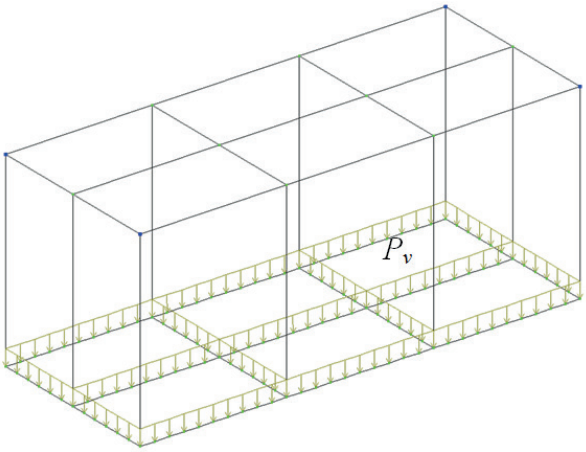

Figure 3 *Calculation scheme of the frame for the I loading mode*

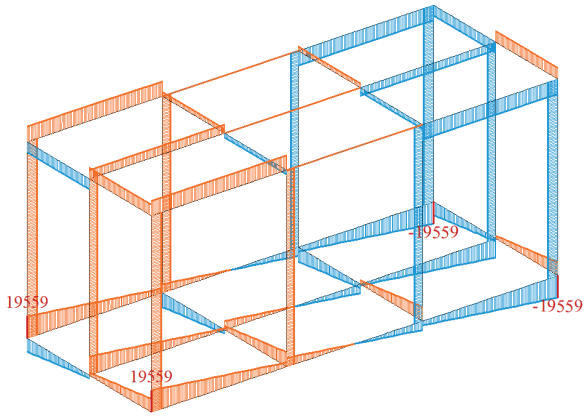

Figure 5 *Scheme of the lateral forces acting in the frame (N)*

and behavior of buildings during the installation period, etc. [15].

In this case, the frame is considered as a rod system. Two frame loading schemes are taken into account:

- vertical loading of the frame when it is lifted by the upper corner fittings (I loading mode);
- longitudinal loading of the frame during the transportation by rail transport (II loading mode).

The calculation scheme of the frame when it is lifted by the upper corner fittings is shown in Figure 3.

The fact that the container frame is secured by the upper corner fittings is taken into account. The vertical loading P_v is transferred to the lower part of the frame, which is intended for placing floor boards. It is also taken into account that the vertical load P_v is determined by the weight of the transported cargo and the container's own weight, i.e. gross weight of the container. In this case, the conditional load was considered using the full carrying capacity of the container. Taking this into account, the schemes of longitudinal (Figure 4) and lateral forces (Figure 5) acting in the frame, as well as the scheme of bending moments (Figure 6) were obtained. Here, in Figures 4 - 6, "extension" is indicated in orange, and "compression" is indicated in blue.

The analysis of a scheme shown in Figure 4 leads to the fact, that the longitudinal forces in individual sections of the frame are constant. This is explained by the fact that the elements in individual sections were considered as one whole rod that experiences a given type of internal force (tension or compression).

Therefore, the maximum value of the longitudinal force occurs in the vertical struts and equals 31.6 kN. This is due to the fact that they act as an intermediate adapter between the anchor point and the area of application of force to the container frame.

The maximum value of the lateral force occurs in the intermediate vertical struts. Its value is 19.6 kN.

These struts connect the bottom part of the container frame with the lower one. Therefore, in the case of loading the lower part of the frame, the maximum values of this force occur here.

The maximum value of the bending moment also occurs in the intermediate vertical struts and equals 13.6 kNm. The scheme of frame movements under the action of vertical loading is shown in Figure 7.

At the same time, the longitudinal beams of the

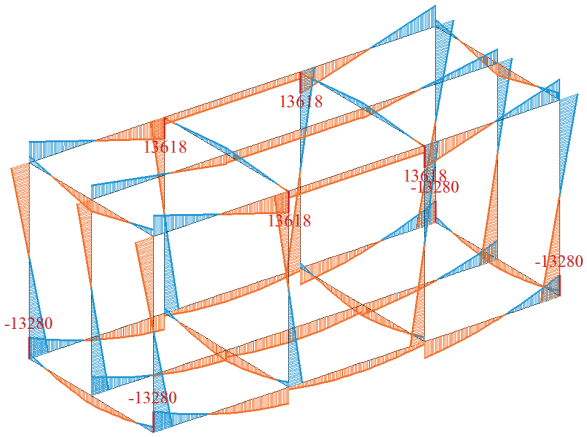

Figure 6 *Scheme of the bending moments acting in the frame (N m)*

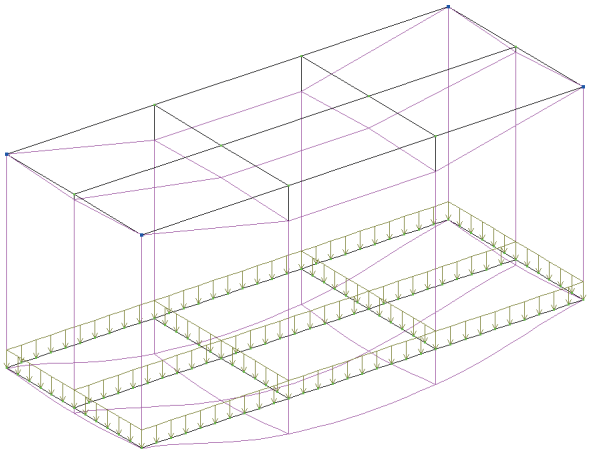

Figure 7 *Scheme of the frame movements under the action of vertical loading*

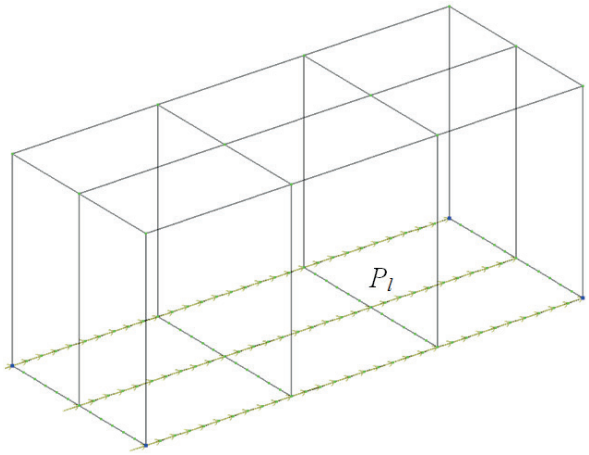

Figure 8 *Calculation scheme of the frame for the II loading mode*

upper and lower parts of the frame experience the largest movements. This is due to the fact that an evenly distributed loading is applied to the beams that form the lower part of the frame.

In addition, as part of the study, the calculation of the container frame under longitudinal loading was carried out, taking into account its transportation by rail transport (on a flat wagon as a part of a train). The calculation scheme of the frame is shown in Figure 8.

In this case, the longitudinal loading P_l was applied to the beams forming the lower part of the frame, namely to the longitudinal beams. This scheme is explained by the fact that the load on the lower frame of the container when transported by a flat wagon is transferred from the corner fittings, which interact with the fitting stops. The movement of cargo relative to the container was not taken into account. The frame was secured in corner fittings.

To determine the amount of the longitudinal force, a mathematical model, formed in the previous work of the authors [16], was used. However, this model was further developed to determine the longitudinal loading of a container placed on a flat wagon when a longitudinal force is applied to it. In view of this, the model has the following form:

$$\begin{cases} M_{FW} \cdot \ddot{q}_1 = P - \sum_{i=1}^{n} (F_{FR} \cdot sign(\dot{q}_1 - \dot{q}_2)), \\ M_c \cdot \ddot{q}_2 = (F_{FR} \cdot sign(\dot{q}_1 - \dot{q}_2)), \end{cases} \quad (1)$$

here M_{FW}, M_C - inertial coefficients, which characterize, respectively, the mass of the frame of the flat wagon and the container; P - force acting on the stops of the automatic coupling device of the flat wagon; F_{FR} - frictional force between the frame of the flat wagon and the containers; q_1 and q_2 - generalized coordinates characterizing the movement of a flat wagon and a container, respectively.

The calculation was carried out under the condition that a longitudinal force of 2.5 MN [17] is applied to the stops of the automatic coupling. It was considered that this force acts in the form of a “jerk” with a constant value.

It is important to note that it is necessary to take into account the value of forces that are characteristic of their operating conditions in the case of using this model

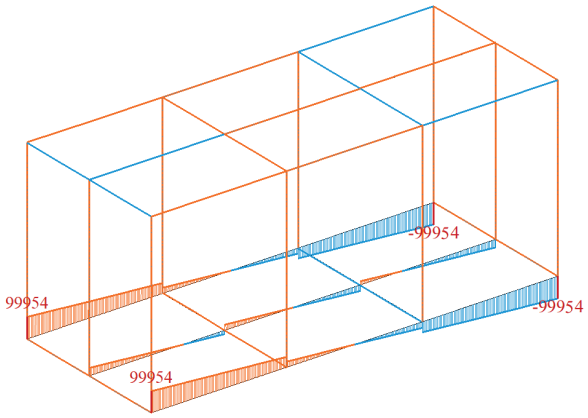

Figure 9 *Scheme of the longitudinal forces acting in the frame (N)*

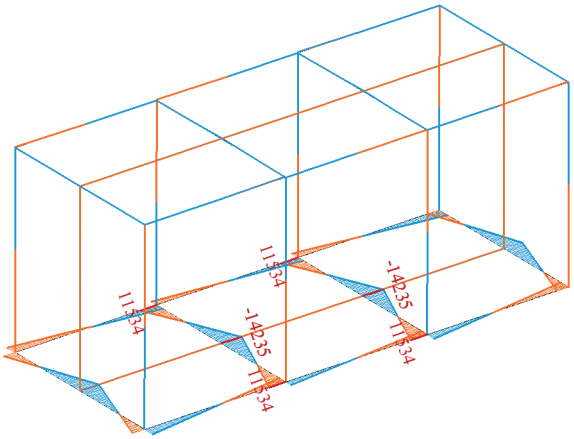

Figure 11 *Scheme of the bending moments acting in the frame (Nm)*

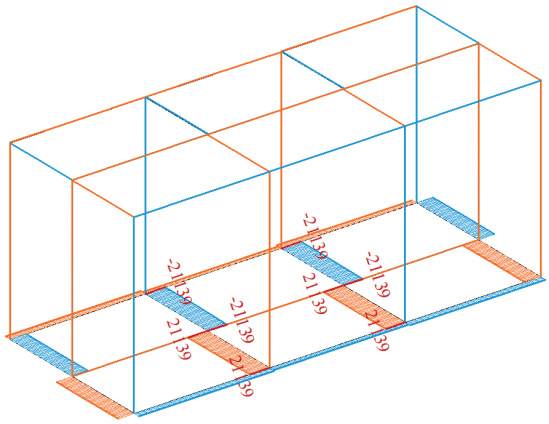

Figure 10 *Scheme of the lateral forces acting in the frame (N)*

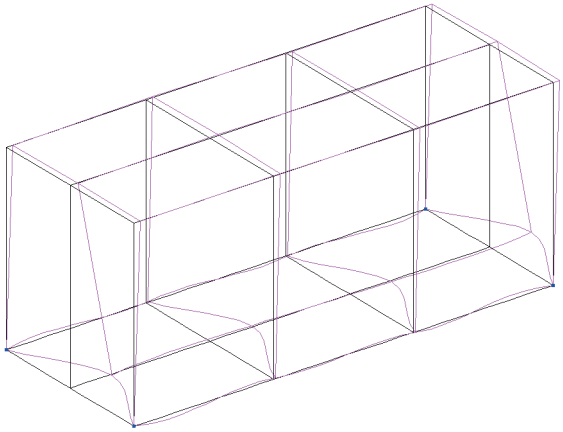

Figure 12 *Scheme of the frame movements when a longitudinal force is applied to it*

for a 1435 mm gauge car equipped with a screw tie.

The solution of the mathematical model was carried out by the method of variation of arbitrary constants, with initial conditions close to zero [18-19]. Based on the calculations, it was established that the longitudinal acceleration acting on the container is about 20 m/s^2.

This value of acceleration is taken into account when constructing the loading scheme of the container frame in the II loading mode. The calculation results are shown in Figures 9 - 11. Analyzing the data of the scheme, one can conclude that the maximum value of the longitudinal force occurs in the bottom part of the frame and equals 100 kN (Figure 9). This can be explained by the fact that it was secured by the lower corner fittings. The maximum value of the lateral force was recorded in the longitudinal beams and amounted to 21.1 kN (Figure 10). This is explained by the same argument as for the situation with longitudinal forces. The maximum bending moment occurs in the bottom part of the frame and is equal to 14.2 kNm (Figure 11).

The scheme of the frame movements in the II calculation mode is shown in Figure 12.

At the same time, the lateral beams of the lower part of the frame experience maximum displacement. This circumstance is caused by the fact that it is fixed by the lower corner fittings, and the longitudinal force is applied to the lateral beams.

Based on the obtained results, the moment of resistance of the section of the container frame execution profile was determined. In this case, the following dependency was used [20]:

$$W = \frac{M}{[\sigma]}, \tag{2}$$

here M - value of the maximum bending moment acting in the section of the frame; [σ] - allowable stresses for the material of the frame execution (steel grade 09G2S, [σ] = 210 MPa [13]).

It should be noted that grade 09G2S steel is standard for the manufacture of containers.

The cross-sectional area of the frame execution profile was considered, as well. In this case [20]

$$A = \frac{F}{[\sigma]}, \tag{3}$$

here F - value of the longitudinal force acting in the frame.

It must be said that according to the results of

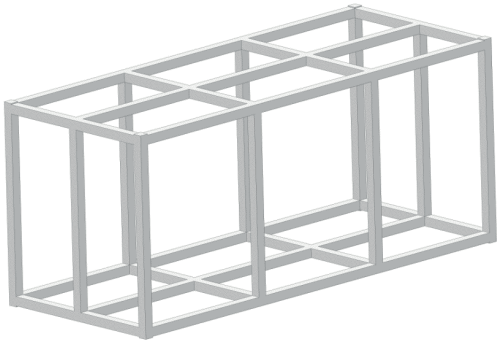

Figure 13 *the 3-D model of the container frame*

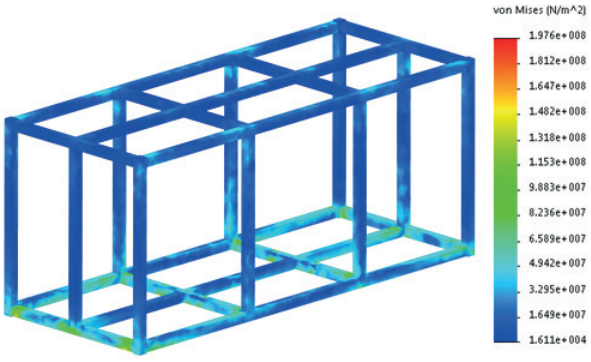

Figure 14 *Stressed state of the container frame*

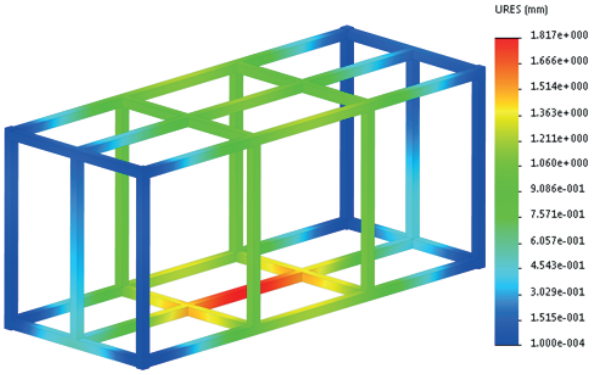

Figure 15 *Displacements in the nodes of the container frame*

calculations, the selection of the section parameters of the frame was carried out according to Equation (2), since here the value of the moment of resistance, from the point of view of ensuring the strength of the frame execution profile, is more important. Taking into account the conducted calculations, it was established that the profile of the frame execution is a square pipe with the following parameters: $H = B = 120$ mm, $S = 4$ mm, $W = 67.05$ cm^3. Based on the specified parameters, the mass of the container frame will amount to about 500 kg.

At the next stage of the research, a spatial model of the container frame was built (Figure 13) and its FEM analysis was carried out in SolidWorks Simulation [21-22].

The results of the calculation of the container's strength under the II loading mode are shown in Figures 14 and 15.

The maximum stresses occur in the lateral beam and amount to 197.6 MPa (Figure 14), that is, they are lower than permissible. The maximum displacements occur in the middle part of the longitudinal beam and amount to 1.8 mm (Figure 15). Therefore, the strength of the container frame under operational loadings is ensured [17].

4 Conclusions

1. The force factors that take place in the structure of the container frame during the operational loading modes are determined. At the same time, the two schemes are considered: the effect of the vertical loading on the frame of the container when it is lifted by the upper corner fittings (I loading mode) and the effect of the longitudinal loading on the frame during the transportation by rail transport (II loading mode). It was found that the maximum value of the longitudinal force in the I mode occurs in vertical struts and equals 31.6 kN. The maximum value of the lateral force is recorded in the intermediate vertical struts and equals 19.6 kN. The maximum value of the bending moment also occurs in the intermediate vertical struts and is equal to 13.6 kN m.
To determine the longitudinal force acting on the frame of the container, mathematical modeling of its dynamic loading when placed on a flat wagon was carried out. It was established that the longitudinal acceleration acting on the container is about 20 m/s^2. In view of this, the calculation of the container frame in the II mode was carried out. The maximum value of the longitudinal force occurs in the bottom part of the frame and equals 100 kN. The maximum value of the lateral force was recorded in the longitudinal beams and amounted to 21.1 kN. The maximum bending moment occurs in the bottom part of the frame and is equal to 11.5 kNm.
2. The profile of the container frame execution was selected - a square pipe with parameters:

$H = B = 120$ mm, $S = 4$ mm, $W = 67.05$ cm^3. Here, the mass of the container frame was about 500 kg. The strength of the container frame was calculated. The calculation results showed that the maximum stresses occur in the lateral beam and amount to 197.6 MPa. The maximum displacements occur in the middle part of the longitudinal beam and amount to 1.8 mm. Therefore, the strength of the container frame under the considered operational loadings is ensured.

The conducted research could contribute to creation of recommendations and developments in the sphere of designing modern structures of vehicles of a modular type.

Acknowledgment

This publication was prepared thanks to support from the Cultural and Educational Grant Agency of the Ministry of Education of the Slovak Republic in the project KEGA 031ZU-4/2023: Development of key competencies of the graduate of the study program Vehicles and Engines; from the Slovak Research and Development Agency of the Ministry of Education, Science, Research and Sport in the project and VEGA 1/0513/22 "Investigation of the properties of railway brake components in simulated operating conditions on a flywheel brake stand; funding by the EU NextGenerationEU through the Recovery and Resilience Plan for Slovakia under the project No. 09I03-03-V01-00131; Funding by the EU NextGenerationEU through the Recovery and Resilience Plan for Slovakia under the project No. 09I03-03-V01-00129.

Conflicts of interest

The authors declare that they have no known competing financial interests or personal relationships that could have appeared to influence the work reported in this paper.

References

[1] DIZO, J., HARUSINEC, J., BLATNICKY, M. Structural analysis of a modified freight wagon bogie frame. *MATEC Web of Conferences* [online]. 2017, 134, 00010. eISSN 2261-236X. Available from: https://doi.org/10.1051/matecconf/201713400010

[2] DIZO, J., HARUSINEC, J., BLATNICKY, M. Computation of modal properties of two types of freight wagon bogie frames using the finite element method. *Manufacturing Technology* [online]. 2018, 18(2), p. 208-214. ISSN 1213-2489, eISSN 2787-9402. Available from: https://doi.org/10.21062/ujep/79.2018/a/1213-2489/MT/18/2/208

[3] SOUKUP, J., SKOSILAS, J., SKOSILASOVA, B., DIZO, J. Vertical vibration of two axle railway vehicle. *Procedia Engineering* [online]. 2017, 177, p. 25-32. ISSN 1877-7058. Available from: https://doi.org/10.1016/j.proeng.2017.02.178

[4] RZECZYCKI, A., WISNICKI, B. Strength analysis of shipping container floor with gooseneck tunnel under heavy cargo load. *Solid State Phenomena* [online]. 2016, 252, p. 81-90. ISSN 1662-9779. Available from: https://doi.org/10.4028/www.scientific.net/SSP.252.81

[5] NIKITCHENKO, A., ARTIUKH, V., SHEVCHENKO, D., PRAKASH, R. Evaluation of Interaction Between Flat Wagons and Container at Dynamic Coupling of Flat Wagons. *MATEC Web of Conferences* [online]. 2016, 7, 04008. eISSN 2261-236X. Available from: https://doi.org/10.1051/matecconf/20167304008

[6] IBRAGIMOV, N., RAKHIMOV, R., KHADZHIMUKHAMEDOVA, M. Development of a container design for the transportation of fruits and vegetables (in Russian). *Young Scientist* [online]. 2015, 21(101), p. 168 - 173. ISSN 2072-0297, eISSN 2077-8295.

[7] KHADJIMUKHAMETOVA, M. A., MERGANOV, A. M. Development of the design and conditions of operation of containers for transportation of fruit and vegetable products international. *Journal of Recent Technology and Engineering (IJRTE)* [online]. 2020, 8(5), p. 2277-3878. eISSN 2277-3878. Available from: https://doi.org/10.35940/ijrte.E4856.018520

[8] GIRIUNAS, K., SEZEN, H., DUPAIX, R. B. Evaluation, modeling, and analysis of shipping container building structures. *Engineering Structures* [online]. 2012, 43, p. 48-57. ISSN 0141-0296, eISSN 1873-7323. Available from: https://doi.org/10.1016/j.engstruct.2012.05.001

[9] VATULIA, G., LOVSKA, A., MYAMLIN, S., STANOVSKA, I., HOLOFIEIEVA, M., HOROBETS, V., NERUBATSKYI, V., KRASNOKUTSKYI, Y. Revealing the effect of structural components made of sandwich panels on loading the container transported by railroad. *Eastern-European Journal of Enterprise Technologies* [online]. 2023, 1/7(121), p. 48-56. ISSN 1729-3774, eISSN 1729-4061. Available from: https://doi.org/10.15587/1729-4061.2023.272316

[10] VATULIA, G., LOVSKA, A., KRASNOKUTSKY. Y. Research into the transverse loading of the container with sandwich-panel walls when transported by rail. *IOP Conference Series: Earth and Environmental Science* [online]. 2023, 1254, 012140. ISSN 1755-1315. Available from: https://doi.org/10.1088/1755-1315/1254/1/012140

[11] MISHUTA, D. ALGIN, V., MIKHAILOV, V. Assessment of the stress-strain state of a container body of variable volume. *Bulletin of the Belarusian-Russian University*. 2012, 4(37), p. 61-68. ISSN 2077-8481.
[12] EREMIN, V., SEMENNIKOVA, L. Study of the stress-strain state of a container body using the WinMachine automated workplace software package. *CAD and Graphics*. 2004, 7, p. 23-28. ISSN 1211-1082.
[13] TIERNAN, S., FAHY, M. Dynamic FEA modelling of ISO tank containers. *Journal of Materials Processing Technology* [online]. 2002, 124(1-2), p. 126-132. ISSN 0924-0136, eISSN 1873-4774. Available from: https://doi.org/10.1016/S0924-0136(02)00196-6
[14] DSTU 8940:2019. Steel profile pipes. Specifications. Kyiv, Ukraine: State Standard of Ukraine, 2019.
[15] BARABASH, M., SOROKA M., SURIANINOV, M. *Nonlinear structural mechanics with LIRA-SAPR*. Odessa: Ekolohiia, 2018. ISBN 978-617-7046-48-5.
[16] PANCHENKO, S., GERLICI, J., VATULIA, G., LOVSKA, A., PAVLIUCHENKOV, M., KRAVCHENKO, K. The analysis of the loading and the strength of the FLAT RACK removable module with viscoelastic bonds in the fittings. *Applied Sciences* [online]. 2023, 13(1), 79. eISSN 2076-3417. Available from: https://doi.org/10.3390/app13010079
[17] DSTU 7598:2014. Freight wagons. General requirements for calculations and design of new and modernized wagons of 1520 mm track (non-self-propelled). Kiev, Ukraine: UkrNDNTS, 2015.
[18] LOVSKAYA, A. Assessment of dynamic efforts to bodies of wagons at transportation with railway ferries. *Eastern-European Journal of Enterprise Technologies* [online]. 2014, 3(4), p. 36-41. ISSN 1729-3774, eISSN 1729-4061. Available from: https://doi.org/10.15587/1729-4061.2014.24997
[19] ZADACHYN, V., KONYUSHENKO, I. *Numerical methods: textbook* (in Ukrainian). Kharkiv, 2014. ISBN 978-966-676-547-6.
[20] SHVABYUK, V. *Resistance of materials: Textbook* (in Ukrainian). Kyiv: Znannia (Knowledge), 2016. ISBN 978-617-07-0306-4.
[21] PANCHENKO, S., GERLICI, J., VATULIA, G., LOVSKA, A., RYBIN, A., KRAVCHENKO, O. Strength assessment of an improved design of a tank container under operating conditions. *Communications - Scientific Letters of the University of Zilina* [online]. 2023, 25(3), p. B186-B193. ISSN 1335-4205, eISSN 2585-7878. Available from: https://doi.org/10.26552/com.C.2023.047
[22] PANCHENKO, S., VATULIA, G., LOVSKA, A, RAVLYUK, V., ELYAZOV, I., HUSEYNOV, I. Influence of structural solutions of an improved brake cylinder of a freight car of railway transport on its load in operation. *Eureka: Physics and Engineering* [online]. 2022, 6, p. 45-55. ISSN 2461-4254, eISSN 2461-4262. Available from: https://doi.org/10.21303/2461-4262.2022.002638

THE SERVICE LIFE PREDICTION FOR BRAKE PADS OF FREIGHT WAGONS

Sergii Panchenko[1], Juraj Gerlici[2], Alyona Lovska[2], Vasyl Ravlyuk[1,*]

[1]Ukrainian State University of Railway Transport, Kharkiv, Ukraine
[2]University of Zilina, Zilina, Slovak Republic

*E-mail of corresponding author: rvgv@ukr.net

Sergii Panchenko 0000-0002-7626-9933,
Alyona Lovska 0000-0002-8604-1764,
Juraj Gerlici 0000-0003-3928-0567,
Vasyl Ravlyuk 0000-0003-4818-9482

Resume

The analysis of the statistical values of wear of brake pads in operation, based on which a wear model was developed, is presented in this paper. This model can be used for predicting the remaining service life of brake pads according to the wagon mileage.

The distribution function of wear on the upper and lower parts of the pad was determined, which made it possible to find the main qualitative characteristics, namely, the wear intensity, the γ-percentage wear, and the average pad wear at a specified wagon mileage.

The results of the study can be factored for solving complex engineering problems of excessive wear of composite brake pads used for freight rolling stock; they could also help to extend the guaranteed overhaul period and improve the railway traffic safety.

Article info

Received 13 November 2023
Accepted 10 January 2024
Online 29 January 2024

Keywords:

transport mechanics
brake pad
analysis
model
prediction
residual service life

Available online: https://doi.org/10.26552/com.C.2024.017

ISSN 1335-4205 (print version)
ISSN 2585-7878 (online version)

1 Introduction

Nowadays, Ukrainian Railways (Ukrzaliznytsia) is suffering deterioration of the technical condition of the mechanical brake system of rail wagons, which is the key element of the train traffic safety. The analysis of the traffic safety of the rolling stock has demonstrated that the excessive wear of pads can cause many failures in operation [1]. The reason for this is an imperfect design of the brake leverage system of the bogie, which has not been modernized for a long time.

The results of the study have revealed that excessive wear of pads is caused by the design features of the brake leverage system, which decreases the braking efficiency of wagons due to a smaller contact area in the brake pad/wheel tribotechnical pair (Figure 1). Therefore, this leads to frequent repairs of freight rolling stock, additional energy costs of train traction; and less efficient technical and economic performance of railway transport enterprises.

In recent years, leading wagon manufacturers have successfully modernized elements of a typical brake leverage system, which have extended the guaranteed overhaul periods for brake pads and improved the reliability, durability and maintainability of the brake system [2-5].

2 Analysis of recent research and publications

Based on preliminary observations over wagons, conducted under the operational conditions, it was found that the dual wedge-shaped wear of pads depends on the design and state of the brake system of a wagon bogie. If the wagon mileage reaches 75,000 km, the excessively worn composite brake pads with a residual working mass of 39 % are replaced; it implies excessive operating costs, which, however, can be avoided by modernizing the brake leverage system for wagons used as railway and industrial transport means. This will extend overhaul periods and increase the wagon mileage, providing that the service life of brake pads is predicted [6].

The service life of composite brake pads with mesh and wire frame, which is now in full-scale production and used in the wagon brake system, is from 90,000 to 200,000 km, according to [7]. Based on the results of the study, the average mileage per 1 mm of the pad thickness is 3,500 km on average. However, due to

Figure 1 *Unserviceable brake pads with a large residual working body*

the use of innovative materials, special designs, and improvements in the brake leverage system, the service life of a pad can be significantly increased.

In work [8], the authors proposed an approach to the statistical study. Thus, they evaluated the force with which the brake pad presses the wheel, the hardness of the pad material, etc., when determining the brake distance depending on the speed, the track gradient, and the curve radius during the rolling stock braking. The critical slope values of the brake distance, with full-service braking of the rolling stock, were statistically established. However, the authors did not discuss the case when the contact area between the excessively worn pad and the wheel decreases, therefore, the braking efficiency of the train cannot be positively assessed.

The research described in [9] deals with development of a regression friction model of the pad and wheel of industrial transport locomotives under conditions of structural uncertainty; it was the result of a great number of input parameter variables in the models, i.e., the friction coefficient was included. It is difficult to exclude unstable solutions in such a multi-parameter model, although the author suggested his vision of the problem. However, the model did not include the main parameter - the pad wear by thickness - which restricts the use of all types of brake pads (in terms of safety) under the conditions of scheduled preventive maintenance.

Author of article [10] describes the research into the cause of harmful wedge-shaped wear of pads and the possibility to eliminate it. Such a wear can result in the premature replacement of the brake pads with residual working mass within the scheduled overhaul periods. In this study, a statistical approach was used to plan experiments during the trial operation of wagons with standard and modernized brake leverage gears, included in one train. However, the task of predicting their service life was not set.

Another approach is proposed in [11], where, on the example of excessive wear of brake pads, the authors considered the problem of uneven wear of the pad/wheel friction pairs of one wagon; their dynamic processes were described by a complex model. The work deals with cases in which the values of random parameter variables under consideration follow to the normal distribution law.

Study [12] presents the analyses of some typical block brakes, which are advisable for the rolling stock of the Chinese subway. Some of them are advantageously flexible in operation, fast responding and structurally compact. In some countries, block brakes are used in wagon bogies to provide more efficient braking and extend the service life of pads. However, the use of brake blocks in wagon bogies significantly increases the weight, air consumption for braking, time for maintenance and complexity of repair.

In work [13] the authors analyzed the thermally stressed state of the pad using SolidWorks and, based on the results, propose to improve the material of pads, which will reduce their wear intensity and increase the service life.

Study [14] highlights the results of various friction brake devices that increase the braking efficiency. The authors believe that the mechanisms, which use brake pads have a negative impact on both the track and the wheel's rolling surface due to high temperatures in the pad/wheel friction zone, therefore, the disc brakes are preferable.

Thus, disc brakes are in the focus of many specialists; they calculate the thermally stressed state of the brake elements, observe their operation, and thoroughly investigate the temperature modes for some elements of the rolling stock brake system [15-16]. During the braking, the thermal energy develops in the contact zone of the brake pad/wheel tribotechnical pair. This energy gets dissipated by forced convection, conduction and radiation from the exposed surfaces of the brake. Some authors note that the overheating of tribotechnical pairs can cause failure in the brake gears in operation, which may threaten the train traffic safety [17-18]. From this

Table 1 *Numerical characteristics of the wear measured on the composite brake pads X_1 and X_2*

Pad wear measured	Estimated values of characteristics			
	$\overline{x}$	s^2	As^2	Es
Top X_1	31.69	238.38	0.002	2.01
Bottom X_2	31.86	237.51	0.001	2.01

point of view, considerable theoretical work is being done to study the temperature characteristics of composite brake pads used in wagons under different operating conditions at various speeds [19-20].

The above analysis of literature sources has demonstrated that the problems of excessive wear of pads and ways to increase their service life under the normal operating conditions for brake leverage gears in wagons are yet to be studied. Therefore, it is advisable to introduce measures aimed at improving the performance of brake leverage systems with modernized elements; it reduce the operating costs and ensure the train traffic safety, as well.

The purpose of the study is to predict the service life of brake pads used in freight wagons.

To achieve this purpose, the following tasks have been assigned:

- to formulate a wear model of the brake pad on the basis of the statistical values obtained, so that to predict the remaining working body depending on the wagon mileage;
- to study the wear distribution function for different parts of the pad and, based on it, to determine the wear characteristics for a specified wagon mileage; and
- to research into the wear characteristics of the pad, according to the mileage of a wagon with modernized brake leverage systems, the pads of which are worn-out.

3 Creating the model to predict the brake pads wear and the wear distribution

The information collected in the course of the research on the change in the geometric parameters of brake pads depending on the wagon mileage is subject to careful processing. The thickness of the brake pads was checked during the inspection of freight wagons in the arrival park of the sorting station. With help of a measuring tool, the thickness of the pads in the upper and lower parts, as well as their wear, were determined. The results of the measurements were recorded in the developed report for controlling the geometric parameters of the pads, modernized brake lever gears of the bogies. In this regard, the methods of mathematical statistics were used to analyze the brake systems of the freight wagons. Therefore, creating the favorable conditions for the further serial introduction of updated brake lever transmission designs into production at wagon-building plants, or their modernization at wagon repair enterprises of the joint-stock company "Ukrzaliznytsia".

The statistical estimation method was used to predict the wear of pads of the 2TR-11 type used in wagons with modernized gears. The chemical composition of the 2TR-11 type composite pad contains: 20 % of rubber, 47.5 % of baride, 15 % of carbon black, 2.5 % of vulcanizing composition, 15 % of other substances. The wear values on the top and bottom of the pad in operation at the wagon mileages from 0 to 197,800 km were found; the number of tests that formed the sample size was n =106. The optimal number of intervals is adopted from the studies highlighted in the work [21]. With a sample size of n =106, the number l = 5 is taken. This meets the requirements for modern statistical research [22]. Such an approach should be considered, if the results of using the Sturges formula are taken into account. In this case, it is $l = 1 + 3.3221gn \approx 5$. That is, the samples of working hours per service life should be divided into 5 intervals, if the total number of observations exceeds 100 units.

In order To determine the wear on the top X_1 and bottom X_2 of the brake pad, the numerical characteristics were found; they included average value $\overline{x}$, corrected variance s^2, squared asymmetry coefficient As^2, and excess coefficient Es - for the random variables X_1 and X_2. The results are shown in Table 1.

A model of wear of the geometric dimensions of brake pads and estimation of their parameters, based on the results of operation of modernized devices for parallel retraction of brake shoes, has been formulated. The model of wear of the geometric dimensions of wagon brake pads was applied as a statistical function. In this case, the density function $f(x)$, for random wear values of x pads, was determined as follows [6, 23-25]:

$$f(x) = \begin{cases} 0, & x \notin (b,c), \\ \dfrac{1+k}{c-b}\left[1-\left(\dfrac{x-a}{b-a}\right)^{\frac{1}{k}}\right], & x \in [b,a], \\ \dfrac{1+k}{c-b}\left[1-\left(\dfrac{x-a}{c-a}\right)^{\frac{1}{k}}\right], & x \in (a,c], \end{cases} \quad (1)$$

where a is the modal value;
b, c are the lower and upper pad wear limits, respectively;
k is the parameter of the pad wear shape.

Equation (1) is determined with $k > 0$ and $k < -1$, where $b < a < c$ and $b \geq 0$. For Equation (1), the distribution function has the form [23-24]:

$$F(x)=\begin{cases}0, & x\le b\\ \left\{x-b+k(x-a)\times\left[1-\left(\frac{x-a}{b-a}\right)^{\frac{1}{k}}\right]\right\}/(c-b), & b<x\le a\\ \left\{x-b+k(x-a)\times\left[1-\left(\frac{x-a}{c-a}\right)^{\frac{1}{k}}\right]\right\}/(c-b), & a<x\le c\\ 1, & x>c.\end{cases} \quad (2)$$

Here, the lower wear limit is b = 0, and the upper wear limit is c = 65 mm. With these parameters, the mathematical expectation is as follows:

$$M(X)=\frac{(55+55k+165kq+55q)}{2(2k+1)(1+q)}. \quad (3)$$

where q is dimensionless parameter.

The value of parameter q is determined if q of the expression is determined $q = 65q/(1+q)$.

The dispersion is determined using the formula [20, 22]:

$$D(X)=\frac{(c-b)^2(k+1)\left(\begin{matrix}2k^2q+7k^2+7k^2q^2+\\+(4k+1)(q+1)^2\end{matrix}\right)}{12(2k+1)^2(1+q)^2(3k+1)}. \quad (4)$$

For this model, the squared asymmetry is a function of the two variables, and has the following form [6, 21]: $\beta_1^2=\mu_3^2/\mu_2^3$, where μ_k is the central moment of the k-th order,

$$\begin{aligned}\beta_1^2=&\,108(4k^2q^2-4k^2+4k^2q^3-4k^2q^3-4k^2q+\\&+3kq^3+7kq^2-3k-7kq-1-q+q^2+q^3)^2\times\\&\times k^4(3k+1)/((k+1)(2k^2q+7k^2+7k^2q^2+\\&+4k+8kq+4kq^2+1+2q+q^2)^3(4k+1)^2).\end{aligned} \quad (5)$$

The excess is determined by the expression $\beta_2=\mu_4/\mu_2^2$ [24- 25]; it is equal to:

$$\begin{aligned}\beta_2=&\,9(3k+1)(1+90kq^2+60kq+1184k^3q^3+\\&+368k^2q+1011k^5+572k^6+813k^44q^3+366k^3+\\&+6q^2+102k^2+q^4+532k^2q^2+1184k^3q+\\&+1636k^3q^2+1932k^4q+1932k^4q^3+2958k^4q^2+\\&+102k^2q^4+1684k^5q^4+60kq^3+368k^2q^3+\\&+1684k^5q^3+2546k^5q^2+872k^6q^2+4q+15k+\\&+15kq^4)/(5(2k^2q+7k^2+7k^2q^2+4k+8kq+\\&+4kq^2+1+2q+q^2)^5(4k+1)(5k+1)(k+1)).\end{aligned} \quad (6)$$

To estimate the dimensionless parameters k and q, the method of moments was used [24-25]; it included the equating of the theoretical characteristics in Equations (5), (6) and empirical numerical characteristics (Table 1), the coefficient of squared asymmetry and a kurtosis coefficient.

The solution of this system of equations produced the following parameter values of Equation (1): a) for the top k = 0.32, q = 0.78, a = 28.33; b) for the bottom k = 0.32, q = 0.82, a = 29,2.

The parameter values obtained were used to construct the density distribution graphs for the random pad wear values (Figures 2 and 3) and the pad wear distribution function (Figures 4 and 5).

Consider the sensitive characteristics of the distribution law of a random variable and their operational estimates of the pad wear. Since the correlation is not the adequacy of a probable model, consider the functional characteristics of random variables that are sensitive to distribution models. Their form was established according to experimental data and is one of the essential grounds for proximity, which is close to adequacy of the formulated model. One of these characteristics in the reliability theory is the failure rate, hereinafter called the λ-characteristics. The theoretical λ-characteristics is widely used in practice; it is determined using the formula

$$\lambda(x)=\frac{f(x)}{1-F(x)}. \quad (7)$$

The formula looks like:

$$\lambda(x_{(i)})=\frac{n(x_{(i)})}{\left[n-\sum_{j=1}^{i-1}n(x_{(i)})\right](x_{(i)}-x_{(i-1)})}, \quad (8)$$

where $n(x_{(j)})$ - the frequency of the pad thickness x occurrence in the interval $(x_{(i)}, x_{(i-1)})$.

Based on the measurements of the wear rate for 106 composite brake pads of wagons with modernized devices, the empirical and theoretical λ-characteristics with obtained distribution parameters in Equation (1), was constructed (Figure 6). The points of empirical λ-characteristics practically coincide with the points of theoretical λ-characteristics, which indicates the possibility of using Equation (1) for a random size value of the top and bottom wear of composite brake pads of wagons.

Figure 6 shows the λ-characteristics and the empirical estimates of wear on the top and bottom of the brake pads of wagons [6].

Figure 6, a and b, demonstrates that this characteristics has a virtually linear increasing dependency in the range from 0 to 45 mm. Since the empirical estimates of the λ-characteristics are quite close to the theoretical curve of the λ-characteristics, the pad wear model in Equation (1) can be used for research in this area.

The estimate of the μ-characteristics of the average residual service life [6, 23-24, 26] has significantly lower random fluctuations than the estimate of the μ-characteristics calculated using the same parameters.

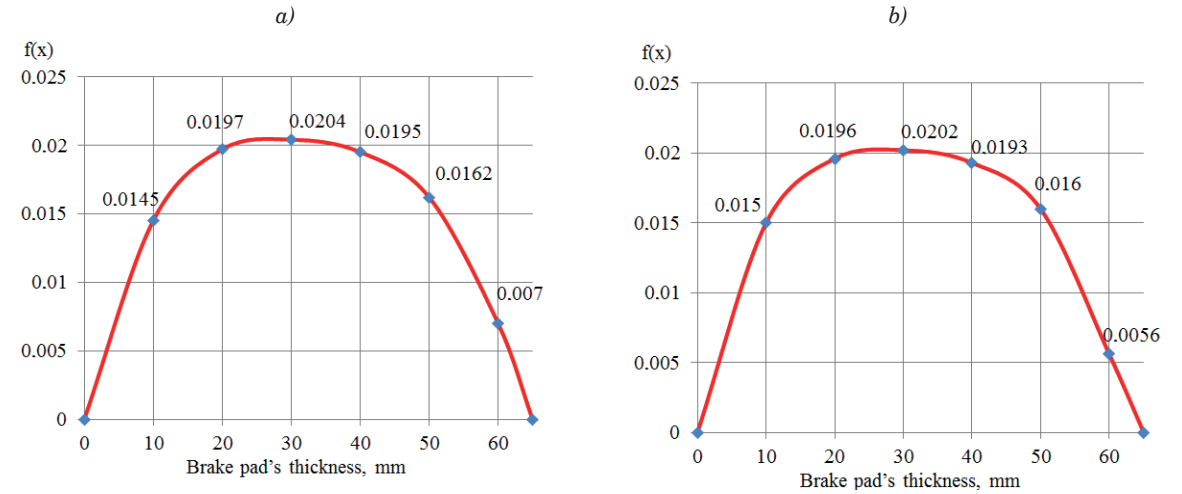

Figure 2 *The theoretical curve of the wear distribution density on top (a) and bottom (b) of the pad with parameter estimates obtained by the method of moments*

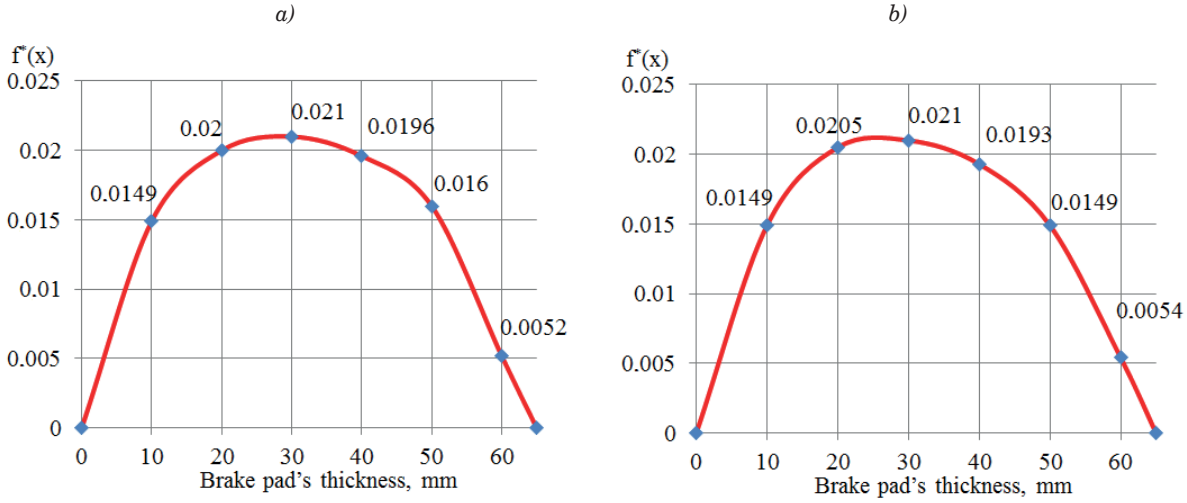

Figure 3 *The empirical curve of wear distribution density on top (a) and bottom (b) of the pad in operation*

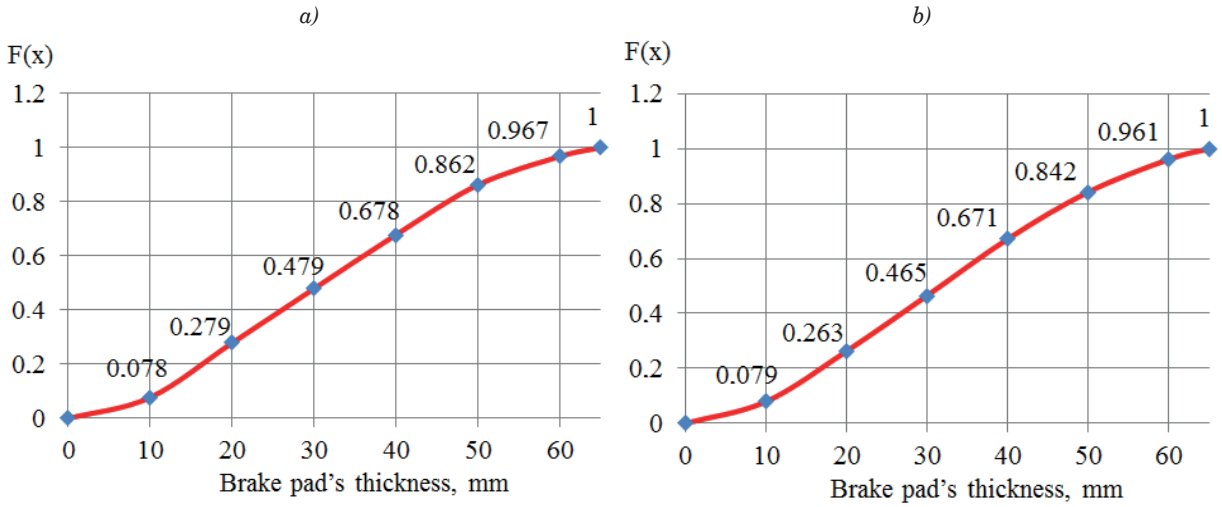

Figure 4 *The theoretical curve of the wear distribution function on top (a) and bottom (b) of the pad with parameter estimates obtained by the method of moments*

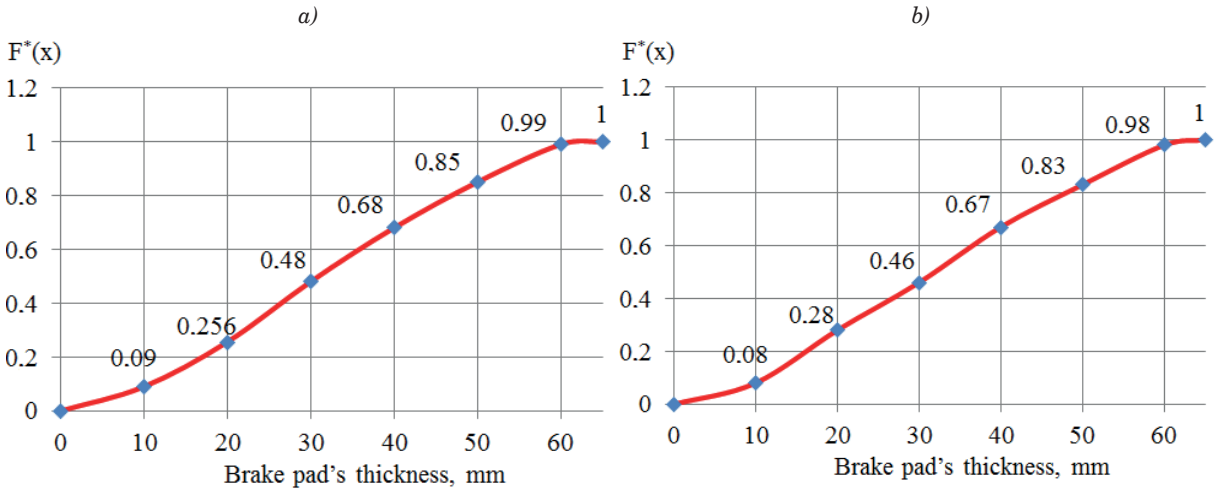

Figure 5 *The empirical curve of the wear distribution function on top (a) and bottom (b) of the pad in operation*

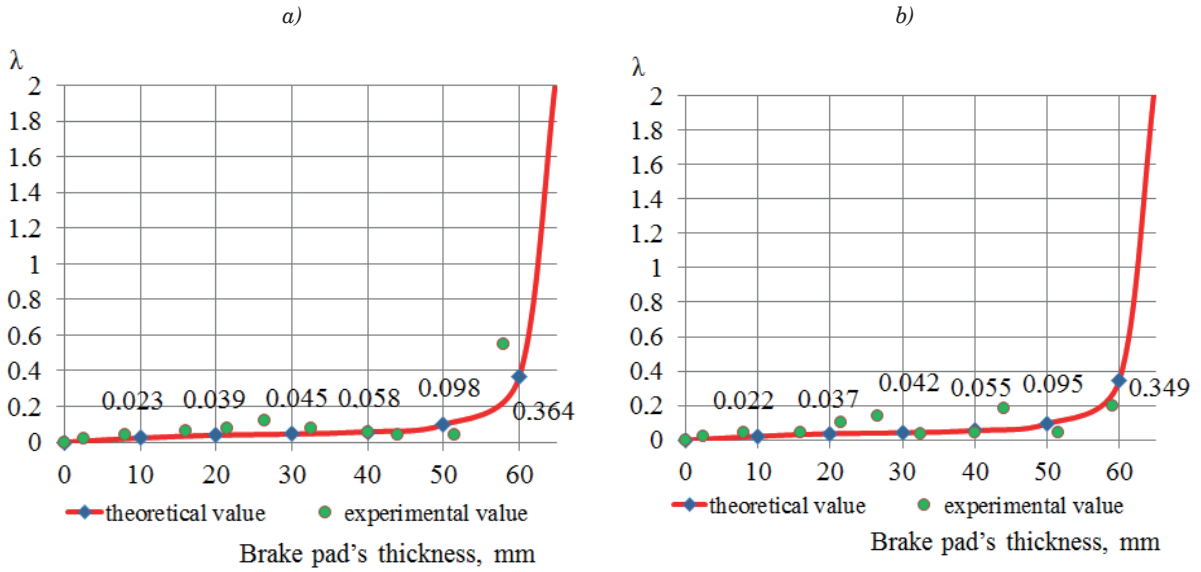

Figure 6 *The graphs of the λ- characteristics of the wear on top (a) and bottom (b) of the composite brake pad and its empirical estimates*

This can be explained by the better statistical quality of the sum estimates compared to the proportion estimates. Moreover, the estimate of the μ-characteristics is sufficiently sensitive to the right-side distribution, which is required for studying the models bounded from the right. It is this characteristics, which will be considered later. Suppose that n tests are conducted, then, at specified values of x, $n \cdot P(X \geq x)$, thus, taking it into account, $n \cdot P(X \geq x + \tau)$. The ratio of these values gives the conditional probability of a value greater than τ, if all these x values have already been present. At the same time, the ordered values are considered:

$$P(X \geq \tau / x) = \frac{P(X \geq x + \tau)}{P(X \geq x)}. \tag{9}$$

The integration of Equation (9) gives $\mu(x)$:

$$\mu(x) = \int_0^\infty \frac{1 - F(x + \tau)}{1 - F(x)} d\tau = \\ = \frac{1}{1 - F(x)} \int_x^\infty (1 - F(z)) dz. \tag{10}$$

To find the empirical estimate $\tilde{\mu}(x)$, it is sufficient to arrange all the values observed in an ascending order, that is, to compile ordinal statistics $x_{(1)}, \ldots, x_{(n)}$. Then, the values are calculated by the expression

$\tau_0^{(j)}(x_i) = \tau_j - x_i$ for those τ_j that are not less than x_i.

If the number of such values is l, then (with a small offset)

$$\mu(x) \approx \overline{\tau}(x_i) = \frac{1}{l} \sum_{i=1}^{l} \tau_0^{(ji)}(x_i). \tag{11}$$

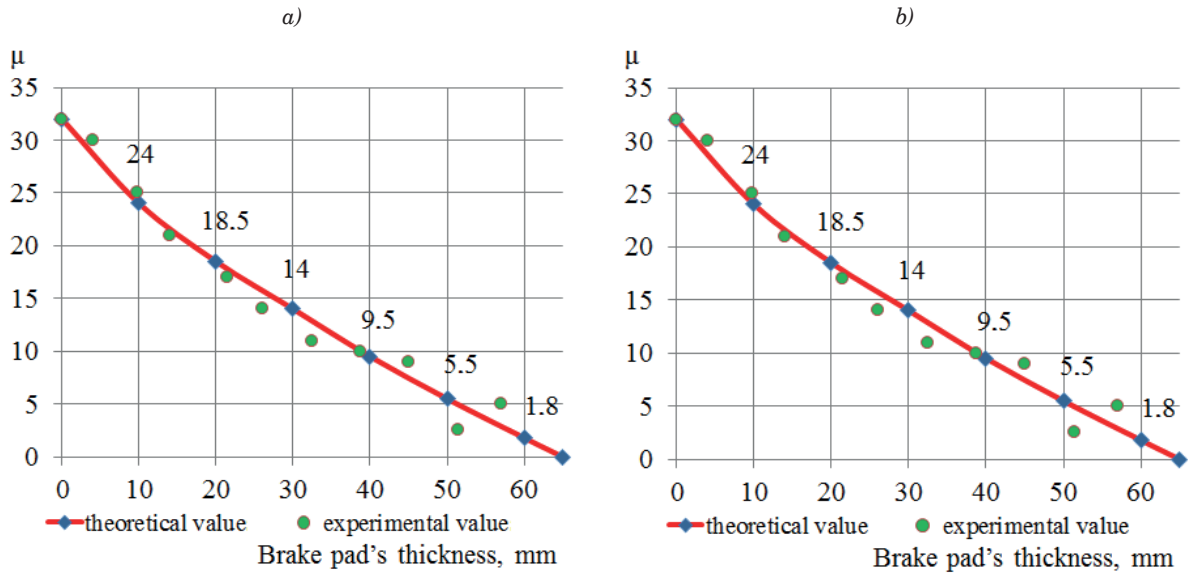

Figure 7 *The graphs of the μ-characteristics of the service life on top (a) and bottom (b) of the composite brake pad and its empirical estimates*

The estimate $\mu(x)$ can be found using the empirical estimates of the distribution function $\tilde{F}(x)$, where $\tilde{F}(x) = \frac{1}{n}\sum_{i=1}^{l} f_i$, and

$$\mu(\tilde{x}) = \frac{1}{\tilde{F}(x)}\sum_{j=1}^{l}\left(1 - \frac{\tilde{F}(x_{j+1}) + \tilde{F}(x_j)}{2}\right)\Delta x_j, \qquad (12)$$

where $x_{j+1} - x_j = \Delta x_j$.

By using Equation (10), the μ-characteristics for the pad service life on the top and bottom can be found using the calculated parameter values of Equation (1) (Figure 7, a and b) and its empirical estimates.

Figure 7 indicates that for the wear values of the wagon brake pad the empirical and theoretical μ-characteristics practically coincide and change similarly, which indicates the proximity of this model to the true model.

The service life characteristics at the test points were found using the mileage of the wagon with modernized brake leverage gears. The study has shown that the relationship between the wear and mileage is close to linear. For the first approximation, take this dependence as $y = \eta(x)$, since for $x = 0$, y should be equal to zero. Using the least squares method, the slope factor η was found. For the upper wear it was $\eta_1 = 5.11$, and for lower wear it was $\eta_2 = 5.28$. By using the dependence and wear distribution in Equation (1), the distribution density of the random mileage y was determined as:

$$f(y) = \begin{cases} 0, & y \notin (\eta b, \eta c), \\ \frac{1+k}{(c-b)\eta}\left[1 - \left(\frac{y/\eta - a}{b-a}\right)^{\frac{1}{k}}\right], & y \in [\eta b, \eta a], \\ \frac{1+k}{(c-b)\eta}\left[1 - \left(\frac{y/\eta - a}{c-a}\right)^{\frac{1}{k}}\right], & y \in (\eta a, \eta c], \end{cases} \qquad (13)$$

For this model, the distribution function has the form:

$$F(y) = \begin{cases} \dfrac{-\eta(b+ka) + y(1+k) + nk(a-b)\left(\frac{y-a\eta}{\eta(a-b)}\right)^{\frac{1+k}{k}}}{\eta(c-b)}, & y \in [\eta b, \eta a), \\ \dfrac{-\eta(b+ka) + y(1+k) + nk(c-a)\left(\frac{y-a\eta}{\eta(c-a)}\right)^{\frac{1+k}{k}}}{\eta(c-b)}, & y \in [\eta a, \eta c], \end{cases} \qquad (14)$$

the next step is to find the empirical and theoretical estimates of the wear intensity and the average residual service life of brake pads taking into account the wagon mileage.

Figure 8, a and b shows the graphs of empirical and theoretical estimates of the wear intensity of brake pads with modernized brake leverage gears, taking into account the wagon mileage. Figure 9, a and b shows the graphs of the empirical and theoretical estimates of the average service life of the brake pad, taking into account the wagon mileage.

By analysing Figures 8 and 9, it can be concluded that the pad wear model, proposed in Equation (1) and obtained Equation (13), can be used to the solve major problems associated with wear of any wagon brake pad used for the rolling stock.

The designed wear model of the wagon pad and the results obtained make it possible to solve the necessary practical problems. The use of service life characteristics can help to predict the main efficiency characteristics of wagons.

The calculations have showed that the threshold of wagon mileage before the composite brake pad gets worn-out on the top is 331,880 km, and on the bottom is

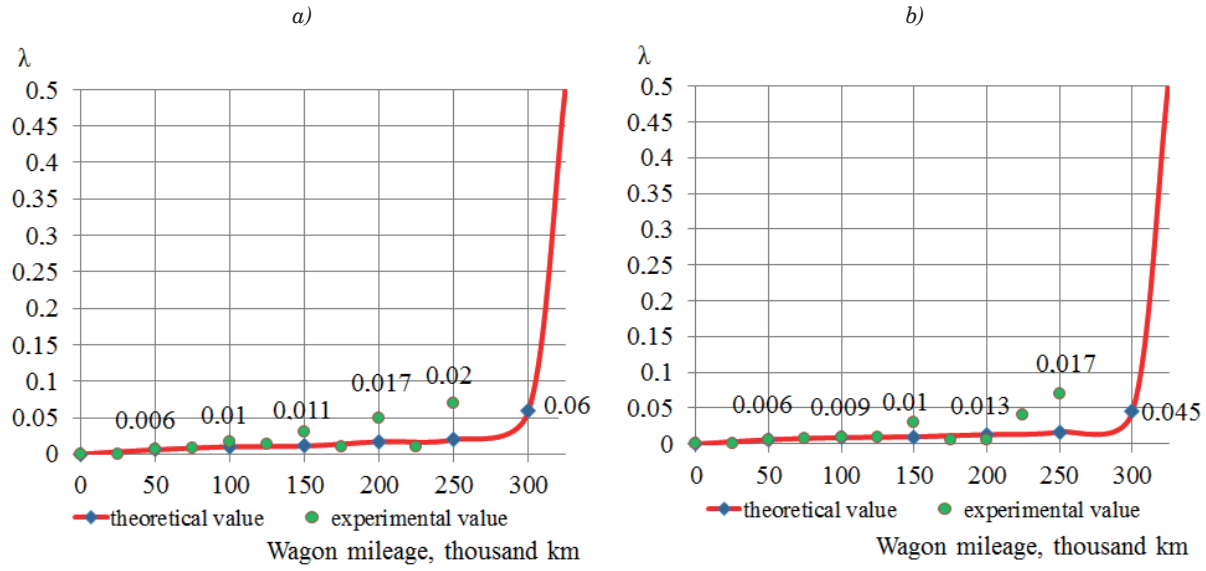

Figure 8 *The graphs of empirical and theoretical estimates of the wear intensity of the pad on top (a) and bottom (b), taking into account the wagon mileage*

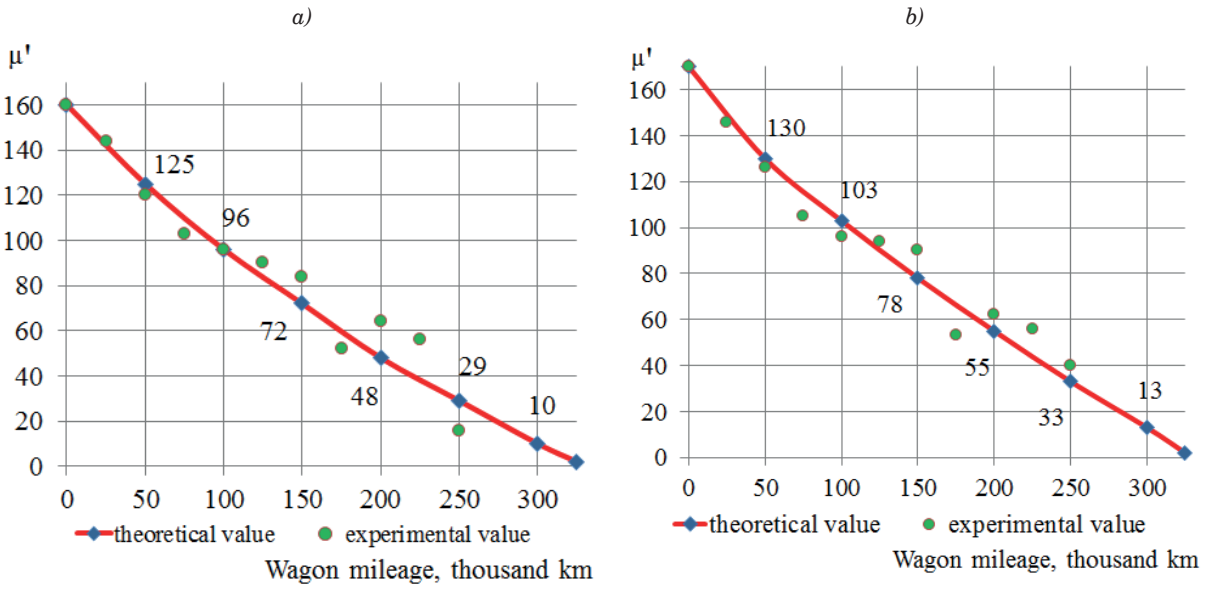

Figure 9 *The graphs of empirical and theoretical estimates of the average residual service life of the pad on top (a) and bottom (b), taking into account the wagon mileage*

343,040 km.

The values of the wear intensity of the composite brake pad of the wagon with a mileage of 250,000 km will account for λ = 0.02 on the top and λ = 0.017 on the bottom.

Given the distribution function $F(x) = P(X < x)$ and estimates of its parameters, it is possible to determine such a characteristics as the probability of the pad wear at point $x_0 - F(x_0)$, and the probability that the pad does not wear at this point $Q(x_0) = 1 - F(x_0)$. Therefore, the probability of wear on the top of the brake pads will be $F(20)$ = 0.27; $F(30)$ = 0.47 and $F(40)$ = 0.67, and on the bottom of the pads is $F(20)$ = 0.26; $F(30)$ = 0.47 and $F(40)$ = 0.67.

Another essential characteristic is the γ-percentage service life, which is determined by the expression $F(x_\gamma) = \gamma/100\%$. For example, for the upper part of the composite brake pad, if $\gamma = 95\%$, the wear is $x_\gamma = 56.79$, and if $\gamma = 90\%$, the wear is $x_\gamma = 52.93$. For the bottom part of the brake pad, if $\gamma = 95\%$, then $x_\gamma = 56.85$, and if $\gamma = 90\%$, then $x_\gamma = 53.02$.

An approximating dependence between the wear and mileage of the wagon with modernized brake leverage gears has been determined, the dependencies found take into account that the pads are worn-out.

It is determined that the average residual service

life of the wagon composite brake pad with a thickness of 40 mm on the top is 9.51 mm, and on the bottom is 9.53 mm. It should be noted that if the wagon mileage is 200,000 km, the average residual service life using the slope factor on the top of the composite brake pad will be $\mu' = 50.39$ mm, and on the bottom - $\mu' = 53.13$ mm.

4 Conclusions

A model of the brake pad wear to predict the remaining service life depending on the wagon mileage was designed using the statistical values obtained. This will make it possible to accurately assess such important qualitative characteristics as the service life threshold, which can be used to predict the performance of brake pads and assess the efficiency of brake leverage gears of wagon bogies.

The wear distribution function for the pad parts has been investigated; it can be used to determine the qualitative wear characteristics (probability of pad wear-out at a specified wear; γ-percentage service life of the pad; wear intensity and average residual service life) for a specified wagon mileage. This will help to solve the practical problems for different parts of the brake pad given a known wagon mileage. The service life characteristics will help to predict the major efficiency characteristics of the wagon. The calculations have demonstrated that the wear intensity of the wagon composite brake pad at a wagon mileage of 250,000 km, on the top is λ = 0.02 and on the bottom is λ = 0.017.

An approximating dependence of the wear and mileage for the wagon with modernized brake leverage gears has been determined. It is found that the average residual resource of the wagon composite brake pad with a thickness of 40 mm is 9.51 mm on the top and 9.53 mm on the bottom.

The results obtained can be used for solving engineering problems related to excessive wear of composite brake pads used for freight rolling stock. They can be used to extend the guaranteed overhaul periods and improve the railway traffic safety, as well.

Acknowledgment

This publication was issued thanks to support from the Cultural and Educational Grant Agency of the Ministry of Education of the Slovak Republic in the project KEGA 031ZU-4/2023 “Development of key competencies of the graduate of the study program Vehicles and Engines”; and support by the Slovak Research and Development Agency of the Ministry of Education, Science, Research and Sport of the Slovak Republic in Educational Grant Agency of the Ministry of Education of the Slovak Republic in the project and VEGA 1/0513/22 “Investigation of the properties of railway brake components in simulated operating conditions on a flywheel brake stand, as well as to funding by the EU NextGenerationEU through the Recovery and Resilience Plan for Slovakia under the project No. 09I03-03-V01-00131.

Conflicts of interest

The authors declare that they have no known competing financial interests or personal relationships that could have appeared to influence the work reported in this paper.

References

[1] Analysis of the state of traffic safety in the structure of JSC “Ukrzaliznytsia” in 2019. Joint-stock company “Ukrainian railway”, Department of traffic safety, 2019.

[2] PANCHENKO, S., GERLICI, J., VATULIA, G., LOVSKA, A., PAVLIUCHENKOV, M., KRAVCHENKO, K. The analysis of the loading and the strength of the FLAT RACK removable module with viscoelastic bonds in the fittings. *Applied Sciences* [online]. 2023, **13**(1), 79. eISSN 2076-3417. Available from: https://doi.org/10.3390/app13010079

[3] LOVSKAYA, A. Assessment of dynamic efforts to bodies of wagons at transportation with railway ferries. *Eastern-European Journal of Enterprise Technologies* [online]. 2014, **3**(4), p. 36-41. ISSN 1729-3774, eISSN 1729-4061. Available from: https://doi.org/10.15587/1729-4061.2014.24997

[4] DIZO, J., HARUSINEC, J., BLATNICKY, M. Structural analysis of a modified freight wagon bogie frame. *MATEC Web of Conferences* [online]. 2017, **134**, 00010. eISSN 2261-236X. Available from: https://doi.org/10.1051/matecconf/201713400010

[5] DIZO, J., BLATNICKY, M. Investigation of ride properties of a three-wheeled electric vehicle in terms of driving safety. *Transportation Research Procedures* [online]. 2019, **40**, p. 663-670. ISSN 2352-1465. Available from: https://doi.org/10.1016/j.trpro.2019.07.094

[6] RAVLYUK, V. G., RAVLYUK, M. G., KYRYCHENKO, I. K., LAMNAUER, N. Y, MELNYCHUK, A. K. Probabilistic statistical model of wear of brake pads of freight cars. *Science and Progress of Transport. Bulletin of the Dnipropetrovsk National University of Railway Transport named after Academician V. Lazaryan* [online]. 2020, **5**(89), p. 116-133. ISSN 2307-3489, eISSN 2307-6666. Available from: https://doi.org/10.15802/stp2020/217633

[7] VORONCHIKHIN, A. I., NALEV, I. A., BYCHKOV, V. N., NAJSHEV, A. A., VUKOLOV, L. A., SIMONOVA, T. S. Railway vehicle brake shoe (versions). RU 2386561 C2. 2008.
[8] ZHAROV, I. A., MAKAS, A. A. Methods for statistical processing of braking distance measurement results when assessing the effectiveness of rolling stock brakes. *VNIIZHT Bulletin*. 2009, **5**, p. 29-33. ISSN 2223-9731, eISSN 2713-2560.
[9] KOPTOVETS, A. N. Identification of the state of the brake of mine locomotives under conditions of structural uncertainty. *Geotechnical Mechanics: Interdepartmental Collection of Scientific Papers.* 2014, **119**, p. 241-246. ISSN 1607-4556, eISSN 2309-6004.
[10] RAVLYUK, V. G. Study of the features of dual pad wear in the brake system of freight cars. *Science and Progress of Transport. Bulletin of the Dnipropetrovsk National University of Railway Transport named after Academician V. Lazaryan* [online]. 2019, **2**(80), p. 111-126. ISSN 2307-3489, eISSN 2307-6666. Available from: https://doi.org/10.15802/stp2019/166114
[11] KOROPETS, P. A., CHERNIKOV, V. D., KOSTYUKEVICH A. I. On uneven wear of moving friction pairs. *Bulletin of SNU named after Dalya.* 2010, **5**(147), p. 41-45. ISSN 1998-7927.
[12] ZHANG, Y., ZHANG, M. The application status of unit brakes on metro vehicles in China. *IOSR Journal of Mechanical and Civil Engineering* [online]. 2018, **3**(15), p. 17-23. ISSN 2320-334X, eISSN 2278-1684. Available from: https://doi.org: 10.9790/1684-1503031723
[13] CHAUBEY, A. O., RAUT, A. A. Failure analysis of brake shoe in Indian railway wagon. *IPASJ International Journal of Mechanical Engineering.* 2015, **3**, p. 37-41. ISSN 2321-6441.
[14] SHARMA, R. C., DHINGRA, M., PATHAK, R. K. Braking systems in railway vehicles. *International Journal of Engineering Research and Technology*. 2015, **4**, p. 206-211. ISSN 2278-0181, eISSN 2278-0181.
[15] GUPTA, V., SAINI, K., GARG, A. K., KRISHAN, G., PARKASH, O. Comparative analysis of disc brake model for different materials investigated under tragic situations. *Asian Review of Mechanical Engineering* [online]. 2016, **5**(1), p. 18-23. ISSN 2249-6289. Available from: https://doi.org/10.51983/arme-2016.5.1.2409
[16] SARIP, S. Design development of lightweight disc brake for regenerative braking - finite element analysis. *International Journal of Applied Physics and Mathematics* [online]. 2013, **3**(1), p. 52-58. eISSN 2010-362X. Available from: https://doi.org/10.7763/IJAPM.2013.V3.173
[17] DAY, A. J. A finite element approach to drum brake analysis. *Proceedings of the Institution of Mechanical Engineers.* 1979, **193**, p. 401-406. ISSN ISSN 0954-4062.
[18] DAY, A. J. Drum brake interface pressure distributions. *Proceedings of the Institution of Mechanical Engineers, Part D: Journal of Automobile Engineering*. 1991, **205**, p. 127-136. ISSN 0954-4070, eISSN 2041-2991.
[19] PANCHENKO, S., GERLICI, J., VATULIA, G., LOVSKA, A., RAVLYUK, V., HARUSINEC, J. Studying the load of composite brake pads under high-temperature impact from the rolling surface of wheels. *EUREKA: Physics and Engineering* [online]. 2023, **4**, p. 155-167. ISSN 2461-4254, eISSN 2461-4262. Available from: https://doi.org/10.21303/2461-4262.2023.002994
[20] PANCHENKO, S. V., VATULIA, G. L., LOVSKA, A. O., RAVLYUK, V. G. Determination of the thermal stress state for the composite brake pad of a wagon at operational loads. *IOP Conference Series: Earth and Environmental Science* [online]. 2023, **1254**, 012141. ISSN 1755-1315. Available from: https://doi.org/10.1088/1755-1315/1254/1/012141
[21] LAMNAUER, N., KUPRIYANOV, A., SKORKIN, O., KONDRATYUK, A. Probabilistic-statistical model of durabilityof parts under cyclic loading. In: *Advances in Design, Simulation and Manufacturing III. DSMIE 2020. Lecture Notes in Mechanical Engineering. Advances in Design, Simulation and Manufacturing* [online]. IVANOV, V., TROJANOWSKA, J., PAVLENKO, I., ZAJAC, J., PERAKOVIC, D. (Eds.). Cham: Springer, 2020. ISBN 978-3-030-50793-0, eISBN 978-3-030-50794-7, p 285-294. Available from: https://doi.org/10.1007/978-3-030-50794-7_28
[22] RAVLYUK, V., ELYAZOV, I., AFANASENKO, I., RAVLIUK, M. Determination of forces in the elements of the brake rigging of bogies of freight cars. *E3S Web of Conferences* [online]. 2020. **166**, p. 1-7. eISSN 2267-1242. Available from: https://doi.org/10.1051/e3sconf/202016607003
[23] BIDYUK, P. I., TKACH, B. P., HARRINGTON, T. *Mathematical statistics*. Kyiv: Personal Publishing House, 2018. ISBN 978-617-02-0234-5.
[24] SLYUSARCHUK, Y. M., KHROMYAK, Y. Y., JAVALA, L. L., TSYMBAL, V. M. *Probability theory, mathematical statistics and probabilistic processes*. Lviv: Lviv Polytechnic Publishing House, 2015. ISBN 978-617-607-775-6.
[25] SARMA, K. V. S., VARDHAN, R. V. *Multivariate statistics made simple. a practical approach* [online]. New York: Chapman and Hall/CRC, 2018. eISBN 9780429465185. Available from: https://doi.org/10.1201/9780429465185
[26] DONCHENKO, V. S., SIDOROV, M. V.-S., SHARAPOV, M. M. *Probability theory and mathematical statistics*. Kyiv: Alma mater "Academy", 2009. ISBN 978-966-580-297-6.

COMPARISON OF THE MOLDING PARAMETERS EFFECTS ON METAL INJECTION MOLDED SPECIMENS IN THE REAL EXPERIMENTAL AND SIMULATION ENVIRONMENTS

György Ledniczky[1,2,*], Zoltán Weltsch[2]

[1]Department of Innovative Vehicles and Materials, GAMF Faculty of Engineering and Computer Science, John von Neumann University, Kecskemet, Hungary
[2]Department of Road and Rail Vehicles, Szechenyi Istvan University, Gyor, Hungary

*E-mail of corresponding author: ledniczky.gyorgy@nje.hu

György Ledniczky 0009-0001-0949-572X, Zoltán Weltsch 0000-0002-6366-8281

Resume
This article presents a technology that is not widely known. Previous research has investigated the effect of metal injection molding parameters on product shrinkage. The technology is mostly limited by the variations caused by deformation, so it is of paramount importance to focus on shrinkage. Consequently, within this study the injection molding simulations with 17-4PH type material was performed and its results were compared to the previously determined curve characters. The results obtained allow conclusions to be drawn regarding the accuracy of the simulation. Changing the parameters of the injection molding process can significantly affect the shrinkage factor. Changes in mold temperature, melt temperature and holding pressure affect the product dimensions. These parameters are also modified in the simulation setup and compared to the previous real measurements.

Article info
Received 13 November 2023
Accepted 9 January 2024
Online 8 February 2024

Keywords:
metal injection molding
simulation
molding

Available online: https://doi.org/10.26552/com.C.2024.018

ISSN 1335-4205 (print version)
ISSN 2585-7878 (online version)

1 Introduction

Metal Injection Molding (MIM) is a very rapidly developing technology, which can be best compared to a combination of powder metallurgy and plastic injection molding. In recent years, it has spread to a growing number of fields, with applications in a wide variety of areas outside the defense, healthcare and automotive industries. Based on the idea of plastic injection molding, metal powder particles are embedded in a binder and the resulting pellets are pressed into a durable mold by an injection molding machine [1-6]. The resulting granules are commonly called feedstock.

The product that falls out of the mold is the so-called green product. The product in this state is a semi-finished preform, with further steps to achieve metallic properties. So, the next step is to reduce the resulting product in a binder and form an open pore structure, which is true for the entire cross section of the product. In the raw material mixture, it is expected that the individual powder particles, which must be surrounded by a very thin film of binder, are in close contact with each other. There are several types of binder removal, depending on the type of binder system. These can be solvent-based, catalytic, water-based or supercritical binder systems. The bottom line is that the binder must work in such a way that the product is porous, but still has enough binder to hold the particles together.

The binder-reduced product is called the brown product. The product is the most fragile in this state, so it is not recommended to move the product at this stage. In the sintering phase, the product is heated in a high temperature furnace at temperatures below the melting point [7-10]. The process is shown in Figure 1.

Most researchers investigated the influence of the metal powder properties on technology, the rheological properties of the binder and the effect of technology on shrinkage [11-14].

Some researchers analyzed the geometrical effect of the finished workpiece and the limiting value of solvent binder removal [15-17]. These studies contributed greatly to a better understanding of this less known

technology and to a better exploitation of its potential, but beyond that, little attention is paid to preliminary parameterization or modelling.

In the MIM, it is difficult to gain sufficient knowledge for optimal process development from experiments alone. Therefore, we investigate the applicable software to the process in addition to experimental research at Neumann János University, Department of Innovative Vehicles and Materials. A range of necessary equipment, including a computer-controlled injection molding machine, a decomposition furnace and a high-temperature sintering furnace, are organised in an easily adaptable way with data acquisition systems for different physical quantities.

Through their experiments, Barriere et al. have developed a combined application of modelling and numerical simulations to MIM to ensure that parts are free from defects and have the required mechanical properties. Modelling of the injection stage, based on the two-phase flow composition of the powder-binder mixture, has enabled an access to the powder deposition during the injection and an understanding of injection defects [18].

Results from authors' previous research showed that the shrinkage properties of parts manufactured with MIM do not behave like plastics, so the simulations were operformed to investigate its applicability for the characterization of deformations [19-20].

We have started to produce a green product using additive manufacturing linked to the technology presented earlier and are already working on chip testing of sintered test pieces based on previous studies. [21-22].

2 Material

The selected material is martensitic stainless steel, commercially known as 17-4PH, and its main components are listed in Table 1 [23]. This material is commonly used in both MIM and additive manufacturing processes, which is why it is advantageous to use it [24]. Opposed to moststainless steel grades, this exhibits excellent mechanical properties, making it widely utilized in various industrial applications. It is frequently applied in aerospace and space technology, as well as in the oil and gas industry. It is used for the production of screws, springs, nails, gears, and it finds applications in the medical field for manufacturing surgical instruments, as well. The binder used in the process consists of two main components: polypropylene and wax, which are mixed with the metal powder at a ratio of 6 % by weight [25]. The connection between the binder and the metal powder is shown in Figure 2.

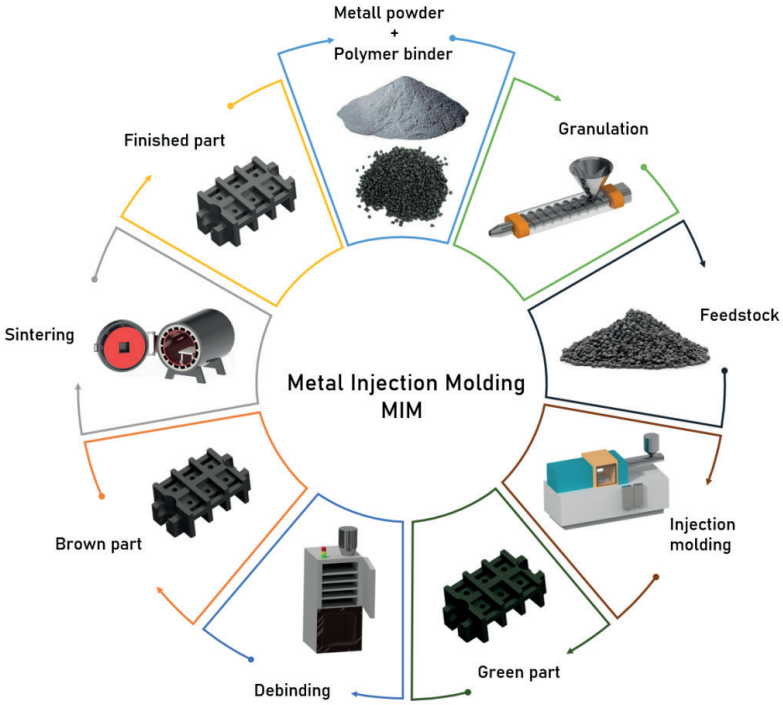

Figure 1 *The metal injection molding process*

Table 1 *17-4PH stainless steel chemical composition [24]*

%	Cr	Mn	Si	Ni	Cu
Min	15.0	--	--	3.50	3.00
Max	17.5	1.00	1.00	5.00	5.00

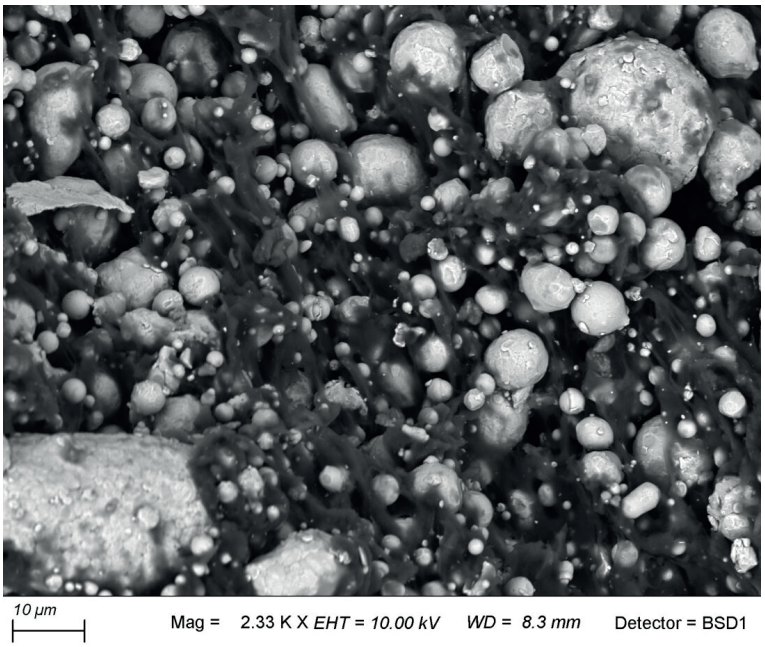

Figure 2 *the SEM image of the 17-4PH powder embedded in binder*

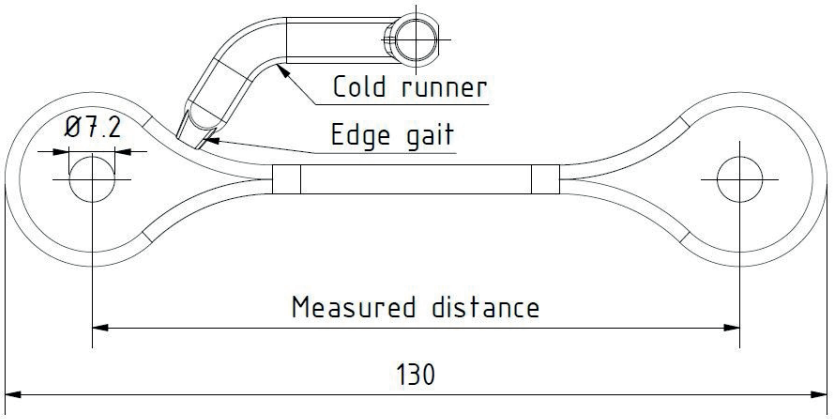

Figure 3 *Test specimen measures*

3 Methodology of injection molding experiments

Molding shrinkage values were determined by measuring the spacing of holes in a test specimen of a dog-bone geometry, Figure 3. It is important to note that the product was tested in "green" condition. In an intermediate step, the row of locking bars in the holes was removed using a reamer. Measurements were taken using an optical measuring device to ensure accuracy.

3.1 Tool used for testing

For conducting the experiments, we employed a specialized molding tool, that was designed for production of a test specimen, weighing around 36 grams. This mold is versatile and can accommodate various types of tests. It is equipped with cooling channels on both sides and includes a central heated nozzle that feeds the mold cavity through a short cold runner.

Figure 4 provides an illustration of the mold utilized in the experiment.

AFT Hungary Ltd generously supplied us with the tool and the opportunity to perform testing with it.

3.2 Molding parameters

The melting temperature was set to correspond to the average processing temperature of the polyethylene (PE) component in the binder, and the holding pressure was set at the midpoint between the two extreme processing limits. The highlighted parameters can be viewed in Table 2. The ideal mold temperature

Figure 4 *The tool used for the test*

Table 2 *The defined processing parameters*

Parameter	Value
Injection volume	6.56 cm^3/s
Injection pressure	903 bar
Postpress time	2 s
Post pressure	827 bar
Cooling time	15 s
Tool temperature	45°
Melt temperature	205 °C

Table 3 *The changed parameters and corresponding values*

Variable	Back press., bar	Tool temp., °C	Melt temp., °C
Deviation -	550	25	195
Deviation -	690	35	200
Average value	827	45	205
Deviation +	965	55	210
Deviation +	1103	65	215
Deviation +	1241	75	220

was determined based on practical observations and experiments. The main objective in designing the experiments was to vary the critical parameters - melt temperature, mold temperature and holding pressure - independently of each other. The variables are shown in Table 3. Consequently, this resulted in production of 16 different process settings. To ensure process stability and thermal equilibrium, the first 5 cases were eliminated. Subsequently, 10 test pieces were produced for each configuration. Out of those, 5 were left as green parts, while the remaining 5 were binder removed and sintered.

Table 4 *The varied parameters and corresponding values*

Parameters type	Set value
Molding Material	Catamold 17-4PH : BASF
Process controller	Process controller defaults
Injection molding machine	Default injection molding machine
Mold material	Tool Steel S-1
Solver parameters	Thermoplastic injection molding solver

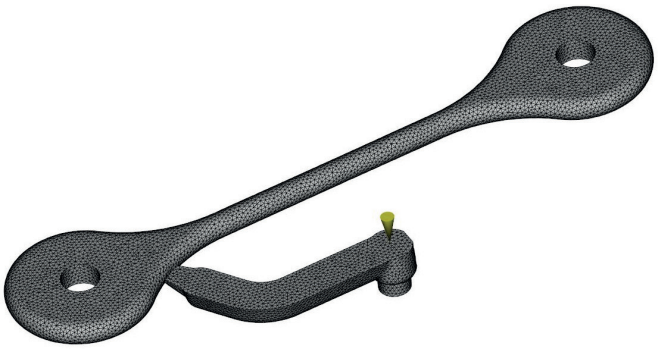

Figure 5 *The simulation model built with a volumetric mesh*

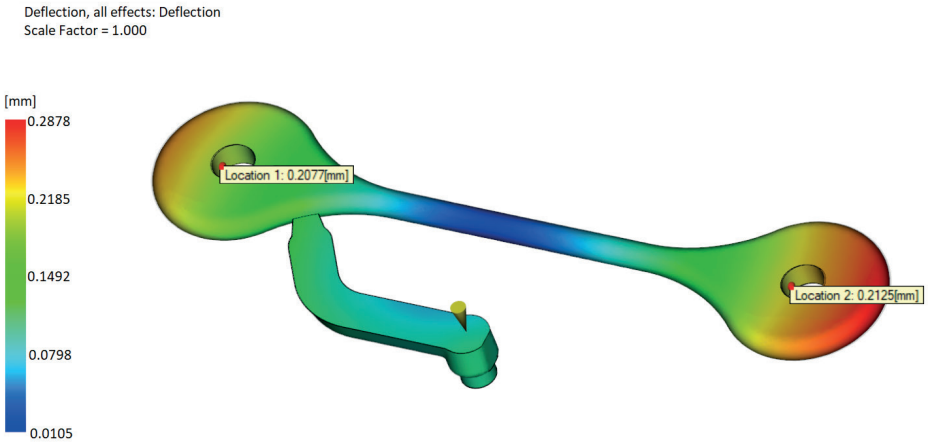

Figure 6 *The simulation model obtained after deformation with the two measurement points*

4 Simulation method

A simulation was performed to evaluate the correlation between the actual measured values and the simulation on the test specimen.

For the simulation, we used Autodesk Moldflow software, a tool specifically designed for simulation of the polymer injection molding, as shown in the set parameters. The simulation included filling and packaging processes. Table 4 shows the set values of the simulation.

The test material consisted of 94 % metal powder (17-4PH) and 6 % binder (PP and wax) granules. In contrast, the raw material selected for the simulation contains 17-4PH metallic powder, but has a catalytic binder removal system (Catamold) manufactured by BASF.

4.1 Definition of shrinkage values in the simulation software

The primary objective of the study was to assess the measurability of linear shrinkage of the product under simulation conditions.

The simulation model was created using a 3D volume mesh consisting of 0.8 mm edge length tetrahedrons, as shown in Figure 5. It consists of 10 layers in thickness.

Figure 5 illustrates the simulation model constructed with the spatial mesh. The product was made with the same gate and inlet as the injection molded part. The basic injection molding parameters, including filling time (injection time), holding pressure and cooling time, remained consistent for both the simulation and real tests.

To determine the linear shrinkage, measurements

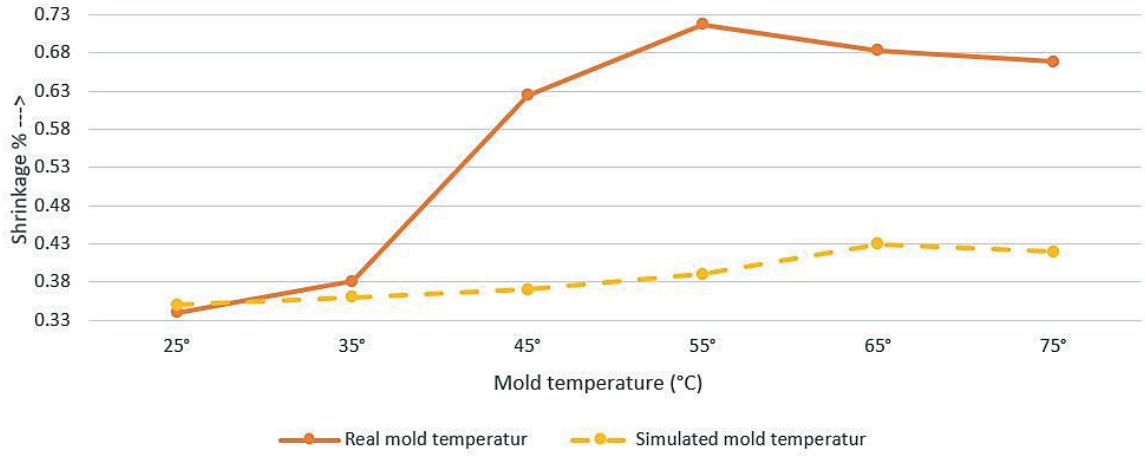

Figure 7 *Real and simulated mold temperature curve*

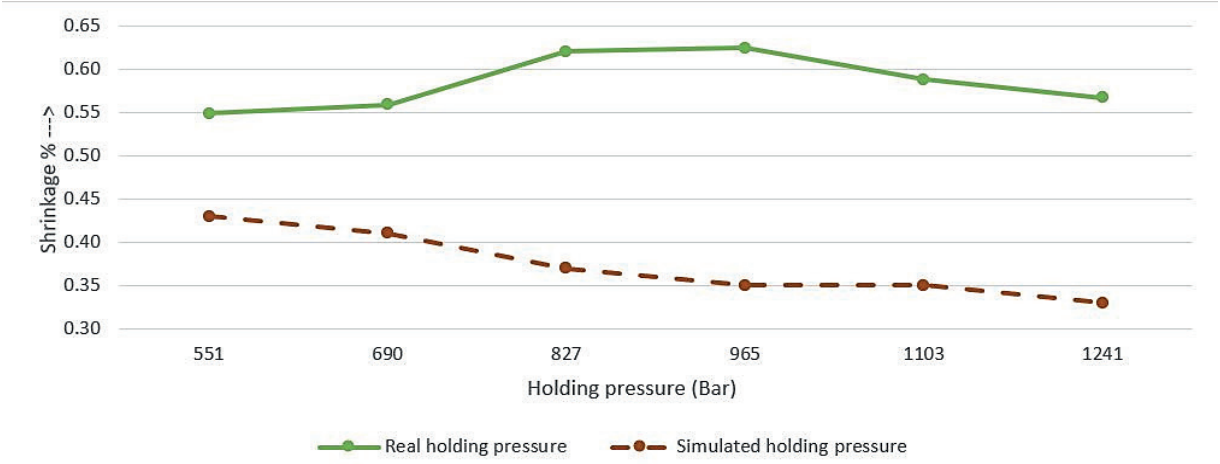

Figure 8 *Real and simulated holding-pressure curve*

were taken on the axial spacing of the holes as shown in Figure 6. The distance (displacement) between the two marked points was evaluated on the simulated image. Based on this distance measurement, the software calculates the shrinkage value based on the product's deformation with shrinkage compensation turned off.

5 Results

The hole distances of samples from the real injection molding tests were measured and the shrinkage value as a function of the parameter was shown in a diagram. The shrinkage value was determined using the following formula.

$$Shrinkage = \left(\frac{tool\ distance}{part\ distance} - 1\right) \cdot 100 \qquad (1)$$

In the simulation, the measurements were carried out according to the same principle and plotted in a diagram.

The main factor affecting the size of the product is the temperature of the mold, as illustrated in Figure 7. Shrinkage ranged from 0.34% to 0.72%, a significant variation, which translates into a dimensional deviation of approximately 0.4 mm over a 100 mm test length.

The solid-line curves always represent the real test results, while the broken-line curves represent the simulation results.

5.1 Modifying the working temperature of the tool

The curve shows an upward trend similar to plastic injection molding, but only up to 55 °C. Beyond this temperature the shrinkage value starts to decrease. During the experiments, it was observed that at higher mold temperatures the products exhibit a "wet" appearance, probably due to the wax extraction from the binder, as shown in Figure 7. Consequently, the metal particles can replace the precipitated wax, resulting in a reduction of the shrinkage factor. It is assumed that this can be quantified based on the percentage composition of the component. For the simulation results it was observed that the shrinkage values show an increase when the temperature is increased, similarly to

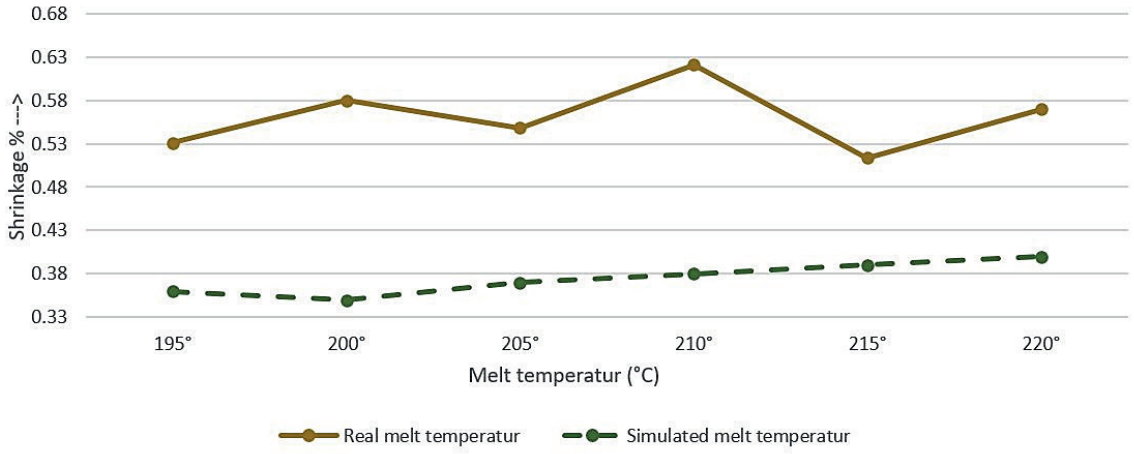

Figure 9 *Real and simulated melt temperature curve*

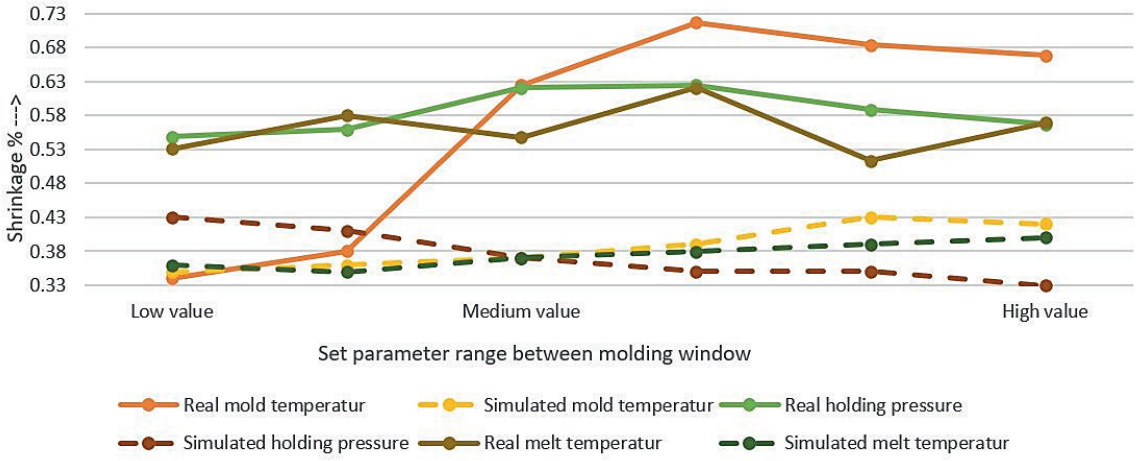

Figure 10 *Combined shrinkage curve*

the real injection molding tests. It is observed that the nature of the curves is similar and peaks at 65 °C mold temperature.

5.2 Modifying the holding-pressure of the injection molding

The relationship between the shrinkage and the change in holding pressure is different as for polymers. The results show that shrinkage reaches a maximum around 900 bar, as shown in Figure 8, leading to reduced shrinkage at higher or lower pressure levels. It is essential to stress that the effect of the applied pressure on shrinkage is much less important than that of the mold temperature. The holding-pressure curve shows a similar character to the injection molding of plastic polymers, but differs significantly from the results obtained in real experiments, both in characteristic and in magnitude.

5.3 Variation of the melt temperature

Deviations from standard plastic processing parameters can be attributed to a variety of factors, but a comprehensive study is needed to fully understand them.

Of all the parameters studied, the variation of the melt temperature had the least effect on product dimensions and the curve showed a significant variation of deviations, as shown Figure 9. The curve generated from the change of the melt temperature shows a similar character to the injection molding of plastic polymers, but differs significantly from the results obtained in real experiments in nature, as well as in magnitude.

5.4 Combined shrinkage factor graph

We combined the results in a common graph to better understand the effect of the different parameter

variations on the shrinkage of the product, Figure 10., Different parameters are plotted on the horizontal axis with a common characteristics, as low, medium and high values. Those values represent the limits of the processing window. A solid line indicates the real results and the broken line indicates the simulation results.

6 Summary and conclusions

The experiments were carried out with the aim of facilitating the simultaneous application of modelling and numerical simulations and the comparison of the actual measured results within the MIM process. To minimize the deformation of the MIM parts, it is important to know the effects of injection molding parameters.

Summary of research results:

- Simulation results at lower temperatures are closer to real measurements, however,
- with increasing temperature, there was a significant discrepancy between the simulation and real tests.
- The variation of the holding-pressure parameter shows a different characteristics.
- The difference in the magnitude of the discrepancies may be caused by the binder system not being exactly the same, but the out-of-character behavior may be caused by the simulation model itself. The assumption is supported by the correspondence of the characteristics of the curves obtained from the simulation to the properties characteristic of the polymers, which, in the present case for metal injection molding, can only be accepted conditionally if a material with a solvent binder system is processed with the used injection molding machine.
- To clarify these discrepancies, the exact material properties required for the simulations should be measured in later stages.

Acknowledgements

We thank AFT-Hungary Kft. for their generous help in securing the raw materials and technology.

Project no. TKP2021-NVA-23 has been implemented with the support provided by the Ministry of Technology and Industry of Hungary from the National Research, Development and Innovation Fund, financed under the TKP2021-NVA funding scheme.

This work was supported by the Janos Bolyai Research Scholarship of the Hungarian Academy of Sciences (ZW).

Conflicts of interest

The authors declare that they have no known competing financial interests or personal relationships that could have appeared to influence the work reported in this paper.

References

[1] GERMAN, R. M., HENS, K. F. Key issues in powder injection molding. *American Ceramic Society Bulletin*. 1991, **70**(8), p. 1294-1302. ISSN 0002-7812.

[2] GERMAN, R. M. Technological barriers and opportunities in powder injection molding. *Powder Metallurgy International*. 1993, **25**(4), p. 165-169. ISSN 0048-5012.

[3] KULKARNI, K. M. Future looking bright for PIM. *Metal Powder Report* [online]. 2000, **55**(10), p. 40-42. ISSN 0026-0657. Available from: https://doi.org/10.1016/S0026-0657(00)80068-5

[4] BALLARD, C., ZEDALIS, M. Advances in powder injection molding. In: Annual Technical Conference ANTEC: proceedings. Vol. 1. 1998. p. 358-361.

[5] HAUCK, P. A. Powder injection molding: current and long term outlook. *International Journal of Powder Metallurgy*. 2000, **36**(3), p. 29-30. ISSN 0888-7462.

[6] GERMAN, R. M. Scientific status of metal powder injection molding. *International Journal of Powder Metallurgy*. 2000, **36**(3), p. 31-36. ISSN 0888-7462.

[7] HONG, S., KANG, J., YOON, K. Correlation between thermal contact resistance and filling behavior of a polymer melt into multiscale cavities in injection molding. *International Journal of Heat and Mass Transfer* [online]. 2015, **87**, p. 222-236. ISSN 0017-9310, eISSN 1879-2189. Available from: https://doi.org/10.1016/j.ijheatmasstransfer.2015.03.061

[8] LUCCHETTA, G., MASATO, D., SORGATO, M., CREMA, L., SAVIO, E. Effects of different mold coatings on polymer filling flow in thin-wall injection molding. *CIRP Annals* [online]. 2016, **65**(1), p. 537-540. ISSN 0007-8506, eISSN 1726-0604. Available from: https://doi.org/10.1016/j.cirp.2016.04.006

[9] SARDARIAN, M., MIRZAEE, O., HABIBOLAHZADEH, A. Influence of injection temperature and pressure on the properties of alumina parts fabricated by low pressure injection molding (LPIM). *Ceramics International* [online]. 2017, **43**(6), p. 4785-4793. ISSN 0272-8842, eISSN 1873-3956. Available from: https://doi.org/10.1016/j.ceramint.2016.11.208

[10] ZHANG, Y., PEDERSEN, D. B., GOTJE, A. S., MISCHKOT, M., TOSELLO, G. A Soft Tooling process chain employing Additive Manufacturing for injection molding of a 3D component with micro pillars. *Journal of Manufacturing Processes* [online]. 2017, **27**, p. 138-144. ISSN 1526-6125, eISSN 2212-4616. Available from: https://doi.org/10.1016/j.jmapro.2017.04.027

[11] DE SOUZA, J. P., ATRE, S. V., SURI, P. K., THOMAS, J. A., GERMAN, R. M. Understanding homogeneity of powder-polymer mixtures-effect of mixing on tungsten powder injection molding feedstock. *Metalurgia e Materials*. 2003, **59**(Suppl. 7), p. 16-19. ISSN 0104-0898.

[12] SUPATI, R., LOH, N. H., KHOR, K. A., TOR, S. B. Mixing and characterization of feedstock for powder injection molding. *Materials Letters* [online]. 2000, **46**(2-3), p. 109-114. ISSN 0167-577X, eISSN 1873-4979. Available from: https://doi.org/10.1016/S0167-577X(00)00151-8

[13] DROPMANN, M. C., STOVER, D., BUCHKREMER, H. P., DIEHL, W., VASSEN, R. Injection molding with ultra high solids loading. In: Powder Injection Molding Symposium: proceedings. Vol. 92. 1992. p. 287-293.

[14] LI, Y., JIANG, F., ZHAO, L., HUANG, B. Critical thickness in binder removal process for injection molded compacts. *Materials Science and Engineering: A* [online]. 2003, **362**(1-2), p. 292-299. ISSN 0921-5093, eISSN 1873-4936. Available from: https://doi.org/10.1016/S0921-5093(03)00613-0

[15] WESTCOT, E. J., BINET ANDRANDALL, C., GERMAN, R. M., In situ dimensional change, mass loss and mechanisms for solvent debinding of powder injection molded components. *Powder Metallurgy* [online]. 2003, **46**(1), p. 61-67. ISSN 0032-5899, eISSN 1743-2901. Available from: https://doi.org/10.1179/003258903225010442

[16] LIU, D.-M., TSENG, W. J. Influence of solids loading on the green microstructure and sintering behaviour of ceramic injection moldings. *Journal of Materials Science* [online]. 1997, **32**(24), p. 6475-6481. ISSN 0022-2461, eISSN 1573-4803. Available from: https://doi.org/10.1023/A:1018646824219

[17] TSENG, W. J. Statistical analysis of process parameters influencing dimensional control in ceramic injection molding. *Journal of Materials Processing Technology* [online]. 1998, **79**(1-3), p. 242-250. ISSN 0924-0136, eISSN 1873-4774. Available from: https://doi.org/10.1016/S0924-0136(98)00019-3

[18] BARRIERE, T., LIU, B., GELIN, J. C. Determination of the optimal process parameters in metal injection molding from experiments and numerical modeling. *Journal of Materials Processing Technology* [online]. 2003, **143-144**, p. 636-644. ISSN 0924-0136, eISSN 1873-4774. Available from: https://doi.org/10.1016/S0924-0136(03)00473-4

[19] LEDNICZKY, G., WELTSCH, Z. Molding simulation of metal injection molded automotive parts. In: 38th International Colloquium on Advanced Manufacturing and Repair Technologies in Vehicle Industry: proceedings. 2023. ISBN 9789639058484, p. 51-54.

[20] LEDNICZKY, G., WELTSCH, Z. Effects of injection Molding Parameters on the Produced Parts / A femfroccsontes parametereinek hatasa a gyartott alkatreszekre (in Hungarian). *Acta Materialia Transylvanica* [online]. 2023, **6**(1), p. 33-37. ISSN 2601-1883. Available from: https://doi.org/10.33923/amt-2023-01-06

[21] KONYA, G., FICZERE, P. The effect of layer thickness and orientation of the workpiece on the micro- and macrogeometric properties and the machining time of the part during 3D printing. *Periodica Polytechnica Mechanical Engineering* [online]. 2023, **67**(2), p. 143-150. eISSN 1587-379X. Available from: https://doi.org/10.3311/PPme.21473

[22] BOGNAR, A., KUN, K. Design of a heating unit for photopolymerization-based 3D printing technology. In: 38th International Colloquium on Advanced Manufacturing and Repair Technologies in Vehicle Industry: proceedings. 2023. p. 46-50.

[23] Ametek specialty metal products. Specialty powders. 17.4 PH alloy powder - Ametek special metal products [online] [accessed 2013-06-21]. Available from: https://www.powderclad.com/products/specialty-powders/17-4-ph-alloy-powder

[24] SINGH, G., MISSIAEN, J.-M., BOUVARD, D., CHAIX, J.-M. Additive manufacturing of 17-4 PH steel using metal injection molding feedstock: analysis of 3D extrusion print-ing, debinding and sintering. *Additive Manufacturing* [online]. 2021, **47,** 102287. ISSN 2214-8604, eISSN 2214-7810. Available from: https://doi.org/10.1016/j.addma.2021.102287

[25] HAMIDI, M. F. F. A., HARUN, W. S. W., KHALIL, N. Z., GHANI, S. A. C., AZIR, M. Z. Study of solvent debinding parameters for metal injection molded 316L stainless steel. *IOP Conference Series: Materials Science and Engineering* [online]. 2017, **257**, 012035. ISSN 1757-899X. Available from: https://doi.org/10.1088/1757-899X/257/1/012035

TESTING OF RAILWAY EQUIPMENT FOR THE IMPACT ON THE TRACK AND TURNOUTS

Seidulla Abdullayev[1], Gabit Bakyt[2,*], Assel Abdullayeva[3], Bakytzhamal Duisembayeva[4], Yerlan Askenov[1], Galymzhan Ashirbayev[2], Rustam Besekenov[1]

[1]Satbayev University, Almaty, Republic of Kazakhstan
[2]Academy of Logistics and Transport, Almaty, Republic of Kazakhstan
[3]International University of Information Technology, Almaty, Republic of Kazakhstan
[4]L. N. Gumilyov Eurasian National University, Almaty, Republic of Kazakhstan

*E-mail of corresponding author: gaba_b@bk.ru

Seidulla Abdullayev 0000-0001-5028-8143,
Assel Abdullayeva 0000-0001-5188-3008,
Gabit Bakyt 0000-0001-5558-9316,
Galymzhan Ashirbayev 0000-0002-7044-9968

Resume

The indicators of dynamic qualities that ensure the traffic safety, as well as the permissible impact on the railway track, with the obligatory fulfillment of which the railway rolling stock can be used in the transportation process, are presented in this article. The purpose of this work was to carry out the complex dynamic (running), and the impact on the railway track, tests of the rolling stock, during which simultaneous registration of dynamic processes on the railway rolling stock, and in the elements of the superstructure of the track, is carried out, as well as in elements of turnouts. Dynamic tests were carried out on the track switches from the minimum speed to the maximum possible speed of 50 km/h by the TE33A diesel locomotive during the freight traffic. Meeting the requirement of reproducibility of test conditions and having a typical design of the track structure on wooden or reinforced concrete sleepers.

Article info

Received 30 September 2023
Accepted 24 January 2024
Online 6 February 2024

Keywords:

railway track
railway rolling stock
dynamic indicators
turnouts
dynamic testing

Available online: https://doi.org/10.26552/com.C.2024.020

ISSN 1335-4205 (print version)
ISSN 2585-7878 (online version)

1 Introduction

To ensure the growing volumes of traffic with traction resources, urgent measures are needed to modernize the existing and purchase new rolling stock. In addition, at present, changes have been made to the track maintenance standards, the requirements for certification of locomotives, which require the determination of permissible levels of dynamic qualities that evaluate the vibration-protective properties of the mechanical part of locomotives, the strength and reliability of the railway track, while ensuring the unconditional traffic safety indicators [1].

In the Republic of Kazakhstan, locomotives of the TE33A series were put into operation (Figure 1). When creating a new rolling stock of railways, the greatest importance is attached to the study of its dynamic and running properties, as well as the assessment of traffic safety conditions.

Test object - Diesel locomotive TE33A (Evolution ES44ACi) - a freight locomotive with asynchronous traction motors and electric drive, developed by General Electric (USA) and manufactured by the "Locomotive Kurastyru Zauyty" locomotive plant in Astana in 2010 [2].

The connection of the bogie frame with the wheel pairs is carried out through the jaw boxes. The locomotive uses wheel-to-wheel braking using one brake cylinder per wheel with shoe brakes [3-4].

The tests were carried out to establish the compliance of the locomotive performance with the safety standards NB ZhT TsT 02-98. The list of indicators determined during the tests and their allowable values are given in Table 1.

2 Methods

To measure the dynamic performance, the diesel locomotive was equipped with displacement sensors to

Figure 1 *General view of the TE33A diesel locomotive*

Table 1 *Defined indicators*

The name of the indicator, characteristics	Item number NB ZhT TsT 02-98	The value of the indicator to regulatory documents	Method for determining the indicator
1	2	3	4
Deviation of the actual value of the mass of the diesel locomotive from the designed one, %, no more than	7.1	2	tests
Deviation of the actual value of the load from each wheel pair on the rails from the value specified in the terms of reference, %, no more than	-	3	tests
The difference in loads on the wheels of the wheel pair, %, no more than	7.2	4	tests
Difference of loads along the axes of one bogie, %, no more than	7.3	3	tests
Difference of loads on the sides of the locomotive, %, no more than	7.4	3	tests
Frame forces in straight, curved track sections and turnouts, kN, no more than	2.1, 8.4	91.1	experimental-computational
Coefficient of vertical dynamics of the first stage of suspension, no more than	2.2, 8.5	0.4 0.25	tests
Stresses in the outer and inner edges of the rail sole, MPa, no more than	2.3	240	tests
Stresses in the outer edge of the blades in standardized sections, MPa, no more than	2.4	275	tests
The ratio of the maximum horizontal load to the average vertical load of the rail on the sleeper, no more than	2.5	1.4	tests
Stability factor against derailment, not less than	8.2	1.4	tests
Margin for relative movements of crew members	9	Lack of touch	Visual control
Braking distance, m	14	At V_{nom} = 100 km/h, no more than 800	tests

record the movements of the bogie frame relative to the wheel set in the vertical direction and the movements of the body relative to the bogie in the vertical direction. The signals from the sensors were transmitted via cables to the input of the measuring and computing complex "MIC-036" and recorded on the hard disk of a portable computer. Before the testing, all the measuring circuits were calibrated [5-6].

The dynamic performance of the diesel locomotive and the level of its impact on the superstructure of the track and turnouts were measured on the operating main tracks of the Kazakhstan Temir Zholy company. Prior to the start of testing, the locomotive was operated in TCEU-28. In Almaty, by the beginning of the tests, the mileage of the diesel locomotive was 11107 km (Figure 2) [4].

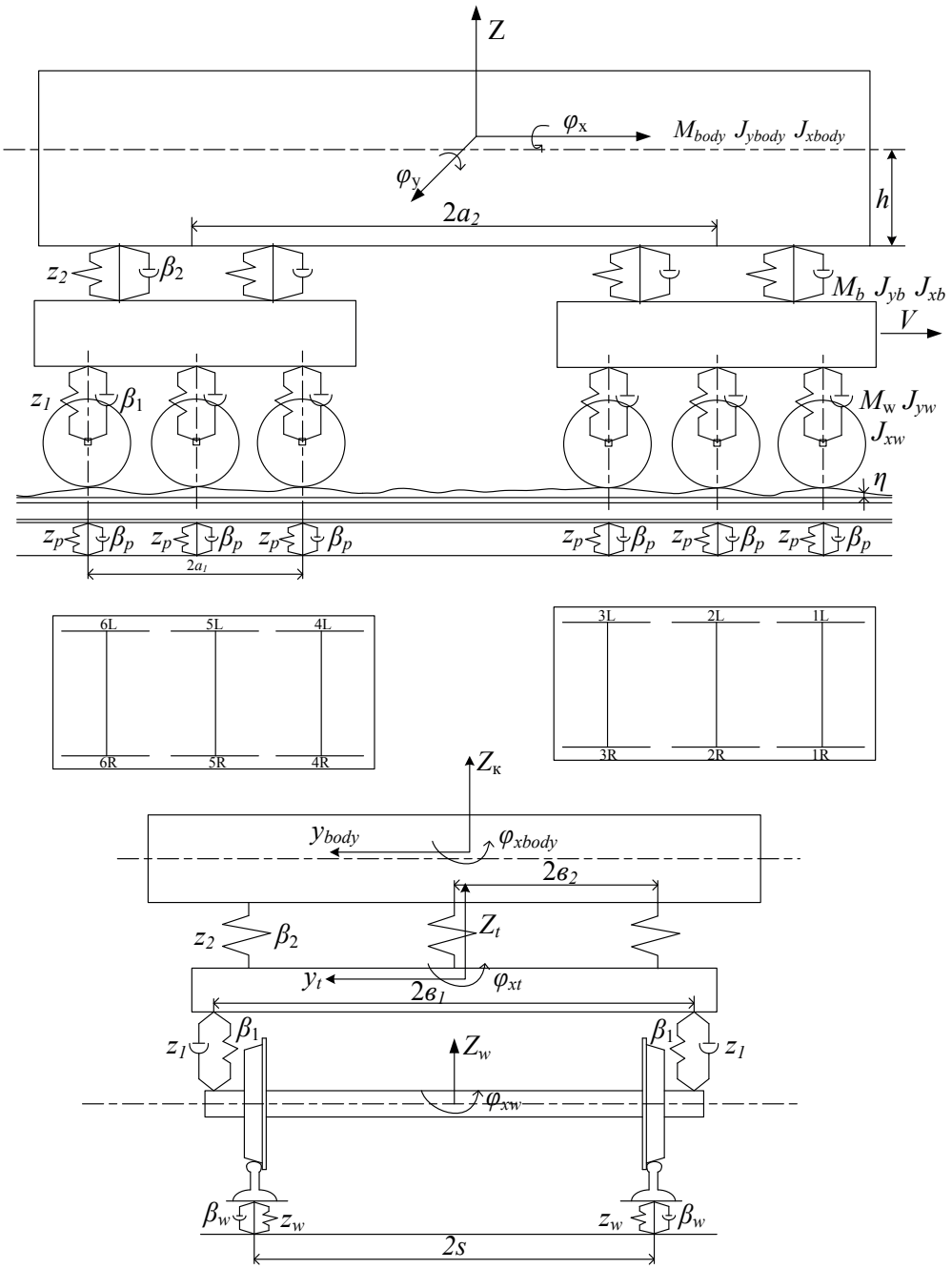

Figure 2 *Kinematic diagram of the TE33A diesel locomotive model*

On the calculated kinematic scheme, the following designations are accepted [4]:

M_{body}, M_t - mass of the body and track, respectively;

M_b - sprung mass of bogies;

M_w - masses of wheelsets;

J_{ybody}, J_{xbody} - moments of inertia of the body relative to the y and x axes, respectively;

J_{yb}, J_{xb} - moments of inertia of bogie frames relative to the y and x axes, respectively;

J_{yw1}, J_{xw2} - moments of inertia of the wheel pairs of the first and second bogies relative to the x axis, respectively;

β_1 - is the damping factor in the box stage of the spring suspension;

z_1 - rigidity of the box stage of the spring suspension;

z_2 - is the damping coefficient in the central stage of the spring suspension;

z_2 - rigidity of the central stage of the spring suspension;

β_w - attenuation coefficient in the way;

z_p - rigidity of the path;

$2a_2$ and $2a_1$ - the base of the body and bogies, respectively;

$2b_2$ and $2b_1$ - the distance between the elastic and dissipative elements of the central and pedestal stages of the spring suspension across the track axis;

$2s$ - is the distance between the points of contact with the rails of the wheels of one wheel pair;

η_r and η_l - equivalent geometrical irregularities on the right and left rails, taken as a disturbance, respectively.

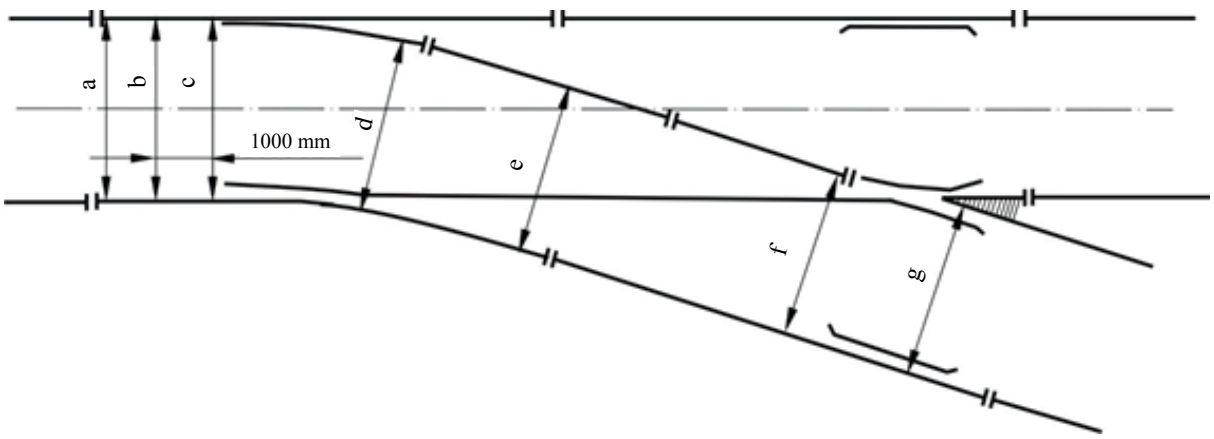

Figure 3 *Places of control measurements on the turnout*

Table 2 *Geometric dimensions of the turnout switch No. 2 Sary-Oba station*

Place of measurement	The designation of the measurement location in Figure 3	Switch R65 1/11 before testing
At the junction of the frame rail	a	1526/5
At a distance of 1000 mm from the point of the wit	b	1520/6
At the sharp edge	c	1522/4
At the root of the wit on the side path	d	1517/2
In the middle of the conversion curve	e	1524/6
At the end of the conversion curve	f	1525/0
In the cross on the lateral path (core section 40 mm)	g	1520/4

Table 3 *Dimensions of the conversion curve, mm*

Number sleepers	22	25	28	31	34	37	40	44	47	50	53
Width	1517	1517	1520	1522	1524	1524	1525	1525	1526	1524	1525
Elevation	2	0	0	4	5	4	3	2	2	2	0

3 Results

Tests of the diesel locomotive on turnouts were carried out when the diesel locomotive was passing turnout No. 2 Sary-Oba station from the odd main path to a side path. The ambient temperature is from 6 to 17 °C, the wind force is not more than 6 m/s.

Turnout switch No. 2 of type R65, grade 1/11, is installed on wooden beams. Before the testing, using a manual template, the geometric dimensions of the turnout were measured according to [7]. Measurement locations are shown in Figure 3.

Measurement data are shown in Table 2.

In addition, the track width and elevation of the outer rail in the transfer curve were measured every two sleepers. The data obtained are shown in Table 3.

During the tests, all the indicated dimensions during the transition from one speed to another were controlled by measurements using the TsUP3 template. In this case, the change in the geometry of the turnout was within 1 mm, which is comparable with the measurement error.

The experimental train consisted of a diesel locomotive TE33A. The direction was considered to be a straight line when the locomotive was ahead in the direction of travel and passed the turnout in the direction of wool. In this case, the first wheel pair of the locomotive was the guide [8].

Registration of dynamic processes in all r the aces began and ended on the straight sections of the track.

The processing of dynamic processes was carried out as follows. In each race, one maximum value of the frame forces was determined, taking into account the quasi-static component. The obtained data were grouped by directions and velocities.

The maximum probable values were calculated with a confidence level of 0.994 using the formula [4]:

$$X_{mp} = X_{res} + 2.5 \cdot \sigma, \quad (1)$$

where X_{res}, σ - respectively, the arithmetic mean and standard deviation of the measured maximum frame forces at a given speed in the selected direction of travel.

The maximum observed value of the frame forces

Table 4 *Frame forces during the movement of the diesel locomotive TE33A along the turnout R65 brand 1/11, kN*

Speed, km/h	Maximum probable value						Maximum observed value					
	Forward run			Reverse run			Forward run			Reverse run		
	Wheel set number											
	1	2	3	1	2	3	1	2	3	1	2	3
15	64.2	65.3	48.5	49.7	58.2	50.4	57.2	59.2	42.1	43.3	51.7	43.6
25	80.2	71.0	64.9	63.3	64.8	64.0	75.8	68.9	60.2	61.4	63.3	54.4
40	85.1	83.0	81.8	80.8	77.3	64.6	78.6	74.8	73.4	71.8	69.3	59.7
50	96.4	87.6	86.6	85.3	84.5	67.4	88.7	80.7	78.5	77.7	77.2	54.8

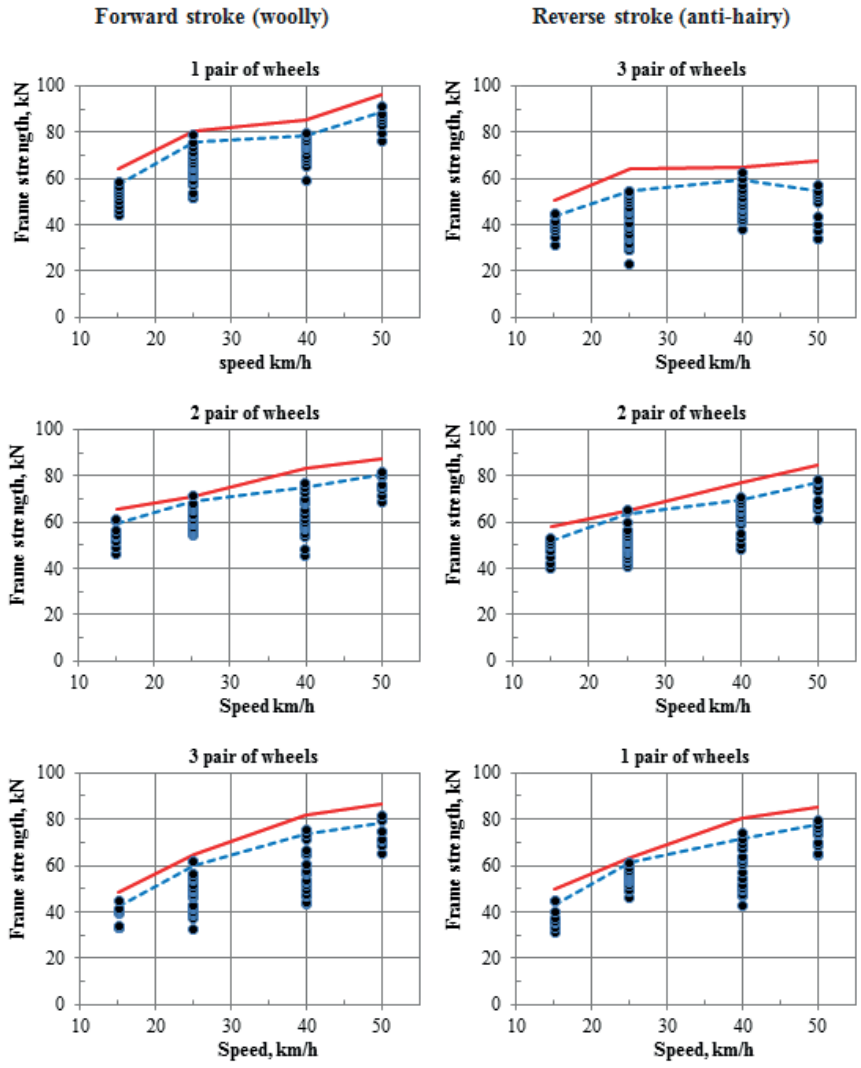

Figure 4 *Frame forces during the movement of the diesel locomotive TE33A-0023 on turnout R65 brand 1/11*

was determined as the arithmetic mean of the three largest values in each group.

The dependence of the frame forces, measured during the passage of the diesel locomotive on the turnout R65 brand 1/11, on the speed is shown in Figure 4.

The allowable value of frame forces for a diesel locomotive of the TE33A type is 23.23 · 9.8 · 0.4 = 91.1 kN. According to Table 4 and Figure 4, it can be seen that at a speed of 50 km/h, the level of frame forces exceeds the permissible value by 5.8 %. Up to a speed of 40 km/h, the maximum probable value of frame forces

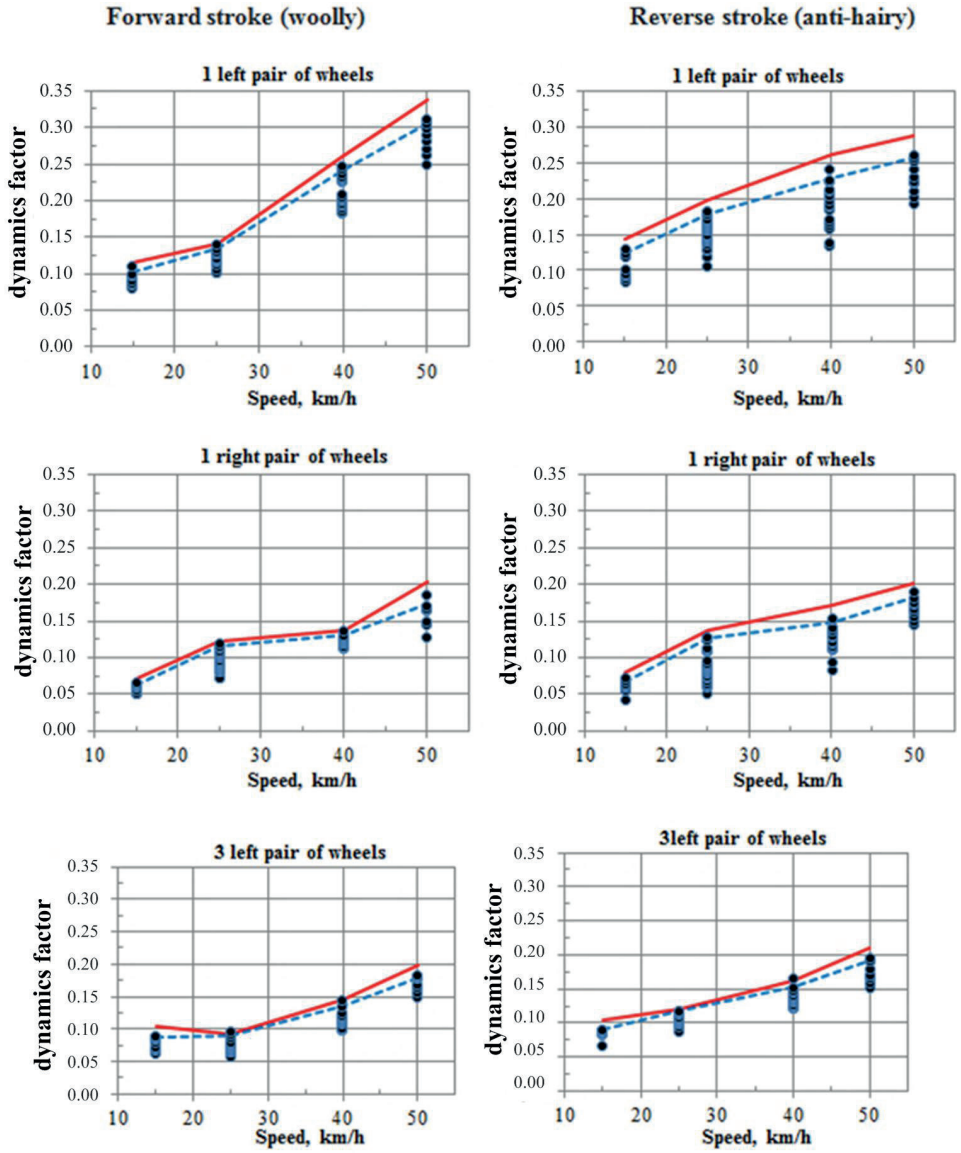

Figure 5 *Coefficient of vertical dynamics of the first suspension stage when the diesel locomotive TE33A moves along the turnout R65 of brand 1/11*

during the cross-country passage of the turnout does not reach the allowable value by 6.6 % does not exceed the permissible limits up to a speed of 50 km/h.

The coefficient of vertical dynamics of the first suspension stage was determined as the ratio of the dynamic vertical displacements of the wheel pair box relative to the bogie frame in the vertical direction to the static deflection of the first suspension stage. According to the data provided by the manufacturer, the static deflection of the locomotive's first suspension stage is 131.5 mm.

The vertical displacements of the box relative to the bogie frame were measured for the first wheel set on the left and right, and for the third wheel set on the left [9].

Dynamic vertical displacements of the box relative to the bogie frame were processed without taking into account the quasi-static component. All measurements were divided into speeds and directions of movement. In each race, one maximum amplitude value of the dynamic process was selected.

Based on the results of data processing at a given speed, separate arrays were formed for each sensor. Based on these arrays, the maximum probable and maximum observed values of the vertical dynamics coefficient of the first suspension stage were found. In the calculations, the same methodology was used as in the calculations of the maximum probable and maximum observed values of the frame forces.

The results of the data processing to determine the coefficient of vertical dynamics of the first suspension stage are shown in Figure 4.

The highest value of the coefficient of vertical dynamics of the first stage was registered on the guide wheel sets of the bogie. At the same time, at the speed

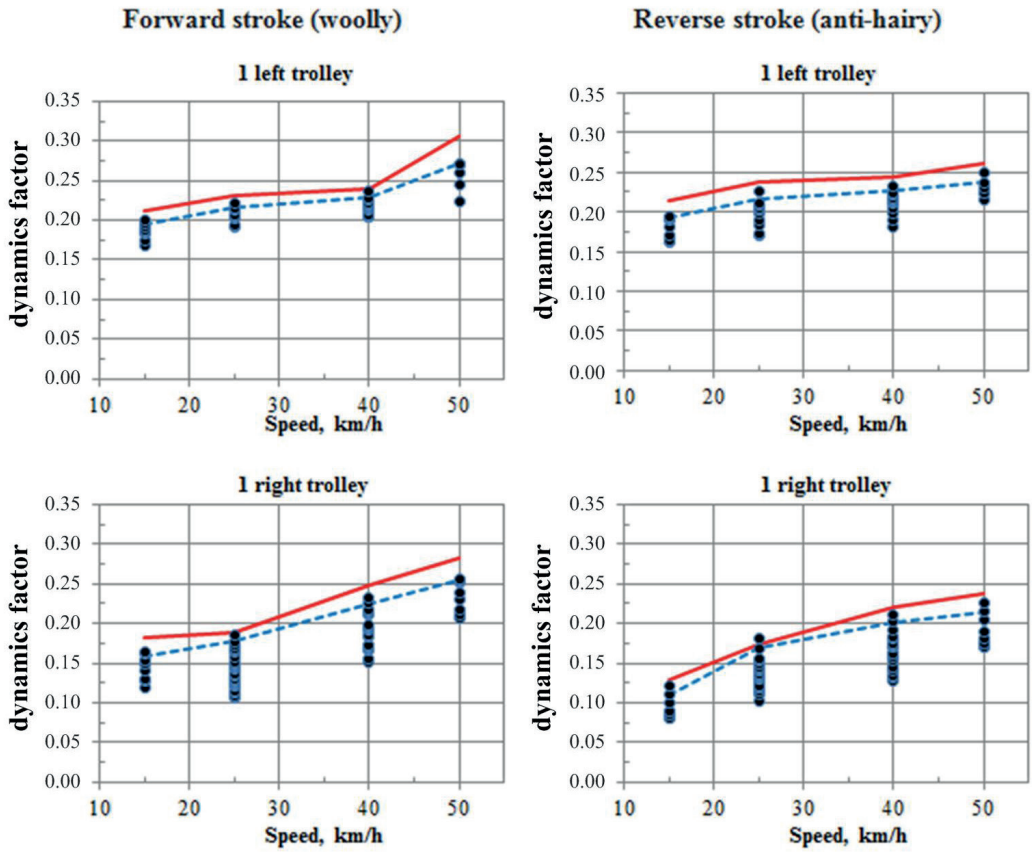

Figure 6 *Coefficient of vertical dynamics of the second suspension stage when the diesel locomotive TE33A moves along the turnout R65 of grade 1/11*

Table 5 *Coefficient of vertical dynamics of the first suspension stage when moving along a turnout type R65, grade 1/11*

Value	Speed, km/h	Forward run			Reverse run		
		Wheel set number					
		1		3	1		3
		left	right	left	right	left	right
maximum probable	15	0.11	0.07	0.10	0.14	0.08	0.10
	25	0.14	0.12	0.09	0.20	0.14	0.12
	40	0.26	0.14	0.14	0.26	0.17	0.16
	50	0.34	0.20	0.20	0.29	0.20	0.21
maximum observed	15	0.10	0.06	0.09	0.12	0.07	0.09
	25	0.14	0.12	0.09	0.18	0.13	0.12
	40	0.24	0.13	0.14	0.23	0.15	0.15
	50	0.31	0.17	0.18	0.26	0.18	0.19

Table 6 *Coefficient of vertical dynamics of the second suspension stage when moving on a turnout type P65 of grade 1/11*

Speed, km/h	Maximum probable value				Maximum observed value			
	Forward run		Reverse run		Forward run		Reverse run	
	left	right	left	right	left	right	left	right
15	0.21	0.18	0.21	0.13	0.20	0.16	0.19	0.11
25	0.23	0.19	0.24	0.17	0.22	0.18	0.22	0.17
40	0.24	0.25	0.24	0.22	0.23	0.23	0.23	0.20
50	0.31	0.28	0.26	0.24	0.27	0.25	0.24	0.22

of 50 km/h, on the first wheel pair of the locomotive, the vertical dynamics coefficient increases significantly and reaches a value of 0.34, without exceeding the permissible norms [2, 10].

Similarly, the coefficient of vertical dynamics of the second stage of suspension is determined, based on the fact that the static deflection of the second stage of suspension of the diesel locomotive is 10.3 mm (side supports). The results obtained are shown in Figure 5.

The coefficient of vertical dynamics of the second suspension stage during the rough movement at a speed of 50 km/h exceeds the permissible norms by 24 %, and up to a speed of 40 km/h it is within the permissible limits.

Based on the data of Figures 5 and 6, Tables 5 and 6 are compiled, which show the maximum probable and maximum observed values of the vertical dynamics coefficient of the first and second stages of the locomotive suspension when moving along the R65 turnout of grade 1/11 [11].

The obtained results show that the dynamic performance of the diesel locomotive (frame forces, coefficients of vertical dynamics of the first and second stages of suspension) when moving along a turnout type R65 brand 1/11 up to speeds of 40 km/h are within acceptable limits. At a speed of 50 km/h, the vertical dynamics coefficient of the first stage is also within acceptable limits, and the frame forces and the vertical dynamics coefficient of the second stage exceed the permissible norm [12-13].

4 Conclusions

In connection with this research goals, the following main tasks were solved:

- determination of the main dynamic indicators of a diesel locomotive;
- determination of the level of diesel locomotive impact on the track and turnouts;
- To achieve the set goals, the following work has been carried out:
- a kinematic diagram of the TE33A diesel locomotive has been compiled with the main values of the main parameters of the mechanical part;
- it was found that for the TE33A diesel locomotive, the permissible value of the frame forces reaches when passing the track switch at a speed of 40 km/h with a margin of 6.6%. This, in turn, makes it possible to determine the critical speed of the TE33A diesel locomotive by the switch.
- graphs of the dependence of the coefficients of the vertical dynamics of the first and second suspension stages of suspension when moving a TE33A diesel locomotive at a speed of up to 50 km/h are constructed. It is determined that, when moving at a speed of 50 km/h, the coefficient of vertical dynamics of the first stage is within acceptable limits, and the coefficient of vertical dynamics of the first second stage exceeds the permissible norm.

Thus, as a result of the experimental study carried out, it should be concluded that the maximum and safe speed for the TE33A diesel locomotive along the track switch with R65 rails is 40 km/h.

Grants and funding

The authors received no financial support for the research, authorship and/or publication of this article.

Conflicts of interest

The authors declare that they have no known competing financial interests or personal relationships that could have appeared to influence the work reported in this paper.

References

[1] SUN, Y., COLE, C., SPIRYAGIN, M., DHANASEKAR, M. Vertical dynamic interaction of trains and rail steel bridges. *Electronic Journal of Structural Engineering* [online]. 2013, **13**(1), p. 88-97. ISSN 1443 9255. Available from: https://doi.org/10.56748/ejse.131641

[2] WAN, C., MARKINE, V. L., SHEVTSOV, I. Y. Improvement of vehicle-turnout interaction by optimising the shape of crossing nose. *Vehicle System Dynamics* [online]. 2014, **52**(11), p. 1517-1540. ISSN 0042-3114, eISSN 1744-5159. Available from: https://doi.org/10.1080/00423114.2014.944870

[3] ABDULLAYEVA, A., KALABAYEVA, A., IVANOV, A., ABDULLAYEV, S., BAKYT, G. Methods for identification of complex industrial control objects on their accelerating characteristics. *Communications - Scientific Letters of the University of Zilina* [online]. 2022, **24**(3), p. B239-B246. ISSN 1335-4205, eISSN 2585-7878. Available from: https://doi.org/10.26552/com.C.2022.3.B239-B246

[4] ABDULLAYEV, S., BAKYT, G., KAMZINA, A., SARSANBEKOV, K., ABDULLAYEVA, A. Interaction of the TE33a diesel locomotive and the railway track on curved section with radius 290 m. *Communications - Scientific Letters of the University of Zilina* [online]. 2023, **25**(4), p. B315-326. ISSN 1335-4205, eISSN 2585-7878. Available from: https://doi.org/10.26552/com.C.2023.069

[5] ANTOLIN, P., ZHANG, N., GOICOLEA, J. M., XIA, H., ASTIZ, M. A., OLIVERA, J. Consideration of nonlinear wheel-rail contact forces for dynamic vehicle-bridge interaction in high-speed railways. *Journal of Sound and Vibration* [online]. 2013, **332**(5), p. 1231-1251. ISSN 0022-460X, eISSN 1095-8568. Available from: https://doi.org/10.1016/j.jsv.2012.10.022

[6] SENINI, S., FLINDERS, F., OGHANNA, W. Dynamic simulation of wheel-rail interaction for locomotive traction studies. In: 1993 IEEE/ASME Joint Railroad Conference: proceedings [online]. IEEE. 1993. ISBN 0-7803-0963-4, p. 27-34. Available from: https://doi.org/10.1109/RRCON.1993.292967

[7] ANDERSON, W. F., KEY, A. J. Model testing of two-layer railway track ballast. *Journal of Geotechnical and Geoenvironmental Engineering* [online]. 2000, **126**(4), p. 317-323. ISSN 1090-0241, eISSN 1943-5606. Available from: https://doi.org/10.1061/(ASCE)1090-0241(2000)126:4(317)

[8] KALIVODA, J., BAUER, P. Roller rig testing at the Czech technical university. *Science and Transport Progress. Bulletin of Dnipropetovsk National University of Railway Transport* [online]. 2016, **4**(64). ISSN 2307-6666. Available from: https://doi.org/10.15802/stp2016/77994

[9] VUONG, T., MEEHAN, P. A., EADIE, D. T., OLDKNOW, K., ELVIDGE, D., BELLETTE, P. A., DANIEL, W. J. Investigation of a transitional wear model for wear and wear-type rail corrugation prediction. *Wear* [online]. 2011, **271**(1-2), p. 287-298. ISSN 0043-1648, eISSN 1873-2577. Available from: https://doi.org/10.1016/j.wear.2010.10.008

[10] YAZDI, M. A question on using fuzzy set theory and its extensions in safety and reliability. *Computational Research Progress in Applied Science and Engineering*. 2020, **6**(3), p. 203-209. eISSN 2423-4591.

[11] IMASHEVA, G., ABDULLAYEV, S., TOKMURZINA, N., ADILOVA, N., BAKYT, G. Prospects for the use of gondola cars on bogies of model ZK1 in the organization of heavy freight traffic in the republic of Kazakhstan. *Mechanika* [online]. 2018, **24**(1), p. 32-36. ISSN 1392-1207, eISSN 2029-6983. Available from: https://doi.org/10.5755/j01.mech.24.1.17710

[12] YAN J., MENG, Y., YANG, Q., LUO, X., GUAN, X. Privacy-preserving localization for underwater sensor networks via deep reinforcement learning. *IEEE Transactions on Information Forensics and Security* [online]. 2020, **16**, p. 1880-1895. ISSN 1556-6013, eISSN 1556-6021. Available from: https://doi.org/10.1109/TIFS.2020.3045320

[13] MASSEL, A. Experimental tracks and their role in testing of rolling stock and railway infrastructure. *Railroad Problems: Railway Report* [online]. 2021, **192**, p. 153-170. ISSN 0552-2145, eISSN 2544-9451. Available from: https://doi.org/10.36137/1923E

APPRAISAL RELIABILITY OF ELECTROMECHANICAL EQUIPMENT OF RAIL SERVICE CAR

Ziyoda Mukhamedova Gafurdjanovna[1,*], Sherzod Fayzibayev Sabirovich[2], Dilbar Mukhamedova Gafurdjanovna[3], Gulshan Ibragimova Ruslanovna[4], Shokhrukh Kayumov Sharof Ogli[4]

[1]Department "Transport and Cargo Systems", Faculty Management of Transport Systems, Tashkent State Transport University, Tashkent, Uzbekistan
[2]Department "Locomotives and Locomotive Establishment", Faculty Railway Transport Engineering, Tashkent State Transport University, Tashkent, Uzbekistan
[3]Department of Psychology, Faculty of Social Science, National University of Uzbekistan, Tashkent, Uzbekistan
[4]Department "Organization of Transport System", Faculty Management of Transport Systems, Tashkent State Transport University, Tashkent, Uzbekistan

*E-mail of corresponding author: mziyoda1987@gmail.com

Ziyoda M. Gafurdjanovna 0000-0002-1825-2447,
Dilbar M. Gafurdjanovna 0009-0005-4451-5895,
Shokhrukh K. Sharof Ogli 0000-0002-6239-3001
Sherzod F. Sabirovich 0000-0003-1420-3581,
Gulshan I. Ruslanovna 0000-0002-5998-533X,

Resume

This study conducts an in-depth exploration into the principal factors that influence the reliability of specialized rail cars and auto-rail vehicles. It places a particular emphasis on key performance metrics including the average operational duration prior to failure, the proba¬bility of faultless operation, the rate of failure, and the gamma-percentage resource. Addition¬ally, the paper examines various methodologies for computing these metrics and quantitatively evaluating their respective values. It elucidates how specific units of electromechanical equip¬ment, which operate in conjunction with asynchronous motors and clutches, exhibit distribution patterns during failure that overlap between exponential and normal distributions. The study further presents a mathematical formula to approximate the reliability density of the distribution, a critical factor in recalibrating the metrics associated with specialized rail cars.

Article info

Received 2 September 2023
Accepted 22 January 2024
Online 8 February 2024

Keywords:

rail service car
reliability indicators
electromechanical equipment
synchronous generator
electric motors
percentage resource
gamma exponential law

Available online: https://doi.org/10.26552/com.C.2024.021

ISSN 1335-4205 (print version)
ISSN 2585-7878 (online version)

1 Introduction

The work presented in this paper includes an in-depth exploration of the underlying reasons and specific nature of the damage that significantly compromises the operational effectiveness of the distinctive rolling stock compositions under the stewardship of the Joint-Stock Company, "Uzbekistan Railways". Comprehensive data analysis unveils that the majority of these adverse events (50 %) are primarily due to mechanical breakdowns, followed by electrical dysfunction (31.8 %), and issues concerning the hydraulic machinery (18.2 %) [1].

With these significant challenges at the forefront, it becomes an imperative requirement to conceptualize and implement an innovative approach to modernize the rail service cars during their overhaul stages. This initiative aims to substantially augment their technical diagnostics, thereby promoting overall operational efficiency. This particular research concentrates primarily on rail service cars, specifically the ADM-1 type, which comprise a significant portion of the fleet, with 145 units in operation under the umbrella of the "Uzbekistan Railways" Joint Stock Company [2].

The systematic maintenance of the requisite reliability standards of rail service cars and railway inspection vehicles, especially within the context of a market economy, hinges decisively on the strategic decisions made concerning their maintenance and repair (M&R). The reliability of the rail service cars is largely contingent upon the capability of its individual mechanical, electrical, and hydraulic components to sustain their initial technical characteristics during

operational periods. This feature considerably impacts the overarching effectiveness of the railway transportation.

This overarching effect is quantitatively evaluated using the technical-economic efficiency metric, which encapsulates the performance spectrum of the rail service car functionalities. This includes the integral consideration of financial expenditure, labour contributions, and material costs. The troubleshooting process for the rail service car involves identifying potential failure points, tracking key performance indicators during operations, and appraising the technical processes that require the integration of complex mechanical, electrical, and hydraulic systems. This calls for a harmonized approach across the deployment location, aiming at maintaining both static and dynamic stability, which, in turn, ensures the seamless functionality of the primary contact network.

The novelty of this study is in obtaining the probability of distribution before the failure of the rail service car main equipment of, by superimposing exponential and normal Gaussian distribution laws. The results of this study could make it possible to adjust the indicators of separate and joint optimal frequency of the rail service car.

Reliability is the most important qualitative characteristics of the main equipment of the rail service car, as well as all the products of engineering facilities. According to [3], this is the property that the object must perform the specified functions, keeping in time the values of the established operational indicators within the specified limits corresponding to the specified modes and conditions of use, maintenance, repairs, storage and transportation. The reliability of the rail service car and equipment in detail is a complex property, including reliability, durability, maintainability and preservation [4].

2 Related works

The research conducted by numerous scientists has played a crucial role in shaping the contemporary designs of railway rolling stock. This body of work has largely addressed the significant challenges of assessing static and dynamic loads on rail carriages, with substantial contributions from researchers such as Anyakwo[5], Bogdevicius.[6], Bureika [7], Chao [8], EulitzKotte [9], Fan et al. [10], Kuznetsov et al. [11], Popp and Schiehlen [12], Sharma et al. [13], Sebesan and Baiasu [14]. Their theoretical insights, regulatory and technical solutions, as well as methods and algorithms for assessing the residual life of rail transport rolling stock, continue to be integral in the railway industry.

Furthermore, dynamic strength and reliability calculation theories for mechanical systems on railway transport have been significantly advanced by Spiryagin. et al. [15], Sosnovsky and Scherbakov [16], Tretyakov [17-19], Vasilyev [20] and others. Today, over 25 organizations across Russia, Ukraine, Belarus, Kazakhstan, Latvia, Lithuania, Georgia, and Uzbekistan have taken practical strides to extend the lifespan of different rail vehicles types.

The reliability of specialized rail car is a field with extensive research. In terms of electromechanical equipment units, Zhou et al. [21] investigated the dynamics effect of wheel flats on the railway vehicle system. They found that the wheel flats exacerbate wheel-rail impact and locomotive component vibrations. Moreover, they identified that defects like wheel flats can be detected by analysing the frequency spectrum of current signals in a traction motor, providing insights for efficient monitoring and maintenance, which aligns with our focus on technical diagnostics.

In the realm of railway vehicle multi-body models, Bruni et al. [22] reviewed models for railway vehicle suspension components, discussing the required level of detail in view of the overall simulation model's accuracy. Their work underscores the need for precision in modelling components, which aligns with our approach of using a system analysis model for maintenance and repair. Similarly, Bruni et al. [23] emphasized the role of control and monitoring technologies in railway vehicle dynamics. Their findings underlined the need for comprehensive technical diagnostics in enhancing rail car reliability.

Evans and Berg [24] explored the challenges in the simulation of rail vehicle dynamics. They emphasized the importance of appropriate modelling choices for different applications and the increasing importance of validating simulation results, which this study takes into account. They also emphasized the role of simulation as an essential part of the design process for new vehicles and for investigating service problems with existing vehicles, thus validating our approach to calculate failure metrics through the system analysis.

Carlbom [25] discussed the combination of multibody and finite element models for the rail vehicle dynamics analysis, using the real track data as input. His work illustrates the importance of integrating different models to accurately assess vehicle behavior and validates our method of calculating overhaul life based on the failure probability indices.

Finally, Auciello et al. [26] proposed an innovative semi-analytic procedure for wheel-rail contact point detection, recognizing its substantial impact on the contact force direction and intensity. Their work highlights the significance of understanding the complex interplay between different rail car components, which resonates with our approach of studying overlapping failure distribution patterns in specialized rail cars.

Together, these studies demonstrate the rich, multifaceted understanding of the rail vehicle reliability and that it is an influencing factor. Building upon their insights, our research objective was to enhance the rail

Figure 1 *Photos of an ADM type rail service car*

car reliability through the strategic assessment and adjustment of the key operational metrics.

However, the contemporary literature still faces a gap in addressing the theory of oscillations and reliability of body frames, spring suspensions, and chassis of the rail service car. Those studies must also consider the optimization of dynamic characteristics and the rational design and modernization methodologies. The performance of the whole railway transport depends heavily on the adherence to the electric locomotives' movement schedule, with technical and economic indicators significantly influenced by the reliability of the rail service car mobile composition.

The reliability of rail service car is largely contingent on its electromechanical equipment, which must maintain optimal performance of designated functions, while preserving the operational indicator values within specified storage limits. Those limits correspond to the use, maintenance, and repair systems over time. The initial data to define reliability indicators are often statistical operation data from the functional units [27].

The object of this research of the rail service car is a self-propelled two-axle carriage. A load-bearing cabin is located on the front console. On the rear console there is a crane manipulator unit capable of mounting and dismantling contact network supports, loading and unloading various cargoes on railways. The mounting platform is located in the middle part of the rail service car. In addition, in the middle part under the frame of the rail service car there is a power plant that transmits power through hydraulic transmission to a three-phase generator.

The photographs of the object of study, taken by the authors during the survey of the rail service car operated by Uzbek Railways JSC, are shown in Figure 1.

3 Methods

We conducted a collection and record procedure of the primary reliability information based on the guidelines stipulated in the documents "Procedure for conducting technical inspection" and "Checking the technical condition of the rail service car" [28]. Those procedures were carried out using the data from the "Mechanization Department" of the "Uzbekistan Railways". An assumption was made that the initial statistical information is objective, reliable, and selected [29] according to the sampling method provisions, ensuring sufficient volume for estimates with a given

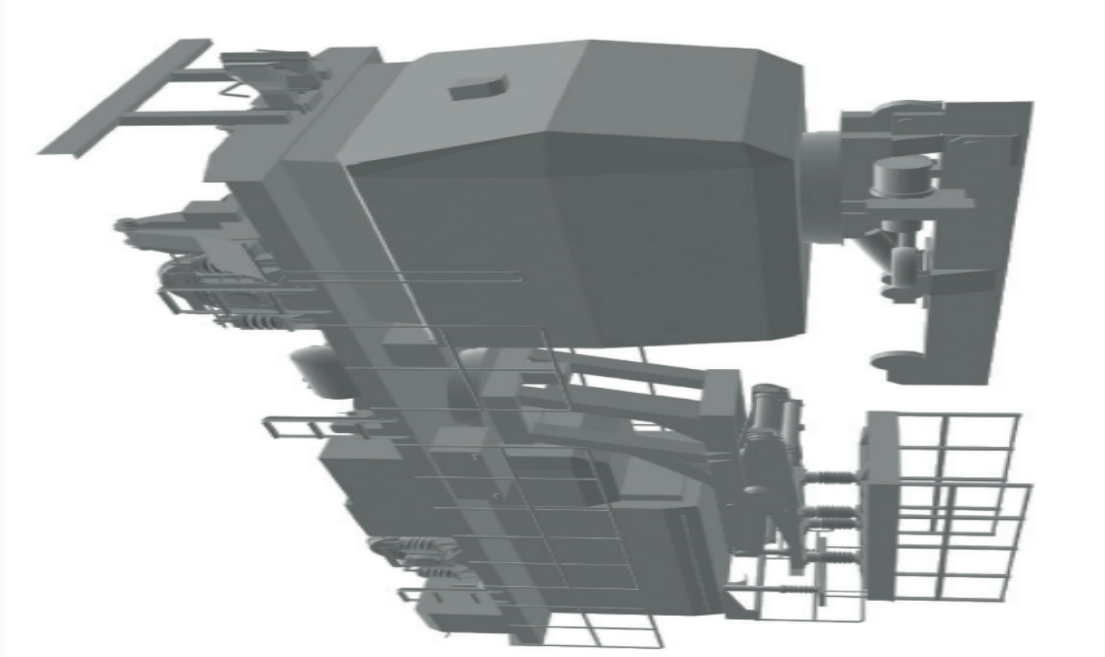

Figure 2 *The 3D model of the ADM type rail service car*

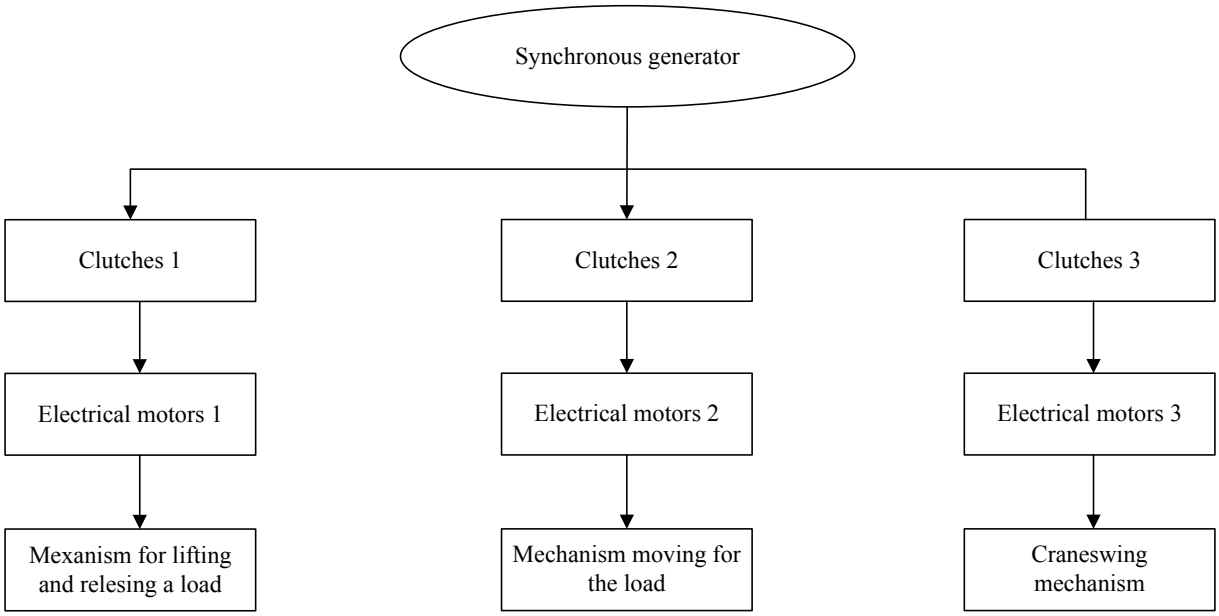

Figure 3 *A calculation scheme of the reliability of electrical equipment of the rail service car of the ADM type*

confidence level and accuracy. The analysis of statistical operation data for the rail service car types ADM from "Uzbekistan railways" JCS indicates that the technical condition of mechanical, hydraulic, and electrical equipment of the rail service car is a complex object, warranting a holistic consideration for assessing reliability indicators for each equipment type.

A 3D model of the rail service car is shown in Figure 2.

The reliability of electromechanical equipment significantly impacts the efficacy of the entire rail service car system. All the technical blocks of the electromechanical equipment (EE) consist of a synchronous three-phase current generator and three electric motors (EM1, EM2, EM3), each responsible for different mechanisms: lifting and lowering the load, load movement, and the crane swing. These are all connected to the synchronous generator via three clutches.

The power electric circuits of the rail service cars, type ADM are standardized. The 12 kW synchronous three-phase alternator is the electrical energy source. Each actuator is driven through electromagnetic clutches by the electric motors M1 for the load lifting and releasing mechanism (type ASVT-52), M2 for the load trolley moving mechanism (type 4AC100), M3 for the crane swing mechanism (type MKTF). These are

Table 1 *Summary table of reliability ratings for mechanical, electrical and hydraulic control equipment of the rail service car type ADM*

d	1	2	3	4	5	6	7	8	9	10	11	12	13	14	15	16
t_i, hour	61	79	80	81	92	94	101	104	111	123	132	140	142	202	213	217

Table 2 *Summary table of assessments of reliability indicators of mechanical, electrical and hydraulic equipment*

Types of equipment controls		Mechanical	Electrical	Hydraulic
		[*N, U, T*]	[*N, U, T*]	[*N, U, T*]
Observation plan	N	50	50	50
Estimates of the reliability indicators	d	12	14	16
Failure rate	λ_{av}; 1/h	$0.3661 \cdot 10^{-3}$	$0.370 \cdot 10^{-3}$	$0.444 \cdot 10^{-3}$
Lower confidence limit failure rate	λ_{L}; 1/h	$0.149 \cdot 10^{-3}$	$0.1575 \cdot 10^{-3}$	$0.169 \cdot 10^{-3}$
Upper confidence limit failure rate	λ_{av}; 1/h	$0.386 \cdot 10^{-3}$	$0.407 \cdot 10^{-3}$	$0.457 \cdot 10^{-3}$
Point estimate of mean time to failure	$\lambda_{u}H$; h	3266.9	2702.9	2252.2
Lower confidence limit of operating time	λ_{L}; h	2589.3	2457.0	5917.2
Upper confidence limit of operating time	$\lambda_{u}B$; h	6711.4	6349.2	2188.2
Probability of failure-free operation over the operating time	$P(t)$	0.54	0.69	0.41
Lower confidence limit of probability of failure-free operation	$P(t)_{L}$	0.74	284.7	0.401
Upper confidence limit of probability of failure-free operation	$P(t)_{u}$	0.74	284.7	0.713
Resource at $\gamma = 90\%$	T; h	344.2	258.7	237.3
Lower bound of the confidence resource at $\gamma = 90\%$	T_{L}; h	272.8	258.8	230.5
Upper confidence limit of probability of failure-free operation	T_{u}; h	707.1	668.9	623.4

N - number of items, d - number of failures

termed as electric executive units.

From a reliability perspective, this electric circuit system operates so that a failure in one unit leads to a failure of the entire rail service car, but does not impact the reliability of other executive unit blocks. This structure is known as a system with serially connected elements in reliability theory (Figure 3).

Hence, the structural reliability of the object in question over time t can be expressed as [2]:

$$P(t) = P_{EE}(t) \cdot P_{CSM}(t) \cdot P_{MML}(t) P_{CS}(t), \quad (1)$$

where:

$P_{EE}(t)$ represents the failure-free operation probability of the synchronous electric generator, an hour (h).

$P_{CSM}(t)$ is electromagnetic clutch of the load lifting and releasing motor, h.

$P_{MML}(t)$ is load moving motor, h.

$P_{CS}(t)$ is crane rotation motor within a specified tolerance, h. [30].

Expressing $P(t)$ in terms of failure rate allows to rewrite Equation (1) as:

$$P(t) = \exp\left[-\sum_{i=1}^{u} \int_{0}^{t} \lambda_i(x)dx\right]. \quad (2)$$

A total of 145 rail service cars units, with unified power electrical circuits, were observed over three years to determine the failure rate of electromechanical equipment. The observation included types of ADM rail service cars. The total number of devices observed was $N = 40$. After the failure, the devices were not replaced. Observations were conducted until the run $L = 100 \cdot 10$ km, within which $d = 10$ items of electromechanical equipment failed, with operational times t_i = 8.3; 40.4; 40.6; 45.4; 47.7; 53; 69.1; 100.3; 161.9; 168.5 hThe law of probability distribution for failure for the rail service car is known to be exponential. In the railway transport, the reliability of the rail service car is commonly assessed by mileage, i.e., the distance an object travels while in working condition [31].

For the rail service car, a plan, (N, U, T_o), is recommended, where N represents the number of items under observation, U indicates plans where failed items were not replaced, and T_o estimates the duration of observations or, in general, the established mileage after which the rail service cars functionality is restored. A summary of results of the rail service cars basic equipment scores, based on many years of observations, is presented in Tables 1 and 2.

$$\begin{matrix} \sum t_{m.hour} = 1198 \cdot \sum t_{e.hour} = \\ = 1536 \cdot \sum t_{hyd.hour} = 1466 \end{matrix}. \quad (3)$$

Table 3 *The probability of failure-free operation of rail service cars and operating time hours*

Mileage in hours	200	500	1000	2000	2500	3000	4000
P(l)	0.93	0.85	0.72	0.52	0.44	0.37	0.27

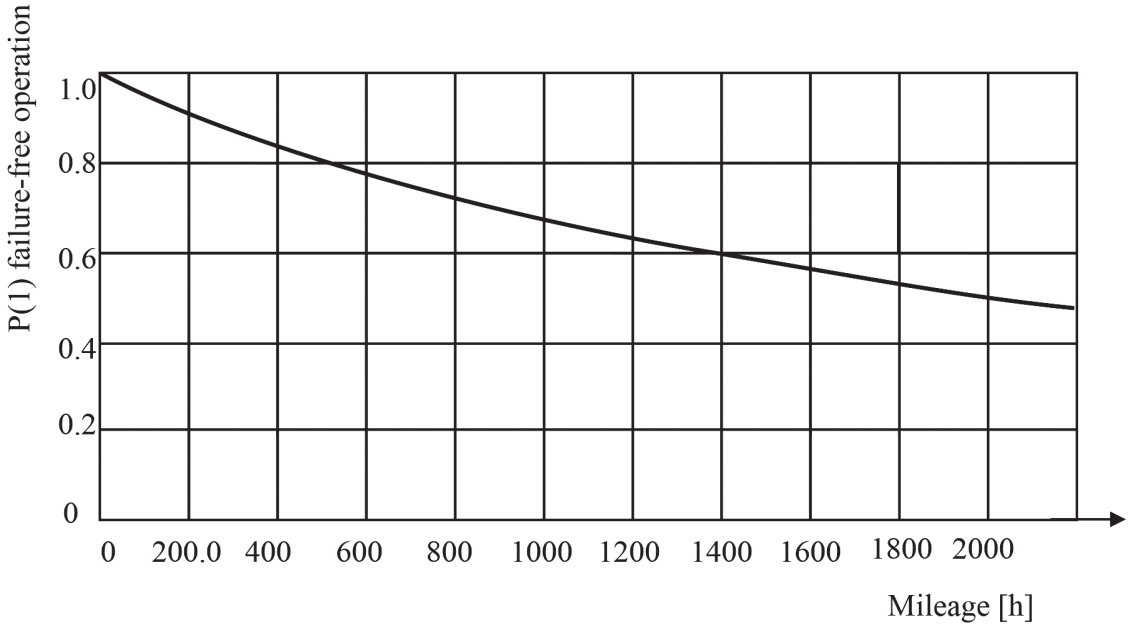

Figure 4 *Graph of the probability of failure-free operation of the rail service car with an exponential distribution law*

4 Results and discussion

The dignity plan (N, U, T_o) allows for a shorter observation period since there is no need to wait until the failure of all objects is reached. Using this monitoring plan, it is possible to assess the following indicators of the main equipment of rail service car: the average time to failure of the items, the probability of trouble-free operation at various runs of the rail service car, the lower and upper failure rates and the percentage resource of the main equipment of rail service car.

As a result, this plan can be efficiently used in practice to assess reliability indicators, given the large number of rail service cars 144 units for "Uzbekistan railways" JSC.

In the data given in Table 2, the following notation applies:

- T_o - is the mean time to failure,
- $P(l)$ - is the probability of failure-free operation at $l = 400 \cdot 10^3 km$,
- $\lambda(l)$ - is the intensity of the failure,
- $\gamma = 90\%$ - denotes the gamma percent resource.

For the selected plan, the average intensity of refusal was calculated as:

$$\hat{\lambda} = \frac{d}{\sum_{i=1}^{d} + (N-d) \cdot T_0} = \\ = \frac{10}{[739.2 + (40-10)] \cdot 10^3 km} = 60 \cdot 10^{-6} \frac{1}{km}. \quad (4)$$

For the calculated λ, the two-sided confidence limits were defined, with a confidence level $\beta = 0.9$.

The lower limit:

$$\lambda_L = \frac{\hat{\lambda} N \chi^2_{\frac{1-\beta}{2}, 2d}}{d\left(2N - d + \frac{1}{2}\chi^2 \frac{1-\beta}{2}, 2d\right)} = \\ = \frac{2.60 \cdot 10^{-6} \cdot 40 \cdot \chi^2_{1\frac{1-0.9}{2}, 2 \cdot 10}}{10 \cdot \left(2 \cdot 40 - 10 + \frac{1}{2}\chi^2_{1\frac{1-0.9}{2}, 2 \cdot 10}\right)} = \\ = 0.115 \cdot 10^{-6} \frac{1}{km} \quad (5)$$

The upper limit:

$$\lambda_u = \frac{\hat{\lambda} N \chi^2_{\frac{1+\beta}{2}, 2d}}{d\left(2N - d + \frac{1}{2}\chi^2_{\frac{1+\beta}{2}, 2d}\right)} = \\ = \frac{2.60 \cdot 10^{-6} \cdot 40 \cdot \chi^2 \frac{1+\beta}{2}, 2d}{10 \cdot \left(2 \cdot 40 - 10 + \frac{1}{2}\chi^2_{2\frac{1+0.9}{2}, 2d}\right)} = \\ = 3.599 \cdot 10^{-6} \frac{1}{km}. \quad (6)$$

Values for $\chi^2_{1\frac{1-0.9}{2}, 2 \cdot 10}$ and $\chi^2_{2\frac{1+0.9}{2}, 2d}$.

We note that $x_1^2 < x_2^2$, therefore, the significance of the chosen law does not contradict the experimental data. The calculated values λ_u and λ_L are covered with a probability of 0.9; the true values of the parameter λ.

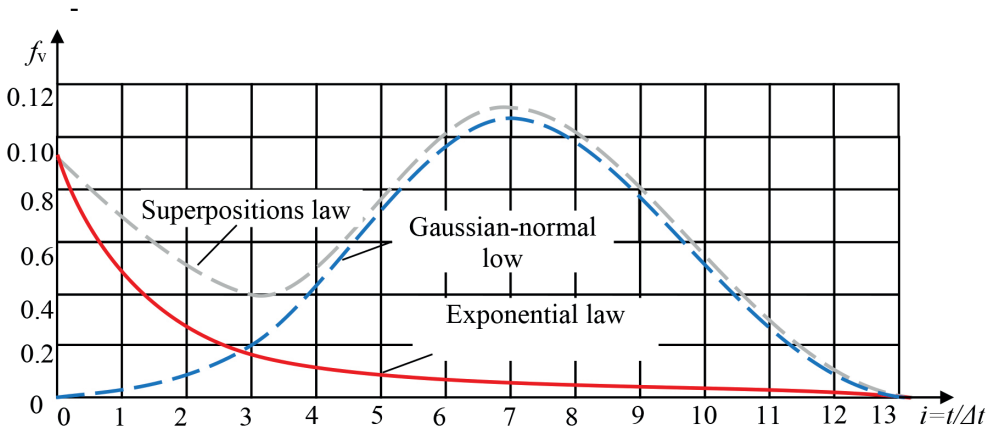

Figure 5 *Overlay of exponential and normal Gaussian laws of distribution of the rail service car time to failure Δt = 1000 km (The colours in this picture have no semantic characters)*

The point estimate of the mean time to failure is:

$$\hat{L} = \frac{1}{\hat{\lambda}} = \frac{1}{2.60 \cdot 10^{-6}} = 384.61 \cdot 10^3 \, km \, . \tag{7}$$

The lower and upper confidence limits of the mean time to failure are:

$$\begin{aligned} L_{av.H} &= \frac{1}{\lambda_L} = \frac{1}{3.599 \cdot 10^{-6}} = 0.277 \cdot 10^6 km; \\ L_{av.B} &= \frac{1}{\lambda_u} = \frac{1}{0.115 \cdot 10^{-6}} = 8.695 \cdot 10^6 km. \end{aligned} \tag{8}$$

Probability of the trouble-free operation, for a mileage l = *400 x 10³* km, is:

$$P(l) = e^{-\hat{\lambda} l} = e^{-2.60 \cdot 10^{-6}} \cdot 400 \cdot 10^3 = 0.361 \, . \tag{9}$$

The probability of failure-free operation is provided in Table 3.

It's worth noting that the probabilities of no-failure operation for runs of *50 x 10³*, *100 x 10³*, *200 x 10³*, *300 x 10³*, and *400 x 10³* km are respectively 0.878, 0.771, 0.594, 0.45, and 0.361 (refer to Figure 4).

Based on the Table 3, we built a Figure 4.

The two-sided confidence limits for P(l) are determined by the calculated values of λ_u and λ_L as:

$$P(l) = e^{-\hat{\lambda}_L l} = e^{-0.115 \cdot 10^{-6} \cdot 400} = 0.9999 \, , \tag{10}$$

$$P(l)_u = e^{-\hat{\lambda}_u l} = e^{-3.599 \cdot 10^{-6} \cdot 400} = 0.99985 \, . \tag{11}$$

The 90 %-gamma percentage resource (γ = *90 %*) is determined as:

$$\begin{aligned} L_{\gamma L} &= \frac{1}{\lambda_L}(-\ln 0.9) = \frac{1}{3.599 \cdot 10^{-6}}(-\ln 0.9) = \\ &= 29.27 \cdot 10^3 km, \end{aligned} \tag{12}$$

$$\begin{aligned} L_{\gamma u} &= \frac{1}{\lambda_u} = \frac{1}{0.115 \cdot 10^{-6}}(-\ln 0.9) = \\ &= 915.6 \cdot 10^3 km. \end{aligned} \tag{13}$$

The ADM type of the rail service cars share a characteristic feature that their failures can be caused by more than one simultaneously acting causes. For example, three-phase actuator motors can fail under the influence of their rotor, causing the phenomenon of eccentricity, wear of internal and external bearing rings, wear of electrical insulation of motors under the influence of heating and overvoltage. Depending on which of the processes develops more intensively, failure of one or joint action of other types occurs. Thus, the total probability of distribution of duration of operation up to the failure of the electromechanical equipment having a clutch, and working on different kinds of loading is a mix, a superposition of several distributions.

The statistical data on duration of operation up to failure of electromechanical equipment of separate units of the rail service car, especially asynchronous motors, working together with a clutch, suggest an overlay of the exponential law and the normal Gaussian law. Figure 5 presents the distribution of distance travelled by the rail service car of the ADM type before failure, confirming the presence of two superposition's.

This superposition can be described by the formula for density distribution:

$$f(l) = K_1 f_1(l) + K_2 f_2(l) \, , \tag{14}$$

where K_1=*0.2* and K_2=*0.8* represent the share of failures distributed exponentially (Exponental law Curve 1 red color) and normally (Gaussian Curve 2 blue color) respectively, as depicted in Figure 4. In the same figure, (Superpositions low Curve 3 grey) represents the total superimposed laws distribution: $f_1(l)$; $f_2(l)$ respectively denote the distribution densities under exponential and normal conditions.

$$\begin{aligned} f_1(l) &= \frac{1}{L_{av.1}} \cdot \exp f_1(l) = \left(-\frac{l}{L_{av.1}}\right) = \\ &= \frac{1}{384.61 \cdot 10^3} \cdot \exp\left(-\frac{400 \cdot 10^3}{384.61 \cdot 10^3}\right) = , \\ &= 0.918 \cdot 10^{-3} \frac{1}{km} \end{aligned} \tag{15}$$

$$f_2(l) = \frac{1}{2\pi\delta} \cdot \exp\left[-\frac{(l - l_{av.2})^2}{2\delta^2}\right] = \\ = \frac{1}{2 \cdot 3.14 \cdot 0.15} \cdot \exp\left[-\frac{(400 - 277)^2}{2 \cdot 0.15^3}\right] = \\ = 0.021 \cdot 10^{-3} \frac{1}{km}, \quad (16)$$

where δ = *0.15* - tis the relative error of the mean value, selected according to the recommended values [3]. We can find the total distribution density by substituting Equations (15) and (16) into Equation (14), resulting in

$$f(l) = 0.2 \cdot 10^{-3} \frac{1}{km}.$$

5 Conclusions

A comprehensive analysis of statistical data, concerning the operation of the ADM type Joint-Stock Company rail service cars, particularly focusing on their power electromechanical equipment, elucidates that the operational state of mechanical, hydraulic, and electrical equipment exhibits complex interdependencies. These dynamically interconnected entities operate across various modes, which underscores the need for a systematic exploration of the quantitative reliability indicators that bear a significant influence on their effective utilization.

The observation plan denoted as [N, U, L_0] facilitates the ascertainment of essential indicators and provides an estimate of the following parameters: L_{av}, denoting the mean time to failure; *P(l)*, representing the probability of failure-free operating time across different runs; *λ(l)*, indicating the lower and upper boundaries of failure rates, and the gamma percent resource when γ is equivalent to *9 0%*.

By applying the test and basing the analysis on the numerical values at specific levels of significance, authors can affirm that the selected law does not contravene the experimental data. The total probability distribution, concerning the failures of electromechanical equipment tends to align with a superposition of both exponential and normal Gaussian laws. The calculation of these distribution densities is of the utmost importance for determining and adjusting the crucial reliability indicators during both the design and operation phases of the rail service car.

By factoring parameters of the main units in the operating mode, the model installation site, the average costs associated with current repairs, and the expenditure incurred during the emergency recovery operations, a mathematical model has been formulated. This model aids in determining the optimal maintenance intervals utilizing uncertain Lagrange multipliers.

The practical implications of this mathematical model extend to the design process and the investigation of fundamental reliability characteristics of the main units. For instance, this model can be effectively applied to assembly platforms of the rail service cars at “Uzbekistan Railways” JSC. This exemplifies the practical application of these models in assessing and enhancing the reliability of rail service car in real exploitation operational scenarios.

Acknowledgments

This work was supported by Agency of innovative development under the Ministry of higher education of the Republic of Uzbekistan [women’s grant number AL-662204208].

Conflicts of interest

The authors declare that they have no known competing financial interests or personal relationships that could have appeared to influence the work reported in this paper.

References

[1] KHROMOVA, G., MUKHAMEDOVA, Z., YUTKINA, I. *Optimization of the dynamic characteristics of emergency recovery railcars*. Tashkent: Scientific Publish, “Science and technology”, 2016. ISBN 978-9943-11-263-6.

[2] Development strategy of Uzbekistan Temir Yollari JSC for the 2015-2019 [online]. Available from: https://www.railway.uz/ru/gazhk/strategiya_razvitiya

[3] GOST 53480-2009. Product diagnostics. General requirements. Publishing House of Standards, 2011.

[4] Instructions for the motorcar. Diesel assembly ADM-1. Operating manual 77.020-00.00.000. Operating instructions of JSC Tikhoretsky Machine. Tikhoretsk: Building Plant named after V.V. Vorovsky, 2003.

[5] ANYAKWO, A., PISLARU, C., BALL, A., GU, F. Modelling and simulation of dynamic wheel-rail interaction using a roller rig. *Journal of Physics: Conference Series* [online]. 2012, **364**(1), 012060. ISSN 1742-6596. Available from: https://doi.org/10.1088/1742-6596/364/1/012060

[6] BOGDEVICIUS, M., ZYGIENE, R. Simulation of dynamic processes of rail vehicle and rail with irregularities. *Journal of KONES. Powertrain and Transport* [online]. 2015, **21**(2), p. 21-26. ISSN 1231-4005, eISSN 2354-0133. Available from: https://doi.org/10.5604/12314005.1133858

[7] BUREIKA, G., SUBACIUS, R. Mathematical model of dynamic interaction between wheel-set and rail track. *Transport* [online]. 2002, **17**(2), p. 46-51. ISSN 1648-4142, eISSN 1648-3480. Available from: https://doi.org/10.3846/16483480.2002.10414010

[8] CHAO, W. Research on fatigue test method of car body for high-speed trains. *IOP Conference Series: Earth and Environmental Science* [online]. 2018, **189**, 062002. ISSN 1755-1315. Available from: https://doi.org/10.1088/1755-1315/189/6/062002

[9] EULITZ, K., KOTTE, K. Damage accumulation - limitations and perspectives for fatigue life assessment. In: Materials Week 2000: proceedings. 2000. p. 25-28.

[10] FAN, S., PING, B., YI, Z., YE, S. Fatigue evaluation of railway vehicle bogie frame by different methods. In: International Conference on Mechanics and Civil Engineering: proceedings [online]. 2014. ISSN 2352-5401, p. 844-852. Available from: https://doi.org/10.2991/icmce-14.2014.150

[11] KUZNETSOV, B., KARDAS-CINAL, V., LUKASHOVA, E., PETRENKO, N., NIKONOV, O., NIKONOV, D. Evaluation of the effectiveness of using an electromechanical shock absorber in a subway car. *Eksploatacja i Niezawodnosc / Maintenance and Reliability* [online]. 2022, **24**(4), p. 603-611. ISSN 1507-2711, eISSN 2956-3860. Available from: https://doi.org/10.17531/ein.2022.4.1

[12] POPP, K., SCHIEHLEN, W. *System dynamics and long-term behaviour of railway vehicles. Track and Subgrade* [online]. Berlin, Heidelberg: Springer Science and Business Media, 2013. ISBN 978-3-642-07864-4. Available from: https://doi.org/10.1007/978-3-540-45476-2

[13] SHARMA, R. CH., DHINGRA, M., PANDEY, R. K., RATHORE, Y., RAMCHANDANI, D. Dynamic analysis of railway vehicles. *Journal of Science*. 2015, **5**(3), p. 193-198. ISSN 2277-3282, eISSN 2277-3290.

[14] SEBESAN, I., BAIASU, D. Mathematical model for the study of the lateral oscillations of the railway vehicle. *UPB Scientific Bulletin. Series D: Mechanical Engineering*. 2012, **74**(2), p. 51-66. ISSN 1454-2358.

[15] SPIRYAGIN, M., COLE, C., SUN, Y. Q., MCCLANACHAN, M., SPIRYAGIN, V., MCSWEENEY, T. *Design and simulation of rail vehicles* [online]. CRC Press, 2014. ISBN 9781498733526. Available from: https://doi.org/10.1201/b17029

[16] SOSNOVSKY, L., SCHERBAKOV, S. Concepts of material damage. *Bulletin of TNTU*. 2011, Special volume 1, p. 14-23. ISSN 2071-7296. https://elib.bsu.by/handle/123456789/12309

[17] TRETYAKOV, A. *Managing the individual resource of wagons in operation*. Saint Petersburg, OM-Press Publishing House LLC, 2004. ISBN 5-901739-08-6.

[18] TRETYAKOV, A. *Extending the service life of rolling stock*. Publishing house OM Press St. Petersburg, 2011. ISBN 978-5-902445-56-2.

[19] TRETYAKOV, A. *Managing the individual resource of wagons in operation*. Saint Petersburg, OM-Press Publishing House LLC, 2004. ISBN 5-901739-08-6.

[20] VASILYEV, V. *A short course on the strength of materials with the basics of the theory of elasticity: textbook*. St. Petersburg: Ivan Fedorov, 2001. ISBN 5-87685-045-4.

[21] ZHOU, Z., CHEN, Z., SPIRYAGIN, M., ARANGO, E., WOLFS, P., COLE, C., ZHAI, W. Dynamic response feature of electromechanical coupled drive subsystem in a locomotive excited by wheel flat. *Engineering Failure Analysis* [online]. 2021, **122**(1-2), 105248. ISSN 105248. ISSN 1350-6307, eISSN 1873-1961. Available from: https://doi.org/10.1016/j.engfailanal.2021.105248

[22] BRUNI, S., VINOLAS, J., BERG, M., POLACH, O., STICHEL, S. Modelling of suspension components in a rail vehicle dynamics context. *Vehicle System Dynamics* [online], 2011, **49**(7), p. 1021-1072. ISSN 0042-3114, eISSN 1744-5159. Available from: https://doi.org/10.1080/00423114.2011.586430

[23] BRUNI, S., GOODALL, R., MEI, T., TSUNASHIMA, H. Control and monitoring for railway vehicle dynamics. *Vehicle System Dynamics* [online]. 2007, **45**(7-8), p. 743-779. ISSN 0042-3114, eISSN 1744-5159. Available from: https://doi.org/10.1080/00423110701426690

[24] EVANS, J., BERG, M. Challenges in simulation of rail vehicle dynamics. *Vehicle System Dynamics* [online]. 2009, **47**(8), p. 1023-1048. ISSN 0042-3114, eISSN 1744-5159. Available from: https://doi.org/10.1080/00423110903071674

[25] CARLBOM, P. Combining MBS with FEM for rail vehicle dynamics analysis. *Multibody System Dynamics* [online]. 2001, **6**, p. 291-300. ISSN 1384-5640, eISSN 1573-272X. Available from: https://doi.org/10.1023/a:1012072405882

[26] AUCIELLO, J., MELI, E., FALOMI, S., MALVEZZI, M. Dynamic simulation of railway vehicles: wheel/rail contact analysis. *Vehicle System Dynamics* [online]. 2009, **47**(7), p. 867-899. ISSN 0042-3114, eISSN 1744-5159. Available from: https://doi.org/10.1080/00423110802464624

[27] LEE, Y.-L., PAN, J., HATHAWAY, R., BARKEY, M. *Fatigue testing and analysis: theory and practice*. 1. ed. Burlington: Elsevier Butterworth-Heinemann, 2004. ISBN 9780750677196. eISBN 9780080477695.

[28] MUKHAMEDOVA, Z. G., IBADULLAEV, A. S., MAMAEV, S. I. Calculation of remaining life and extending the service life of special self-propelled rolling stock. *Universum: Technical Sciences* [online]. 2022, **2**(95), p. 1-5. ISSN. 2311-5122. Available from: https://7universum.com/ru/tech/archive/item/13085

[29] KRUTOVA, V. A., FEDOTOV, K. A. Analysis of the causes of malfunctions in diesel motor trails during their operation. *Bulletin of the Rostov State Transport University*. 2022, **3**(87), p. 72-79. ISSN 0201-727X.

[30] ROMEN, Y. S. Wheel pair for studying the forces of interaction between the rail vehicle and the way. In: *Rail vehicle dynamics and associated problems*. Gliwice: Silesian University of Technology, 2005. ISBN 83-7335-239-2, p. 115-121.

[31] KHROMOVA, G., MUKHAMEDOVA, Z., YUTKINA, I. Mathematical model of oscillations of bearing body frame of emergency and repair railcar. *Transport Problems* / *Problemy Transportu* [online]. 2017, **12**(1), p. 93-103. ISSN 1896-0596. Available from: https://doi.org/10.20858/tp.2017.12.1.9

EFFECT OF ENVIRONMENTAL CONDITIONS ON CURING OF POLYURETHANE ADHESIVE INVESTIGATED WITH FTIR ANALYSIS

Péter I. Kovács[1,2], Zoltán Weltsch[2], Miklós Berczeli[1,*]

[1]Department of Innovative Vehicles and Materials, GAMF Faculty of Engineering and Computer Science, John von Neumann University, Kecskemet, Hungary
[2]Department Road and Rail Vehicles, Szechenyi Istvan University, Gyor, Hungary

*E-mail of corresponding author: berczeli.miklos@nje.hu

Péter I. Kovács 0000-0003-1268-9362, Zoltán Weltsch 0000-0002-6366-8281, Miklós Berczeli 0009-0004-7187-9064

Resume
The use and significance of adhesives in various industries are explored, highlighting the growth of the adhesive market and the crucial role of time in adhesive bonding. The composition of adhesives, particularly polyurethane adhesives (PUR), is detailed, emphasizing their sensitivity to environmental factors, like moisture and UV radiation. Various factors influencing adhesive properties, such as reactivity and curing-induced shrinkage, are discussed, along with the importance of catalysts in adjusting reaction rates. One-component moisture-curable PUR adhesives are presented as versatile and continually improving alternatives in structural adhesive applications. The research's focus was to investigate the curing speed of Sikaflex-252 1-component PUR structural adhesive under different conditions, including room temperature, room temperature with ~30 % humidity, and room temperature with ~100 % humidity.

Article info
Received 8 November 2023
Accepted 21 December 2023
Online 7 March 2024

Keywords:
polyurethane
curing
influence of environment

Available online: https://doi.org/10.26552/com.C.2024.024

ISSN 1335-4205 (print version)
ISSN 2585-7878 (online version)

1 Introduction

The majority of PUR adhesives are quite insensitive to moisture penetration [1]. For adhesives that cure with moisture, saturation with moisture does not lead to a reduction in values. The PUR adhesives consist of hard and soft segments. The soft segments are usually derived from hydroxyl-terminated polyester, polyether, polybutadiene or polyisobutylene polyols, while the hard segments (HS) contain isocyanates and diamine chain-extending moieties [2]. Increasing the HS content generally increases the elastic modulus and reduces elongation. Therefore, by varying these two types, the properties of PUR adhesives can be varied [3]. Polyurethanes are mainly made up of difunctional and trifunctional OH-terminated molecules that react with di- or triisocyanates [4]. The length and stiffness of the chain determine the mechanical properties of the final polymer. The chain can be made up of polyethers, which makes them flexible and hydrophilic, polyesters, which provide greater stiffness, polycarbonates or other OH- or NH-terminated molecules [5].

The concentration of the trifunctional molecules, which can be either the OH or isocyanate component, determines the cross-linking density, a factor influencing the stiffness pattern [6-7]. A structural adhesive must have trifunctional groups to guarantee a covalent three-dimensional network, otherwise it would have thermoplastic properties. In some places, curing-induced volume shrinkage plays a prominent role. If a thick layer of adhesive is not allowed or able to move during the curing due to spacers or other design constraints, shrinkage will cause significant stress, reducing the load-bearing capacity of the bond. The PURs based on prepolymers show less shrinkage and thermal expansion during curing. The building blocks of adhesives also have different reactivity, and catalysts are needed to adjust these reaction rates. However,

too fast reactions can cause problems in wetting, as the liquid adhesive must first fully wet the surface to achieve adhesion before it solidifies, and if solidification is faster than wetting, adhesion can be significantly reduced [8-9].

Moisture curing adhesives cure by the diffusion of moisture into the adhesive, a process controlled only by the rate of water diffusion, which also depends on temperature and humidity, and hydrophilic/hydrophobic properties. Water must be added to accelerate the cross-linking reaction of the moisture-curing adhesive. This is not easy, because even very small amounts of water are difficult to mix into a water-repellent, highly viscous material, but it can be done by adding a specially formulated water paste (booster) [10]. Curing takes place slowly through the humidity, even without a booster. Booster systems are used when thick bond lines are required for materials with no or slow diffusion of water vapour. A problem in such applications may be a tendency to bubble formation caused by rapid curing with large amounts of water [11]. Adhesives are strongly influenced by the properties of the environment in which they are used [12-13]. One example is the PUR type adhesive we use as our primary adhesive, which crosslinks more quickly as the humidity in the environment increases. In addition to ambient humidity, another influencing factor is temperature, although this is more important for two-component adhesives. In addition to the two factors mentioned above, boosters are the third accelerating factor, but these are optional. Without a booster, the process is slower and may not be complete, but the reaction does not take place below water (humidity) or below a minimum temperature. During our experiments we did not use the help of boosters.

The aim of our research was to investigate the speed of different cross-linking processes; to compare the reaction rates of Sikaflex-252 1-component PUR structural adhesive crosslinked at room temperature, crosslinked at room temperature and ~30 % humidity, crosslinked at room temperature and ~100 % humidity.

2 Description of adhesives tested and test methods

2.1 SIKAFLEX-252

Sikaflex-252 is a structural adhesive. The adhesive is a one-component polyurethane (PUR) that crosslinks when exposed to moisture. It is suitable for bonding under dynamic loads. It can be applied on many faces to substrates of different materials, such as wood, plastics, ceramics, aluminium, steel and other metals. It also has good vibration damping, is electrically non-conductive and has a high elongation at break. The bonding of sikaflex-252 adhesive is not among the fastest bonding adhesives, nor even among the fast ones, as it bonds to moisture [9].

3 Description of the test procedure

3.1 Fourier transform infrared spectroscopy

The measurement instrument is a JASCO 4600 FT-IR spectrometer, characterized by a measurement range spanning from 7800 to 350 cm^{-1}. With a resolution capability of up to 0.7 cm^{-1}, this instrument is versatile, accommodating both transmission and reflection measurements. Additionally, it features a rapid scan function, allowing for the swift data acquisition at a rate of up to 7-8 measurements per second.

3.2 Description of the test procedure

In our experimental investigations, our primary objective was to assess the cross-linking kinetics and reaction rates of adhesives. This encompassed examining the variation in cure rates among different formulation types and assessing the cross-linking rate of specific single-component adhesives (PUR) undergoing curing in the presence of moisture across diverse humidity conditions. To ensure precise measurements, each sample was positioned on polyethylene foil with spectroscopy serving as a recorded background. Furthermore, each sample was affixed to a wooden sample holder, which remained undisturbed until the completion of the tests. Samples subjected to 100 % humidity for cross-linking were placed in a desiccator containing water, as opposed to silica gel typically used for drying and dehumidification. This modification aimed to establish the appropriate humidified environment within the enclosed system. Our measurements demonstrated a remarkable consistency across all adhesive materials. The process involved meticulous sample placement, selection of the background assigned to each sample, and execution of the measurement program in the FTIR, generating results from 64 measurements recorded in transmittance. The post-measurement steps included identifying the reaction group, applying baseline fitting if necessary, and converting results to absorbance. The recorded data were documented within absorbance-converted measurements. Subsequent to this, results were calculated using the method described below and graphically plotted, providing a visual representation of the obtained data.

4 Results and evaluation

In the presentation of our findings, a comprehensive analysis of the binding speed for each sample is provided, along with an examination of the variation in binding

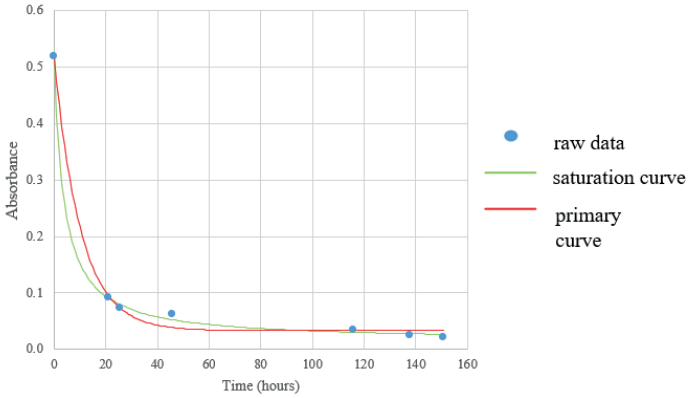

Figure 1 *Cross-linking of sample A*

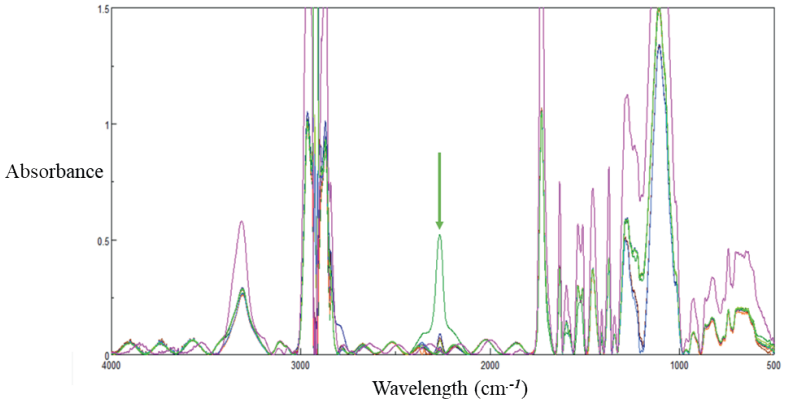

Figure 2 *Results of measurement "A" in FTIR Spectra Analysis*

speed among sample pairs. It is important to note that the sample pairs exclusively pertain to the single-component polyurethane structural adhesive and the single-component silicone sealant adhesives. All the measurements and cross-linking were performed at the accredited laboratory permissible temperature. The results never reach 0 or a certain number, so they were considered cross-linked only when the values of the reaction groups had not been greatly reduced. The values do not remain constant even for "fully" cross-linked adhesives, either because of minimal inaccuracy of the measuring equipment or because of the continuous decomposition and re-bonding of the reaction groups. To minimise the influence on the results of the measurement, the samples were placed in a separate holder for each of them. Thus, each adhesive was named with an assigned letter.

4.1 Sikaflex-252

4.1.1 "A" Sample - Investigation of curing chemical composition in normal 50% humidity condition

The aim of sample A was to find the reaction group and to know the total cross-linking time. Here a problem arose, as shown in Figure 1, that during the first 20 hours, shown in Figure 2, the absorbance of the material decreased sharply, making the calculation of the reaction rate inaccurate.

For this reason, the half hourly time interval measurements were required for the first 4 hours of the glue. More frequent measurements would have affected adhesives that crosslinked at 100% humidity.

In Sikaflex-252, a polyurethane, one-component adhesive, the reaction group is located around ~2265. In Figure 3, the green arrow indicates the location of the reaction group. In Figure 4, the reaction direction is visible.

Given groups are located at a given wavenumber, these general locations are shown in Figure 5, they can only be shifted slightly. Based on Figure 6, the reaction group is isocyanide. Isocyanide (also known as isonitrile or carbylamine) is an organic compound with the functional group $N \equiv C$. It forms bonds through nitrogen.

4.1.2 "B" Sample - Curing mechanism in outdoor, unconditioned environment of PUR adhesive

The "B" pattern is a nearly 100% cross-linked adhesive. The sample was measured in FTIR in an outdoor environment with 30-40% humidity.

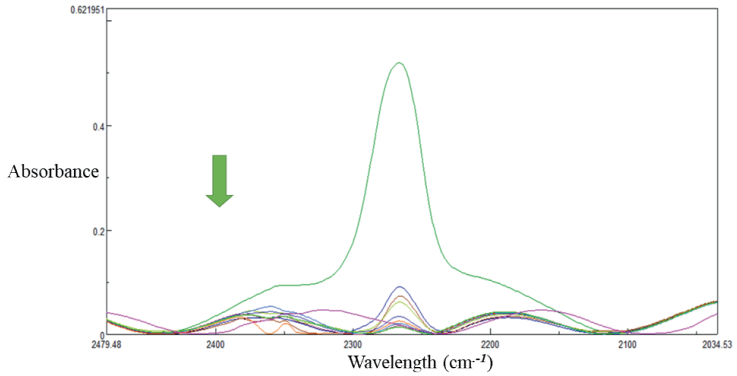

Figure 3 *Results for reaction groups in sample A with direction of change in absorbance*

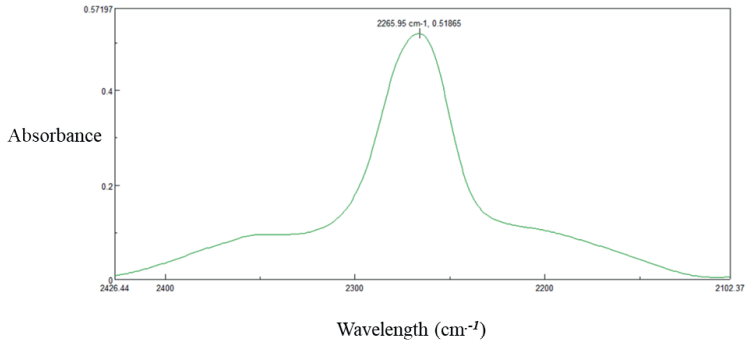

Figure 4 *Reaction group with peak at wavelength 2265*

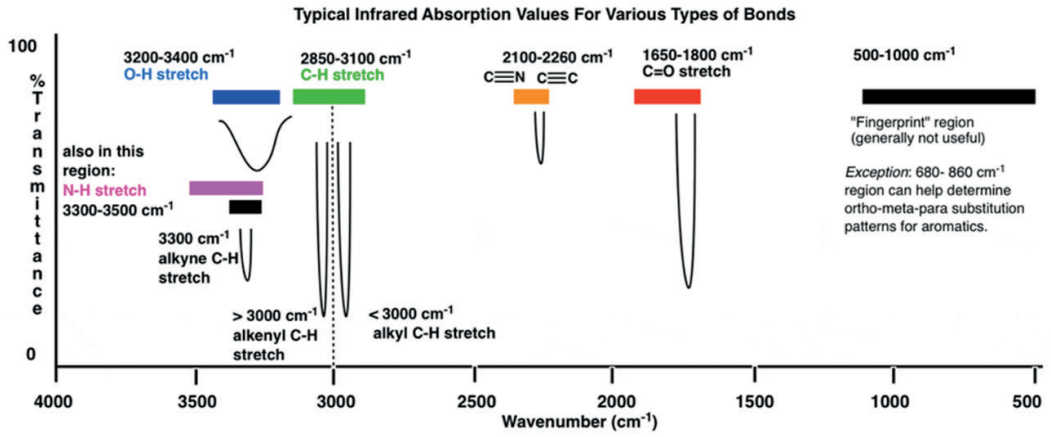

Figure 5 *General locations of different joints*

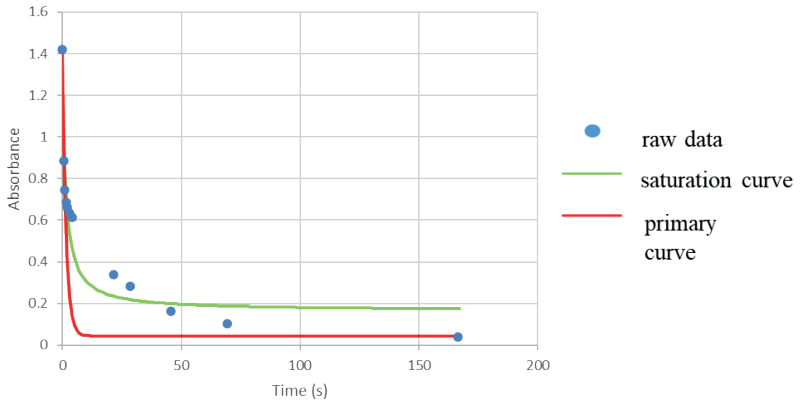

Figure 6 *Cross-linking of sample B*

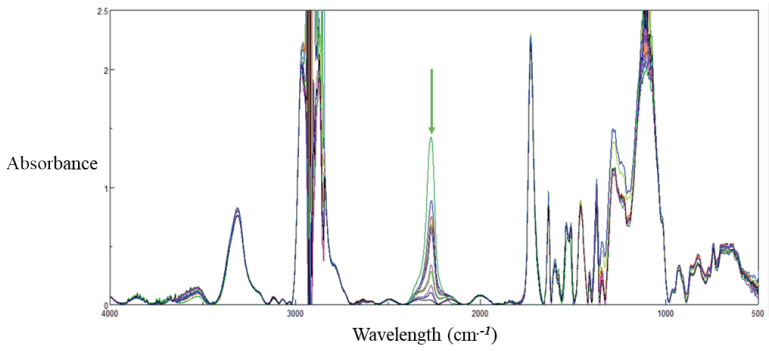

Figure 7 *Results of measurement "B" in FTIR Spectra Analysis*

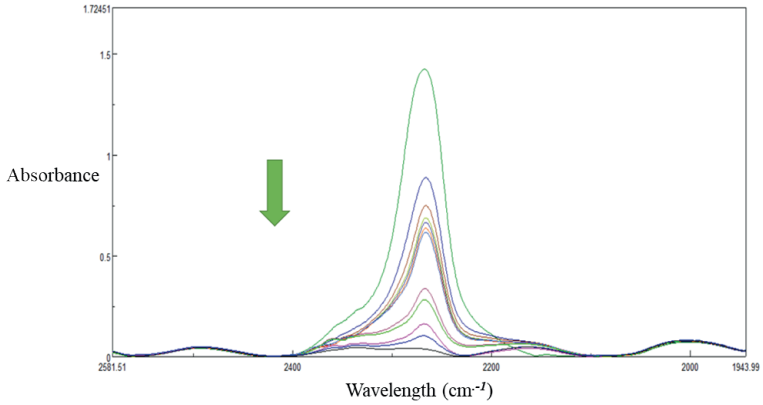

Figure 8 *Results for reaction groups in sample B with direction of change in absorbance*

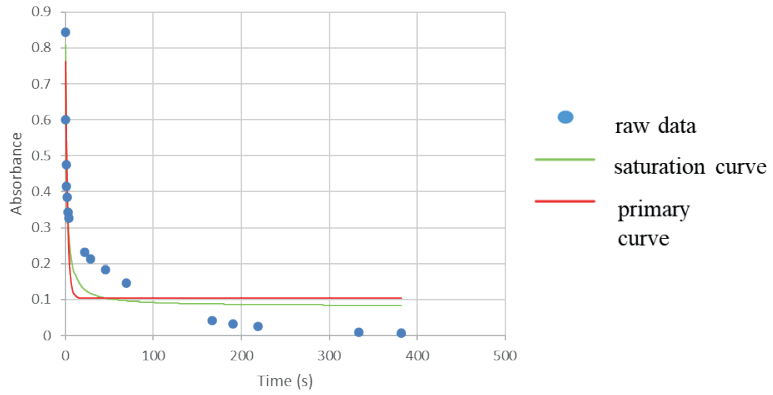

Figure 9 *Cross-linking of sample "C"*

As can be seen, the absorbance varied steeply during the first 4 hours (Figure 7). The reaction rate was the highest here and as time went on, the cross-linking process slowed down as the number of reactive groups decreased (Figure 8).

4.1.3 „C" sample - Curing mechanism in 30% humidity in laboratory, controlled environment of PUR adhesive

In Figure 9 sample C was solidified in a laboratory environment of ~30 % humidity and 24 ± 5 °C. As seen in sample B, the reaction is the fastest in the first 4 hours and gradually slows down (Figure 10). The decreasing of the absorbance in the FTIR results can be seen in higher resolution in Figure 11.

4.1.4 Comparison of samples B and C to determine the humidity difference

In Figure 12 the results show that the glue in the humid environment reached the cross-linked state one day earlier, but it is difficult to distinguish the onset of the cross-linked state, as the initial state is considered to be similar for both samples.

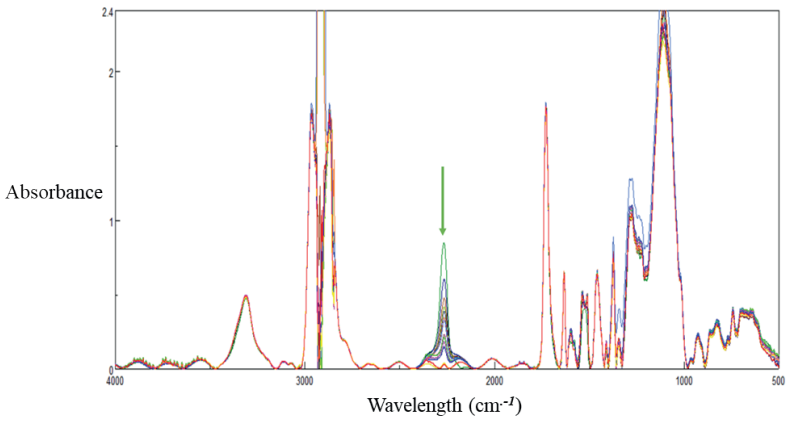

Figure 10 *"C" measurement results in the FTIR Spectra Analysis program*

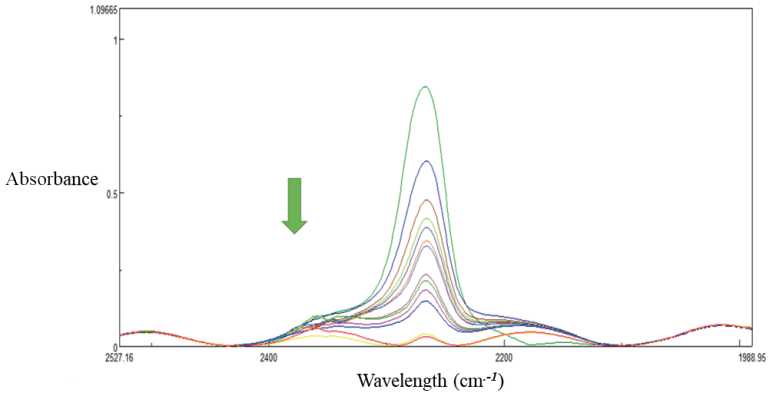

Figure 11 *Results for reaction groups in sample C with direction of change in absorbance*

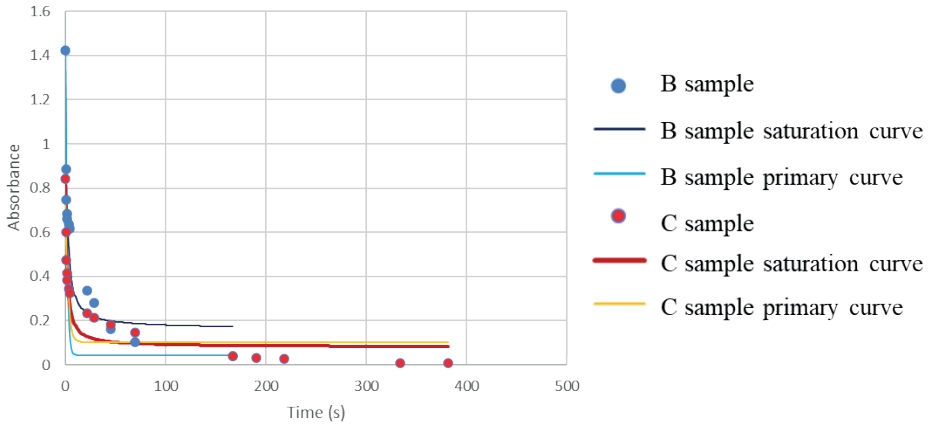

Figure 12 *Crosslinking speed of sample pair B and C relative to each other*

4.1.5 „D" sample - Curing mechanism in 80% humidity in laboratory, controlled environment of PUR adhesive

The results of the higher 80% humidity samples can be seen in Figures 13 and 14. The results show that higher humidity increases the starting procedure of curing or PUR. In Figure 15 a decreasing tendency of absorbance can be seen in the chemical groups during the FTIR.

4.1.6 „E" sample - Curing mechanism in 60% humidity in laboratory, controlled environment of PUR adhesive

The curing of sample E, at 60% humidity, took 14 days (Figure 16). Thus, confirming the claim that in a humid environment, the reaction rate is faster. In Figures 17 and 18 the decreasing tendency of the absorbance of reaction groups can be seen in details.

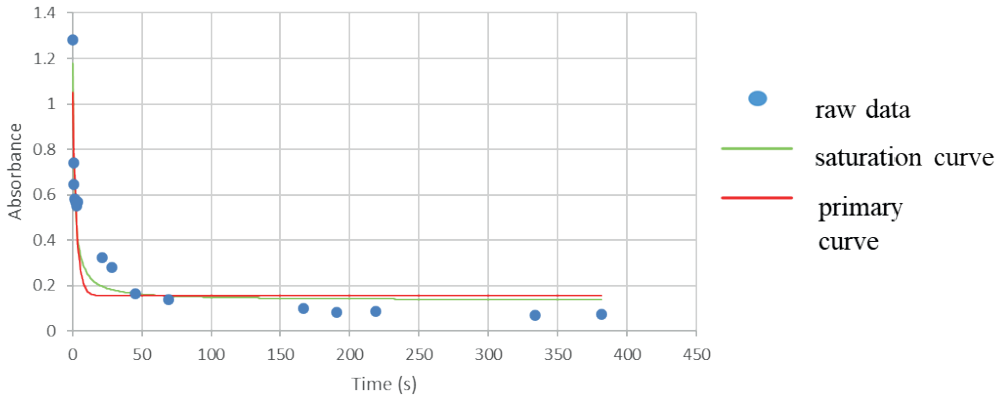

Figure 13 *Cross-linking of sample D*

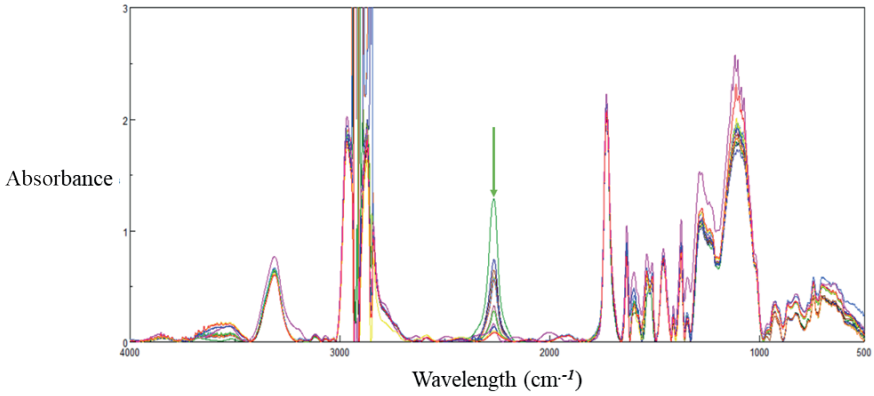

Figure 14 *"D" measurement results in FTIR Spectra Analysis*

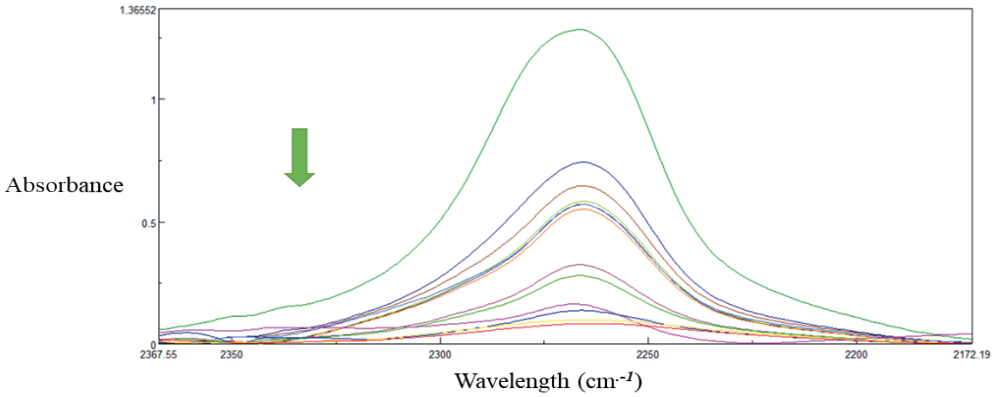

Figure 15 *Results for reaction groups in sample D with direction of change in absorbance*

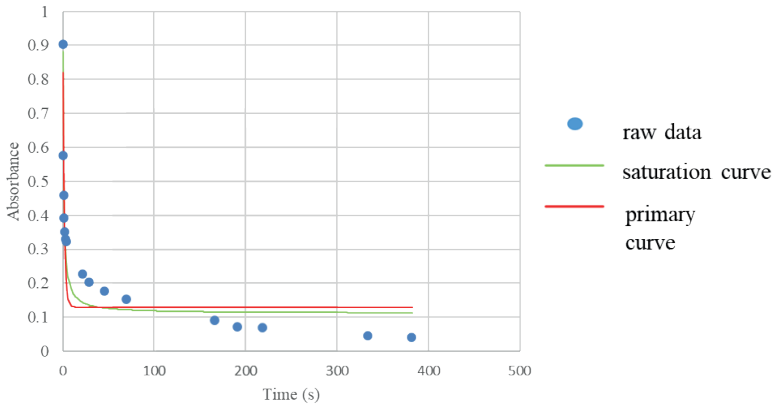

Figure 16 *"E" sample cross-linking*

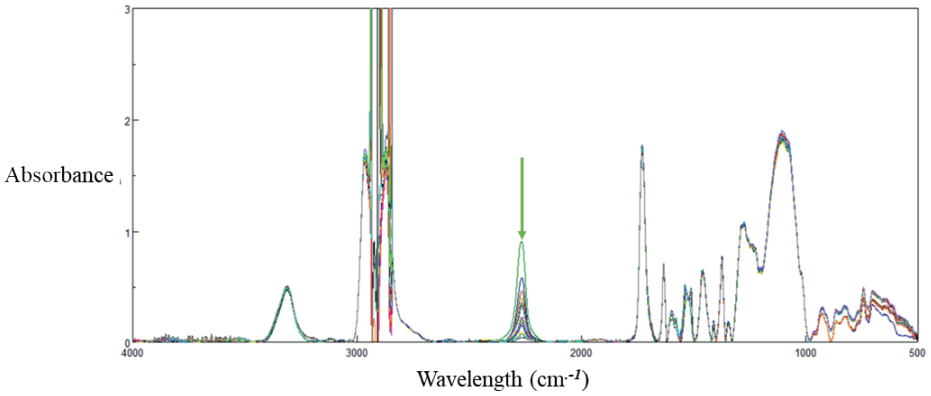

Figure 17 *"E" measurement results in FTIR Spectra Analysis*

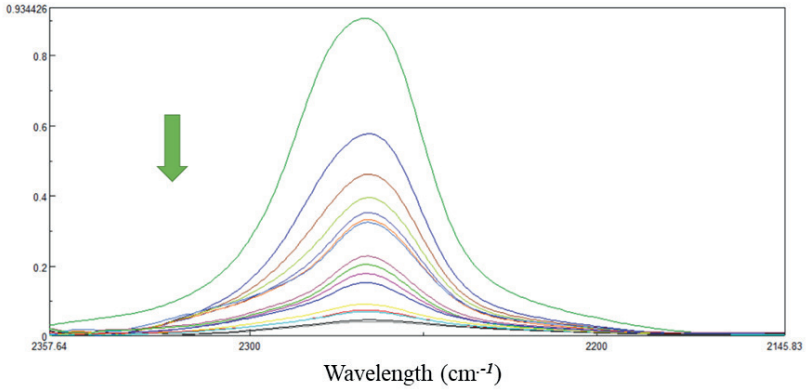

Figure 18 *Results for reaction groups in sample E with direction of change in absorbance*

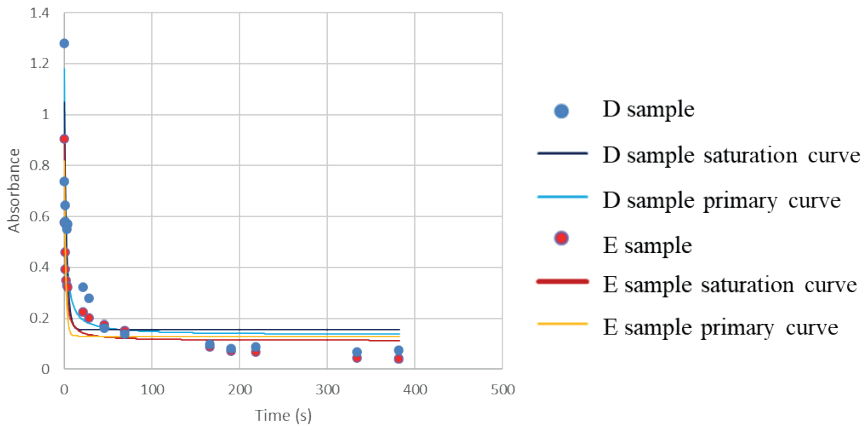

Figure 19 *Cross-linking speed of sample pair "D" and "E" relative to each other*

4.1.7 Comparison of "D" and "E" sample to investigate the effect of humidity

In Figure 19. The results show that adhesive in the higher humidity environment cured much faster. Here, as in the two measurements above, the first 4-8 hours have the highest reaction rate. The results obtained show that the humidity plays an increasingly important role towards the end of the crosslinking process, with almost no difference between the two environments at the beginning and a steadily increasing role as the crosslinking process progresses.

5 Summary

The first objective of this research was to study the Sikaflex-252 structural adhesive; reaction group that induces cross-linking and the speed and difference of this cross-linking with respect to a counterpart in

another environment. This study was concerned with the reaction rate constants of the reaction groups of the material. The results suggest that the cross-linking rate of the adhesive varies significantly with the environment. Humidity plays an increasingly important role in bond formation over time. The second objective was to investigate the cross-linking rates of other types of adhesives and to gain a broader understanding of them. Upon scrutinizing the results, we have arrived at the conclusion that the environmental factors are not to be neglected in the context of bonding. Consequently, the surrounding environment holds significant importance in the application of adhesives. In our forthcoming research, authors aim to further enhance their understanding of adhesives and explore materials that were not included in the current experiments. Additionally, authors plan to conduct the further research employing alternative methodologies.

Acknowledgements

This work was supported by the 2020-1.1.2-PIACI-KFI-2021-00260 Grant. The authors are grateful to the scholars cited in this paper, and their research results have given a lot of inspiration to this work. Special thanks to the department of Innovative Vehicles and Materials at John von Neumann university for their support.

Conflicts of interest

The authors declare that they have no known competing financial interests or personal relationships that could have appeared to influence the work reported in this paper.

References

[1] PETRIE, E. M. *Handbook of adhesives and sealants*. McGraw Hill Professional, 2004. ISBN 978-1260440447.

[2] BURCHARDT, B. Advances in polyurethane structural adhesives. In: *Advances in structural adhesive bonding* [online]. DILLARD, D. A. (ed.). Woodhead Publishing, 2010. ISBN 978-1-84569-435-7, p. 35-65. Available from: https://doi.org/10.1533/9781845698058.1.35

[3] DA SILVA, A. L. D., MARTIN-MARTINEZ, J. M., BORDADO, J. C. M. Influence of the free isocyanate content in the adhesive properties of reactive trifunctional polyether urethane quasi-prepolymers. *International Journal of Adhesion and Adhesives* [online]. 2006, **26**(5), p. 355-362. ISSN 0143-7496, eISSN 1879-0127. Available from: https://doi.org/10.1016/J.IJADHADH.2005.06.001

[4] NARAGHI, T., NOBARI, A. S. Identification of the dynamic characteristics of a viscoelastic, nonlinear adhesive joint. *Journal of Sound and Vibration* [online]. 2015, **352**, p. 92-102. ISSN 0022-460X, eISSN 1095-8568. Available from: https://doi.org/10.1016/J.JSV.2015.05.010

[5] GAMA, N., FERREIRA, A., BARROS-TIMMONS, A. Cure and performance of castor oil polyurethane adhesive. *International Journal of Adhesion and Adhesives* [online]. 2019, **95**, 102413. ISSN 0143-7496, eISSN 1879-0127. Available from: https://doi.org/10.1016/J.IJADHADH.2019.102413

[6] Adam, B., Weltsch, Z. Thermal and mechanical assessment of PLA-SEBS and PLA-SEBS-CNT biopolymer blends for 3D printing. *Applied Sciences* [online]. 2021, **11**(13), 6218. eISSN 2076-3417. Available from: https://doi.org/10.3390/app11136218

[7] An introduction to MMA structural adhesives - SciGrip [online] [accessed 2023-06-22] Available from: https://www.compositesworld.com/cdn/cms/cw_whitepaper_scigrip_mma_intro.pdf

[8] KUN, K., LISKA, J., WELTSCH, Z. Replication of microstructures formed by femtosecond laser during injection moulding. In: *Advances in manufacturing engineering and materials II* [online]. CHATTOPADHYAYA, S., KROLCZYK, G. M., PUDE, F., KLICHOVA, D., HLOCH S. (Eds.). Cham: Springer International Publishing, 2021. ISBN 978-3-030-71955-5, eISBN 978-3-030-71956-2, p. 11-290. Available from: https://doi.org/10.1007/978-3-030-71956-2_24

[9] BERCZELI, M., WELTSCH, Z. Enhanced wetting and adhesive properties by atmospheric pressure plasma surface treatment methods and investigation processes on the influencing parameters on HIPS polymer. *Polymers* [online]. 2021, **13**(6), 901. eISSN 2073-4360. Available from: https://doi.org/10.3390/polym13060901

[10] Polyurethane adhesives market size worldwide from 2016 to 2026 (in million US dollars) - Statistics [online] [accessed 2023-06-22] Available from: https://www.statista.com/statistics/1304804/global-polyurethane-adhesives-market-size/

[11] TAJTI, F., BERCZELI, M. Development of high power femtosecond laser microstructures on automotive stainless steel. *IOP Conference Series: Materials Science and Engineering* [online]. 2020, **903**, 12025. ISSN 1757-899X. Available from: https://doi.org/10.1088/1757-899X/903/1/012025

[12] KUN, K., WELTSCH, Z. Research of the effect of macrogeometric structures on the melt front using simulation. In: *Advances in manufacturing engineering and materials II* [online]. CHATTOPADHYAYA, S., KROLCZYK, G. M., PUDE, F., KLICHOVA, D., HLOCH S. (Eds.). Cham: Springer International Publishing, 2021. ISBN 978-3-030-71955-5, eISBN 978-3-030-71956-2, p. 282-289. Available from: https://doi.org/10.1007/978-3-030-71956-2_23

[13] Automotive adhesive tapes market - Straits [online]. Available from: https://straitsresearch.com/report/automotive-adhesive-tapes-market

PITS TRANSPORTING SYSTEM FROM PITTER FRUIT MACHINE - CASE STUDY

Łukasz Nowakowski, Piotr Kurp*, Michał Skrzyniarz, Sławomir Błasiak, Wojciech Depczyński

Faculty of Mechatronics and Mechanical Engineering, Kielce University of Technology, Kielce, Poland

*E-mail of corresponding author: pkurp@tu.kielce.pl

Łukasz Nowakowski 0000-0002-2425-7295,
Michał Skrzyniarz 0000-0003-4590-5842,
Wojciech Depczyński 0000-0001-5574-4937
Piotr Kurp 0000-0002-1001-5033,
Sławomir Błasiak 0000-0001-7333-4026,

Resume

The paper presents the construction and technological aspects of a device for pitting fruit, especially cherries, on an industrial scale.
The presented work includes design solutions related to the transport of pits removed from pitted fruit, as well as a gravity chute, with an indication of potential operational problems related to the machine design. The authors proposed the use of a screw conveyor, especially in the case of longer drums, to optimize the process. Some analyses are also presented, including friction occurring during the transport of pits. Ultimately, a specific design concept is presented that integrates the screw conveyor with the pitting drum. The presented conclusions point to practical technological and engineering aspects related to fruit processing, suggesting the potential for innovative solutions in the design of pitters.

Article info

Received 23 January 2024
Accepted 5 March 2024
Online 11 March 2024

Keywords:

pits transport
stone transport
screw conveyor

Available online: https://doi.org/10.26552/com.C.2024.025

ISSN 1335-4205 (print version)
ISSN 2585-7878 (online version)

1 Introduction

Removing the pit (stone[1]) from the fruit is necessary when preparing preserves, jams or compotes, and in the production of e.g. candied fruit, for decorating baked goods, etc. [1-2]. Initially, this activity was performed manually using simple and generally available tools. Currently, this activity is performed using specialized equipment for industrial scale applications. A pitter is a device used to remove pits from drupes (those with pits) such as cherries, sweet cherries, Mirabelle plums, plums, olives and others. Unlike pulpers, the pitter minimally damages the fruit, leaving it whole. Generally, devices of this type can be divided into manual, semi-automatic and automatic. In addition, pitting machines can be devices for home-use and industrial-use. In the case of home-use pitters, we distinguish between manual and mechanical pitters. They generally have a simple structure and are characterized by low efficiency. Industrial pitters are automated devices with high efficiency of up to 300 kg/h - some devices offered on the market have a capacity of up to 1200 kg/h. Such devices can be generally divided into drum pitters (the element with slots for fruit is a drum) and belt pitters (the element with slots for fruit is a belt or ribbon) [3-5].

The system for transporting pits from pitters should be designed in such a way as to minimize losses, ensure the efficiency of the process and maintain high quality pits (used in further processing, e.g. for planting or as an intermediate product for pellet production). Adapting the system to the specific needs and pit type is key to achieving optimal results.

Currently used solutions for the system of transporting pits from a fruit pitting device in the form of a pitter, especially a drum pitter, use a chute (inclined plane). After pitting the fruit, the pit falls into the chute, which has a ramp set at an appropriate angle, allowing the pit to move by gravity and thus evacuate it from the pitting machine. A diagram of the current solution is shown in Figure 1.

This solution is very simple and effective. However, a problem occurs when the drum used has more than

1 *Pit fruit (stone fruit) - the seed or stone in the middle of various foods such as: olives, peaches, cherries, apricots, avocados, and plums*. The authors of this paper decided to use the name "pit", but it is an equal name "stone".

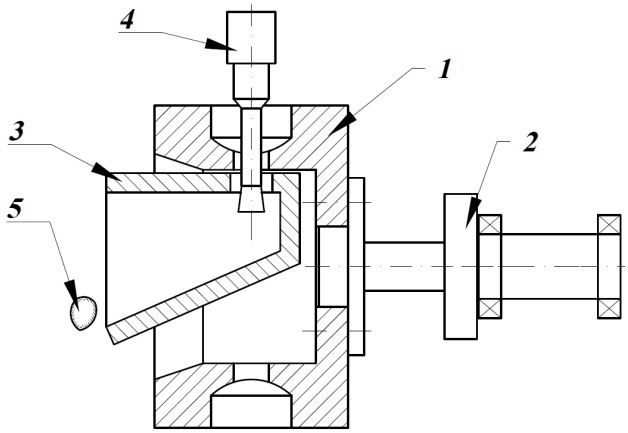

Figure 1 *Scheme of the solution for evacuating a cherry pit using a gravity chute. 1 - pitter drum with fruit slots, 2 - drum drive shaft, 3 – gravity chute, 4 – pitter tip, 5 – evacuated pits*

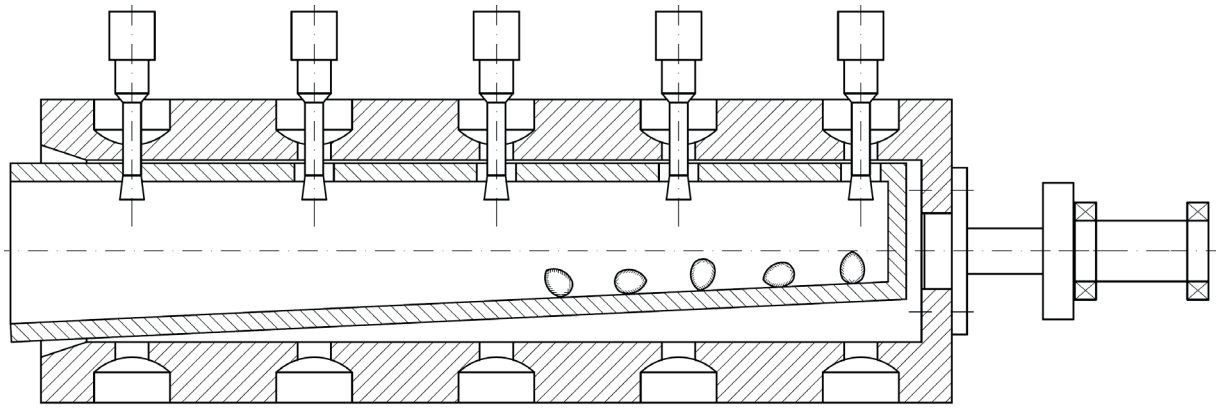

Figure 2 *Chute for a longer drum. The angle of discharge decreases significantly*

one row of slots located around its circumference. In this case, the length of the entire drum increases and, as a result, the angle of inclination of the chute decreases. This is schematically shown in Figure 2.

If the internal diameter of the drum is (standard) 60 mm (which allows for the arrangement of eight sockets around the circumference) and its length, determining the length of the chute, is 300 mm, the angle of the chute is reduced below 1.5°. It is assumed that the minimum effective angle of gravity chute should be 5° to 8° (typically, due to the most reliable evacuation of the pits, the angle is between 30° to 60°). At an angle of 1.5° and less, there is a high probability that the pits will not slide down the chute by gravity and will get stuck on its surface. This state of affairs is determined by the fact that the pit itself is covered with juice and fruit remains, which gives it certain adhesive properties and increases the possibility of "sticking" to the surface of the chute with too small an angle of inclination.

One of the ways to improve the efficiency of the pits' evacuation from the chute is to increase the angle of inclination, which requires increasing the internal diameter of the drum for a given length of the chute. Due to design reasons, this solution is not always possible, as it would significantly increase the overall dimensions of the entire device. The second solution used in such a case is a water jet, whose task is to rinse the pits. The disadvantage of this solution is the need to use clean water, which must be discharged into the sewage system or subjected to a purification process. Therefore, the authors of this article propose to use a screw conveyor for the process of transporting pits, which is driven directly from the stoner drum.

2 Materials and methods

The material for research and analysis were the cherry pits, the dimensions and properties of which are presented in Figure 3 and Table 1. The research was carried out on 100 cherry pits. The measurements were calculated according to the following relationships [6-7]:

$$d_g = \sqrt[3]{a \cdot b \cdot c}\,, \tag{1}$$

$$S = \frac{d_g}{b} \cdot 100\,, \tag{2}$$

$$\upsilon = \frac{a \cdot b \cdot c}{6} \cdot \pi, \tag{3}$$

where: d_g is a geometric mean diameter, mm,
a, b, c are main dimensions of the pit, mm (see: Figure 3),
S is a sphericity, %,
υ is a volume, kg/m^3.

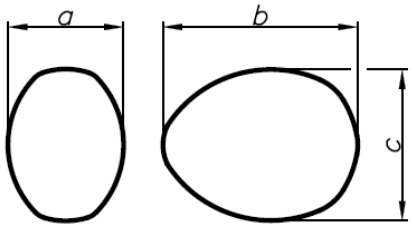

Figure 3 *Schematic presentation of the dimensions of the cherry pit being the subject of the analysis*

Table 1 *Geometrical properties, mass and friction coefficient of cherry pits (averaged results) [7-10]*

Physical properties		Value
Dimensions, mm	a	9.00
	b	12.00
	c	10.00
Geometric mean diameter d_g, mm		7.00
Sphericity S, %		60.00
Mass m, g		0.45
Friction coefficient f, - (for galvanized mild steel surface)		0.70

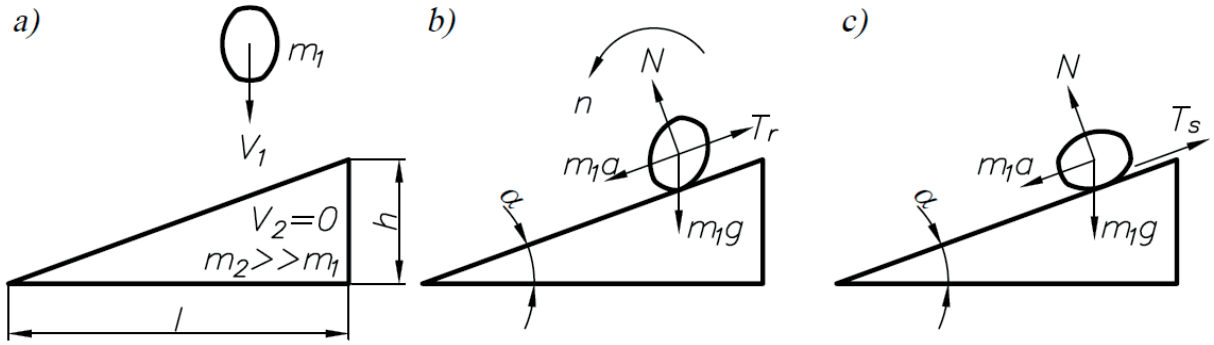

Figure 4 *Diagram of the considered possibilities: a) elastic/inelastic collision, b) rolling friction, c) sliding friction*

2.1 Analysis of transport efficiency using a gravity chute

A gravity chute can be treated as a classic inclined plane. Analyzing the efficiency of pits transport along an inclined plane is possible after introducing the following aspects - Figure 4.

a) elastic/inelastic collision of pit with an inclined plane,
b) transport on an inclined plane using the rolling friction,
c) transport on an inclined plane using the sliding friction.

When reviewing the structure of the stone pitters, it can be concluded that the standard devices of this type, i.e. pitters with a short drum, have an inclined plane installed with an angle of inclination of at least $\alpha = 30°$, i.e., $tg\alpha \backsimeq 0.6$. This corresponds to the height of the inclined plane h to its length l in the ratio 1.0/1.5 and is the maximum percentage of the radius of the inner diameter of the drum:

$$tg\alpha = \frac{h}{l} \tag{4}$$

where: h is the inclined plane height, mm,
l is the inclined plane length, mm.

Such proportions ensure sufficient geometric parameters of the device for transporting pits outside the pitter and placing such a chute inside the pitter drum. It was also observed that during the transportation of the pits, in the first phase it bounces off the surface of the chute at least once, and finally "rolls" out of it. Due to the irregular shape of the pit and its surface covered with pulp remnants, it is very difficult to model how the pits behave during transport. The first problem is to determine whether the collision of the pit (which has a certain initial velocity after the pitting V_1) with the surface of the chute is an elastic or inelastic collision. Regardless of the type of collision, in both cases, it should be considered that it is a collision of a body

(pit, m_1) with a stationary body (inclined plane, m_2) having a very large mass $m_2 >> m_1$ and velocity equal $V_2 = 0$. According to the principle of conservation of momentum and energy, the velocities of both bodies can be determined from the following relationship:

$$m_1 \cdot V_1 + m_2 \cdot V_2 = m_1 \cdot V_1' + m_2 \cdot V_2', \quad (5)$$

$$\frac{1}{2} m_1 \cdot V_1^2 + \frac{1}{2} m_2 \cdot V_2^2 = \frac{1}{2} m_1 \cdot V'^2_1 + \frac{1}{2} m_2 \cdot V'^2_2, \quad (6)$$

where: V_1, V_2 are the velocities of the pit and inclined plane, respectively, before the collision, m/s,
V'_1, V'_2 are the velocities of the pit and inclined plane, respectively, after the collision, m/s
m_1, m_2 are the masses of the pit and inclined plane, respectively, kg.

For elastic collisions, when determining $m_2 >> m_1$ and $V_2 = 0$:

$$V_1' \approx - V_1, \quad (7)$$

$$V_2' \approx 0. \quad (8)$$

For inelastic collisions, when determining $m_2 >> m_1$ and $V_2 = 0$:

$$V_1' + V_2' \approx 0 \quad (9)$$

In the first case, the velocity of the pit after the collision will have the same value, but in the opposite direction. In the second case, the pit's velocity will be "suppressed" by the mass of the plane. In fact, the rebound of the pit is "between" elastic and inelastic collision. The irregular shape and adhesive properties of the pulp remaining on the pit complicate the calculations.

Let us now consider the case of the possibility of the pit rolling with a rotational motion. According to the law of dynamics for progressive motion:

$$m_1 \cdot a = m_1 \cdot g \cdot \sin\alpha - T_r, \quad (10)$$

where: a is an acceleration, m/s^2,
g is an acceleration of gravity, m/s^2,
T_r is the rolling friction force without slipping, N.

According to the law of dynamics for rotational motion:

$$I \cdot \varepsilon = r \cdot T_r, \quad (11)$$

$$a = \varepsilon \cdot r, \quad (12)$$

where: I is a moment of inertia (we assume for a sphere), kgm^2,
ε is an angular acceleration, rad/s^2,
r is a pit (sphere) radius, m.

After solving the above equations, assuming that the pit is a sphere and assuming no slip, the translational motion of the body is uniformly accelerated, then the linear velocity can be written:

$$V = \sqrt{g \cdot h}. \quad (13)$$

Analogously, for the case of a pit sliding off an inclined plane without slipping (T_s is a sliding friction force), using Equation (11) and making the appropriate transformations, one obtains:

$$V = \sqrt{2 \cdot g \cdot h \cdot (1 - ctg\alpha)}, \quad (14)$$

Analyzing Equations (13) and (14) one can see that for $h \to 0$, $V \to 0$ aswell.

2.2 Analysis of transport efficiency using a screw conveyor

Of course, the above considerations are very simplified and do not fully reflect the real conditions. However, based on the above relationships and the engineering intuition, one can assume that for the small plane angles, transport of the pits outside the pitter will not be possible.

Therefore, the authors proposed a solution consisting in transporting the pits using a screw conveyor. The movement of the working element of the conveyor (spiral) can be carried out using a separate drive or integrated (connected via a clutch) with the main drive of the pitting machine drum.

To calculate such a conveyor, the relationships presented in sources [11-15] can be used. We assume that, for the purposes of the solution, the conveyor operates at an angle of inclination $\alpha = 0$. The velocity of pits' movement in the trough can be found from the relationship:

$$V = \frac{p \cdot \omega}{2\pi}, \quad (15)$$

where: p is a screw pitch, m,
$\omega = 2\pi n$ is an angular speed of the screw, rad/s,
n is a rotational speed, rps.

The volumetric efficiency Q_v, m^3/h, and the mass efficiency of the horizontal conveyor Q_m, t/h are calculated from the relationships:

$$Q_v = 450 \cdot \lfloor (D + 2\delta)^2 - d^2 \rfloor \cdot p \cdot \omega \cdot \lambda, \quad (16)$$

$$Q_m = 450 \cdot \lfloor (D + 2\delta)^2 - d^2 \rfloor \cdot p \cdot \omega \cdot \lambda \cdot \rho_s, \quad (17)$$

where: D is an external diameter of the screw, m,
d is an internal diameter of the screw, m,
δ is a radial clearance between the screw and the trough housing, m,
λ is a trough filling factor (see: Table 2),
ρ_s is a bulk density, t/m^3.

Traction force on the drive shaft F_H, N, is:

$$F_H = q \cdot l \cdot k\,, \tag{18}$$

where: q is a unit load of the conveyor, N/m,
l is a length of the conveyor, m,
k is a motion resistance coefficient (see: Table 2).

Conveyor driving power, P, W, is:

$$P = \frac{Q_v \cdot l \cdot \rho_s \cdot g}{3600} \cdot k\,. \tag{19}$$

Based on the above assumptions and calculations, a solution involving the mechanical transport of pits was presented. It was decided to use a screw conveyor in the form of a spiral made of steel wire with a square cross-section, which is integrated with the pitting machine drum and rotates simultaneously with it. The operation diagram is presented in Figure 5. A cross-section of the proposed solution is shown in Figure 6.

The principle of operation is as follows. The pitting machine drum 1 is driven directly by the drive shaft 2 (the drum and the shaft are connected with a prismatic key). The conveyor screw 3 is connected to the drive shaft 2 via a clutch. The conveyor screw is mounted on a slide bearing installed in the evacuation channel 4. The evacuation channel 4 is attached to the frame of the device - the pitting machine (not shown in the diagram) in such a way that it is immobilized. The pitting machine drum 1 and the conveyor screw 3 rotate simultaneously using a motor connected to the drive shaft 2. With each revolution of the drum and screw, the pitted pit is moved towards the outlet until it is completely evacuated.

3 Conclusions

In the fruit processing, an effective method of evacuating pits from pitted fruit, e.g. cherries, plays a key role in maintaining high efficiency of the production process. The issue of transporting pits, especially in the context of the construction of pitters with drums of increased length, is quite important due to the possibility of material blocking in the form of pits from pitted cherries. For that reason, the screw conveyors become a promising solution to these problems while eliminating the need to increase the angle of inclination of the chute. An innovative approach to the design of pitters has the potential to significantly improve both the efficiency and quality of the pit transport.

The proposed new design solution, supported by the field tests, is crucial for the safe handling of pitted pits, minimizing the risk of their blocking. The authors focused on improving the transport technology and

Table 2 *Calculation parameters for various types of transported materials [12]*

Material	λ	k
Light, free-flowing and non-abrasive materials, e.g. grain, rapeseed, groats, ground coal	0.45 ÷ 0.50	1.25
Medium-weight, non-abrasive, fine-grained materials, e.g. beans, soybeans, gravel, coal dust	0.38 ÷ 0.40	1.45 ÷ 1.85
Low-abrasion, fine-grained materials, e.g. coal, walnut, ash, lime, salt	0.30	2.10 ÷ 2.60
Medium abrasive materials, e.g.: cement, gypsum, fine limestone, foundry sand, sulfur, sodium acid phosphate	0.25	3.20 ÷ 4.00

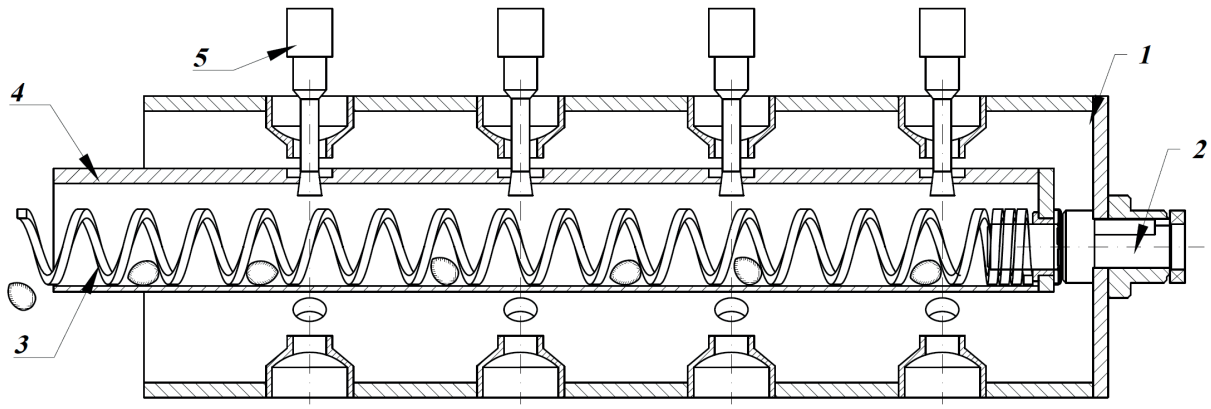

Figure 5 *Operational diagram of the pit evacuation system from the fruit pitting device. 1 - pitter drum with slots for cherries, 2 - drum drive shaft with clutch, 3 – conveyor screw, 4 – escape channel, 5 – pitter tips*

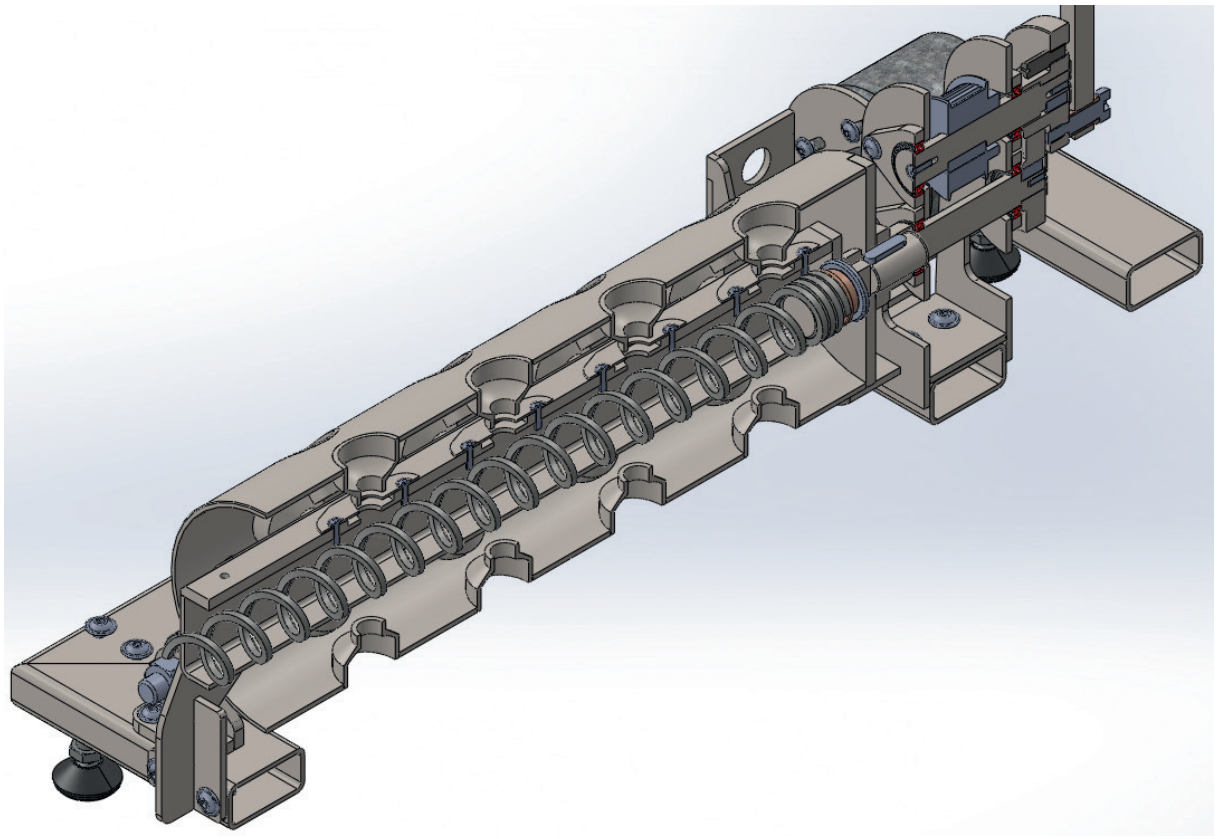

Figure 6 *Cross-section of the proposed solution for a ready-made drum pitter design*

designing a new chute to increase the reliability of the entire process, while eliminating the potential problems related to blocking of the evacuated pits. Another very important aspect of the developed structure is ease of use and hygiene maintenance, which is so important in all the fruit treatment processes.

The next step in improving the efficiency of pitting may be the introduction of automation and monitoring of the entire process, which will translate into an additional increase in efficiency, quality and reliability of the pitting process.

Acknowledgements

The research reported herein was supported by a grant from The Agency for Restructuring and Modernisation of Agriculture (ARMA) involving founds of European Agricultural Fund for Rural Development (EAFRD) for the years 2014-2020 under action 16 "Cooperation". Grant title: "Technological, process and product innovation in pitting cherries in such a way that the structure of the fruit is disturbed as little as possible in cooperation with the Kielce University of Technology", contract number: 00028. DDD.6509.00125.2019.13.

Conflicts of interest

The authors declare that they have no known competing financial interests or personal relationships that could have appeared to influence the work reported in this paper.

References

[1] FELLOWS, P. *Food processing technology: principles and practice*. 2. ed. Cambridge, England: Woodhead Publishing Limited and CRC Press LLC, 2000. ISBN 1-85573-533-4.

[2] VALERO, D., SERRANO, M. *Postharvest biology and technology for preserving fruit quality* [online]. 1. ed. Boca Raton: CRC Press Taylor and Francis Group, 2010. ISBN 9780429093333. Available from: https://doi.org/10.1201/9781439802670

[3] A peach stoning machine that can be used also for other fruits [online] [accessed 2023-12-15]. Available from: https://www.freshplaza.com/europe/article/9417062/a-peach-stoning-machine-that-can-be-used-also-for-other-fruits/
[4] Stainless stoning machine for peaches of every type[online] [accessed 2023-12-15]. Available from: https://www.italianfoodtech.com/stainless-stoning-machine-for-peaches-of-every-type/
[5] Aonla de-stonning machine [online] [accessed 2023-12-15]. Available from: https://cish.icar.gov.in/destoning.php
[6] MOHSENIN, N.N. *Physical properties of plant and animal materials*[online]. New York: Routledge, 2020. eISBN 9781003062325.Available from: https://doi.org/10.4324/9781003062325
[7] ARANA, I. *Physical properties of foods. Novel measurement techniques and applications* [online]. Boca Raton: CRC Press Taylor and Francis Group, 2012. eISBN9780429105944. Available from: https://doi.org/10.1201/b11542
[8] PLANINSIC, G., LIKAR, A. Speed, acceleration, chameleons and cherry pit projectiles. *Physics Education* [online].2012, **47**(1), p. 21-27. ISSN 1361-6552. Available from: https:/doi:10.1088/0031-9120/47/1/21
[9] ALTUNTAS, E., OZTURK, B., KALYONCU, H.I. Bioactive compounds and physico-mechanical attributes of fruit and stone of cherry laurel (prunus laurocerasus) harvested at different maturity stages. *Acta Scientiarum Polonorum Hortorum Cultus* [online]. 2018, **17**(6), p. 75-84. Available from: https:/doi:10.24326/asphc.2018.6.8
[10] MOUSA, A.M., GHANEM, H.G. Mechanical behavior of apricot and cherry pits under compression loading. *Journal of Soil Sciences and Agricultural Engineering* [online]. 2019, **10**(12), p. 867-872. ISSN 1644-0692, eISSN 2545-1405. Available from: doi:10.21608/jssae.2019.79682
[11] PN-ISO 1050:1998. Continuous mechanical handling equipment for loose bulk materials - screw conveyors.
[12] PN-M-46553:1993. Continuous mechanical handling equipment for loose bulk materials. Screw conveyors. Design rules for drive power.
[13] WULANTUYA, WANG, H., WANG, CH., QINGLIN. Theoretical analysis and experimental study on the process of conveying agricultural fiber materials by screw conveyors. *Engenharia Agricola/Agricultural Engineering* [online]. 2020, **40**(5), p. 589-594. ISSN 0100-6916, eISSN1809-4430. Available from: https://doi.org/10.1590/1809-4430-Eng.Agric.v40n5p589-594/2020
[14] RENFENG, Z., LEI, G., WEICHENG, G., XUDONG, X., YANWEI, L. Structure optimization design of screw conveyor based on EDEM. *Journal of Physics: Conference Series* [online]. 2022, **2200**(1), 012002. ISSN 1742-6596. Available from: https://doi.org/10.1088/1742-6596/2200/1/012002
[15] TAN, Y., RACKL, M., YANG, W., FOTTNER, J., MENG, W., KESSLER, S. A comparative study on design standards of screw conveyors in China, Germany and the USA - part I: Theoretical calculation and quantitative analysis. *Particuology* [online]. 2022, **69**, p. 61-76. eISSN 2210-4291. Available from: https://doi.org/10.1016/j.partic.2021.11.011

DEVELOPMENT OF THE BONDING TECHNOLOGY OF MODERN AUTOMOTIVE MATERIALS WITH ENVIRONMENTALLY FRIENDLY SOLUTIONS

Zoltan Weltsch[1,*], Ferenc Tajti[2], Miklós Berczeli[2]

[1]Department of Road and Rail Vehicles, Szechenyi Istvan University, Gyor, Hungary
[2]Department of Innovative Vehicles and Materials, GAMF Faculty of Engineering and Computer Science, John von Neumann University, Kecskemet, Hungary

*E-mail of corresponding author: weltsch.zoltan@sze.hu

Zoltán Weltsch 0000-0002-6366-8281, Ferenc Tajti 0000-0003-3643-9261, Miklós Berczeli 0009-0004-7187-9064

Resume
The significance of bonding technology for modern vehicle structural materials is increasingly acknowledged, driven by the adoption of new materials to reduce weight. This is important not only for quality and economic reasons but to address environmental pollution, as well. Traditional joining methods like riveting, screwing, welding, and brazing, are often unsuitable or limited for modern materials. Soldering, an economical and almost waste-free technology, is becoming more widespread. Through optimization, it achieves a strong, durable bond. There is a potential to favourably alter interface properties, including using high energy density surface treatments. Research showed that the laser surface treatment of high-strength steel sheets could improve the mechanical properties of soldered joints.

Article info
Received 4 November 2023
Accepted 7 February 2024
Online 12 March 2024

Keywords:
surface treatment
DP600
soldering
laser beam

Available online: https://doi.org/10.26552/com.C.2024.026

ISSN 1335-4205 (print version)
ISSN 2585-7878 (online version)

1 Introduction

Today, steel continues to be predominantly used in vehicle production, primarily because it is one of the most readily available raw materials, rendering it more cost-effective than other metals with similar properties. Its significant advantage lies in the ability to modify its properties within wide limits at relatively low costs. Furthermore, steel can be recycled without any loss of quality. The only drawback is its heavy weight. This feature is causing more and more problems nowadays, because the environmental protection regulations are becoming increasingly strict. To reduce consumption and emissions, the approach involves either incorporating metals that are lighter but more expensive, such as aluminum-magnesium alloys, or adopting the high-strength steels capable of satisfying strength requirements with thinner sheet thicknesses. Steel or aluminum plates of lower basic strength are used in energy-absorbing places, but high-strength steel is used in places important for safety. Such places are the roof of the car, the A- and B-pillars and the doors, and in certain places, such as the doors, they can also be supplemented with super high-strength steel. With these steels, it is possible to increase safety and still achieve weight reduction [1]. To be able to connect these steels of different strengths problem-free, it is necessary to ensure the appropriate joining technology and the factors affecting it. In bonding technology, the surface of materials being joined and characteristics of interfaces represent one of the most crucial aspects [2-4].

Vehicle weight reduction is a critical task for lowering consumption. Thinner yet high-strength steel plates offer a viable solution for achieving this weight reduction. It is advisable to design the connection of these plates in such a way that it does not significantly increase the weight of a vehicle. It is possible to improve bonding technologies with surface treatment technologies. Laser surface treatment with a high energy density affects the interfacial energy of the treated surface, thus its wetting ability, which plays an important role in the creation of adhesive bonds [5-7].

The core principle of laser surface treatment involves inducing stresses on the material's outer

surface that are crucial for stress management. The primary objectives include enhancing the surface's strength and load-bearing capacity, establishing more favourable friction conditions, improving wear resistance, optimizing residual stresses to boost fatigue resistance, and enhancing the corrosion resistance. Laser treatment cannot be economically used for mass property modification, however, it can be used for very precise surface treatments, when it is important to change the properties of the raw material only on the surface layer. Utilizing this method allows for the alteration of the surface oxide layer, the interfacial energy, and creation of a surface microstructure that influences wetting. The extent to which the laser beam is absorbed by the material significantly dictates its applicability for various tasks. To enhance absorption, the surface may be coated with graphite spray. The interaction between the laser beam and the material is basically determined by the following technological parameters [8-10]:

- Laser power [W]
- Wavelength [nm]
- Beam shape, size [mm]
- The nature of the intensity distribution within the irradiated area (TEMij)
- Scanning (forward) speed [m/s].

Hao et al. utilized CO_2 laser surface treatment on corrosion-resistant steel, resulting in nearly a doubling of the O_2 concentration in the steel's interfacial layer and a 10 % increase in surface energy. [1].

Khadka et al. team applied a Nd:YAG laser treatment to a magnesium alloy, with the effects assessed using distilled water. The treatment led to a decrease in the contact angle of distilled water droplets on the surface from 81° to 41°, marking a significant enhancement in wetting [11].

Rotella et al. conducted treatments on DP500 high-strength and AISI 304 corrosion-resistant steel using a wire laser, aiming to improve wetting and thereby enhance the bonding strength. The investigation also covered changes in surface roughness, reporting a notable improvement in the wetting properties of both steels, alongside an increase in surface roughness [12].

Bonds are categorized into dissolvable and non-dissolvable types. If a bond can be removed without destruction with some tool or aid, then the given bond type is classified as a dissolvable bond; however, if the bond can only be removed by destruction, it is classified as a non-dissolvable bond. Dissolvable joint technologies include, for example, rib joints, screw joints and latch joints. The non-dissolvable ones include riveting, welding, soldering and gluing. The solid joints fall into both categories, as their classification as dissolvable or non-dissolvable depends on the extent of part overlap and the assembly technology used, determining whether such joints can be separated without causing destruction.

In the present work, soft soldering is preferred because it is one of the possible joining technologies for joining high-strength steels. Riveting and screwing would also be a good technology, but if the goal is to reduce the weight of vehicles, these fastening methods are not the solution, because those fasteners increase the weight of vehicles. Welding and brazing do not greatly increase the weight of a vehicle, but with these technologies, a melt is formed, which can change the fabric structure of the raw material or even deform it due to the high heat input [13].

Soldering is a widely used joining technology nowadays. The benefit lies in the ability to form a soft-soldered joint at temperatures low enough to preserve the fabric structure of the base material, resulting in minimal deformation. The quality of the joint depends largely on the wetting of the solder. By improving the wetting, the strength of the bond can be further increased.

Drawing from literature data and existing knowledge, it is posited that laser surface treatment on steel material can effectively alter the oxide layer, thereby enhancing the wetting properties and increasing the strength of soft-soldered joints. In the course of the research, the changes in interfacial energy, resulting from the CO_2 laser surface treatment, and its impact on soft-soldered joints are thoroughly investigated.

2 Materials and methods

The DP600 type steel was selected for the tests because of its common application in vehicle

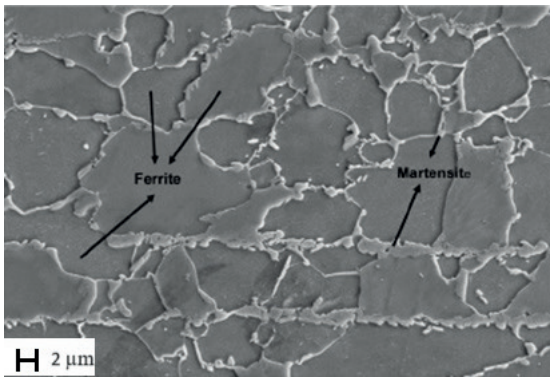

Figure 1 *Metallographic image of DP600 steel [15]*

manufacturing. The numbering of DP steels indicates the tensile strength. Dual phase steels consist of islands of hard martensite embedded in soft, malleable ferrite, the amount of which is usually 10-40 %, depending on the desired mechanical properties (Figure 1) [14].

During the series of experiments, a cold-rolled 25 x 55 mm DP600 steel plates of a thickness of 1 mm were used. The plates were cut in such a way that their longer sides were parallel to the rolling direction. The results of the research can be impaired by a contaminated surface, so the surfaces were cleaned on-site with 96 % methanol, directly before the treatment, which was applied to the surface with a sterile cotton swab and wiped off. The plate was then dried immediately after cleaning using a hot air dryer.

During the laser surface treatment, a laser with a CO_2 source was used, specifically a Unisonic 900 type engraving laser, capable of a maximum power of 100 W. Furthermore, the treatment parameters were determined experimentally. In this case, the focus diameter was fixed at 0.1 mm, and the increment was also set to the same amount.

During the laser beam surface treatment, the variable parameters were power and scanning speed, the set power values were: 35 W, 50 W, 65 W and 80 W, while the speed values were 25 mm/s, 37 mm/s, 48 mm/s and 60 mm/s. With this set of parameters, the extreme values of the machine's application range are covered (Figure 2).

The wetting was investigated using the resting drop method. The temperature in the measuring room was 20 ± 1°C. The treated steel plate was placed on the stage, 5 µl of distilled water was drawn into the micropipette, and it was then positioned in the pipette holder on the stand. The water drop was gently squeezed to prevent dripping, causing it to hang at the end of the pipette tip. Subsequently, the plate, along with the stage, was raised to bring the water drop into contact with the plate's surface, resulting in the water drop jumping onto the plate. The stage was then lowered to position the drop at the center of the camera's view. To capture a photograph, the focus was adjusted using the micrometers on the microscope stage. When the image appeared sharp on the camera, the drop was photographed using a remote control with a 2-second delay to reduce errors caused by camera shake. These processes were also carried out using ethylene glycol, and the photos were saved in separate folders on the computer.

The photographs taken in this manner were opened in a computer program, where the two contact points between the liquid drop and the surface had to be manually marked. Subsequently, two tangents were manually drawn, and the program calculated the edge angle, which was then saved in an Excel file. Four measurements were taken from each photograph to minimize measurement errors.

SMIC lead-free EcoSolder solder paste was used for soldering due to its safety as a lead-free option.

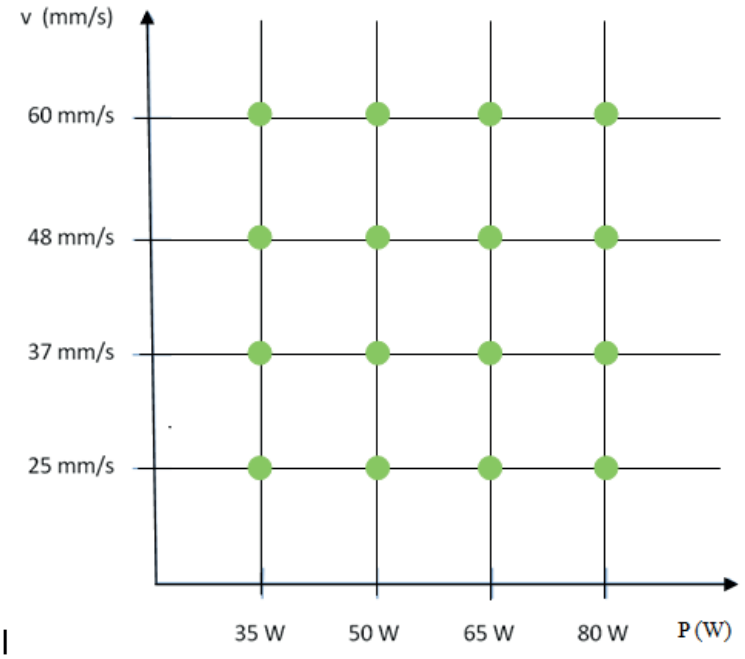

Figure 2 *The parameters of the laser surface treatment*

Table 1 *Chemical composition of M705-GRN360-K1-V solder paste [16]*

%	Sn	Pb	Sb	Bi	Cu	Au	In	Ag	Al	As	Cd	Fe	Ni	Zn
M705	96.5	0.05 max	0.1 max	0.1 max	0.5 max	0.05 max	0.1 max	3 max	0.001 max	0.03 max	0.002 max	0.02 max	0.01 max	0.01 max

A big advantage is that those pastes are available in a wide range of products according to different soldering temperatures. The solder paste utilized carries the type number M705-GRN360-K1-V, with a melting point of around 220 °C according to the manufacturer's data. The chemical composition of the solder paste is shown in Table 1.

3 Result and discussions

Based on the results, it can be seen that compared to samples with untreated surfaces, the wetting values were improved with the CO_2 laser beam (Figure 3). Regarding the trend of the results, it can be said that by increasing the amount of energy input and reducing the feed speed, the value of the wetting edge angle can be reduced. On the DP600 steel plate, wetting improved by 62° for ethylene glycol (Figure 3/b) and 86.5° for distilled water (Figure 3/a), resulting in an improvement of 93.9% and 97.7%, respectively. The alteration of the edge angle values is presumably due to changes in the oxide layer, which was modifiable with the laser beam.

For this treatment, the total interfacial energy was calculated as well, based on the Fawkes relation, as indicated in (Figure 4). The figure shows that the surface energy increases proportionally with increasing power and decreasing feed rate. The surface energy was

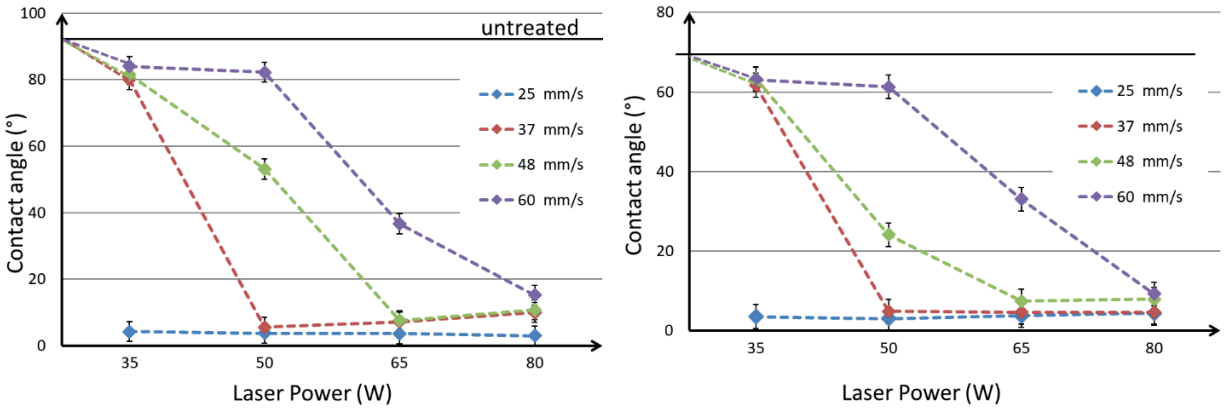

Figure 3 *Effect of the DP600 steel laser surface treatment on the wetting edge angle measured with a) distilled water, b) ethylene glycol liquids*

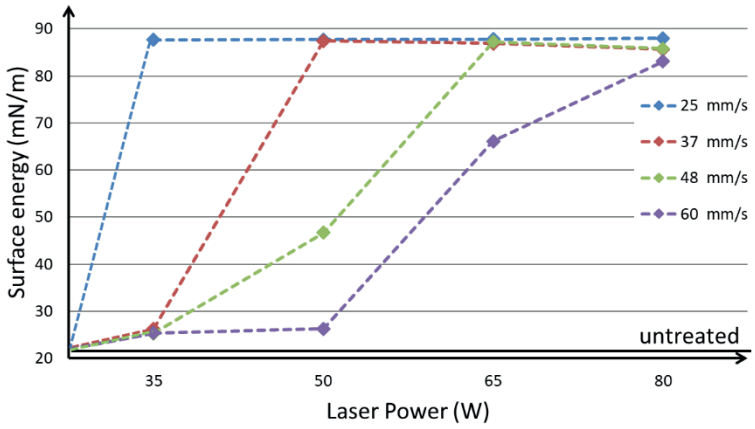

Figure 4 *The change in the interfacial energy as a result of the laser beam surface treatment of DP600 steel*

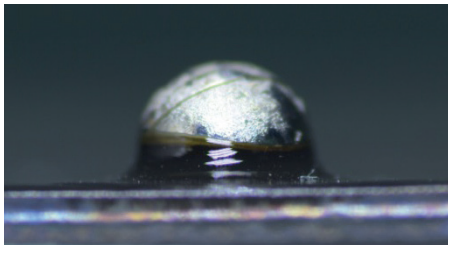

Figure 5 *Contact conditions during the soldering experiment on a laser-treated DP600 steel plate*

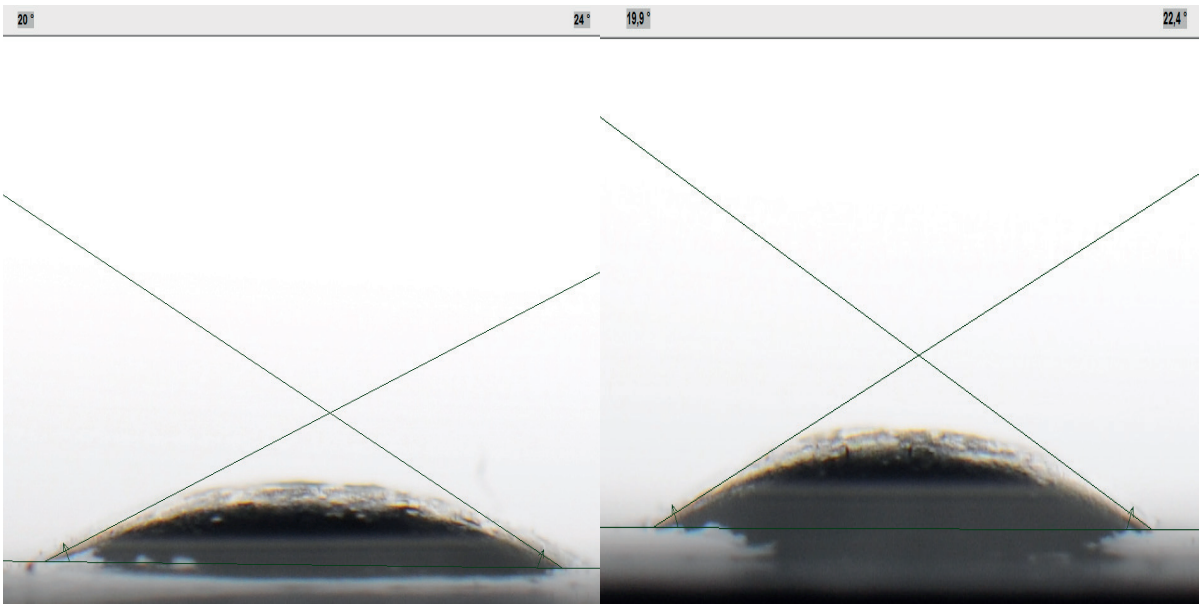

Figure 6 *Images of contact angle measurements of soldering made on an untreated DP600 plate*

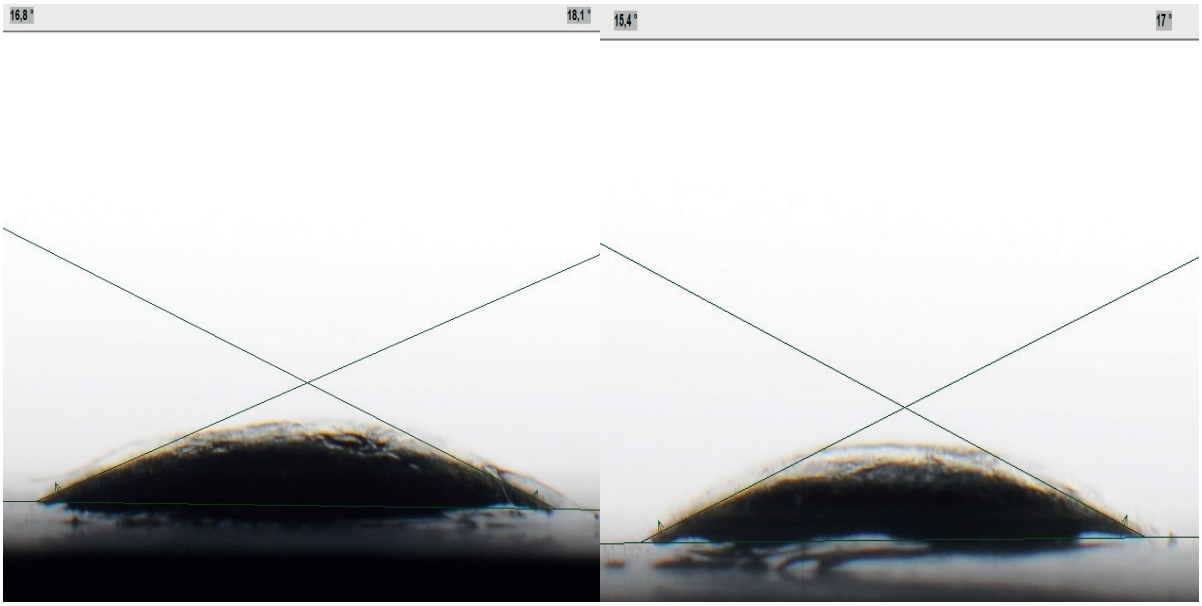

Figure 7 *Images of contact angle measurements of soldering made on laser treated DP600 plate*

almost quadrupled compared to the untreated plate.

A soldering experiment was also performed on the plate treated with the ALFA-LCE 2 laser machine. In this case, the plate was soldered using a power of 50 W and a speed of 37 mm/s. In Figure 5 can be observed that the edge angle of the solder material increased significantly, possibly due to the high temperature, causing the effect of the laser surface treatment to disappear. As a result, the soldering experiment did not yield any results. However, an improvement in bonding is expected with adhesive bonding technologies where the high temperatures are not involved.

Figure 6 shows the soldering measured on the untreated plate, while Figure 7 shows the soldering of the plate treated with 300 W. Each soldering photo was evaluated four times, and the angles were then averaged. The average of the peripheral angle of the soldering on the untreated plate is 20.6°, while the average of the peripheral angle of the soldering measured on the plate treated with 300 W is 16.8°.

Compared to the untreated case, a significant difference can be discovered of the edge angle values of the solder material of the DP600 plate treated with the 300 W laser energy wave. On the one hand, there is an average difference of more than 4°, so the laser beam treatment improves the wetting properties by that much. The standard deviation of the perpendicular angle measurements was improved by approximately

40 %, as well, which further strengthens the assumption that the laser treatment does not only result in surface activation, but also in the surface homogenization, which remains even at the soldering temperature.

4 Conclusion

The findings of the study reveal significant enhancements in the wetting values following the CO_2 laser beam surface treatment, in comparison to untreated samples. The trend observed indicates that the increasing energy input and reducing the feed rate contribute to a reduction in the wetting edge angle. On the DP600 steel plate, wetting improved by 62° for ethylene glycol and 86.5° for distilled water, resulting in remarkable improvements of 93.9 % and 97.7 %, respectively. These changes of the edge angle values are likely attributed to modifications in the oxide layer, achievable through the laser beam treatment. Furthermore, the investigation included calculating the total interfacial energy using the Fowkes relation. The results depicted in Figure 4 illustrate that the surface energy increases proportionally with higher power and decreased feed rate. Notably, the surface energy was nearly quadrupled compared to untreated plates, showcasing the effectiveness of the laser surface treatment. However, in the context of soldering experiments, performed on the plate treated with the ALFA-LCE 2 laser machine, using a power of 50 W and a speed of 37 mm/s, an unexpected increase in the edge angle of the solder material was observed. That increase may be attributed to the high temperature during the soldering process, which could nullify the beneficial effects of the laser surface treatment. Consequently, the soldering experiment did not yield the expected results. In summary, the study underscores the beneficial effects of CO_2 laser beam surface treatment on enhancing the wetting values and surface energy. However, the effects on soldering require further investigation, and adhesive bonding methods may be a promising avenue for improved bonding in the laser-treated materials.

Acknowledgements

Project no. TKP2021-NVA-23 has been implemented with the support provided by the Ministry of Technology and Industry of Hungary from the National Research, Development and Innovation Fund, financed under the TKP2021-NVA funding scheme.

This work was supported by the Janos Bolyai Research Scholarship of the Hungarian Academy of Sciences (ZW).

Supported by the UNKP-23-5-SZE-110 New National Excellence Program of the Ministry for Culture and Innovation from the source of the National Research, Development and Innovation Fund.

Conflicts of interest

The authors declare that they have no known competing financial interests or personal relationships that could have appeared to influence the work reported in this paper.

References

[1] HAO, L., LAWRENCE, J., LI, L. The wettability modification of bio-grade stainless steel in contact with simulated physiological liquids by the means of laser irradiation. *Applied Surface Science* [online]. 2005, **247**(1-4), p. 453-457. ISSN 0169-4332, eISSN 1873-5584. Available from: https://doi.org/10.1016/j.apsusc.2005.01.163

[2] BENDEFY, A., PIROS, A., HORAK, P. Arbitrary vehicle steering characteristics with changing ratio rack and pinion transmission. *Advances in Mechanical Engineering* [online]. 2015, **7**(12), p. 1-12. ISSN 1687-8132, eISSN 1687-8140. Available from: https://doi.org/10.1177/1687814015619279

[3] PIROS, A., TRAUTMANN, L., BAKA, E. Error handling method for digital twin-based plasma radiation detection. *Fusion Engineering and Design* [online]. 2020, **156**, 111592. ISSN 0920-3796, eISSN 1873-7196. Available from: https://doi.org/10.1016/j.fusengdes.2020.111592

[4] KUN, K., WELTSCH, Z. Research of the effect of macrogeometric structures on the melt front using simulation. In: *Advances in manufacturing engineering and materials II. ICMEM 2021. Lecture notes in mechanical engineering* [online]. In: CHATTOPADHYAYA, S., KROLCZYK, G. M., PUDE, F., KLICHOVA, D., HLOCH, S. (Eds.). Cham: Springer International Publishing, 2021. ISBN 978-3-030-71955-5, eISBN 978-3-030-71956-2, p. 282-289. Available from: https://doi.org/10.1007/978-3-030-71956-2_23

[5] PUSZTAI, Z., KOROS, P., SZAUTER, F., FRIEDLER, F. Vehicle model-based driving strategy optimization for lightweight vehicle. *Energies* [online]. 2022, **15**(10), 3631. eISSN 1996-1073. Available from: https://doi.org/10.3390/en15103631

[6] SCHWEIGHARDT, A., VEHOVSZKY, B., FESZTY, D. Modal analysis of the tubular space frame of a formula student race car. *Manufacturing Technology* [online]. 2020, **20**(1), p. 84-91. ISSN 1213-2489, eISSN 2787-9402. Available from: https://doi.org/10.21062/mft.2020.013

[7] KOVACS, Z. F., VIHAROS, Z. J., KODACSY, J. Improvements of surface tribological properties by magnetic assisted ball burnishing. *Surface and Coatings Technology* [online]. 2022, **437**, 128317. ISSN 0257-8972, eISSN 1879-3347. Available from: https://doi.org/10.1016/j.surfcoat.2022.128317
[8] BERCZELI, M., WELTSCH, Z. Enhanced wetting and adhesive properties by atmospheric pressure plasma surface treatment methods and investigation processes on the influencing parameters on HIPS polymer. *Polymers* [online]. 2021, **13**(6), 901. eISSN 2073-4360. Available from: https://doi.org/10.3390/polym13060901
[9] KONYA, G, KOVACS Z. F. Effects of machining parameters and tool reconditioning on cutting force, tool wear, surface roughness and burr formation in nickel-based alloy milling. *Materials* [online]. 2023, **16**(22), 7140. eISSN 1996-1944. Available from: https://doi.org/10.3390/ma16227140
[10] ADAM, B., WELTSCH, Z. Thermal and mechanical assessment of PLA-SEBS and PLA-SEBS-CNT biopolymer blends for 3D printing. *Applied Sciences* [online]. 2021, **11**(13), 6218. eISSN 2076-3417. Available from: https://doi.org/10.3390/app11136218
[11] INDIRA, K., SYLVIE, G., ZHONGKE, W., HONGYU, Z. Investigation of wettability properties of laser surface modified rare earth Mg alloy. *Procedia Engineering* [online]. 2016, **141**, p. 63-69. ISSN 1877-7058. Available from: https://doi.org/10.1016/j.proeng.2015.08.1106
[12] ROTELLA, G., ALFANO, M., SCHIEFER, T., JANSEN, I. Enhancement of static strength and long term durability of steel/epoxy joints through a fiber laser surface pre-treatment. *International Journal of Adhesion and Adhesives* [online]. 2015, **63**, p. 87-95. ISSN 0143-7496, eISSN 1879-0127. Available from: https://doi.org/10.1016/j.ijadhadh.2015.08.009
[13] WELTSCH, Z. Comparative study of the joining technologies of vehicle bodywork sheets. *IOP Conference Series: Materials Science and Engineering* [online]. 2018, **448**(1), 012061. ISSN 1757-899X. Available from: https://doi.org/10.1088/1757-899X/448/1/012061
[14] CHEN, H., PENG, J., FU, L., WANG, X., XIE, Y. Solder wetting behaviour enhancement via laser-textured surface microcosmic topography. *Applied Surface Science* [online]. 2016, **368**, p. 208-215. ISSN 0169-4332, eISSN 1873-5584. Available from: https://doi.org/10.1016/j.apsusc.2016.01.167
[15] DAVUT, K., SIMSIR, C., CETIN, B. Strain hardening behaviour characterization of dual phase steels. *Hittite Journal of Science and Engineering* [online]. 2018, **5**(4), p. 301-306. eISSN 2148-4171. Available from: https://doi.org/10.17350/HJSE19030000107
[16] Low-Ag/Ag-free solder alloy - SMIC Senju Metal Industry Co., Ltd. [online]. Available from: https://www.senju.com/en/products/ecosolder/alloy/alloy_low.php

UNIVERSITY
OF ŽILINA

In its over 70 years of successful existence, the University of Žilina (UNIZA) has become one of the top universities in Slovakia.

The mission of UNIZA is to develop education on the basis of science, research and art activities within national and democratic traditions, to develop harmonic personality, knowledge, the good and creativity of a man and to contribute to the advancement of education, science, and culture for the welfare of the whole society.

Professional profile of UNIZA is unique and includes transport (road, railway, water, air), transport and postal services, communications, civil engineering construction, electrical engineering, telecommunications, informatics, information and communication technologies, management and marketing, mechanical engineering, materials and technologies, robotics, machinery design, energies, civil engineering, crisis and security management, civil security, fire protection, forensic engineering, applied mathematics, teacher training, library and information sciences, social pedagogy and high mountain biology. Results of science and research activities of the University have an important influence not only on the educational activities but also on the development of international cooperation or interconnection with practice.

UNIVERSITY PARTS
7 faculties
9 research and educational institutes and centres
3 specialized professional and training workplaces
3 information workplaces
1 economic and administrative department
4 dedicated facilities

EDUCATION
7 faculties:
8 000 students
more than 88 000 graduates
172 study programmes

SCIENCE AND RESEARCH
699 creative workers
785 000 hours, annual research capacity
190 domestic scientific projects
45 foreign projects
30 scientific and technical journals
50 scientific and professional events per year

INTERNATIONAL COOPERATION
The University of Žilina in Žilina has almost 50 valid university-wide bilateral agreements, and cooperates with foreign universities in the EU, Asia, America and Africa. It cooperates on foreign non-research projects and has concluded more than 300 agreements in the ERASMUS + programme.

UNIVERSITY OF ŽILINA
Science & Research Department

Univerzitná 8215/1,
010 26 Žilina,
Slovakia

Ing. Janka Macurová
tel.: +421 41 513 5143
e-mail: janka.macurova@uniza.sk

IMPROVING THE ENERGY EFFICIENCY OF OPERATION OF A MULTI-MOTOR PLATE CONVEYOR IN THE STEADY-STATE OPERATION MODE

Adilbek Kazbekovich Kelisbekov[1,*], Nurlan Asylkhanovich Daniyarov[2], Baurzhan Gilymovich Moldabaev[1]

[1]Department of Transport and Logistics Systems, NJSC "E. A. Buketov Karaganda University", Karaganda, Republic of Kazakhstan
[2]Corporate University of Personnel Service of Kazakhmys Corporation LLP, Karaganda, Republic of Kazakhstan

*E-mail of corresponding author: akelisbekov@mail.ru

Adilbek K. Kelisbekov 0000-0001-8857-8162, Nurlan A. Daniyarov 0000-0002-4476-4569, Baurzhan G. Moldabaev 0000-0002-2102-1834

Resume

The established mode of operation of the conveyor with a nominal linear load is the most economically advantageous from the point of view of increasing the energy efficiency of mineral transportation, in which the cargo flow with minerals corresponds to the nominal productivity of the conveyor. An increase in the linear load of the working branch of the traction-bearing body to a nominal value reduces the share of unproductive consumption due to which energy savings are achieved for a certain period of time, characterized by its hourly average value.

The purpose of the work was to develop a technical solution to increase the energy efficiency of operation of multi-motor plate conveyors.

Article info

Received 5 November 2023
Accepted 19 February 2024
Online 12 March 2024

Keywords:

plate conveyor
automated electric drive
load distribution system
linear load
control unit
increased energy efficiency of operation

Available online: https://doi.org/10.26552/com.C.2024.022

ISSN 1335-4205 (print version)
ISSN 2585-7878 (online version)

1 Introduction

Modern belt conveyors are capable of processing the cargo flows of the largest mines and quarries in the next decade in terms of productivity [1-3]. However, this type of conveyor cannot operate on a curved track, as well as at high angles of inclination, which is typical for open-pit mining conditions. Ensuring the delivery process on curved routes, the possibility of increasing the angle of transportation, improves the technical and economic indicators of mineral extraction in quarries and sections, since at the same time it is possible to change the geometry of open mine workings, which leads to a reduction in unproductive costs by reducing the amount of work on stripping [4].

The practice of operating plate conveyors at mining enterprises in Kazakhstan and the experience of their operation abroad have shown that this type of conveyor, due to its design features, can be successfully applied in various industries in difficult mining, geological and production conditions for transporting a wide range of goods (coal, pellets, agglomerate, rocks and ores). In particular, in Kazakhstan, at the Molodezhny coal mine (Kazakhmys Coal LLP), a plate feeder of the KM PP 2-10-60 type is used to supply coal to the concentrator (Figure 1) with a frequency converter from Mitsubishi Electric E-700 (Figure 2), with which, depending on the volume of the coal flow, it is possible to adjust the frequency, increase or decrease the speed of the electric conveyor drive.

An analysis of the experience of operating plate conveyors at mining enterprises has shown that the use of modern frequency-controlled electric drives is a promising direction in improving the efficiency of operation of multi-motor plate conveyors, providing control of the speed of movement of the bearing web, control of load distribution between drives, elimination of equalizing forces in the conveyor traction circuit, automatic start of a multi-motor conveyor taking into account the elastic-viscous properties of traction-the load-bearing canvas and a number of other factors [5-8].

Figure 1 *Electric plate drive feeder type KM PP 2-10-60*

Figure 2 *Frequency converter of company „Mitsubishi Electric E-700“*

2 Substantiation of the relevance of the study

Technological schemes using the plate conveyors are preferable to conveyors with a belt traction and bearing body, for economic reasons, as well. This is due to the need to install additional crushing complexes in the case of belt conveyors, as well as the arrangement of transshipment points associated with the use of these conveyors on curved transport routes. When using the plate conveyors that bend in plan, the number of mechanisms and machines is significantly reduced, which significantly simplifies the technological scheme of transportation and increases the reliability of operation of the entire complex [9].

It is also possible to note an important design feature of the plate conveyors, characterized by the movement of the traction-bearing body of the conveyor on wheel pairs along a metal frame, which allows for significantly less resistance to movement during the conveyor operation compared, for example, with another type of chain conveyors - scraper conveyors. In these conveyors, the scrapers move along the surface of the metal grate, which leads to a significant increase in the energy consumed by the engines. At the same time, even full loading of the upper branch of the working web of the plate conveyor does not lead to a significant increase in the resistance to movement of the traction-bearing body of the conveyor when it is operating under rated load.

An important advantage of the plate conveyors, in terms of power indicators, is the possibility of transporting large-lump rock mass along a curved highway in one stop without transshipment points at low values of resistance to movement of the load-bearing body. When operating long-range main plate conveyors from 1000 to 6000 m, multi-motor designs are used. At the same time, ensuring a smooth start of a multi-motor chain conveyor is of a great practical importance, and is undoubtedly relevant for controlling and maintaining a workable static and dynamic state of the main plate conveyor structure operated in difficult mining and geological conditions [10-11]. With a non-unloading scheme for transporting the rock mass, due to the presence of a large number of intermediate drives in a plate conveyor, it is also necessary to solve the problem of automatic distribution of the total load between its drives [12-13].

The experience of operating multi-motor plate conveyors at mining enterprises in Kazakhstan shows that the operating modes and technological parameters of industrial conveyors at most coal mines are extremely inefficient in terms of actual electricity consumption.

The actual energy consumption of the leading electric drive of the plate conveyor, as is known, can be determined by the following formula:

$$E = Nt = \frac{W_{ub}\vartheta\, t}{10^3 \eta_p}, \text{ kWh}, \tag{1}$$

where: W_{ub} - is the resistance to movement of the upper branch of the traction-bearing body of the conveyor, N; η_p - is the efficiency of the electric drive gearbox; ϑ - is the linear speed of movement of the conveyor working web, m/s.

The resistance to movement of the upper branch of the traction-bearing body of the conveyor is determined by the following formula:

$$W_{ub} = L_c g[(q_{wb} + q_l)w' \cos\beta + q_{wb} \sin\beta], \text{ N}, \tag{2}$$

where: L_c - conveyor length, m; q_l - linear weight of the load per running meter of the working web of the traction-bearing body, N/m; q_{wb} - linear mass of 1 m of the working branch of the traction-bearing body, N/m; w' - the coefficient of resistance to movement; β - conveyor installation angle, °; g - gravitational acceleration.

Figure 3 shows exponential dependencies reflecting the potential dynamics of changes in energy consumption by the leading electric drive of the P-80K multi-motor plate conveyor in steady-state operation.

The analysis of dependencies presented in Figure 3 shows that with an increase in the linear load on

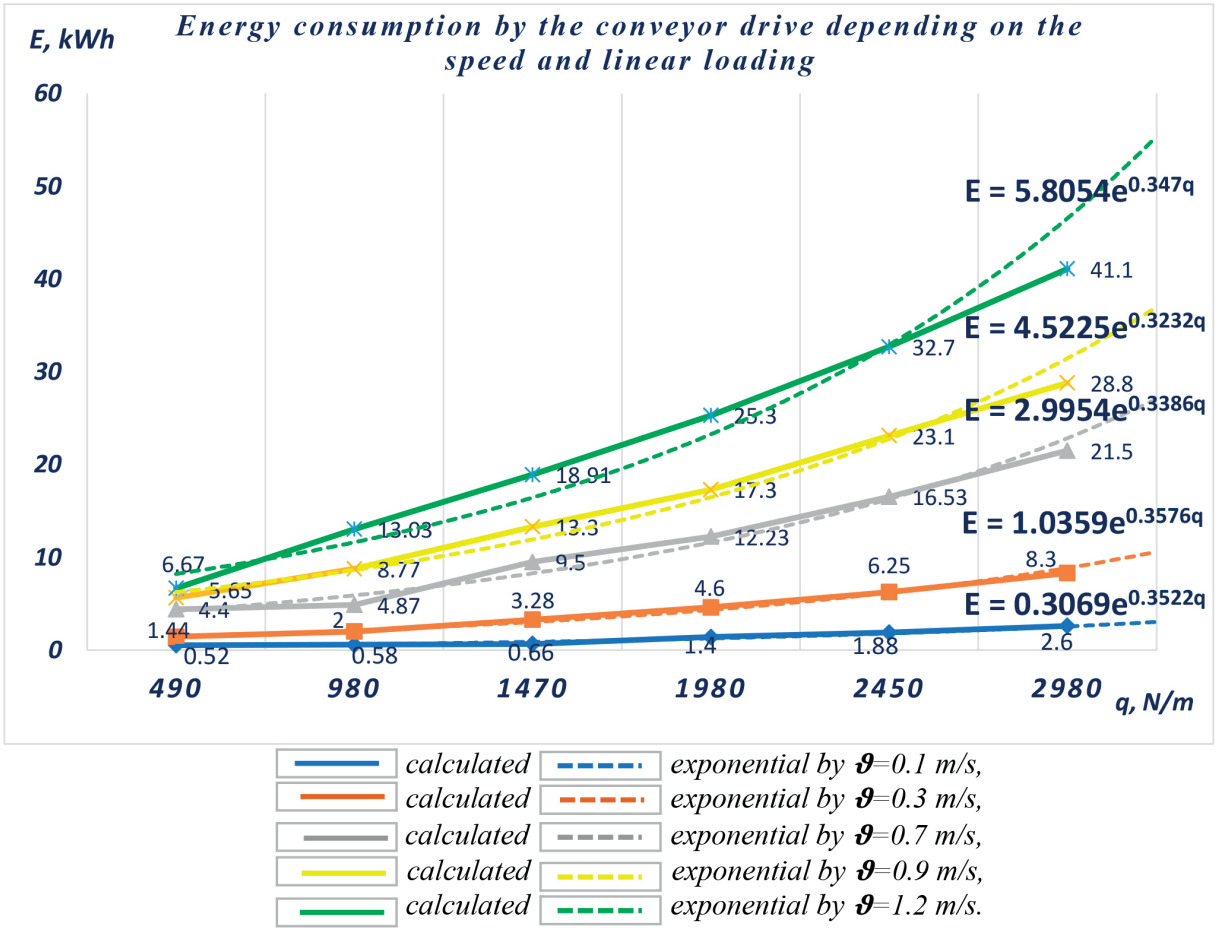

Figure 3 *Dependences of the energy consumed by the electric drive of the P-80K multi-motor plate conveyor on the linear speed of the traction body and the linear load of the working web*

the conveyor working web from 490 to 2980 N/m, at different speeds of the traction body (0.1 - 1.2 m/s), the actual energy consumption of the leading electric drive of the P-80K conveyor increases by 5-6 times. Thus, the problem of unreasonable power consumption in steady-state operation of a multi-motor plate conveyor is an urgent scientific task.

In connection with the above, this work has set the goal of developing a technical solution that would allow for the implementation of measures to increase the energy efficiency of operation of multi-motor plate conveyors.

3 The above diagram and mathematical description of a multi-motor plate conveyor in steady-state operation

After reaching the nominal speed of the traction-bearing body 1, the conveyor begins to load ore from the hopper 2 (Figure 4). When the traction-bearing body is fully loaded with cargo 3, the head drive 4 of the conveyor and the tail driven electric drive 5 of the lower branch 7, respectively, begin to work on moving the loaded upper branch 6 of the traction-bearing body.

The elements of the traction-bearing body of a multi-motor plate conveyor have elasticity, rigidity, inertia - the values of which must be taken into account when developing a mathematical model describing the dynamic processes occurring in various nodes of the conveyor during its operation. To solve the problems of dynamics, the studied conveyor nodes can be represented as separate inertial elements connected by elastic bonds. In addition, for unsteady processes (start-up, braking, speed changes), it is necessary to take into account the influence of rotating and linearly moving parts of the traction body, the electric drive and the weight of the load. To do that, the method of bringing all the moving masses to the shafts of the corresponding engines was used. Calculation formulas are compiled to fully bring the moments of inertia of rotating parts of gearboxes, a moving traction-bearing body, and the weight of the load to the engine shafts. The above diagram of a multi-motor plate conveyor with asynchronous frequency-controlled electric drives is shown in Figure 5.

The masses of the upper branch of the traction body, the sprocket and the rotating parts of the first gearbox are driven to the rotor of the drive motor; the masses

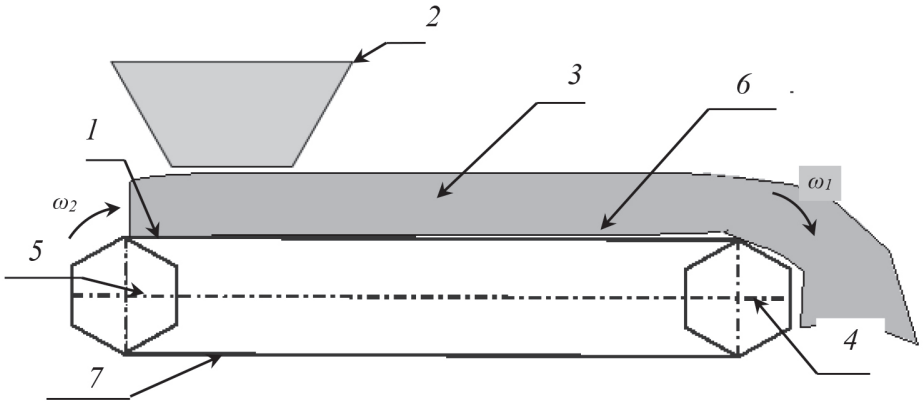

Figure 4 *Diagram of loading a multi-motor plate conveyor with ore*

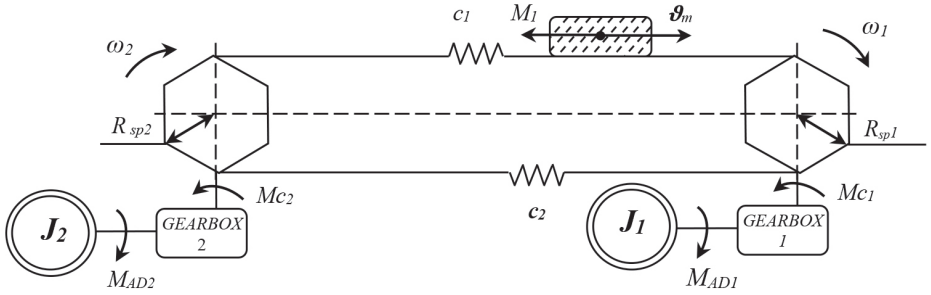

Figure 5 *The above diagram of a multi-motor plate conveyor with asynchronous frequency-controlled electric drives*

of the lower branch of the traction-bearing body, the sprocket and the rotating parts of the second gearbox are driven to the rotor of the driven motor. Thus, the conveyor is replaced by a two-mass system connected by elastic bonds of the lower and upper branches.

The conditions under which the necessary load distribution between the electric drives is ensured (taking into account the limitation of unreasonable dynamic overloads in the traction-bearing body of the plate conveyor) are described by the following system of equations [14]:

$$J_{\Sigma 1}\frac{d\omega_1}{dt} = M_{AD1} - M_{c1} - M_{lm} - \\ - c_1\int(\omega_1 - \omega_2)dt + c_2\int(\omega_2 - \omega_1)dt, \quad (3)$$

$$J_{\Sigma 2}\frac{d\omega_2}{dt} = M_{AD2} - M_{c2} - c_2\int(\omega_2 - \omega_1)dt + \\ + c_1\int(\omega_1 - \omega_2)dt, \quad (4)$$

where: M_{AD1} - is the electromagnetic moment developed by the first master electric motor; M_{c1} - is the static moment reduced to the shaft of the first electric motor; M_{AD2} - is the electromagnetic moment developed by the second slave electric motor; M_{c2} - is the static moment reduced to the shaft of the second motor; M_{lt} - is the moment of resistance forces from the mass of the load transported; ω_1, ω_2 - are the angle speeds of rotation of the first and second electric motors, respectively; $J_{\Sigma 1}$ - is the inertia moment of the upper branch of the traction body taking into account the mass of the load transported reduced to the master electric motor; $J_{\Sigma 2}$ - is the inertia moment of the lower branch of the traction body taking into account the mass of the load transported reduced to the slave electric motor; c_1, c_2 - are the coefficients of rigidity of the upper and lower branches, respectively.

When operating an electric drive of a multi-motor plate conveyor, in the case of placing motors at the ends of the conveyor, the ratio of traction forces of the drives is not equal to the ratio of their installed capacities - this is explained by uneven chain drawing, the difference in loading of empty and loaded branches, which leads to high dynamic loads [15]. To reduce the dynamic forces in the chain, it is advisable to distribute the loads between the drives so that each engine is loaded on its own branch. In the load distribution system, the leading drive is the first head drive loaded on the working branch [16]. The end driven electric drive, accordingly, works to move the lower empty branch of the traction-bearing body.

Figures 6 and 7 show a block diagram and a block diagram of an algorithm for controlling and distributing loads between frequency-controlled electric drives of a multi-motor plate conveyor [17].

The essence of the method of controlling and distributing loads between frequency-controlled asynchronous electric drives of a multi-motor plate

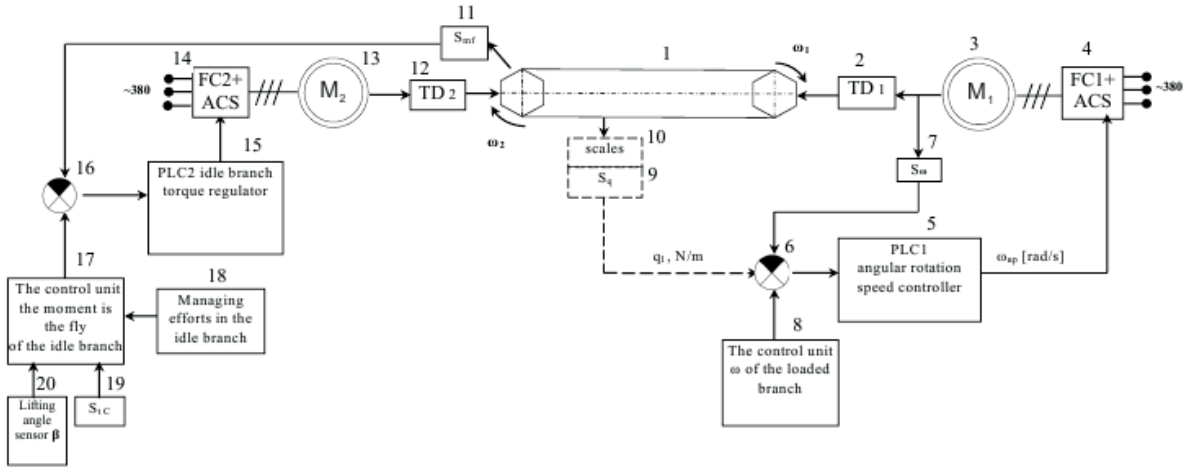

Figure 6 *Structural block diagram of a frequency-controlled electric drive for controlling and distributing loads between drives of a multi-motor plate conveyor*

conveyor, based on measuring the loads of the leading and driven electric drives of the conveyor, correcting the control signal of the driven electric drive in the function of the measured loads and controlling the speed of the leading electric drive, is as follows. The linear loading of the working branch and the forces in the idle branch of the traction-bearing body, the ambient temperature and the lifting angle of the conveyor are measured. In the established modes of operation of the conveyor, in accordance with the changing linear loading, the speed of movement of the working branch is regulated by the driving electric drive, the torque setpoint of the driven electric drive of the idle branch is changed, taking into account the ambient temperature and the angle of lifting of the conveyor, and when the forces in the idle branch change, the traction torque of the driven electric drive is adjusted relative to the torque setpoint of the electric drive of the idle branch [17].

The proposed method can be implemented based on the known technical solutions as follows.

4 Execution of control system units and load distribution between electric drives of a multi-motor plate conveyor

All the blocks can be made based on the known technical solutions [17]. Conveyor 1 includes a steel and a traction-bearing body of the conveyor (a load-bearing cloth made of steel plates attached to a chain traction body), while the first transmission device of the drive electric drive (TD 1) 2 and the second transmission device of the driven electric drive (TD2) 12 are made in the form of standard cylindrical gearboxes. The first asynchronous electric motor of the drive 3, and the second asynchronous electric motor of the driven drive 13, are asynchronous motors with a short-circuited rotor.

The first frequency converter with an automatic control system (FC1+ACS) 4, and a second frequency converter with an automatic control system (FC1+ACS) 14 - standard converters that convert AC mains voltage into variable power supply frequencies of asynchronous electric motors 3 and 13.

The first PLC1 (Programmable Logic Controller), the angular velocity controller 5 of the first electric motor 3 is a programmable logic controller with an adaptive law for regulating the angular velocity of rotation of the rotor of the first electric motor from the actual linear load of the traction-bearing body of the conveyor 1, direct dependence.

The second PLC2, controller 15 is a programmable logic controller with an adaptive law for regulating the traction torque (TT) of the driven second electric drive of the conveyor, taking into account the actual forces in the idle branch of the traction-bearing body.

The first adder of the drive 6 is a standard device that converts information signals (analog or digital) into a signal equivalent to the sum of these signals and, in this case, determines, depending on the linear load of the working branch of the traction-bearing body of the conveyor 1, the difference between the calculated set and the actual measured values of the rotation speed of the first electric motor 3.

Scales 10 is a standard weighing device with a linear load sensor 9 of the upper branch of the traction body. The angular velocity sensor 7 is a standard sensor for measuring the rotational speed of the rotor of the first electric motor 3.

The rotation speed control unit 8 is a standard unit that sets the calculated value of the rotor speed of the first electric motor, made in the form of an analog or digital setpoint. The force sensor on the shaft of the end sprocket 11 is a standard force measurement sensor (tensile moment) applied to the shaft of the end sprocket of the driven drive from the tension of the upper branch

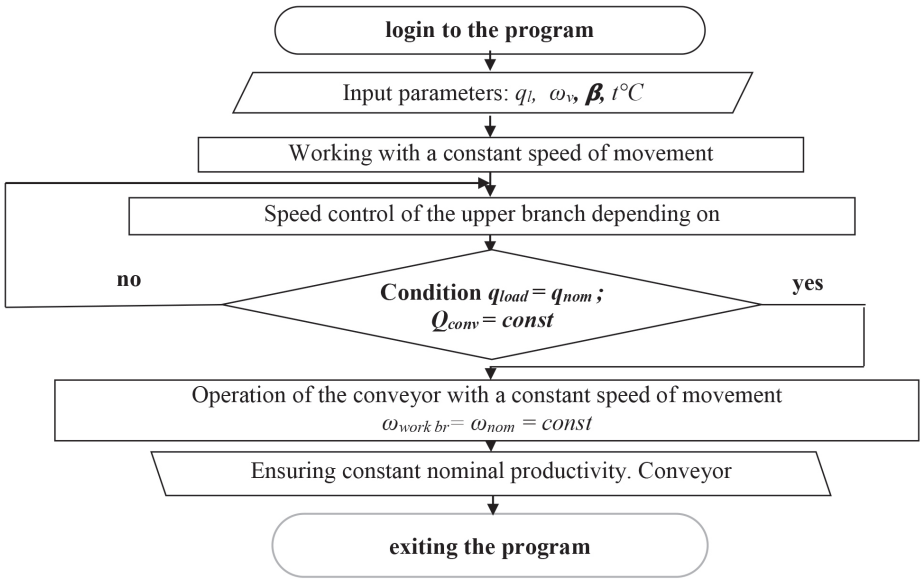

a) ensuring constant conveyor performance

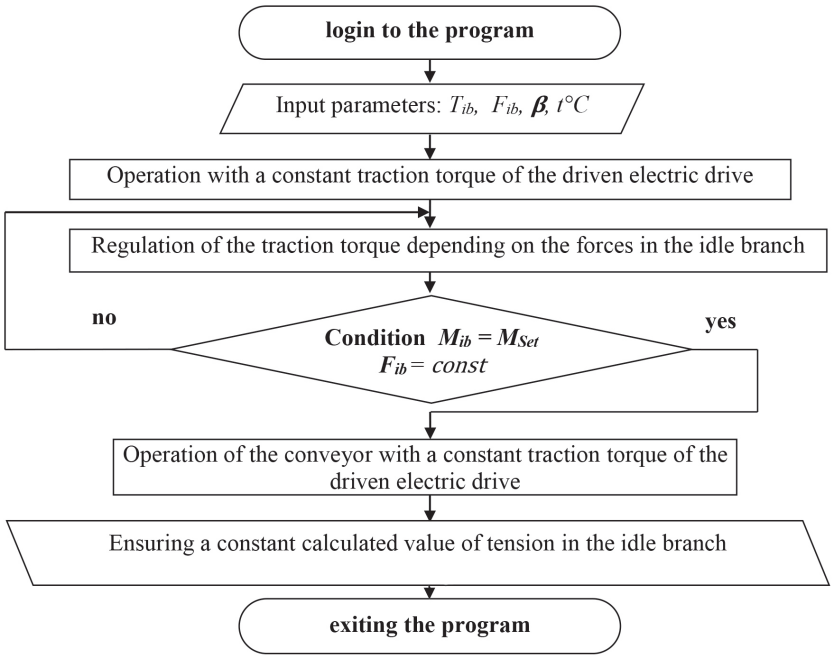

b) ensuring a constant calculated value of tension in the idle branch of the conveyor

Figure 7 *Block diagram of an algorithm for controlling and distributing loads between frequency-controlled electric drives of a multi-motor plate conveyor*

of the traction body. The second adder of the driven electric drive 16 is a standard device that converts information signals (analog or digital) into a signal equivalent to the sum of these signals.

The control unit of the calculated force value in the idle branch of the traction-bearing body 18 is a block that sets the calculated value of the traction torque of the driven electric drive. Temperature sensor 19 is a standard sensor for measuring ambient temperature. The lifting angle sensor 20 is a standard analog or digital sensor that determines the lifting angle (tilt) of a multi-motor plate conveyor.

5 Verification of the proposed technical solution

The developed algorithm for controlling and distributing loads between the frequency-controlled electric drives of a multi-motor plate conveyor was implemented in laboratory conditions in the computer environment of the FR CONFIGURATOR2 program at the stands of Mitsubishi Electric with a frequency converter of the FR-A800 series. The obtained simulation results were positively evaluated by production specialists, who recommended the proposed technical

solution for practical use in the operation of plate conveyors in open-pit mining [15].

Thus, the developed method of controlling and distributing loads between frequency-controlled electric drives of a multi-motor plate conveyor, in authors' opinion, will ensure the necessary operational mode of operation of the conveyor with a nominal linear load, by regulating the speed of movement of the working body of the conveyor. The maximum load of the traction-bearing body of the conveyor in steady-state operation is the most economically advantageous, from the point of view of increasing the energy efficiency of the operation of the plate conveyor. In this regard, the proposed automated control system for a multi-motor electric drive, implemented based on the PLC, is configured in such a way that it measures the linear load of the working web in the real time and regulates the speed of its movement, which ensures the maximum loading of the upper branches and eliminates unreasonable power consumption of the electric drive.

6 Conclusions

The developed method for controlling and distributing loads between frequency-controlled asynchronous electric drives during operation of a multi-motor plate conveyor is based on regulating the linear speed of movement of the traction-bearing body depending on the actual linear load of the working branch.

This ensures the nominal capacity of the conveyor, and, at the same time, the calculated value of the tension of the idle branch is achieved by controlling the traction torque of the driven electric drive of the conveyor in the steady-state operating modes. The results of the proposed technical solution are:

- ensuring the necessary performance of a multi-motor plate conveyor;
- increasing the service life of the elements of the traction-bearing body of the conveyor by reducing dynamic overloads in established operating modes;
- the expected reduction (up to 10-15 %) of unjustified electricity consumption for the empty run of the conveyor, as a result of regulating the speed of movement of the working body.

Acknowledgment

The authors express their deep gratitude to I. V. Breido, Doctor of Technical Sciences, Professor of the Karaganda Technical University named after Abylkas Saginov, for valuable advice in preparing the material for this article.

Conflicts of interest

The authors declare that they have no known competing financial interests or personal relationships that could have appeared to influence the work reported in this paper.

References

[1] SAGINOV, A. S., DANIYAROV, A. N., AKASHEV, Z. T. *Fundamentals of design and calculation of career apron conveyors*. Alma-Ata: Nauka, 1984.

[2] SHESHKO, E. E., GALKIN, V. I. Substantiation of parameters and efficiency of sandwich belt high angle conveyors for deep open pit mines. *Eurasian Mining* [online]. 2022, **37**(1), p. 64-67. ISSN 2072-0823, eISSN 2414-0120. Available from: https://doi.org/10.7580/em.2022.01.13

[3] GALKIN, V. I., SHESHKO, E. E., DYACHENKO, V. P., SAZANKOVA, E. S. The main directions of increasing the operational efficiency of high productive belt conveyors in the mining industry. *Eurasian Mining* [online]. 2021, **36**(2), p. 64-68. ISSN 2072-0823, eISSN 2414-0120. Available from: https://doi.org/10.17580/em.2021.02.14

[4] MUMINOV, R. O., KUZIEV, D. A., ZOTOV, V. V., SAZANKOVA, E. S. Performability of electro-hydro-mechanical rotary head of drill rig in open pit mining: a case-study. *Eurasian Mining* [online]. 2022, **37**(1), p. 76-80. ISSN 2072-0823, eISSN 2414-0120. Available from: https://doi.org/10.17580/em.2022.01.16

[5] BREIDO, J. V. The state and prospects of development of the interconnected multi-motor semiconductor electric drives. In: *DAAAM International Scientific Book 2013* [online]. KATALINIC, B., TEKIC, Z. (Eds.). Vienna: DAAAM International, 2013. ISBN 978-3-901509-94-0, ISSN 1726-9687, p. 193-212. Available from: https://doi.org/10.2507/daaam.scibook.2013.08

[6] WOJCIK, A., PAJCHROWSKI, T. Torque ripple compensation in PMSM direct drive with position-based iterative learning control. In: 2018 18th International Conference on Mechatronics: proceedings. 2019.

[7] SEMYKINA, I. Y., TARNETSKAYA, A. V. Control of energy efficient belt conveyor gearless drum-motor. *EAI Endorsed Transactions on Energy Web* [online]. 2019, **19**(22), p. 144-146. ISSN 2032-944X. Available from: http://dx.doi.org/10.4108/eai.13-7-2018.156435

[8] SEMYKINA, I. Y. Improving the energy and resource efficiency of mining machines by means of a controlled electric drive. Abstract of the dissertation for the degree of Doctor of Technical Sciences, Tomsk, 2014.

[9] MOLDABAYEV, B. G., ROZHKOV, A. V., BALABAYEV, O. T. Determining basic geometric parameters of the apron conveyor drive. *Communications - Scientific Letters of the University of Zilina* [online]. 2023, **25**(3), p. B201-B208. ISSN 1335-4205, eISSN 2585-7878. Available from: https://doi.org/10.26552/com.C.2023.050

[10] BRASLAVSKY, I. Y., ISHMATOV, Z. S., POLYAKOV, V. N. *Energy saving asynchronous electric drive*. Moscow, Russia: Akademiya, 2004. ISBN 5-7695-1704-2.

[11] ESHCHIN, E. K. Model of asynchronous motor in power supply system. *Russian Electrical Engineering*. 2002, **73**(1), p 53-58. ISSN 1068-3712, eISSN 1934-8010.

[12] BREIDO, I. V. *Control principles and methods for the synthesis of controlled electric drives of underground mining machines*. Almaty: Giga Trade, 2012, p. 78-85. ISBN 978-601-07-2004-8.

[13] BREIDO, I. V. Electric drive of the conveyor. A. S. SU1072228A, H02P 5/46. Moscow: USSR State Committee for Inventions and Discoveries, 113035, Zh-35. Publ. 07.02.84. Bul. No. 5.

[14] BREIDO, I. V., KAVERIN, V. V., KELISBEKOV, A. K., DANIYAROV, N. A. Mathematical model of multi-motor plate conveyor traction body with frequency-controlled electric drive. *Eurasian Physical Technical Journal* [online]. 2019, **16**(2), p. 94-100. ISSN 1811-1165, eISSN 2413-2179. Available from: https://doi.org/10.31489/2019No2/94-100

[15] KELISBEKOV, A. K., DANIYAROV, N. A., AKHMETBEKOVA, A. M., ORAZBAYEV, K. N. Control of starting modes of an apron conveyor multi-motor electric drive. *Eurasian Physical Technical Journal* [online]. 2021, **18**(4), p. 74-81. ISSN 1811-1165, eISSN 2413-2179. Available from: https://rep.ksu.kz//handle/data/11879

[16] ALIEV, S. B., BREIDO, J. V., DANIYAROV, N. A., KELISBEKOV, A. K. Control of load distribution between electric drives of a multi-motor plate conveyor for non-overloading coal delivery in surface mining conditions. *Ugol (Coal)* [online]. 2020, **9**, p. 14-17. ISSN 0041-5790, eISSN 2412-8333. Available from: http://dx.doi.org/10.18796/0041-5790-2020-9-14-17

[17] BREIDO, I. V., KELISBEKOV, A. K. Patent of a utility model of the Republic of Kazakhstan. No. ohr. doc.: 4896. electr.: Method of control and distribution of loads between electric drives of a multi-motor plate conveyor [online]. Application 12.10.2023; No. 2020/0147.2; Publ. 30.04.2020; Bul. No. 17. 2023. Available from: https://gosreestr.kazpatent.kz/

THE USE OF RECYCLED CONCRETE POWDER AS SUPPLEMENTARY CEMENTITIOUS MATERIALS FOR MANUFACTURING CONCRETE

Oussama Douidi[1,*], Ahmed Tafraoui[1], Abdelkadir Makani[1], Pedro Serna Ros[2]

[1]Laboratory Eco-Materials Innovations and Applications EMIA (ex LFGM), University TAHRI Mohamed Bechar, Bechar, Algeria
[2]Institute of Concrete Science and Technology ICITECH, Polytechnic University of Valencia, Valencia, Spain

*E-mail of corresponding author: douidi.oussama@univ-bechar.dz

Oussama Douidi 0009-0001-9768-3009,
Ahmed Tafraoui 0000-0002-0287-935X,
Abdelkadir Makani 0000-0002-4027-9929,
Pedro Serna Ros 0000-0001-8754-1165

Resume

Construction development is inevitable, while despite its advantages and its benefits, it may lead to several problems related to landfill and its storage, referring to the high volumes of concrete waste currently generated annually, almost 2.0 ton/per capita according to Eurostat. In Algeria, the government has integrated waste management strategy [3] provision to recovering 60% of construction waste by 2035, which can translate to an urgent need to find innovative ways to recycle concrete waste. One is using those wastes to produce aggregates; however, around 20% of those aggregates represent fines, wich can lead to several issues if not considered in the concrete mixture. This work is an investigation that allows for using this fine fraction as partial replacement of cement. The result confirms the feasibility of using this material efficiently by applying an optimization process, ensuring an optimal cement replacement percentage.

Article info

Received 17 October 2023
Accepted 22 January 2024
Online 6 February 2024

Keywords:

recycle concrete powder
characterisation
mortar
concrete

Available online: https://doi.org/10.26552/com.C.2024.019

ISSN 1335-4205 (print version)
ISSN 2585-7878 (online version)

1 Introduction

Many construction works are being implemented and many projects will be born in the future to serve the development of Algeria's infrastructure, and one of the effective strategies around the world is the sustainability development that became an obligation [1]. The concept is to try to find possibilities for recycling and reusing those waste to thereby drive the institution of a circular economy [2], Algeria is also imposing itself by raising and integrate the waste management strategy, it is expecting to recovery more than 60% of construction waste in 2035 [3]. The construction sector is responsible for 25% of the total CO_2 emissions [4], whereas only the cement production is responsible for about 8% of those emissions. This is among the reasons that pushed Algerian government to enter many agreements, among them the treaty with the Federal Ministry of Germany and the European Union, for the German Society for International Cooperation "GIZ" program, which is an ambitious program to contribute to the reduction of greenhouse gas emissions targeting at least 7% by 2030. This program includes several points, among them the protection of the environment and biodiversity of the Algerian coast and sustainably strengthen value chains in waste management. In addition, create a waste collection and recycling system and also develop and introduce new offers of qualifications and specific training for the waste sector [5]; it also puts several strategies such as National Strategy for Integrated Waste Management by 2035 (SNGID-2035). In addition the realization of eight technical land-fill centres for inert waste across the national territory will allow rational management of this waste and recovery in construction, as well as the National Strategy and Action Plan for Biodiversity 2016 - 2030, the National Action Plan on sustainable consumption and production patterns by 2030 (PNA-MCPD) [6].

In Algeria, millions of tons of waste are generated every year from the construction sector, according to the

Figure 1 *The concrete recycling procedure until obtaining the fine fraction*

report of National Waste Agency in 2020 about the state of waste management. The quantity of construction and demolition waste produced in 2020 is estimated at 13 million tones and it increases every year, the estimate of this inert waste that comes from the construction and demolition sector will be around 27 million tons in 2035 [3]. Hence, the urgent need to adapt to the sustainable development approach by finding effective techniques for managing waste and, above all, reusing it in various applications.

Recent researches tend to find new ways of recovering waste to fully fulfil their obligations; they proceed to the valorisation of this waste generated by construction sector, either in the form of aggregates for reuse instead of natural aggregates [7-11]. In addition, in the manufacture of fines and valued as new materials that can be used as a partial replacement for cement [12]. Moreover, that is what we were investigating in this research, because this practice is often limited due to the side effects often related to their very high water absorption and especially when we use the coarser aggregate. Therefore, this investigation is one of those solutions that could be very beneficial, about the feasibility of using finely ground concrete from waste concrete as a component of concrete. Instead of using fine recycled concrete as aggregates, we propose to use them as mineral addition (supplementary cementing material SCM). After the usual recycled concrete aggregate manufacturing process, in which the concrete was broken in small pieces, and crushed, we proceed to an additional process of crushing and sieving until obtaining a powder with maximal diameter lower than 80 µm. In the following, this powder can be used as a substitute for usual addition, such as limestone filler, silica fume, or blast furnace slag or even fly ash, what would reduce quarrying of natural resources.

Nevertheless, the use of recycled aggregate fines in the manufacture SCM is now a research and development path as an addition to clinker.

The objective of this study was to evaluate the possibility for use of those fines in manufacturing mortar, the appropriate replacement percentage by evaluating the performance of a common concrete composed using them, and to assess that we started by reporting a physical and chemical characterization investigation on those recycled concrete fines. Then, the evaluation of its influence on the mechanical resistances to be able to draw approaches and recommendations for an optimal use of those fines.

In view of results from this work, it is therefore possible to use the powder from the fines recycled concrete in the raw to be used as a mineral addition in cementitious materials, by incorporating them into mortar and subsequently into concrete.

Figure 2 *The manufacturing process of recycled concrete powder in the laboratory*

Table 1 *Results of chemical analysis of recycled concrete powder*

Sample of Recycled Concrete Powder	Component (%)
Calcimeter Tests $CaCO_3$	48.80
Chlorine Test (Cl^-)	0.25
Sulphate Test	≥ 0.01
The insoluble matters	50.95

2 Materials and methods

2.1 Materials preparation

The recycling process that has been adopted in this work-study for the manufacturing process to obtain recycled aggregate, more precisely, the fine fraction (recycled concrete powder) that was used in those experiments, is shown in Figure 1.

The research has been carried out using the raw materials from concrete waste; the concrete has been recovered for test specimens, which come from several construction sites located in the region of Bechar-ALGERIA. The recycled concrete powder manufacturing process started by crushing, and screening, then passed to the grinding using a micro-grinder and then sieving at 80 μm. Figure 2 illustrates the laboratory material employed and schematization of the manufacturing process.

2.2 Characterization of fines from concrete recycling

2.2.1 Chemical characterization:

For a better understanding of the nature of those fines (recycled concrete powder) a basic chemical characterization tests were carried out on this material for identifying minerals, the results are shown in Table 1.

Chemical identification tests revealed that:

- Calcimeter Tests using Bernard Calcimeter: about half of those fines is limestone, which make sense given the calcareous nature of the gravels in this region.
- Chlorine Test: revealed that the amount of chlorine does not exceed 0.25 %.
- Sulphate Test: we detected only traces (less than 0.01), which is largely far from the limit, which is 0.80 %. The rest of the material constitutes of minerals insoluble, which represent around half of the materials.

Those analyses conducted lead to the conclusion that recycled concrete powder is compatible for introduction into cementitious matrices. Additionally, even if there exists a potential variation in the chemical composition between different concrete waste sources, that is attributed to the components, nature, and origins of recycled concrete and its aggregates. According to the literature, recycled concrete may often contain high percentages of calcite or limestone, with quartz being the most common, together with small amounts of lime, portlandite, and some iron oxides [12-14].

Acknowledging to these potential variation, preliminary assessments indicate that those fluctuations do not significantly compromise the properties of the concrete, although this aspect requires validation in future researches.

To better quantify and comprehend the extent of these variations, further analyses based on XRD have been conducted.

2.2.2 Physical characterization

We determined the apparent density of Recycled Concrete Powder according to standard EN 196-6 [15], to compare it to that of the additions and that of the binders.

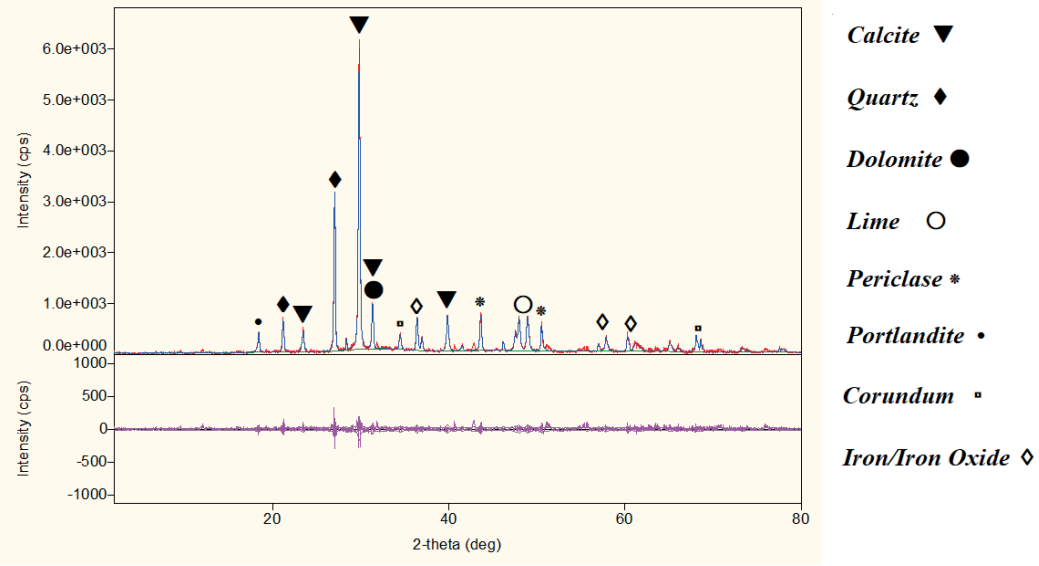

Phase	Formula	Content (%)
Calcite	$CaCO_3$	56.04
Quartz	SiO_2	19.59
Dolomite	$CaMg(CO_3)_2$	9.17
Lime (Calcium oxide)	CaO	5.51
Periclase (Magnesium oxide)	MgO	4.02
Portlandite (Calcium hydroxide)	CaH_2O_2	2.16
Corundum (Aluminum)	Al_2O_3	2.13
Iron/iron oxide	Fe/ Fe_2O_3/FeO	1.38

Figure 3 *The results of XRD analysis of recycled concrete powder*

The density of Recycled Concrete Powder is 650 kg/m^3, which is comparable to that of other additions, such as silica fume (400 to 650 kg/m^3), and limestone fillers (500 to 700 kg/m^3).

2.2.3 XRD characterization

To better understand the recycled concrete powder, we have proceeded to the X-ray diffraction "XRD" tests, which has been made with the following operating parameters: Cu Kα radiation, 45 kV, 200 mA power generator. An angular range of 5-70° 2θ was measured with a scan speed of 5° per minute, the results are presented in Figure 3.

The XRD analysis reveals that these fines are mainly composed of calcite and quartz, which makes sense when we relate it to the nature of the aggregates in the region of Bechar, Algeria; small amounts of lime, portlandite, and some iron oxides were observed, as well.

Other researchers as Oksri-Nelfia et al noted that they had found that the recycled concrete fine containing 73% of $CaCO_3$, as well as around 2.4% of portlandite [12]. Liu et al. found that the recycled concrete powder contain 52.53% of CaO, 27.87% of SiO_2, 7.04% of Al_2O_3, 4.9% of Fe_2O_3, 3.53% of MgO, 1.27% of K_2O, and finally 0.05% of SO_3 [16]. Cantero et al., mention, in their review about construction and demolition, waste powder that can contain between 36% and 70% of SiO_2, 6% to 19% of Al_2O_3, 3% to 6% Fe_2O_3, as well as less than 20% of CaO, along with traces of other oxides; it may prove to be a suitable Supplementary Cementitious Material [17].

Although the results found are in accordance with the literature, however, the chemical components can vary, and there is sometimes a difference in the proportions of materials. This variation is often due to the nature of the aggregates used, as aggregates typically make up 60 to 75% of the volume as fillers in concrete materials [18].

2.3 Materials used for mortar formulation

For the formulation of mortar in this case we used a cement which is CEM I 42.5 N-SR 3 from Lafarge-Algeria (MOUKAOUEM), and for the sand we used a quarry sand (0-3) from the region of Bechar-Algeria; these characteristics are given in Table 2.

Table 2 *Characteristics of sand*

Sand	Value	Description
Sand fineness	mf = 2.05 (1.8 ≤ mf ≤ 2.2)	sand mostly fine grain
Equivalent sand test	esp. = 85.6 (esp. ≥ 80)	very clean sand

Table 3 *Composition of mix mortar*

Replacement share (%)	0	5	10	15	20	25	30	35	40	45	50
Sand (g)	1350	1350	1350	1350	1350	1350	1350	1350	1350	1350	1350
Water (ml)	225	225	225	225	225	225	225	225	225	225	225
Cement (g)	450	422.5	405.0	382.5	360.0	337.5	315.0	292.5	270.0	247.5	225.0
Recycle Concrete Powder (g)	0	22.5	45.0	67.5	90.0	112.5	135.0	157.5	180.0	202.5	225.0

Table 4 *The effect of percentage of replacement share on mechanical strength in MPa*

Mechanical strength (MPa) \ Replacement share (%)	0	5	10	15	20	25	30	35	40	45	50
Flexural strength (7 days)	5.5 (±0.5)	5.0 (±1.0)	5.0 (±1.0)	4.5 (±1.0)	4.5 (±0.5)	4.0 (±1.0)	4.0 (±1.0)	3.5 (±1.0)	3.0 (±1.0)	2.5 (±1.0)	2.0 (±1.0)
Flexural strength (28 day)	6.0 (±0.5)	6.0 (±0.5)	6.5 (±0.5)	6.0 (±1.0)	5.5 (±1.5)	5.5 (±0.5)	5.0 (±1.0)	5.0 (±0.5)	4.0 (±1.0)	4.0 (±0.5)	3.0 (±1.0)
Compressive strength (7 day)	22.5 (±2.0)	23.0 (±1.0)	23.0 (±2.0)	22.5 (±2.0)	22.0 (±2.0)	21.0 (±2.0)	20.0 (±1.0)	19.0 (±1.0)	16.0 (±1.0)	13.0 (±2.0)	10.0 (±2.0)
Compressive strength (28 day)	29.5 (±1.0)	29.5 (±1.5)	30.0 (±1.0)	29.0 (±1.5)	27.5 (±2.0)	26.5 (±1.5)	24.5 (±2.0)	22.0 (±2.0)	19.0 (±1.0)	17.0 (±2.0)	14.0 (±2.0)

2.3.1 Preparation of mortar

These materials were used to make a mortar (1/3) with a W/C = 0.5, according to the standard EN 196-1 [19], with different percentages of cement replacement by recycled concrete powder.

Procedure: Mix the standardized sand with the cement to be tested and the water in the following proportions: 450 ± 2 g of cement, 1350 ± 5 g of standardized sand and 225 ± 1 g of water.

The quantities for all the components are summarized in Table 3.

The mix is made homogeneous by using the equivalent binder by adding the recycled concrete powder, however, it has been noticed that the workability appears to decrease with the increase of the amount of fines on the recycled concrete, it started to be noticeable after reaching 40 % of replacement. The mortar was filled into the molds using vibration, with adjustments made based on the mortar's workability ensuring an effective compaction of the specimens.

Once the mortar was ready, it was put into 40x40x160 mm prismatic molds. The installation was carried out by vibration. The samples were identified and stored in a container filled underwater, at a temperature of 25°C ± 1°C until the compressive and flexural strengths tests (7 and 28 days).

3 Results

The destructive tests, carried out on mortars after the curing period, consist of studying the tensile and compressive strengths of mortars, made without and with different replacement level of recycled concrete powder at 7 days and 28 days, according to the standards. For defining the resistance classes of mortars, to evaluate the contribution of additions to the mechanical performance of mortars, the specimens (six for each mixture) were drawn from the pans and tested in bending and compression.

3.1 Effect of replacement share on mechanical strength

The compressive, and flexural strengths of the mortar, as a function of the addition replacement percentage, are represented in Table 4 and Figure 4.

From the obtained results, it was observed that within the range of 0 to 15 % cement replacement with

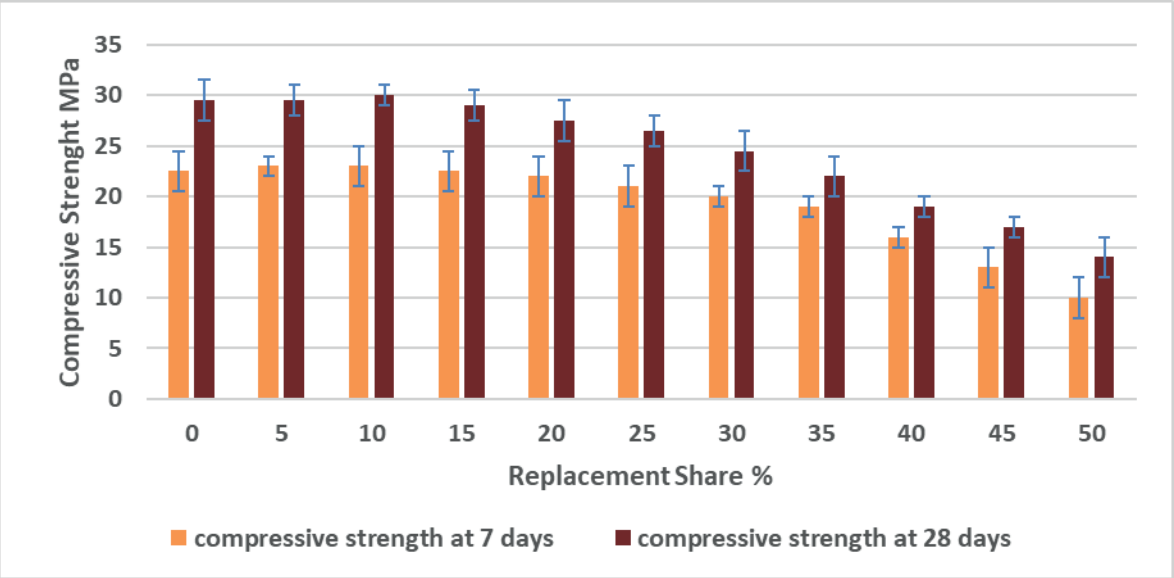

Figure 4 *The effect of replacement share on compressive strength in MPa*

Table 5 *Recycled concrete powder passing percentage depending on fineness size*

Size (μm)	Passing (%)
800	95
500	80
315	70
250	60
160	50
125	40
80	25

recycled concrete powder, the optimal point lies in this interval with very slight differences. It was also revealed that from an economic standpoint, it could achieve up to 20 % or 25 % replacement to at least maintain the normalized resistances.

3.2 Effect of finesse size on mechanical strength

It is noticed that the manufacture of fines at 80 μm is quite difficult, and consumes enormous amount of energy. That is why we tried to find the ideal fineness size of the recycled concrete powder by varying the fineness from 80 to 800 μm, to preserve a maximum of energy in the manufacture of fines, to be more profitable, however, the fineness of the fines could modify the properties of the mortars.

The recycled concrete powder in this experiments result using the output collected after crushing and grinding the same recycled concrete, the resulting material shown after sieving a grading presented in Table 5.

Then, the study was conducted about the effect of the fineness of the used recycled concrete powder on the mechanical resistance of the mortar. A mortar 1/3 with W/C = 0.5 with 20 % replacement of cement by recycled concrete powder, was made with different fractions of the recycled powder: 0/80 μm, 0/125 μm, 0/160 μm, 0/250 μm, 0/315 μm, 0/500 μm, and 0/800 μm. Table 6 presents the results concerning the compressive strength at 7 and 28 days of mortar according to recycled concrete powder fineness. Additionally, Figure 5 provides a more elucidated illustration of the compressive strength results at 28 days for the mortar based on the fineness of the recycled concrete powder.

From results in Table 6 and Figure 5 it can be observed that, for a fineness up to 160 μm, the compressive strength remained consistent. It was slightly affected and decreased marginally in the range from 250 to 315 μm. On the other hand, it is worth noting that the strength becomes more affected with fineness variations exceeding 500 μm.

3.3 Evaluation of water absorption and the necessary correction

It has been noticed that the workability decreases greatly, especially at the high replacement shares, so it was decided to evaluate and quantify the water demand

Table 6 *The compressive strength of mortar according to recycled concrete powder fineness*

Strength (MPa) \ Powder size (μm)	80	125	160	250	315	500	800
compressive strength (7 days)	22.0 (± 2.0)	22.0 (± 2.0)	22.0 (± 2.0)	22.0 (± 1.5)	21.5 (± 2.0)	21.0 (± 2.0)	21.0 (± 1.0)
compressive strength (28 days)	27.5 (± 2.0)	27.5 (± 2.0)	27.5 (± 1.5)	27.0 (± 2.0)	27.0 (± 1.0)	26.5 (± 1.0)	25.0 (± 1.0)

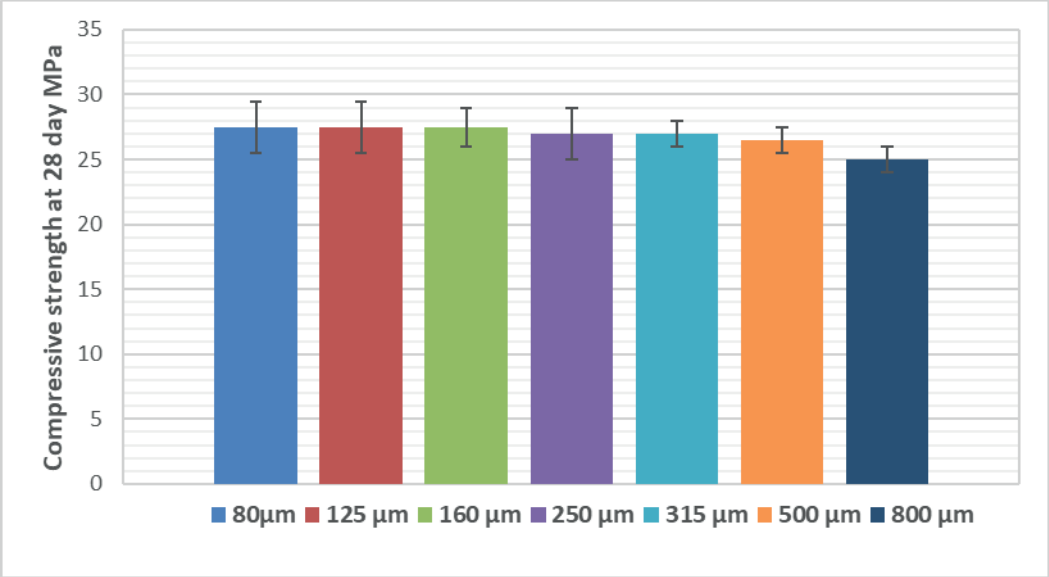

Figure 5 *The compressive strength of mortar according to recycled concrete powder fineness*

Table 7 *The effect of cement replacement by recycled concrete powder on water demand.*

Replacement share (%)	Water (%) over binder	Consistency value needle depth D (mm)
0	27	5
10	27	7
20	28	6
30	29	6
40	30	6
50	31	6

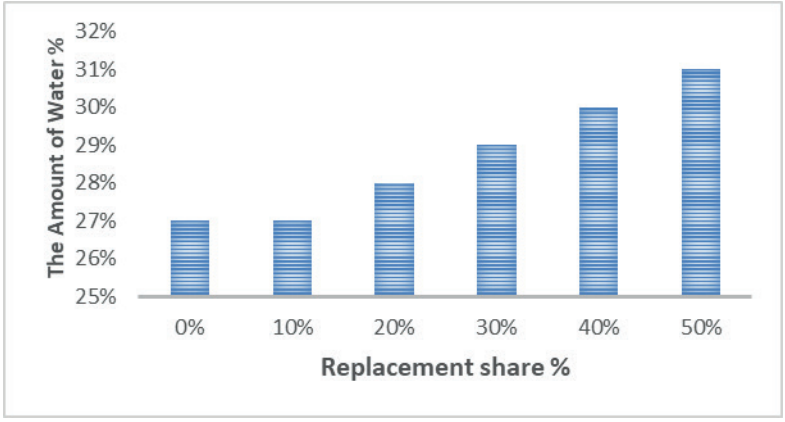

Figure 6 *The effect of replacement share on water demand*

Table 8 *Concrete Mixture (kg/m³)*

Materials	Formulation A	formulation B
Cement	875	700
Recycled concrete powder	0	175
Sand 0/4	900	900
Gravel 3/8	730	730
Water	245	254
Super-plasticizer	26	21
Gravel/Sand	0.81	0.81
Super-plasticizer/Cement	0.03	0.03
Water/Binder	0.28	0.29
Cement/Binder	1.00	0.80

using the Vicat device, equipped with its consistency probe in accordance with the standard EN 196-3 [20], to evaluate the necessary correction for the amount of water. Table 7 and Figure 6 present the results of experiments about the effect of cement replacement by recycled concrete powder on water demand.

Indeed, the decrease in workability is depending on the percentage of recycled content. Beyond 20% replacement, it is necessary to make a water correction.

Based on observations, it appears that there is a need for approximately 1% of additional water for each 10% increase in cement replacement by recycled concrete powder.

Although the increasing replacement of cement by recycled concrete powder appears to causes a drying of the fresh mixture, in which it requires an addition of water for correction to maintain consistent workability, it is noteworthy, based on visual observations, that this adjustment does not affect the mixture's homogeneity, which remains intact and uniform.

3.4 Influence of recycled concrete powder on concrete

A concrete is manufactured based on previous formulations [21-24], so we applied an optimization based on the interpretations of the previous results, in this investigation. The goal was to achieve a concrete mix with satisfactory workability and exceptionally high strength, particularly in terms of compression resistance. This iterative process involved adjusting the key factors, such as the water-cement ratio, aggregate properties, and the use of additives. The aim was to develop a concrete mix that not only met, but also exceeded the performance expectations.

Table 8 presents the basic mixture (Formulation A) that was used it as a reference formulation, as well as the mixture with the integration of recycled concrete powder (Formulation B). In this formulation, 20% of cement "CEM I 42.5 N-SR 3" was replaced by the recycled concrete powder and some parameters were optimized as indicated. The sand used is a coarse sand (0-4), clean, with a very high limestone content, exceeding 95%. The gravel utilized is a 3-8 gravel with a mass loss of less than 20% in the Micro-Deval test [25]. These aggregates are recommended for use in the production of high-performance concrete; and finally, the super-plasticizer used is Sika® ViscoCrete®-4032 RMX. The concrete mixing process was carried out during 15 minutes in a horizontal manner, for ensuring an optimal mixing of the components.

Using the formulation provided in Table 8, has led to a successful production of fluid concrete, which appears stable and shows no initial signs of segregation.

3.4.1 Influence on the fresh state (spreading)

The workability of fresh concrete was tested using Abrams cone, the flow of each formulation was measured after 15 minutes of mixing. The results represent the average of three tests for each formulation. The founding are represented in Figure 7.

The observations indicate a slight reduction in the workability of the concrete, while it still maintains its ability to flow. This suggests that workability remains manageable, and the concrete retains its fluid properties when producing concrete with a 20% of cement replacement by recycled concrete powder.

A remarkable variation regarding the flow has been observed, which suggests that this concrete is likely responsive to specific factors, including mixing conditions, duration, and the moisture content of the aggregates.

3.4.2 Influence on the hardened state (compressive strength)

The evaluation of the compressive strength of concrete was conducted on cubic specimens with side

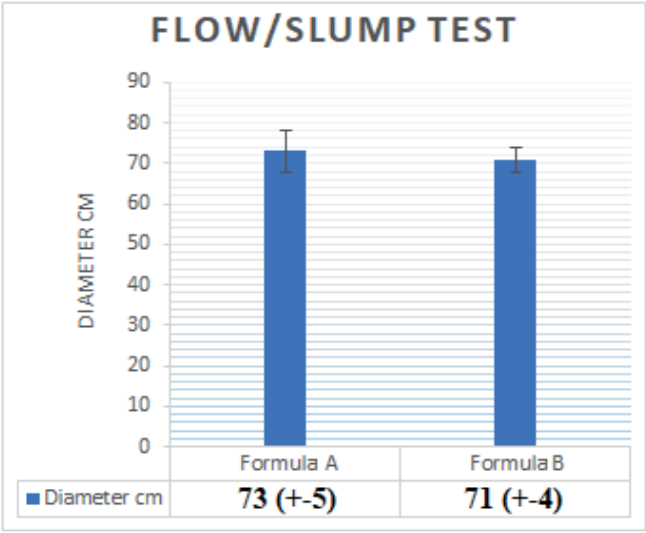

Figure 7 *The effect of recycled concrete powder on concrete flow.*

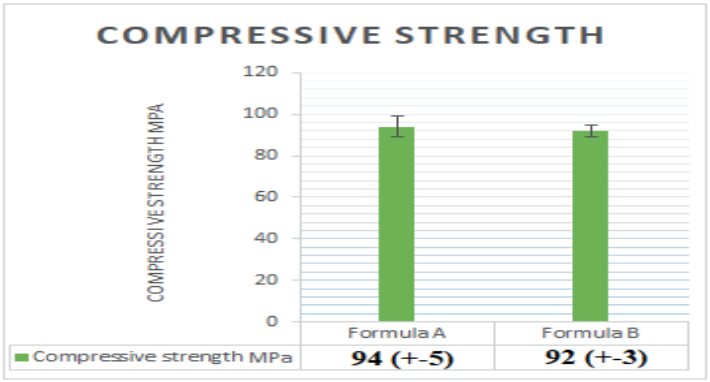

Figure 8 *The effect of recycled concrete powder on compressive strength of concrete at 28 day*

measuring 150 mm at 28 day of cure; the presented results in Figure 8 represent the average compressive strength of six specimens for each mixture, to quantify the effect of recycled concrete powder on compressive strength of concrete at 28 day.

It is noticeable that the compressive strength was not significantly affected, with only a minor variance of approximately 2% observed, when incorporating the recycled concrete powder. The concrete has effectively maintained its robust compressive strength.

Furthermore, the examination revealed that the concrete exhibited a wholly brittle breakage mode, indicating that, in this formulation, the inclusion of fibers is necessary.

4 Conclusions

From the results obtained, it is possible to assess to what extent the recycle concrete powder is compatible with cementitious matrices, therefore, the following conclusions were drawn:

1. The mortars were prepared without and with ranging from 5 to 50% of the cement replacement by recycled concrete powder; it has been found that, up to 10%, replacement had no adverse effects and the concrete kept its properties well, and the effects are acceptable, sometimes rather negligible up to a 20% of replacement share. However, beyond 25% we observe a start of significant decrease of mechanical properties.
2. Other mortars were prepared with 20% of cement substitution by recycled concrete powder, varying the fineness size of it; we found that for a fineness up to 160 μm, the compressive strength remained consistent. Then, it starts to become slightly affected and decreased marginally in the range from 250 to 315 μm. However, when the finesse exceed a 500 μm the strength becomes significantly affected.
3. For the water demand, it is necessary to make a water correction from 20% replacement, and this correction must be around 1% of the binder mixing water for each 10% of additional replacement share.
4. After formulating a concrete mix by applying optimizations deduced from previous results, we were able to obtain fresh and hardened properties

using recycled concrete powder approximately similar to those of the reference concrete.

5. We conclude from these findings that in the formulation of concrete using the recycled concrete powder, the concrete can effectively maintain its key characteristics and essential properties, particularly in terms of workability and compressive strength. This is applicable even to high-performance concrete, as well.
6. From an economic stand point, replacing 20% of the cement quantity, which is notably expensive, by recycled concrete powder, obtained at a minimal cost during the manufacturing of recycled aggregates, proves to be highly advantageous. This approach can offer substantial economic benefits in addition to its environmental advantages.

Based on these conclusions, it can confidently be asserted that substituting a portion of the cement with recycled concrete powder can be done effectively, all while preserving the fundamental properties of the standard concrete. This sustainable practice not only reduces the demand for new cement but contributes to environmentally friendly construction methods, as well. The use of recycled materials in concrete production is an essential step towards achieving greater sustainability in the construction industry.

Acknowledgements

The authors wish to thank the Directorate General for Scientific Research and Technological Development (D.G.R.S.D.T., Algeria) for financial support of this work. Thanks to the professors and students, members of Laboratory of Eco-Materials: Innovations and Applications (EMIA ex. LFGM). Thanks to Erasmus+ KA107 for the scholarship opportunity. Thanks to the professors and students. members of Institute of Concrete Science and Technology ICITECH.

Conflicts of interest

The authors declare that they have no known competing financial interests or personal relationships that could have appeared to influence the work reported in this paper.

References

[1] BRAVI, L., SANTOS, G., PAGANO, A., MURMURA, F. Environmental management system according to ISO 14001:2015 as a driver to sustainable development. *Corporate Social Responsibility and Environmental Management* [online]. 2020, **27**(6), p. 2599-2614. ISSN 1535-3958, eISSN 1535-3966. Available from: https://doi.org/10.1002/csr.1985

[2] KEITH, M., BIRCH, E., BUCHOUD, N. J. A., CARDAMA, M., COBBETT, W., COHEN, M., ELMQVIST, T., ESPEY, J., HAJER, M., HARTMANN, G., MATSUMOTO, T., PARNELL, S., REVI, A., ROBERTS, D. C., SAIZ, E., SCHWANEN, T., SETO, K. C., TUTS, R., VAN DER PUTTEN, M. A new urban narrative for sustainable development. *Nature Sustainability* [online]. 2023, **6**(2), p. 115-117. eISSN 2398-9629. Available from: https://doi.org/10.1038/s41893-022-00979-5

[3] National Waste Agency - Algeria. Report DMA 2020. Household and assimilated waste. Report on the State of Waste Management in Algeria, 2020 [online] [accessed 2020-03-03]. Available from: https://and.dz/site/wp-content/uploads/rapport%20DMA2.pdf

[4] BOUARROUDJ, M. E. K., REMOND, S., GRELLIER, A., BULTEEL, D., MICHEL, F., ZHAO, Z., COURARD, L. Intra granular porosity of mineral powders: modelling and experimentation. *Materials and Structures / Materiaux et Constructions* [online]. 2021, **54**(2), 88. ISSN 1359-5997, eISSN 1871-6873. Available from: https://doi.org/10.1617/s11527-021-01670-5

[5] German Society for International Cooperation "GIZ" in Algeria. Algeria, Environmental Management and Sustainable Development, 2021. [online] Available from: https://www.giz.de/en/downloads/giz-2021-fr-Portfolio-Algerien.pdf

[6] UNSDCF_Algeria, United Nations Cooperation Framework for the Sustainable Development of Algeria 2023-2027 United Nations, 2022 [online] [accessed 2022-11]. Available from: https://unsdg.un.org/sites/default/files/2022-11/UNSDCF_Algeria-2023-2027.pdf

[7] PAVLU, T., BOEHME, L., HAJEK, P. Influence of recycled aggregate quality. *Communications - Scientific Letters of the University of Zilina* [online]. 2014, **16**(4), p. 35-40. ISSN 1335-4205, eISSN 2585-7878. Available from: https://doi.org/10.26552/com.C.2014.4.35-40

[8] AGRELA, F., BELTRAN, M. G., CABRERA, M., LOPEZ, M., ROSALES, J., AYUSO, J. Properties of recycled concrete manufacturing with all-in recycled aggregates and processed biomass bottom ash. *Waste and Biomass Valorization* [online]. 2018, **9**(7), p. 1247-1259. ISSN 1877-2641, eISSN 1877-265X. Available from: https://doi.org/10.1007/s12649-017-9880-6

[9] JONES, M. R., HALLIDAY, J. E., CSETENYI, L., ZHENG, L., STROMPINIS, N. Utilising fine and coarse

recycled aggregates from the Gulf Region in concrete. In: Mediterranean Materials Congress on Energy and Infrastructure Systems TMS Middle East: proceedings [online]. MEMA. 2015. p. 13-23. Available from: https://doi.org/10.1002/9781119090427.ch2

[10] LALDINTLUANGA, H. Study of partial replacement of natural aggregate by recycled aggregate on concrete. *International Journal of Latest Engineering and Management Research* [online]. 2017, **2**(11), p. 1-6. ISSN 2455-4847.

[11] VELAY-LIZANCOS, M., VAZQUEZ-BURGO, P., RESTREPO, D., MARTINEZ-LAGE, I. Effect of fine and coarse recycled concrete aggregate on the mechanical behavior of precast reinforced beams: Comparison of FE simulations, theoretical, and experimental results on real scale beams. *Construction and Building Materials* [online]. 2018, **191**, p. 1109-1119. ISSN 0950-0618, eISSN 1879-0526. Available from: https://doi.org/10.1016/j.conbuildmat.2018.10.075

[12] OKSRI-NELFIA, L., MAHIEUX, P. Y., AMIRI, O., TURCRY, P., LUX, J. Reuse of recycled crushed concrete fines as mineral addition in cementitious materials. *Materials and Structures/Materiaux et Constructions* [online]. 2015, **49**(8), p. 3239-3251. ISSN 1359-5997, eISSN 1871-6873.Available from: https://doi.org/10.1617/s11527-015-0716-1

[13] MEHDIZADEH, H., MO, K. H., LING, T. C. (2023). CO2-fixing and recovery of high-purity vaterite CaCO3 from recycled concrete fines. *Resources, Conservation and Recycling* [online]. 2023, **188**, 106695. ISSN 0921-3449, eISSN 1879-0658. Available from: https://doi.org/10.1016/j.resconrec.2022.106695

[14] LIKES, L., MARKANDEYA, A., HAIDER, M. M., BOLLINGER, D., MCCLOY, J. S., NASSIRI, S. Recycled concrete and brick powders as supplements to Portland cement for more sustainable concrete. *Journal of Cleaner Production* [online]. 2022, **364**, 132651. ISSN 0959-6526, eISSN 1879-1786. Available from: https://doi.org/10.1016/j.jclepro.2022.132651

[15] European Committee for Standardization. CEN EN 196-1. Methods of testing cement part 1: determination of strength. Brussels: CEN, 2005.

[16] LIU, X., LIU, L., LYU, K., LI, T., ZHAO, P., LIU, R., ZUO, J., FU, F., SHAH, S. P. Enhanced early hydration and mechanical properties of cement-based materials with recycled concrete powder modified by nano-silica. *Journal of Building Engineering* [online]. 2022, **50**, 104175. eISSN 2352-7102. Available from: https://doi.org/10.1016/j.jobe.2022.104175

[17] CANTERO, B., SAEZ DEL BOSQUE, I. F., SANCHEZ DE ROJAS, M. I., MATIAS, A., MEDINA, C. Durability of concretes bearing construction and demolition waste as cement and coarse aggregate substitutes. *Cement and Concrete Composites* [online]. 2022, **134**, 104722. ISSN 0958-9465, eISSN 1873-393X. Available from: https://doi.org/10.1016/j.cemconcomp.2022.104722

[18] JAMIL, S., SHI, J., IDREES, M. Effect of various parameters on carbonation treatment of recycled concrete aggregate using the design of experiment method. *Construction and Building Materials* [online]. 2023, **382**, 131339. ISSN 0950-0618, eISSN 1879-0526. Available from: https://doi.org/10.1016/j.conbuildmat.2023.131339

[19] European Committee for Standardization. EN 196-6: Methods of testing cement - part 6: determination of fineness. Brussels, Belgium, 2010.

[20] GHOMARI, F., BENDI-OUIS, A. Normal consistency and setting. University of Tlemcen, 2007 [online]. Available from: https://ft.univ-tlemcen.dz/assets/uploads/pdf/departement/gc/tp/consistance_normale_Prise.pdf

[21] SERNA, P., LLANO-TORRE, A., MARTI-VARGAS, J. R., NAVARRO-GREGORI, J. *Fibre reinforced concrete: improvements and innovations. RILEM-fib International Symposium on FRC (BEFIB) in 2020* [online]. Vol. 30. Cham: Springer, 2021. ISBN 978-3-030-58481-8. Available from: https://doi.org/10.1007/978-3-030-58482-5

[22] MEZQUIDA-ALCARAZ, E. J., NAVARRO-GREGORI, J., MARTI-VARGAS, J. R., SERNA-ROS, P. Effects of tension stiffening and shrinkage on the flexural behavior of reinforced UHPFRC beams. *Case Studies in Construction Materials* [online]. 2021, **15**, e00746. eISSN 2214-5095. Available from: https://doi.org/10.1016/j.cscm.2021.e00746

[23] AGHA, N., MAKKANI, A., TAFRAOUI, A., ZAOUAI, S. Improving the physical and mechanical properties of new concrete containing crushed dune sand and demolition waste as coarse aggregate. *The Journal of Engineering and Exact Sciences* [online]. 2023, **9**(5), 16002-01e. eISSN 2527-1075. Available from: https://doi.org/10.18540/jcecvl9iss5pp16002-01e

[24] SALAH, A., TAFRAOUI, A., TAB, B. Effect of recycle fiber on the mechanical properties of high strength concrete. tobacco regulatory science. *Tobacco Regulatory Science* [online]. 2023, **9**(1), p. 3928-3937. eISSN 2333-9748. Available from: https://doi.org/10.18001/TRS.9.276

[25] AMARI, G., GHERICI, M. Valorization of recycled concrete fines in the development of sustainable construction materials [online]. Electronic Theses and Dissertations. ENP-Oran. Algeria, 2010. Available from: https://repository.enp.edu.dz/jspui/bitstream/123456789/4758/1/AMARI.Gherici.PDF

UNIVERSITY
OF ŽILINA

In its over 70 years of successful existence, the University of Žilina (UNIZA) has become one of the top universities in Slovakia.

The journal Komunikácie - vedecké listy Žilinskej univerzity v Žiline / Communications - Scientific Letters of the University of Žilina, Slovakia, began publication in 1999 with the expectation that it would provide sufficient space for presentation of the latest scientific knowledge and trends in the field of transport, telecommunications, and information technology. The scientific scope of the journal was mainly focused on the issues of transport, telecommunications, structures, materials, technologies and new areas of the university development. As of September 2018, the journal has been profiled as a scientific journal focusing on the topic of transportation.

The journal Communications - Scientific Letters of the University of Žilina is now an established open access scientific journal focusing primarily on topics related to the field of transport. The main areas, related to transport, include Civil Engineering, Electrical Engineering, Management and Informatics, Mechanical Engineering, Operations and Economics, Safety and Security, Travel and Tourism Studies.

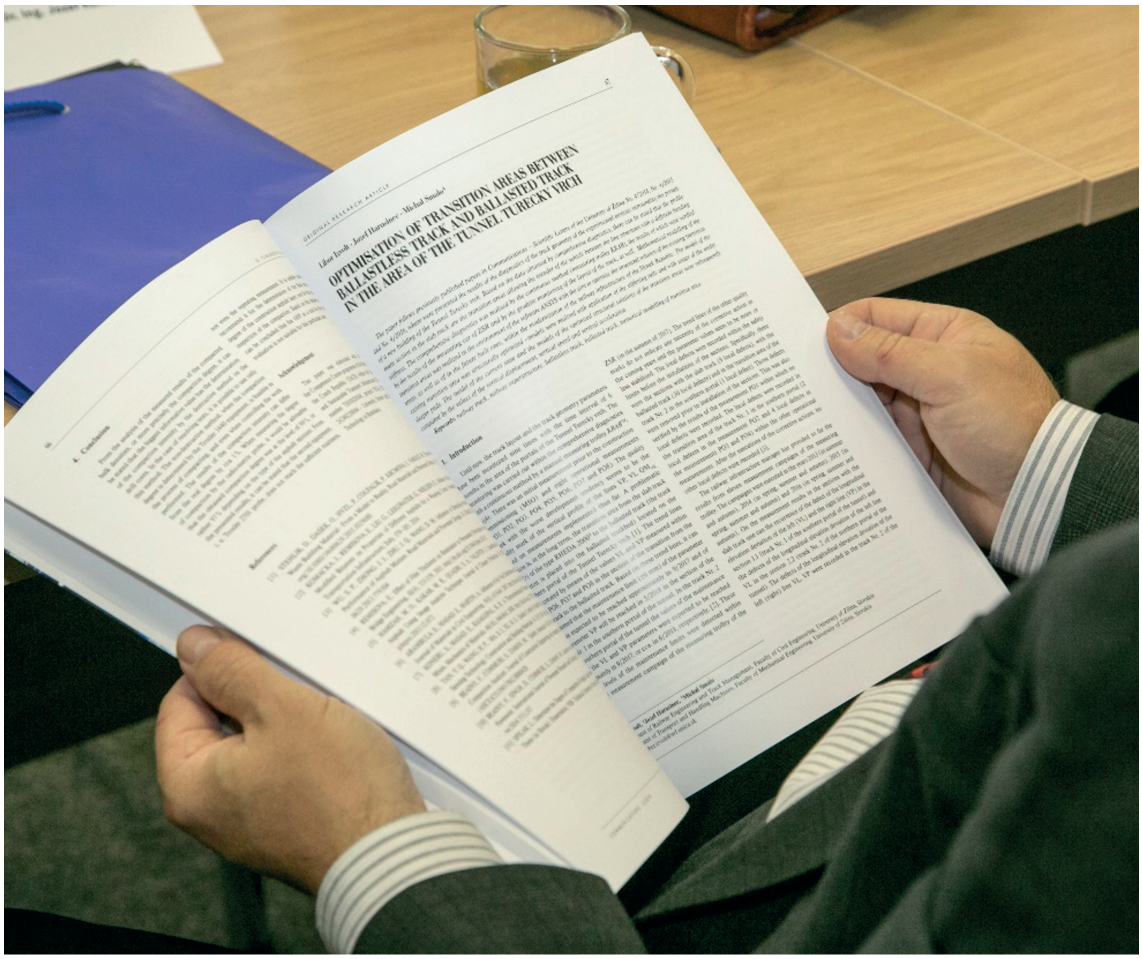

UNIVERSITY OF ŽILINA
Science & Research Department

Univerzitná 8215/1,
010 26 Žilina,
Slovakia

Ing. Janka Macurová
tel.: +421 41 513 5143
e-mail: janka.macurova@uniza.sk

ESTIMATION OF VULNERABLE ROAD USER ACCIDENT FREQUENCY THROUGH THE SOFT COMPUTING MODELS

Saurabh Jaglan[1,*], Sunita Kumari[1], Praveen Aggarwal[2]

[1]Civil Engineering Department, Deenbandhu Chhotu Ram University of Science and Technology, Murthal, Sonepat, Haryana, India
[2]Civil Engineering Department, National Institute of Technology, Kurukshetra, Haryana, India

*E-mail of corresponding author: saurabhjaglan.civil@dcrustm.org

Saurabh Jaglan 0000-0001-8719-4677, Sunita Kumari 0000-0003-3050-5096

Resume

Accident prediction models are mathematical expressions or algorithms used to determine the causal factors for road accidents and road safety engineers are using these models, as well. Modelling this kind of accident is quite challenging and required good quality of data. The results of the artificial neural network model, Gaussian processes model, and support vector machine model are compared for vulnerable road accident frequency in this study. The accident frequency dataset comprises 218 records, with 146 designated for training purposes and 72 reserved for testing. The model's accuracy was contingent on: the mean absolute error, root mean square error and coefficient of correlation. The findings suggest that for predicting the vulnerable road user accidents on roads, the artificial neural network gives better correlation results as (0.912) that the support vector machine (0.879) and Gaussian processes (0.853).

Article info

Received 27 October 2023
Accepted 21 February 2024
Online 11 March 2024

Keywords:

vulnerable road user
accident frequency
artificial neural network
support vector machine and
Gaussian processes

Available online: https://doi.org/10.26552/com.C.2024.023

ISSN 1335-4205 (print version)
ISSN 2585-7878 (online version)

1 Introduction

Almost 400 million trucks and 1.1 billion cars were driven globally in 2015. It is anticipated that 800 million trucks and 2 billion cars would be driven worldwide in 2040 [1]. The increase in vehicular population causes an increase in accidents worldwide, as well as in India. According to Road accidents in India, there has been an alarming annual increase in accidents of 11.9% and a rise in fatalities of 9.4%. These road safety issues in India have been a major concern, and accidents involving vehicles and vulnerable road users (VRUs) are unfortunately common [2]. The VRUs include pedestrians, cyclists, and two-wheeler riders. Several factors, including road characteristics, traffic-related variables, environmental factors, speed characteristics, etc., influence *the* vulnerable road user (VRU) accidents. Since the VRU road accident data is discrete and non-negative, it mostly counts data models used in accident frequency modelling (i.e., the number of accidents on a specified section in known time duration). Various data sets were collected from roadside geometry and first information report (FIR) data collection to estimate the accident frequency. The random division method divides the entire dataset into two parts per the study's requirement. For this study data set was collected on about 364 kms of road length, including different national highway and state highways of Haryana a northern state of India. The roads are then divided into sub-sections based on other geometric data. Two hundred eighteen accident frequency records were divided into two parts. Out of these, 146 samples were used to create the model (training set), and 72 samples were used to test the model in the study. Traditional methodologies are employed using *the* assumed analytical equations to evaluate the impact of various road geometries and accident-related factors, and conducting regression. Nonetheless, those methods prove challenging to apply, and the existing literature offers no completely accurate predictions for vulnerable road user accidents. The flowchart of this investigation is shown in Figure 1. Figure 2 represents the online portal of the Haryana police accident recording application. This portal is used to extract the VRU accident-related information. This portal requires the year, district and police station as input data and then provides the complete details of every accident.

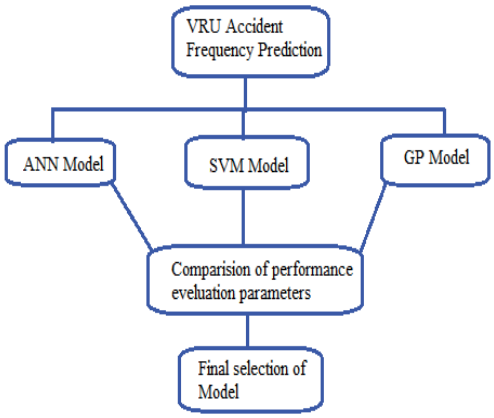

Figure 1 *The process of investigation*

Figure 2 *Haryana Police Online Portal App*

2 Literature review

Various artificial intelligence techniques, including Gaussian processes (GP), support vector machines (SVM), artificial neural networks (ANN), random forest (RF), adaptive network-based fuzzy inference system (ANFIS), M5P model trees, have gained significant popularity and widespread utilization among researchers in different fields [3-5]. Many of these studies suggest that artificial intelligence techniques exhibit considerably high accuracy. Numerous researchers employed the M5P model tree, artificial neural network, random forest model [6-8], with these approaches yielding the best-suited results. This research aims to predict the total VRU Accident frequency by comparing it using GP, SVM, and ANN methods. The recent scenario suggests that the frequency of vulnerable road accidents depends on many variables. Various researchers considered the road parameters and accident characteristics to impact accident frequency [9-11]. Those parameters may be *the* road width, shoulder width, length of section, traffic, median opening, service road, commercial units, etc. Nowadays, different studies are conducted to evaluate the effect of other variables length (L), Shoulder width (SW), road width (RW), median opening (MO), median assess (MA), average daily traffic (ADT), service road (SR) etc. on accidents and the impact of accidents [12-16]. In this study *the* SVM, ANN and GP models were applied using Waikato Environment for Knowledge Analysis, version- 3.9.5 software. The present study meticulously applies various advanced soft computing techniques to address the critical issue of predicting vulnerable road user accident frequency (VRUAF). These innovative and adaptive methodologies, rooted in artificial intelligence and data analysis, offer a dynamic and flexible approach to tackling the complex challenges of road safety for VRUs. The diverse set of soft computing techniques employed in past research includes [15].

2.1 Artificial neural network

This study uses an Artificial Neural Networks (ANN) Model to predict *the* accident frequency involving vulnerable road users. The architecture of an ANN, designed for vulnerable road user accident severity prediction; typically involves multiple layers of interconnected neurons is used [17-18]. The input layer receives relevant features, such as average daily traffic (ADT), Length of section, shoulder width, vehicle

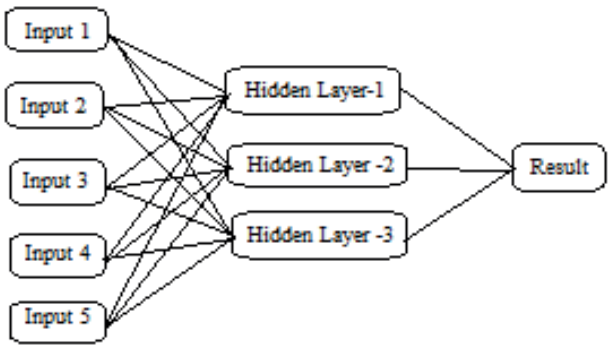

Figure 3 *Nomenclature of ANN model*

speed, time of day, and more. Hidden layers, which can be customized in depth and width, process these inputs to learn intricate relationships and patterns within the data. These layers of the ANN are responsible for processing the input data through a series of weighted connections and non-linear activation functions. Different models were generated through experimentation and optimization to achieve the best predictive performance by changing neurons and the number of hidden layer neurons. Various ANN models were generated with different hidden layers and training times to get better results. Neurons in the hidden layers apply mathematical transformations to the input data to capture complex combinations of input variables. The output layer of the ANN provides the predicted output, which in this study is the estimated frequency of VRU accidents. Typically, there is a single output node for the regression tasks like accident frequency prediction. The output value represents the predicted accident frequency. Following the establishment of the optimal architecture, the dataset comprising a total of 218 accidents should be segregated into two distinct subsets. The first set is for training the network, and the second is exclusively reserved for testing the network's performance. In this study the complete accident data is divided into two parts, i.e., *the* training set and testing set. Firstly, using 70% of the total data, the model is trained using all the parameters for various correlation coefficient (CC) values. The same trial is to be performed many times by changing the neurons in hidden layers. The remaining 30% of the data is utilized to validate the developed model in terms of the best-suited CC value. Figure 3 represents the working of the ANN model with different input variables and hidden layers. Various combinations are formed with different hidden layers, and the best suited model is considered as the result of the ANN model.

2.2 Support vector machines

Regression using support vectors and classification techniques from statistical learning theory are known as support vector machines. The ideal separation of classes is the foundation of classification techniques based on the support vector machines. This approach chooses the linear classifier that minimizes the generalization error, or at least an upper bound on this error, resulting from structural risk minimization, from an infinite pool of potential classifiers, provided that the classes can be distinguished from one another. As a result, the hyperplane that leaves the greatest margin between the two classes will be chosen; according to Cortes and Vapnik (1995), the margin is the total of the hyperplane's distances from the points closest to the two classes [19].

2.3 Gaussian process

One easy to understand and popular family of probability distributions on functions is the Gaussian process (GP). Viewed in this broad context, scholars have researched and employed many varieties of Gaussian processes. However, this focuses on the more focused use of Gaussian processes to predict. Distributions over functions are represented by a Gaussian process using training data and testing data. We have a training data, T= {A,b}, where, A= {a_1, a_2, a_3, …..a_n} matrix have x_i as input examples, and b = [b_1, b_2, b_3, b_4……..b_n] vector have b_j as training output. Training data T = {A,b} with the input test as z* [20]. Where the input vectors of test set matrix are, z* = [z_1,……z_n]

The following equation gives the overall observations:

$$P_i = f(z_i) + \varepsilon, \quad (1)$$

where the P_i is used to predict the results using testing data set. Function $f(z_i)$ is the function/parameters used to prediction and variance and mean zero is taken as ε in the equation.

2.4 Details of Kernel functions

The kernel function concept was proposed on data to simplify it into a higher dimensional feature involving non-linear decision surfaces. Without actually doing

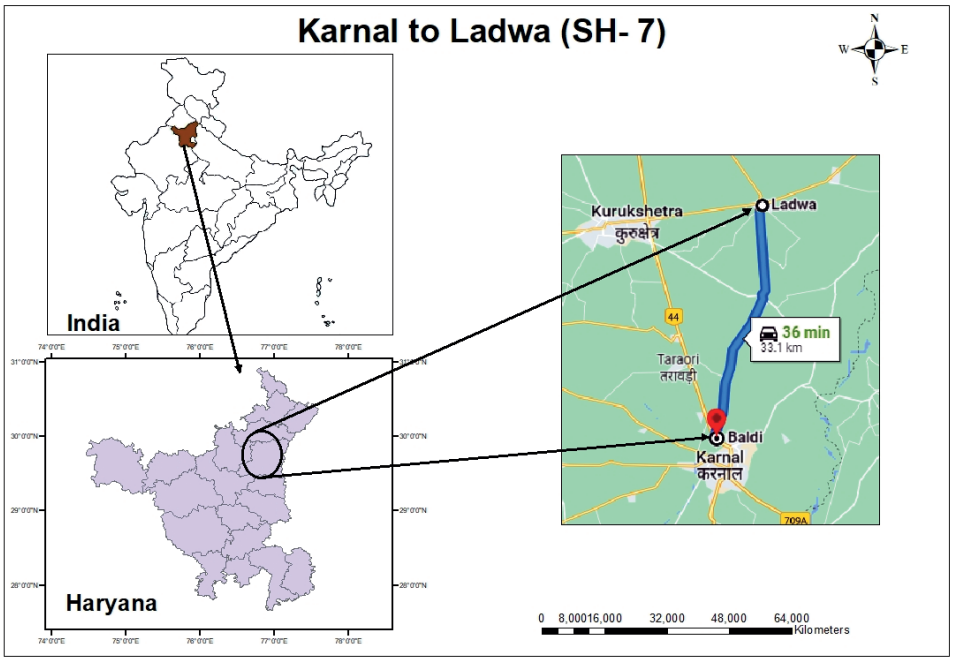

Figure 4 *One of the Study areas for Accident and road geometry data collection*

Table 1 *Description of model variables for accident frequency and severity modelling*

Descriptive Statistics					
	N	Minimum	Maximum	Mean	Std. Deviation
ADT	218	4127	105673	26913.92	30558.705
Ln ADT	218	8.325	11.568	9.7678	0.853
L	218	.7	19.0	5.442	3.589
Ln L	218	-0.356	2.944	1.455	0.745
RW	218	5.5	28.0	13.115	7.062
SW	218	0	6.0	2.349	1.741
Median Width	218	0	4.50	.6709	1.017
Minor Access	218	0	24	8.47	5.989
HC	218	0	18	4.96	4.784
VC	218	0	6	1.44	1.505
MO	218	0	11	4.39	2.996
SR	218	0	4.50	1.406	1.133
CAR %	218	31.330	73.290	49.608	12.000
TRUCK/HV %	218	11.23	44.68	19.837	8.563
Commercial Units	218	0	47	11.57	11.539
B and C	218	0	22	3.57	4.849
SPEED	218	20	110	65.47	21.147
A/Yr	218	1	32	10.26	6.981

Where L = Length of section (km); LnL = Log of Length of section; ADT = Average Daily Traffic; LnADT = Log of Average Daily Traffic; SW = Shoulder Width; RW = Road Width; MO = Median Opening; MA = Minor Access; MW = Median Width; HC = Horizontal Curve; VC = Vertical Curve;

C % = Percentage of cars; T % = Percentage of Truck; B & C = Bridge and Culverts; A/yr = Accidents per year; SR = Service Road.

calculations in a high-dimensional feature space, any selected model can operate there because of a kernel function. The selection of appropriate kernel parameters is crucial and often involves hyperparameter tuning to optimize the model performance. A kernel function provides a way to measure the similarity or dissimilarity between the data points and is a key component in many machine learning models, enabling them to operate effectively in higher-dimensional spaces without explicitly computing the transformed feature vectors. A mathematical function is a kernel function, and any symmetric positive semidefinite function that meets Mercer's requirements can be utilized as a kernel function, according to Cortes and Vapnik (1995) [19]. Several kernel functions are available, but selecting the one that provides the optimum generalization with a particular dataset might be challenging. The selection of kernel should be as per requirement for the underlying structure of the data. Cross-validation and other model selection techniques are often employed to determine the best kernel for a specific problem. The correlation coefficients (CC) and Root Mean Square Error (RMSE) were examined to determine the best selection of these factors. Different models were created using the input dataset as a training set to forecast the VRU accident frequency. The regression model's accuracy is estimated through testing. In the current study, the effectiveness of different models in predicting the efficiency of the VRU accident frequency was evaluated using the correlation coefficient, R2, and the root mean square error (RMSE).

3 Method and materials

Data were derived from several resources, including the Harsamay portal of Haryana Police, field visits, the PWD department, toll plaza, etc. Data was collected for accidents and road-related elements, as shown in Figure 4. The range of accident frequency lies between 0 and 32 at the single road starch. The complete VRUAF dataset comprises 218 data sets divided into training and testing set. The descriptive statics of input and output variables are shown in Table 1. The minimum, maximum, mean and standard deviations are given for each parameter used in the study.

4 Result and discussion

Different models were developed using the collected VRU accident data set to predict the accidents with other influencing parameters. The first and most efficient ANN model is applied by changing the hidden layers from 1 to 5. The different CC, RMSE, and MAE values are calculated for each model approach. The best-suited highest value is taken as the final for three numbers of hidden layers.

4.1 Support vector machine model results

The training and testing sets included 70 % and 30 % of the entire data set, respectively. Several manual trials were performed for the SVM using different Kernel Function based model development. The results in the form of performance evaluation parameters (CC, RMSE, and MAE) are listed in Table 2 for both the training and testing stages. Different models were generated with the help of a training data set of vulnerable road use accidents. After the model development, the same model was applied to the testing data set for evaluating their performance. The conclusions provided in Table 2 show that the Pearson Vii kernel function based SVM model exhibits better results than all the other applicable models. Specifically, the training stage values of CC, RMSE, and MAE are 0.9064, 0.0820, and 0.2586, while the testing stage values are 0.8795, 1.5630, and 2.3681, respectively. The agreement plot between the actual and predicted VRU accident frequency values using the SVM_puk model for the testing stage is shown in Figure 5. All predicted values lie closer to the line of perfect agreement (1:1) line.

Figure 5 shows the plots illustrating the actual VRUs accident frequency distribution and predicted values of the VRUs accident frequency using the SVM_ puk model. The representation of this figure evidently demonstrates that the SVM_puk-based model predicted

Table 2 *SVM model results using different Kernel Function*

S.No	Kernel Function	SVM					
		TRAINING SET (146)			TESTING SET (72)		
		Correlation Coefficients	Mean Absolute Error	Root Mean Square Error	Correlation Coefficients	Mean Absolute Error	Root Mean Square Error
1	SVM_ RBFKernal	0.8728	1.1214	1.5581	0.8589	1.4434	1.9114
2	SVM _Puk	0.9064	0.0820	0.2586	0.8795	1.5630	2.3681
3	SVM_ PolyKernel	0.8475	1.3485	1.8149	0.8326	1.5821	2.4245

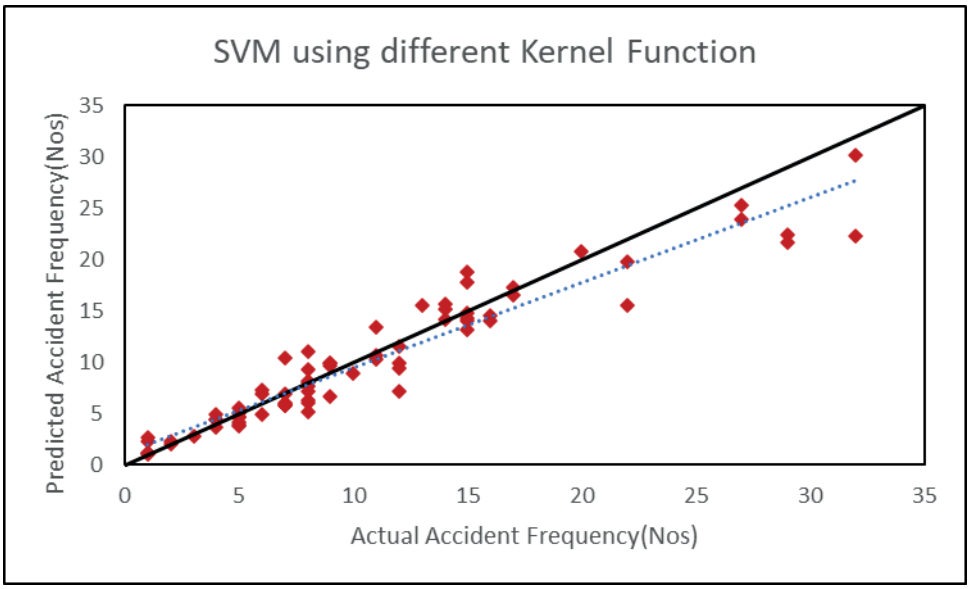

Figure 5 *Variation in scatter values with the actual values of the VRUAFs using SVM Model*

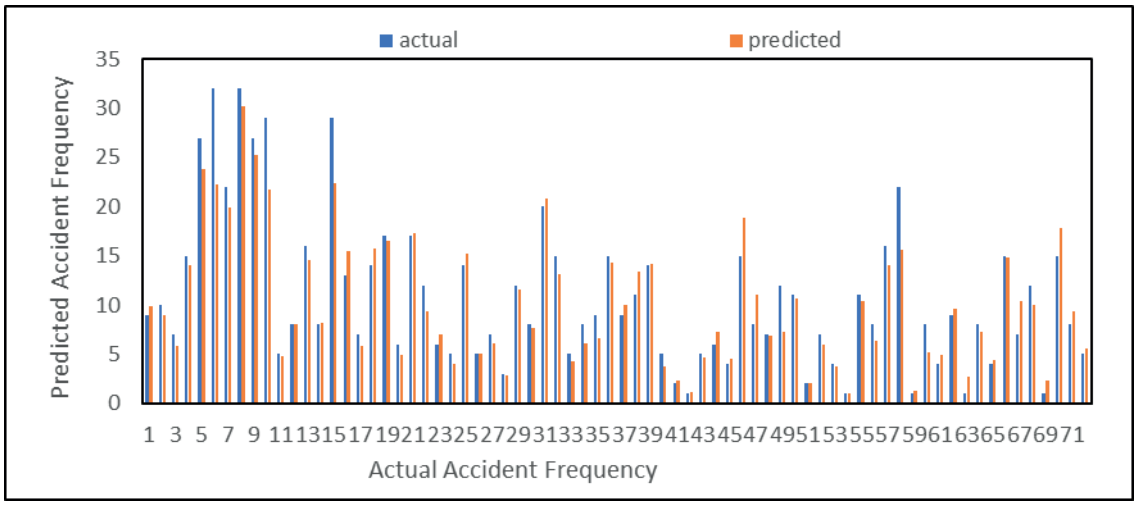

Figure 6 *SVM Model variation in actual and predicted VRUAFs values*

closer values to actual VRUAFs' values in comparison to the other models. The VRUs accident frequency using the SVM Model with actual and predicted values are shown in Figure 6.

4.2 Artificial neural network model results

In this study, the architecture of an ANN designed, for vulnerable road user accident frequency prediction, typically involves multiple layers of interconnected neurons.

The table 3 indicated the results with different hidden layers keeping the training time constant using ANN Model approach. The training time was taken as 1000 for each model formulation. Various models were generated using the value 0.2 of learning rate and 0.1 of momentum. Then, the same model was applied to the testing data set, and the results are given in Table 3. The same procedure was repeated for all five ANN models by changing the hidden layers, and results were calculated in terms of CC, RMSE, and MAE. The best value of ANN-4 is considered in terms of CC, RMSE, and MAE values are 0.9245, 1.458, and 1.123, respectively for the training set. The final ANN-4 model was used for further comparison with other modelling techniques in terms of these three performance indicators for VRUs accident frequency data. The scatter diagram of the actual and predicted VRU accident frequency values using the ANN-4 model in the testing dataset is shown in Figure 7. Figure 8 represents the predicted and actual VRUAF values with the help of the ANN Model.

4.3 Gaussian processes model result

Model development of GP is similar to SVM based model development. The results for training and testing data sets of various kernel function based GP models in for CC, RMSE, and MAE are listed in Table 4. The

Table 3 *Results of neurons-based ANN models*

S. No	Model	No of neurons in hidden Layer	ANN Model					
			TRAINING SET (146)			TESTING SET (72)		
			Correlation Coefficients	Mean Absolute Error	Root Mean Square Error	Correlation Coefficients	Mean Absolute Error	Root Mean Square Error
1	ANN-1	1	0.834	1.183	1.516	0.802	1.245	1.987
2	ANN-2	2	0.878	1.041	1.383	0.852	1.396	1.799
3	ANN-3	3	0.912	0.947	1.252	0.904	1.337	1.741
4	ANN-4	4	0.924	1.124	1.458	0.912	1.198	1.799
5	ANN-5	5	0.895	1.585	1.651	0.860	1.685	1.854

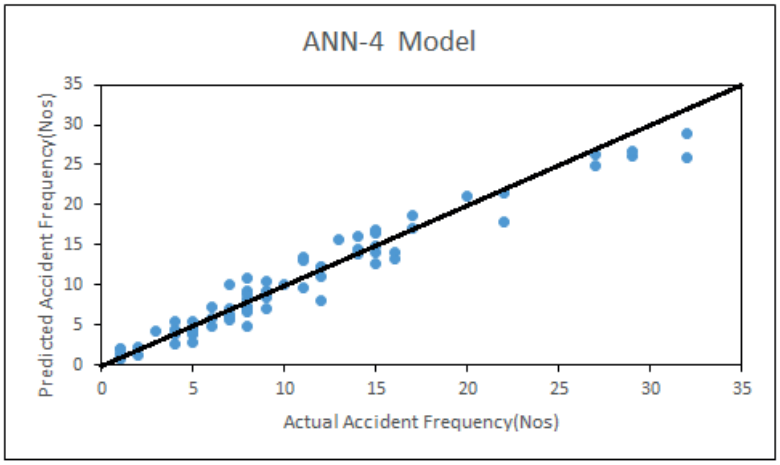

Figure 7 *ANN-4 model results for predicted and actual values of VRUAF*

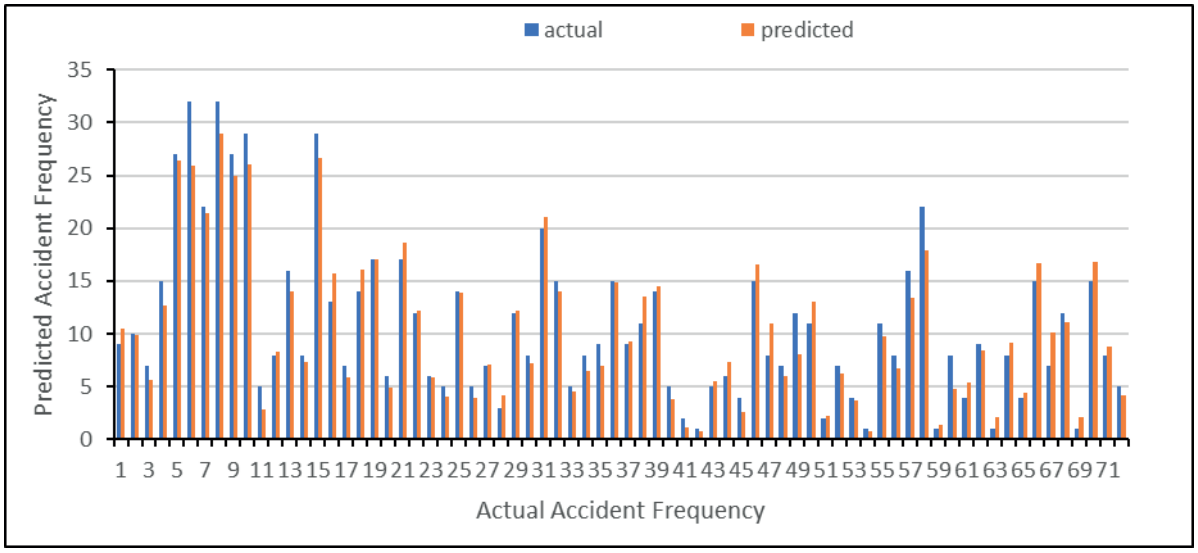

Figure 8 *ANN model comparison of predicted and actual values of VRUAF*

results of Table 4 demonstrate that the Pearson Vii kernel function-based GP model performs the best out of all the applied models. Its CC, RMSE, and MAE values are 0.885, 1.231, respectively, and 1.650 during the training stage and 0.853, 1.807, and 2.963, respectively during the testing stage. The performance of the Polynomial kernel function based GP model is better than the radial basis kernel function based GP model in terms of CC, RMSE, and MAE values are 0.853, 1.610, and 2.058, respectively for the training stage, and 0.839, 1.915 and 2.710, respectively for the testing stage. The agreement plot between the actual and predicted values of the VRUAFs using the GP_puk model for the testing stage is shown in Figure 9. All the predicted

Table 4 *Results of Gaussian Processes using different Kernel Function*

Gaussian processes							
S. No	Kernel Function	TRAINING SET (146)			TESTING SET (72)		
		Correlation Coefficients	*Mean Absolute Error*	*Root Mean Square Error*	Correlation Coefficients	*Mean Absolute Error*	*Root Mean Square Error*
1	GP_RBFKernal	0.820	3.130	3.914	0.853	3.350	4.666
2	GP_Puk	0.885	1.231	1.650	0.853	1.807	2.963
3	GP_PolyKernel	0.853	1.610	2.058	0.839	1.915	2.710

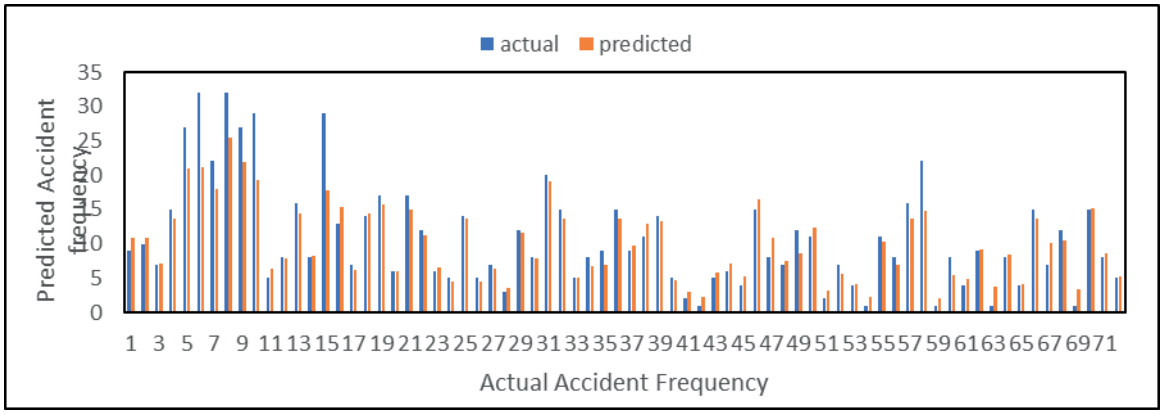

Figure 9 *GP Model comparison of actual and predicted values of VRUAF*

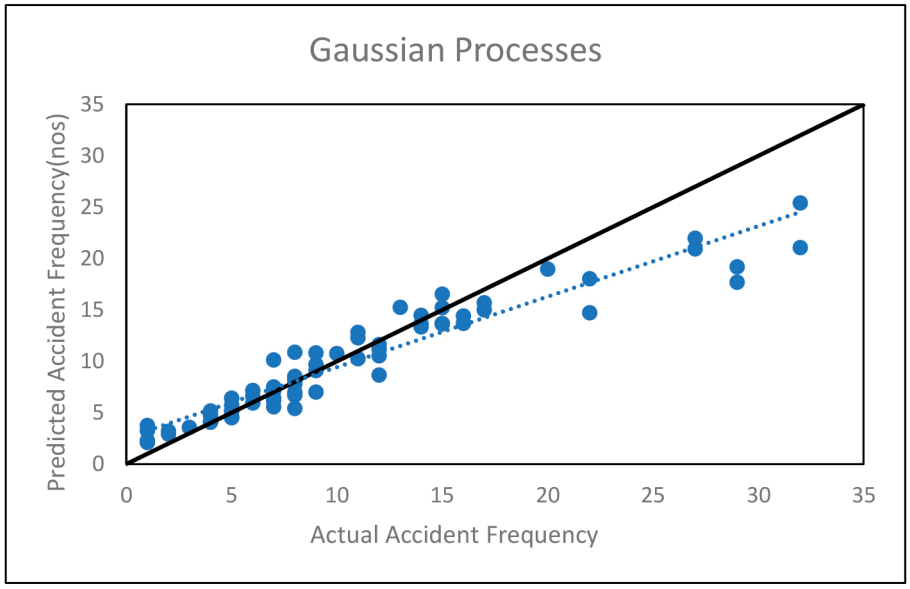

Figure 10 *Variation in scatter values with the actual values of the VRUAFs using the GP Model*

values lie closer to the line of perfect agreement (1:1) line. Figure 10 plots illustrate the distribution of actual VRUs accident frequency and predicted values of the VRUs accident frequency using the GP_puk model. The representation of this figure demonstrates that the GP_puk based model predicted the closer values to actual VRUs accident frequency values than the other models.

5 Comparison of selected artificial neural network model, Gaussian processes model, and support vector machine models

Table 5 summarizes the outcomes of the best selected ANN, SVM, and GP models. The results of this table indicate that the ANN-4 model was the most

Table 5 *Performance evaluation parameters for different modelled VRUAF*

Techniques	Training			Testing		
	CC	RMSE	MAE	CC	RMSE	MAE
ANN-4	0.924	1.124	1.458	0.912	1.198	1.799
SVM_puk	0.906	0.082	0.258	0.879	1.563	2.368
GP_Puk	0.885	1.231	1.650	0.853	1.807	2.963

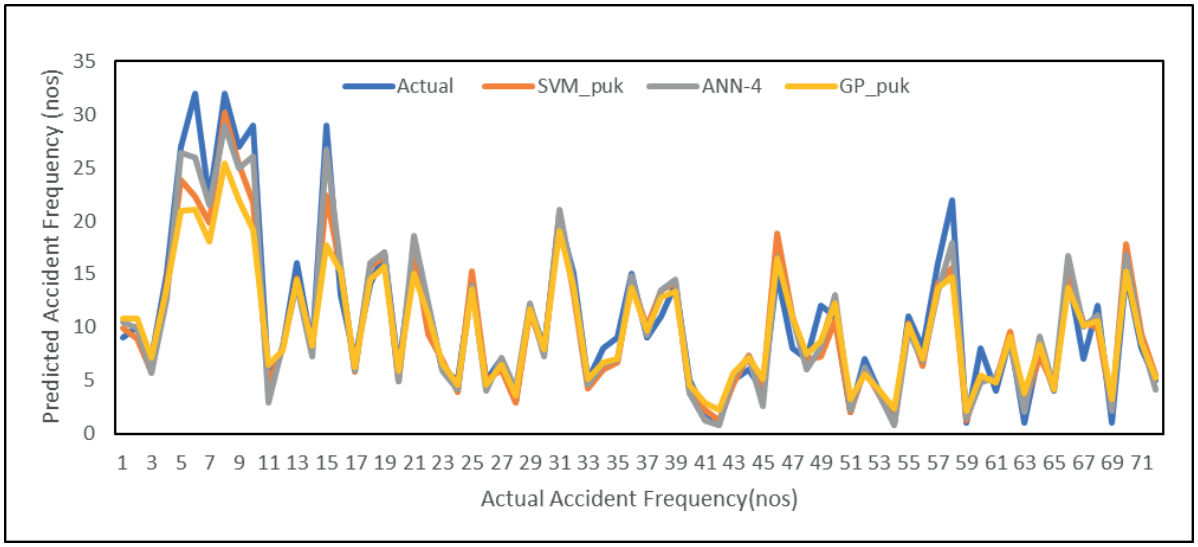

Figure 11 *Variation of the predicted values with the actual values of the VRUAFs using the SVM Model, GP Model, and ANN Model*

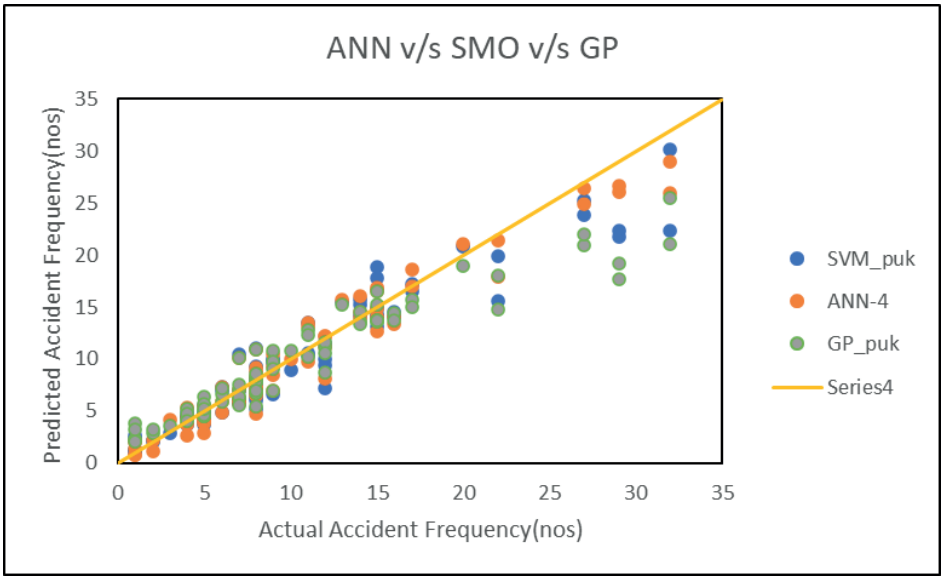

Figure 12 *Variation in scatter values with the actual values of the VRUAFs using SVM Model, GP Model, and ANN Model*

suitable model for accurately predicting the VRUAF with notably low CC and considerably high RMSE and MAE values.

The SVM Model, GP Model, and ANN Model comparison using actual and predicted VRUAF is shown in Figure 11. The ANN Model appears to be the best fit for predicting the VRUAF. The ANN-4 model lines for predicted values follow the same path as the actual values. The SVM, GP and ANN based best performing models are shown for actual and predicted VRUAF values in Figure 12. This figure illustrates that ANN-4 model points are much closer to the agreement line. Hence, the ANN-4 is the best performing model among all other applied models using this data set.

6 Conclusions

This investigation has assessed the performance of three regression-based modelling approaches to provide insights into the most suitable methods for predicting VRU (Vulnerable Road User) accident frequency. These approaches were ANN, SVM, and Gaussian Processes. This study employed various combination models as input variables, with VRUAF as the output. The ANN-4, SVM_Puk and GP_Puk model approach demonstrated exceptional efficiency when used with the ANN, SVM, and Gaussian Processes. According to the analysis, the ANN technique predicts the VRUAF more accurately than *the* GP and SVM. The R values for testing VRUAF data set come from the ANN approaches (0.904) are higher than GP (0.8539) and SVM (0.8795).

Similarly, the ANN model having values of RMSE and MAE (1.337 and 1.741) are much lower than the GP Model (1.807 and 2.963) and SVM model (1.563 and 2.368). Hence, ANN gave a more accurate VRUAF prediction than the GP and SVM models. Sensitivity investigation suggests that the most influential parameters in predicting vulnerable road user accident frequency, using the ANN model with the current data set, are LnL, LnADT, and Speed. Hence, the proper care should be taken when considering these parameters. The implementation of ANN is time-consuming, but it gives better accident prediction results than the actual happening of any accident. Hence, the proposed ANN model can be used to reduce the accident frequency and reduce accident costs and losses in terms of life and property.

Acknowledgment

The authors are thankful to the Public Works Department authorities, Rohtak, India, for the previous year's road geometry data, Toll Plaza National Highway-1, National Highway- 72, for road accident data. We are thankful to the Haryana police for recording road accidents on the online platform. This Harsamay online application collects the road accident data of various stretches.

Conflicts of interest

The authors declare that they have no known competing financial interests or personal relationships that could have appeared to influence the work reported in this paper.

References

[1] BUBELINY, O., DADOVA, I., KUBINA, M., SOVIAR, J. The use of smart elements for the transport operation in the Slovak cities. *LOGI - Scientific Journal on Transport and Logistics* [online]. 2019, **10**, p. 51-60. eISSN 2336-3037. Available from: https://doi.org/10.2478/logi-2019-0015

[2] Road accidents in India [online]. 2021. Available from: www.morth.nic.in

[3] SIHAG, P., TIWARI, N. K., RANJAN, S. Prediction of cumulative infiltration of sandy soil using random forest approach. *Journal of Applied Water Engineering and Research* [online]. 2019, **7**(2), p. 118-142. eISSN 2324-9676. Available from: https://doi.org/10.1080/23249676.2018.1497557

[4] SINGH, B., SIHAG, P., TOMAR, A. SEHGAD, A. Estimation of compressive strength of high-strength concrete by random forest and M5P model tree approaches. *Journal of Materials and Engineering Structures JMES*. 2019, **6**(4), p. 583-892. eISSN 2170-127X.

[5] IVAZ, J., NIKOLIC, R. R., PETROVIC, D., DJOKOVIC, J. M., HADZIMA, B. Prediction of the work-related injuries based on neural networks. *System Safety: Human - Technical Facility - Environment* [online]. 2021, **3**(1), p. 19-37. eISSN 2657-5450. Available from: https://doi.org/10.2478/czoto-2021-0003

[6] PURI, D., KUMAR, R., SIHAG, P., THAKUR, M. S., PERVEEN, K., ALFAISAL, F. M., LEE, D. Analytical investigation of the impact of jet geometry on aeration effectiveness using soft computing techniques. *ACS Omega* [online]. 2023, **8**(42), p. 31811-31825. eISSN 2470-1343. Available from: https://doi.org/10.1021/acsomega.3c03294

[7] GOEL, A. K., KHAN, K., KUSHWAHA, A., SRIVASTAVA, V., MALIK, S., SINGH, A. A machine learning approach to analyze road accidents. In: 2022 IEEE International Conference on Blockchain and Distributed Systems Security ICBDS: proceedings [online]. IEEE. 2022. eISBN 978-1-6654-2832-3, p. 1-5. Available from: https://doi.org/10.1109/ICBDS53701.2022.9935867

[8] SUTHAR, M., AGGARWAL, P. Modeling CBR value using RF and M5P techniques. *Mendel* [online]. 2019, **25**(1), p. 73-78. ISSN 1803-3814, eISSN 2571-3701. Available from: https://doi.org/10.13164/mendel.2019.1.073

[9] SUN, Z., XING, Y., WANG, J., GU, X., LU, H., CHEN, Y. Exploring injury severity of vulnerable road user involved crashes across seasons: a hybrid method integrating random parameter logit model and Bayesian network. *Safety Science* [online]. 2022, **150**, 105682. ISSN 0925-7535, eISSN 1879-1042. Available from: https://doi.org/10.1016/j.ssci.2022.105682

[10] KOMOL, M. M. R., HASAN, M. M., ELHENAWY, M., YASMIN, S., MASOUD, M., RAKOTONIRAINY, A. Crash severity analysis of vulnerable road users using machine learning. *PLoS One* [online]. 2021, **16**, e0255828. eISSN 1932-6203. Available from: https://doi.org/10.1371/journal.pone.0255828

[11] BAMEL, K., DASS, S., JAGLAN, S., SUTHAR, M. Statistical analysis and development of accident prediction model of road safety conditions in Hisar city. *IOP Conference Series: Earth and Environmental Science* [online]. 2021, **889**, 012034. ISSN 1755-1315. Available from: https://doi.org/10.1088/1755-1315/889/1/012034

[12] LEE, J., MANNERING, F. Impact of roadside features on the frequency and severity of run-off-roadway accidents: an empirical analysis. *Accident Analysis and Prevention* [online]. 2002, **34**(2), p. 149-161. ISSN 0001-4575, eISSN 1879-2057. Available from: https://doi.org/10.1016/S0001-4575(01)00009-4

[13] MILTON, J., MANNERING, F. The relationship among highway geometrics, traffic-related elements and motor-vehicle accident frequencies. *Transportation* [online]. 1998, **25**, p. 395-413. ISSN 0049-4488, eISSN 1572-9435. Available from: https://doi.org/10.1023/A:1005095725001

[14] JAGLAN, S., AGGARWAL, P., KUMARI, S. A comparative study of M5P, ANN and RENB models for prediction of vulnerable road accident frequency, n.d.

[15] JAGLAN, S., KUMARI, S., AGGARWAL, P. Development of prediction models for vulnerable road user accident severity. *Optical Memory and Neural Networks* [online]. 2023, **32**, p. 346-363. ISSN 1060-992X, eISSN 1934-7898. Available from: https://doi.org/10.3103/S1060992X23040082

[16] JAGLAN, S., AGGARWAL, P., SINGHAL, D., DASS, S. Vulnerable road user accidents analysis on various roads of Haryana. *AIP Conference Proceedings* [online]. 2023, **2856**, 020003. ISSN 0094-243X, eISSN 1551-7616. Available from: https://doi.org/10.1063/5.0165909

[17] GARCIA DE SOTO, B., BUMBACHER, A., DEUBLEIN, M., ADEY, B. T. Predicting road traffic accidents using artificial neural network models. *Infrastructure Asset Management* [online]. 2018, **5**(4), p. 132-144. ISSN 2053-0242, eISSN 2053-0250. Available from: https://doi.org/10.1680/jinam.17.00028

[18] CODUR, M. Y., TORTUM, A. An artificial neural network model for highway accident prediction: a case study of Erzurum, Turkey. *Promet-Traffic and Transportation* [online]. 2015, **27**(3), p. 217-225. ISSN 0353-532, eISSN 1848-4069. Available from: https://doi.org/10.7307/ptt.v27i3.1551

[19] CORTES, C., VAPNIK, V. Support - vector networks. *Machine Learning* [online]. 1995, **20**, p. 273-297. ISSN 0885-6125, eISSN 1573-0565. Available from: https://doi.org/10.1007/BF00994018

[20] KARCH, J. D., BRANDMAIER, A. M., VOELKLE, M. C. Gaussian process panel modelling - machine learning inspired analysis of longitudinal panel data. *Frontiers in Psychology* [online]. 2020, **11**, 351. eISSN 1664-1078. Available from: https://doi.org/10.3389/fpsyg.2020.00351

Dear colleague,

We would like to send you a copy of the journal Communications - Scientific Letters of the University of Zilina.

Journal Communications - Scientific Letters of the University of Zilina are a well-established open-access scientific journal aimed primarily at the topics connected with the field of transport. The main transport-related areas covered include Civil engineering, Electrical engineering, Management and informatics, Mechanical engineering, Operation and economics, Safety and security, Travel and tourism studies. The full list of main topics and subtopics is available at: *https://komunikacie.uniza.sk/artkey/inf-990000-0500_Topical-areas.php*

Journal Communications - Scientific Letters of the University of Zilina is currently indexed and accepted by CEEOL, Crossref (DOI), DOAJ, EBSCO Host, Electronic Journals Library (EZB), ERIH Plus, Google Scholar, Index Copernicus International Journals Master list, iThenticate, JournalGuide, Jouroscope, Norwegian Register for Scientific Journals Series and Publishers, ROAD, ScienceGate, SCImago Journal & Country Rank, SciRev, SCOPUS, WorldCat (OCLC).

Journal Communications - Scientific Letters of the University of Zilina is preserved in CLOCKSS and Portico to guarantee long-term digital preservation and is archived in the national deposit digitalne pramene.

Authors can share their experiences with publishing in our journal on SciRev.

Journal Communications - Scientific Letters of the University of Zilina is under evaluation for inclusion to Web of Science database.

I would like to invite authors to submit their papers for consideration. We have an open-access policy and there are **no publication, processing or other fees** charged for published papers. Our journal operates a standard single-anonymised review procedure, the successful completion of which is a prerequisite for paper publication.

The journal is issued four times a year (in January, in April, in July and in October).

I would also like to offer you the opportunity of using already published articles from past issues as source of information for your research and publication activities. All papers are available at our webpage: http://komunikacie.uniza.sk, where you can browse through the individual volumes. Our journal offers access to its contents in the open access system on the principles of the license **Creative Commons (CC BY 4.0)**.

For any questions regarding the journal Communications - Scientific Letters of the University of Zilina please contact us at: *komunikacie@uniza.sk*

We look forward to future cooperation.

Sincerely

Branislav Hadzima
editor-in-chief

KOMUNIKÁCIE
COMMUNICATIONS

VEDECKÉ LISTY ŽILINSKEJ UNIVERZITY
SCIENTIFIC LETTERS OF THE UNIVERSITY OF ZILINA

VOLUME 26 Number 2

April 2024

Each paper was reviewed by at least two reviewers.
Individual issues of the journal can be found on: http://komunikacie.uniza.sk
The full author quidelines are available at: https://komunikacie.uniza.sk/artkey/inf-990000-0400_Author-guidelines.php
Published quarterly by University of Žilina in EDIS - Publishing House of the University of Žilina.

Communications is currently indexed, abstracted and accepted by CEEOL, CLOCKSS, Crossref (DOI), digitálne pramene, DOAJ, EBSCO Host, Electronic Journals Library (EZB), ERIH Plus, Google Scholar, Index Copernicus International Journals Master list, iThenticate, JournalGuide, Jouroscope, Norwegian Register for Scientific Journals Series and Publishers, Portico, ROAD, ScienceGate, SCImago Journal & Country Rank, SciRev, SCOPUS, WorldCat (OCLC).
Journal Komunikácie - vedecké listy Žilinskej univerzity v Žiline / Communications - Scientific Letters of the University of Žilina is under evaluation for inclusion to Web of Science database.

Contact:
Komunikácie - vedecké listy Žilinskej univerzity v Žiline
Communications - Scientific Letters of the University of Žilina
University of Žilina
Univerzitná 8215/1
010 26 Žilina
Slovakia

E-mail: komunikacie@uniza.sk
Web: https://komunikacie.uniza.sk

ISSN (print version): 1335-4205
ISSN (online version): 2585-7878

Registered No. (print version): EV 3672/09
Registered No. (online version): EV 3/22/EPP
Publisher, owner and distribution:
University of Žilina, Univerzitná 8215/1,
010 26 Žilina, Slovakia

Company identification number IČO: 00 397 563
Frequency of publishing: four times a year
Circulation: 80 printed copies per issue
Print edition price: free of charge

Publishing has been approved by:
Ministry of Culture, Slovak Republic

UNIVERSITY
OF ŽILINA

In its over 70 years of successful existence, the University of Žilina (UNIZA) has become one of the top universities in Slovakia.

Scientific conferences

organized by University of Žilina

18th International Conference of Railway Communication and Safety Related Systems for Signalling
Date and venue: 22. - 24. 4. 2024, Žilina (SK)
Contact: stancelova.bohuslava@betamont.sk, karol.rastocny@uniza.sk
Web: https://www.betamont.sk/novinky2

15th International Conference ELEKTRO 2024
Date and venue: 20. - 22. 5. 2024, Zakopane (PL)
Contact: peter.hockicko@uniza.sk
Web: https://elektro.uniza.sk

39th International Colloquium Advanced Manufacturing and Repair Technologies in Vehicle Industry
Date and venue: 3. - 5. 6. 2024, Czestochowa (PL)
Contact: lenka.kucharikova@fstroj.uniza.sk
Web: http://kmi2.uniza.sk/

TalentDetector2024_Summer
Date and venue: 17. - 19. 6. 2024, Szczyrk (PL)
Contact: lenka.kucharikova@fstroj.uniza.sk

InvEnt 2024 (Invention Enterprises 2024)
Date and venue: 19. - 21. 6. 2024, Grand Hotel Bellevue (SK)
Contact: martin.krajcovic@fstroj.uniza.sk
Web: https://www.priemyselneinzinierstvo.sk

Unconventional Technologies 2024
Date and venue: 27. - 28. 6. 2024, Budatín (SK)
Contact: jan.moravec@fstroj.uniza.sk
Web: http://kti.uniza.sk/

27th Conference of Slovak Physicists
Date and venue: 2. - 5. 9. 2024, Žilina (SK)
Contact: kudelcik@uniza.sk

40th DANUBIA – ADRIA Symposium on Advances in Experimental Mechanics 2024
Date and venue: 24. - 27. 9. 2024, Gdansk (PL)
Contact: frantisek.novy@fstroj.uniza.sk
Web: https://das2024.pl

UNIVERSITY OF ŽILINA
Science & Research Department

Univerzitná 8215/1,
010 26 Žilina,
Slovakia

Ing. Janka Macurová
tel.: +421 41 513 5143
e-mail: janka.macurova@uniza.sk